Thesis Title: Temperature as a parameter in HPLC optimisation

Abstract

This study focused on the capabilities of elevated temperature chromatography and its potential applications. The effects of separation temperature on compound retention, selectivity and efficiency were studied. The change in retention with temperature was explored using a number of test compound solutions.

A detailed investigation of the importance of system variables like dead volume, mobile phase composition, different stationary phases, and temperature control of column and eluent was performed. The effects of different eluents and different means of temperature control on the separation selectivity and efficiency were investigated and results were compared.

The effect of the mobile phase inlet temperature was then investigated. The influence of the inlet temperature of the mobile phase on the column efficiency at different flow rates was investigated, using different types of temperature control, a range of different commercial stationary phase materials, a range of column dimensions and a standard test mixture. However, no generalised recommendations could be formulated for the optimisation of a separation system.

A number of elevated temperature and superheated water separations were developed. It was shown that it is feasible to transfer reversed phase chromatography separations at standard conditions to elevated temperature conditions. Furthermore, it was possible to estimate compound retention times at elevated temperatures and superheated water conditions from retention data measured at lower temperatures. Examples for the hyphenation of elevated temperature chromatography-mass spectroscopy and of superheated water chromatography-mass spectroscopy are given. Furthermore, the feasibility of superheated water chromatography-nuclear magnetic resonance spectroscopy was shown.

ACKNOWLEDGEMENTS

First and foremost, my thanks go to my supervisor, Professor Roger Smith, for his time, guidance, wise advice and encouragement throughout the course of this research.

Many thanks also to my industrial supervisors, Professor Ian Wilson and Dr Stephen Wren, AstraZeneca, for their advice and support, and for giving me access to use the LC-NMR and the Mass Spectrometer at the AstraZeneca sites in Alderley Park and Macclesfield.

Thank you too to Dr Peter Howe, for his ongoing encouragement and for making it possible for me to use the LC-NMR at Syngenta, Jealott's Hill.

And thanks to my fellow colleagues at Loughborough University; Simi, Shikha, Ruziati, Fabi, Lorna, Dave, Sonia, Ben and Jo, who shared their knowledge and helped to make the challenges of research enjoyable.

Lastly, I would like to thank Mags, for her patience and persistent encouragement and support.

TEMPERATURE AS A PARAMETER IN HPLC OPTIMISATION

By

Margret G. Tebrake

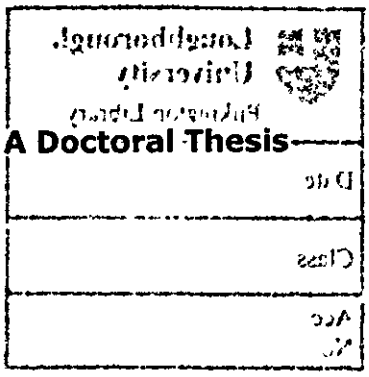

A Doctoral Thesis

Submitted in partial fulfilment of the requirements for the award of

PhD. of Loughborough University

1 INTRODUCTION

The principle of all chromatographic separation is the difference in distribution equilibrium of different analytes between a mobile phase and a stationary phase. The equilibrium distribution between the two phases determines the velocity with which an analyte migrates through the chromatographic system.

Equilibrium separation systems involve the transfer of components between the stationary and the mobile phases. Separation can only be achieved if the molecules of one analyte transfer to a greater extent than those of another [1].

Changing the mobile phase composition, the stationary phase and/or temperature can alter the equilibrium distribution and thus the separation. However, these changes do not happen in isolation. Changes in mobile phase composition will influence the stationary phase, and changes in separation temperature will impact on physico-chemical properties of the mobile phase, the stationary phase and the analyte.

Demands to reduce organic solvent use have increased in recent years [2], therefore an alternative approach to changing mobile phase composition to influence separations was needed. Furthermore, in today's high-throughput laboratories there is a call for shorter analysis times to increase turnover. Using temperature as a parameter for HPLC separation optimisation can potentially achieve both, a reduction in the use of organic solvent and shorter analysis times.

The present work investigates temperature as a parameter in the optimisation of reversed phase HPLC separations. It gives an

overview of how temperature can impact on analyte retention and separation efficiency. Furthermore, a number of elevated temperature applications were developed as examples for the use of temperature as optimisation parameter in reversed phase HPLC.

1.1 The retention factor - definition

The equilibrium distribution of an analyte between the stationary and the mobile phase determines the velocity with which an analyte migrates through the chromatographic system. A retained compound will spend time in the stationary phase as well as in the mobile phase. An un-retained compound will only spend time in the mobile phase.

The retention factor k (Equation 1) is defined as the retention time of the analyte minus the retention time of an un-retained compound divided by the retention time of the un-retained compound.

Equation 1

$$k = \frac{(t_R - t_0)}{t_0}$$

t_R is the retention time of the solute and t_0 is the retention time of an un-retained peak. The difference between the time the analyte spends in the column and the time an un-retained solute spends in the column is the time the analyte spends in the stationary phase. Hence the retention factor expresses the ratio of time the analyte spends in the stationary to the mobile phase. It is also the ratio of the concentration of analyte in the stationary phase to the concentration of analyte in the mobile phase (Equation 2).

Equation 2

$$k = \frac{(c_S * V_S)}{(c_M * V_M)}$$

c_S and c_M are the concentration of the analyte in the stationary and the mobile phases, respectively. The ratio of the concentrations is the distribution or partition coefficient K. V_S and V_M are the volumes of the stationary and the mobile phase respectively. Their ratio is the phase

ratio β. Hence the retention factor is the product of the phase ratio and the distribution coefficient (Equation 3):

Equation 3

$$k = K * \beta$$

From Equation 3 it is obvious that chromatographic retention can be influenced by changes in distribution coefficient of the analyte and the phase ratio. Temperature influences the distribution coefficient and changes the properties of both the stationary and the mobile phase dramatically.

2 TEMPERATURE AS A PARAMETER IN HPLC OPTIMISATION

To appreciate the impact temperature has on reversed phase separations the changes of temperature dependent physical properties of the stationary and mobile phase need to be understood. In the following an overview is given of the properties of mobile and stationary phase and the way they are influenced by temperature.

2.1 Effect of temperature on mobile phase properties

The most significant solvent (i.e. mobile phase) properties affecting separation in reversed phase chromatography are the dielectric constant, surface tension, viscosity, pH and elutropic value of a solvent [3]. The elutropic value of a solvent is an empirical value. Generally, the lower the polarity, the higher is the strength of eluent in reversed phase chromatography. One empirical measure for the elutropic value of a solvent is the polarity index (P') proposed by Snyder [4]. It describes the ability of a solvent to act as proton acceptor, proton donator and its dipole character. However, solvents of similar polarity can have different selectivities for a compound. Snyder describes the solvent selectivity as the ability of a given solvent to selectively dissolve one compound as opposed to another, when the polarities of the two compounds are not obviously different [5].

2.1.1 Dielectric constant

The bulk dielectric constant of a solvent is a measure of its polarity; e.g. water has a high dielectric constant and is a very polar solvent and hence is a weak solvent in RP-HPLC. Increasing temperature causes a decrease of the dielectric constant of water [6, 7]. In 1932 Akerlöf measured the dielectric constant for several aqueous solvent mixtures in the temperature range of 0 to 100 °C. In 1950, in collaboration with Oshry, he developed a method to determine the dielectric constant of water for temperatures up to 370 °C [8]. At 200 °C water was reported to have a similar dielectric constant (ε = 34.59) as pure methanol at room temperature (ε = 32.7) [9, 10].

The intermolecular forces such as hydrogen bonds are weakened and/or broken through increased molecular energy at higher temperatures. The dielectric constant and surface tension are significantly reduced and the solubility of most compounds in water increases with increased temperature [11, 12]. Recent publications showed that it is possible to mimic methanol-water mixtures by raising the column temperature under pressure to 150 to 200 °C [10, 13-15]. It was thus possible to perform reversed phase separations [16-18] and solid phase extractions [19] with a pure water mobile phase without any organic solvent present

2.1.2 Viscosity and surface tension

Two other mobile phase parameters, which are dependent on temperature, are surface tension and viscosity. Lowering the surface tension will reduce retention in reversed phase chromatography and lowering the viscosity will improve mass transfer [13].

The surface tension and viscosity arise from intermolecular attractive forces within the liquid mobile phase. An increase in mobile phase temperature causes an increase in internal energy and weakens

intermolecular forces, which will generally lead to a decrease in surface tension and viscosity of the mobile phase.

The temperature dependence of the viscosity was approximated by Andrade [20] (Equation 4).

Equation 4

$$\ln\eta = A + \frac{B}{T}$$

η is the viscosity, T the absolute temperature and A and B are specific constants of the pure liquid. The specific factors for the temperature dependent viscosity are listed in the literature for pure solvents but are frequently not available for solvent mixtures [21]. However, the majority of reversed phase mobile phases are aqueous mixtures of acetonitrile or methanol.

The viscosity is not only dependent on temperature but also changes with the composition [22]. An aqueous acetonitrile solution for example has its maximum viscosity at a composition of 15 to 20% water. Li and Carr calculated the change of the viscosity with mobile phase composition for acetonitrile/water and methanol/water mixtures at different temperatures [23] employing the Lobe correlation [24]. Figure 1 and Figure 2 show the fitted curves for the change of viscosity with temperature and volume fraction of organic modifier [23].

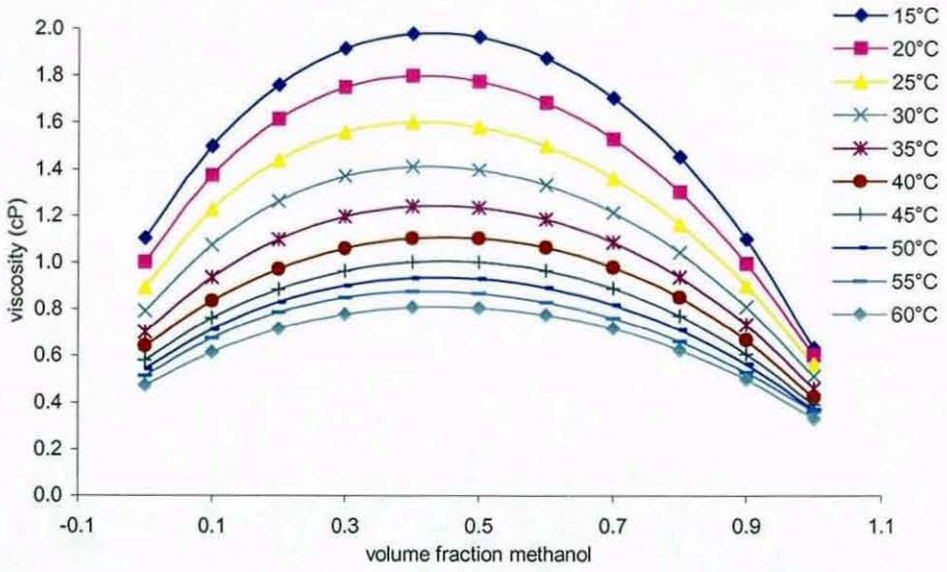

Figure 1: Fitted curves for the viscosity of methanol/water mixtures at different temperature. Viscosity of the mixture versus the volume fraction of organic modifier; data see ref. [23]

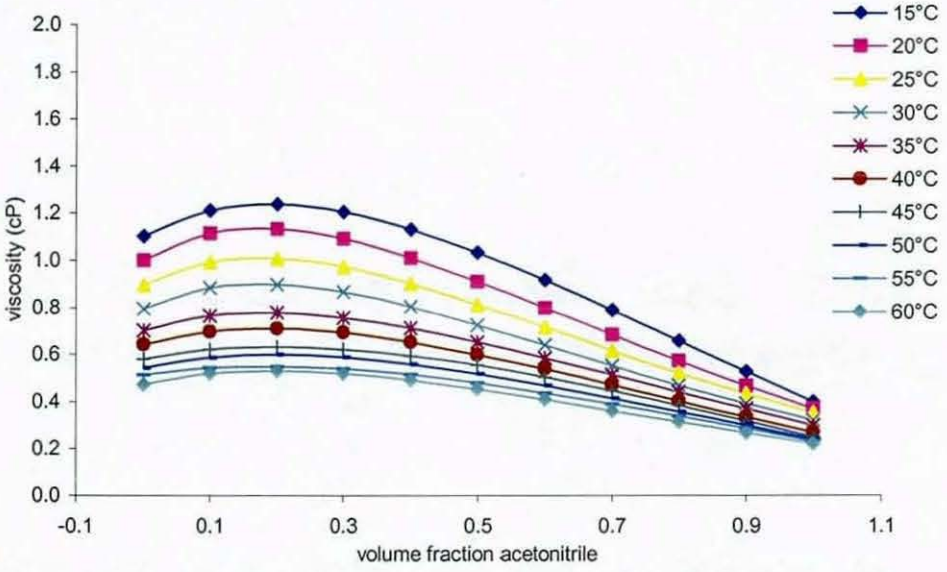

Figure 2: Fitted curves for the viscosity of acetonitrile/water mixtures at different temperature. Viscosity of the mixture versus the volume fraction of organic modifier; data see ref. [23]

A consequence of the lower viscosity at elevated temperatures is a dramatic decrease in inlet pressure when pumping the mobile phase through a separation column. This makes it possible, within the limits of the pump, to use smaller particle-size packing materials, longer columns, and/or higher flow velocities as the pressure drop Δp (Equation 5) along the column is related to mobile phase viscosity η.

Equation 5

$$\Delta p = 1000 \frac{(F * \eta * L)}{(\pi * r^2 * dp^2)}$$

Δp is the pressure drop, F is the flow rate, η is the viscosity, L is the column length, r is the column radius and dp is the particle size.

2.1.3 *Diffusion coefficient*

Chromatographic separations involve the transfer of components between the stationary and the mobile phase. Diffusion is mass transport on a molecular level. A change of separation temperature exerts an impact on diffusion i.e. it changes the rate of mass transfer between stationary and mobile phase. If the rate of mass transfer of one compound is affected to a greater extent than that of another a change in temperature can have an effect on the separation itself.

There are a number of empirical correlations for estimating the diffusion coefficient [25-28], however, the Wilke-Chang equation [29] (Equation 6) is probably most widely applied and best known in chromatography:

Equation 6

$$D = 7.40 * 10^{-8} \frac{\sqrt{\Psi_B * MW_B * T}}{(\eta * V_A^{0.6})}$$

where Ψ_B is the solvent association factor, MW_B is the molecular weight of the solute, T is the absolute temperature, η is the viscosity of the mobile phase and V_A is the molar volume of the solute at its normal boiling point which is usually obtained from a group contribution.

It is obvious from Equation 6 that temperature can significantly alter the diffusion coefficient. The diffusion coefficient is related to

temperature by its square root. Furthermore, the diffusion is related to the reciprocal of the solvent's viscosity, which itself is related to temperature. Thus a change in separation temperature will have a significant impact on the diffusion coefficient of the solute in the solvent i.e. in the mobile phase.

2.1.4 pH value

The pH of a mobile phase can be important if ionic compounds are separated. The reaction of silica, to make a reversed phase material, with long-chain alkylsilyl halides does not cover all available silanol groups. Thus there are residual silanol groups on the surface of reversed phase materials, which can interact in an ion-exchange mechanism with an ionic analyte [30, 31]. Therefore, pH control of the mobile phase can be extremely important in order to control the interactions of ionic analytes and the acidic silanol groups on the stationary phase surface.

A change in the dissociation constant of water with increasing temperature results in a change of pH. Marshall and Franck [32] reported a change of pKw from 13.3 at 50 °C to 11.6 at 150 °C. Kryukov and Perkovets [33] investigated the pH change of buffer solutions over a temperature range of 25 to 150°C. They observed a small increase in pH for phosphate, tartrate, phthalate and tetra-oxalate and a small decrease in pH for borate buffers as temperature increased. Smith and Chienthavorn [34] separated sulphonamides under buffered superheated water conditions. The pKa values of the sulphonamides in the buffered high temperature mode were reported to be very close to the pKa at room temperature. This is in line with the findings of Kryukov and Perkovets.

Even though temperature does not seem to significantly affect the pH of phosphate buffers, the pKa of bases in water was reported to decrease when the temperature is raised [35]. According to the approximate relationship given in Equation 7 the change of pKa per °K

temperature change is more significant for strong bases (large pK_a = small pK_b = strong base).

Equation 7

$$\frac{-d(pK_a)}{dT} = \frac{(pK_a - 0.9)}{T}$$

Equation 7 is valid for aqueous solutions; however, most HPLC mobile phases are aqueous-organic mixtures. The effective pH of a phosphate buffer/organic solvent mixture is higher than in the pure aqueous solution. Furthermore, the pK_a of basic compounds is higher in the presence of organic solvents. Thus, raising the temperature when employing a mixture of aqueous buffer and organic solvent could potentially have a far larger effect on the mobile phase pH and the protonation of the analyte [36].

2.2 Effect of temperature on the stationary phase

In 1973, Knox and Vasvari [37] reported that the peak skewness on a Permaphase ODS column was almost eliminated by running it at 60 °C. Their explanation for this effect was that the polymer layer of the ODS stationary phase became more swollen at higher temperatures and the partition isotherm became more linear through more structural flexibility as the temperature increased.

Morel and Serpinet [38, 39] examined the effect of temperature on a ODS bonded silica by inverse gas chromatography. The van't Hoff plots for column material with a carbon load > 4.0 µmol/m^2 showed a reproducible non-linear shift between 5 and 30 °C. This shift was ascribed to a transition of the bonded C_{18} phase. They proposed a melting of a solid, crystal-like phase to a liquid expanded phase. Linear van`t Hoff plots were reported for less densely coated C_{18} silica.

The studies reported in these papers were not performed under operational HPLC conditions. The packing materials were not exposed to a mobile phase. In a later paper Morel and Serpinet [40] included LC data for the retention of structurally diverse solutes on densely grafted C_{22} silica. They included pure methanol and methanol-water mobile phases in their studies. The carbon load for the slightly longer C_{22} chain bonded to the silica surface was 3.98 $\mu mol/m^2$. A slightly higher transition temperature was observed for the C_{22} chain, 48 °C, as opposed to the C_{18} chain, 27 °C. Under LC conditions with a pure methanol mobile phase, a transition temperature of 46.5 °C was reported. With mixed methanol-water mobile phases up to 50% water, the transition temperature was found to be the same as with neat methanol. The transition temperature was in the same range as with the inverse GC method. However, from above 55% water in the mobile phase the transition temperature shifted from 46 °C to 53 - 54 °C and did not change further with higher concentrations of water. Although non-linear van`t Hoff plots were obtained in all cases the actual transition temperature was dependent on the mobile phase composition, hence on the solvation of the stationary phase in the mobile phase.

Jinno et al. [41] and Cole and Dorsey [42, 43] investigated the effects of changing the mobile phase and the column temperature on the mechanism of retention. Jinno et al. compiled FT-IR data supporting the earlier findings by Morel and Serpinet [40] and Sander et al. [44] that changing the mobile phase caused changes in the conformation of the ODS bonded phase. From solid state NMR data [45] it was evident that a change in temperature caused a drastic change in the stationary phase from solid-like to a liquid-like form. [40] Cole and Dorsey performed retention studies under reversed phase LC conditions and found non-linear van`t Hoff behaviour. They supported the explanation suggested by Morel and Serpinet of a phase transition of the reversed phase stationary phase. For densely packed C_{18}

stationary phases a transition temperature of 22 °C was reported. The phase transition was observed to be more pronounced on high bonding density columns than on low density columns [39, 46].

A more recent study investigated the alkyl chain conformation of bonded C_{18} stationary phases by Raman spectroscopy [47]. The results showed the ability of the bonded alkyl chains to attain different degrees of conformational order depending on temperature. Because of a greater heterogeneity of the environment, the phase transition of the bonded alkylsilanes occurred over a much broader temperature range than with bulk alkylsilanes. Again it was noted that the mobile phase composition and the carbon load influenced the transition temperature.

In 1993 Wheeler at al. comprehensively reviewed of the phenomenon of phase transition [48]. They concluded that phase transition could be a function of virtually every potential variable: bonded chain length, bonding density, bonding reaction (monomeric or polymeric), mobile phase and the choice of solute. In their opinion Van't Hoff plots alone were not an indication of a change in phase structure as non-linearity could arise from other thermodynamic processes than stationary phase changes. Although, differential scanning calorimetry (DSC) [49] experiments indicate a phase transition they were generally not performed under chromatographic conditions. The experiments lacked the influence of mobile phase and pressure on the stationary phase. Wheeler et al. [48] recommended the term phase transition should be applied very loosely as there was not a sharp, distinct change in stationary phase structure but a diffuse change going from a solid-like to a liquid-like state. These transitions occurred over a rather broad temperature range.

Doyle et al. [50, 51] investigated the effect of mobile phase composition and temperature on a C_{18} bonded phase by Raman spectroscopy under operational HPLC conditions. The expected collapse of the C_{18} chains when using water as the mobile phase was not observed but a distinct temperature dependent change in stationary phase conformation was noted. The spectral features of the bonded ligands became increasingly more ordered as the temperature decreased from 45 to 2 °C. There was no sharp transition temperature, rather a continuous change in structural flexibility with temperature. The temperature induced ordering was observed for high and low bonding density phases. The non-linearity of the van't Hoff plot, which has been attributed to possible phase transition by other researchers, was only observed for high bonding density monomeric phases.

2.3 Effect of temperature on retention in reversed phase liquid chromatography

For decades temperature was not appreciated as a parameter for separation optimisation. In 1948 LeRosen and Rivet [52] investigated the movement of a chromatographic zone as a function of temperature. Their work was focused on finding a temperature region in which the retention of substances was least dependent on temperature. They found for all investigated compounds that the retention vs. temperature curves showed a flat region at about 20 to 35°C. Some compounds showed a rapid increase/decrease of retention values outside this range. It was therefore concluded that liquid chromatographic separations should be performed at temperatures between 20 to 35 °C to minimize the impact of temperature.

It was postulated that the solute interactions with reversed phase stationary phases are essentially hydrophobic interactions. The strength of hydrophobic interactions, and thus retention in reversed phase chromatography, was predicted to increase with increasing

temperature [53, 54]. However, experiments showed different behaviour.

Chang [55] investigated a temperature range of –50 to 200 °C and found that dependent on the solvent system, retention values increased or decreased with increasing temperature. In 1967 Locke and Martire [56] proposed an equation for the temperature dependence of retention in liquid-liquid chromatography. It was based on the activity coefficient of the solute and the chemical potentials of stationary and mobile phase. In 1971 Schmit et al. investigated the effect of temperature on reversed phase chromatography separations. They found a linear relationship between log t_R (retention time) and the reciprocal of the absolute temperature [57]. The retention time decreased with increasing temperature. These findings changed the attitude towards the control of temperature from being a mere necessity to being a tool to shorten analysis time.

The temperature dependence of the retention factor in reversed phase chromatography can be expressed in terms of the free energy of a solute when changing from one phase into the other.

The change in free energy ΔG^0 of a solute changing from one phase to another is expressed through Equation 8

Equation 8

$$\Delta G^0 = -RT \ln K$$

where R is the universal gas constant and T is the absolute temperature. The standard free energy can also be expressed as in Equation 9:

Equation 9

$$\Delta G^0 = \Delta H^0 - \Delta TS^0$$

where ΔH^0 is the standard enthalpy change and ΔS^0 is the standard entropy change of solute transfer. Therefore the retention coefficient can be expressed as in Equation 10:

Equation 10

$$\ln k = \ln \beta - \left(\Delta \frac{H^0}{RT} - \Delta \frac{S^0}{R} \right)$$

This expression is the basis of the temperature dependence of retention. The enthalpy is given by the slope of the curve when $1/T$ is plotted against ln k, in a van't Hoff plot. Larger molecules usually have larger enthalpy changes than small molecules. Thus ln k of a larger molecule will be more affected by a change in temperature [21]. Non-linearity in the enthalpy change associated with the transfer of solute between mobile phase and stationary phase can be caused by not linearly increasing adsorption enthalpy within the temperature range, different desorption kinetics of different functional groups or temperature related changes of the mobile phase [58].

Retention generally decreases with increasing temperature and studies were performed to compare the effect of changing temperature with a change in solvent composition [59]. However, there are some exceptions. Greibrokk et al. [60] reported increased retention for the dipeptide leucine-phenylalanine at low pH and high % acetonitrile at elevated temperatures. Furthermore, increased retentions for carotenoids on C_{30} stationary phases were reported by a number of researchers [61, 62].

2.3.1 Retention mechanisms

During the mid/late 1970's Melander and Horvath developed a comprehensive retention model for reversed phase chromatography, the solvophobic model [22, 63, 64]. They applied an extra-thermodynamic approach to analyse retention data. The term extra-thermodynamic denotes the fact that they fall short of a rigorous thermodynamic foundation [22, 64] and many of these relationships are termed linear free-energy relationships [65]. The solvophobic model of retention proposed by Horvath et al. [22, 63, 64, 66] did not

consider that the bonded stationary phase played an active part in retention and explained the change in retention with temperature merely as changes in mobile phase properties.

They used the enthalpy-entropy compensation approach, which manifested itself in a linear dependence of the overall free energy changes on the corresponding enthalpy changes for similar physico-chemical phenomena.

Enthalpy-entropy compensation can be expressed using Equation 11,

Equation 11

$$\Delta H^0 = \beta \Delta S^0 + \Delta G_\beta^0$$

where ΔH^0 is the enthalpy β is the temperature, ΔS^0 is the entropy and ΔG_β^0 is the free energy change at temperature β. Looking at Equation 11 the linear relationship implies that close to β changes in ΔH^0 are offset by changes in ΔS^0. If this compensation of enthalpy and entropy is observed the values for β and ΔG_β^0 are invariant and β is called the compensation temperature. Combining Equation 11 with the thermodynamic expression for the retention factor (Equation 10) they developed an expression (Equation 12) to investigate the enthalpy-entropy compensation of the reversed phase chromatographic process:

Equation 12

$$\ln k_T = -\Delta \frac{H^0}{R}\left(\frac{1}{T} - \frac{1}{\beta}\right) - \Delta \frac{G_\beta}{R_\beta} + \ln \varphi$$

in this equation φ denotes the phase ratio. By plotting $-\Delta H$ vs. *ln k* for different mobile phases and solutes they showed that all data points fell on the same line, thus these points shared compensation behaviour. From these findings they concluded that the mechanism of interaction with the hydrocarbonaceous stationary phase was the same irrespective of eluent composition and the electrostatic properties of the solute.

They derived a set of equations to transform retention data for a specific solute obtained at a given temperature and solvent composition to a different set of experimental conditions [66]. It was proposed to be feasible to calculate, at a given solvent composition, the column temperature, which is equivalent in its effect on retention to another mobile phase composition at a different temperature.

Dill and Dorsey [67, 68] developed the partition model and pointed out that Melander and Horvath did not distinguish between the stationary phase and the mobile phase adsorption of the solute, in that the stationary phase bonded alkane chains were treated as a bulk alkane liquid. According to Dill and Dorsey the stationary phase could not be treated as a bulk alkane phase because the bonded alkane chains do not have the same freedom of movement. They assigned an active role to the stationary phase as well as to the mobile phase. They proposed influence of phase transition in the stationary phase on retention and provided a possible explanation for a number of findings of an increased retention with increased temperature such as reported by Sander et al. [61]. They found distinctly different effects of temperature on retention for carotenoids, if C_{30} and C_{34} stationary phases were used, compared to C_{18}phases.

For example, lutein and xanthin showed non-linear van't Hoff plots. The plots appeared to flatten out as the temperature was decreased. It was suggested that the retention of polar carotenoids involved interactions with silanols near the surface of the silica and the retentions resulted from a combination of mechanisms. For the C_{18} stationary phase the van't Hoff plot was linear. The increased order of the structure of the stationary phase induced by the lower temperature prevented the solute from penetrating the stationary phase and interacting with the surface silanols on reaching the silica surface, thus changing the relative contributions of solute-silanol and solute-bonded phase interactions to retention.

In 1993 Tchapla et al. [69] comprehensively summarised the discussion about the different models of retention, the solvophobic model and the partition model, in reversed phase HPLC at that time.

Although several mechanisms have been proposed to account for the retention in reversed phase chromatography most of these could only be applied to the retention behaviour of a limited range of solute and mobile phase compositions [70]. There is no overall model of retention processes, including those caused by the stationary phase effects, to explain retention behaviour in reversed phase chromatography.

2.4 Effects of temperature on selectivity

The difference in the interaction of two solutes between the mobile and the stationary phase is generally defined as the selectivity (Equation 13).

Equation 13

$$\ln \alpha = \frac{k_2}{k_1} = -\Delta\left(\frac{\Delta G}{RT}\right)$$

k_2 and k_1 are the retention factors of the second and the first eluting solutes respectively, ΔG is the Gibbs free energy of transfer between the mobile and the stationary phase, R is the gas constant and T is the absolute temperature. Retention and selectivity are mostly adjusted by changing the mobile phase, either through changing the solvent strength or the solvent selectivity respectively [71].

Sander and Wise [72, 73] investigated the effect of temperature on the separation of PAH mixtures on monomeric and polymeric stationary phase materials. They used the selectivity for PAHs,

benzo[a]pyrene (BaP) and tetrabenzonaphthalene (TBN) to classify stationary phases as follows:

$\alpha_{TBN/BaP} \geq 1.7$ monomeric like selectivity

$\alpha_{TBN/BaP} < 1$ polymeric like selectivity

$\alpha_{TBN/BaP} < 1.7$ intermediate selectivity

Separations were carried out at both elevated temperatures and sub-ambient temperatures with various mobile phases. It was found that for the polymeric stationary phases the selectivity decreased with increasing temperature and increased on lowering the temperature. For monomeric phases selectivity increased at lower temperatures and changed only slightly as the temperature was raised and became nearly constant above 45 °C. The selectivity was observed to be nearly independent of the mobile phase composition for polymeric stationary phases. On the basis of this data Sander and Wise [73] proposed a model of temperature induced selectivity changes based on the morphology of the bonded phase.

Jinno et al. [41] performed studies on the dependence of the stationary phase morphology on temperature in order to investigate the retention mechanism in reversed phase chromatography. They found a more solid-like structure of the bonded phase at lower temperatures. The solid-like phase preferably retained planar PAHs more strongly than non-planar PAHs. The data indicated that the ordering of a polymeric phase at lower temperatures was large enough to alter the recognition of the planarity in molecules. The planar molecules, which could most efficiently align with the ordered more rigid chains were most efficiently retained.

More studies have been carried out to investigate the increased shape selectivity of reversed phase material at subambient temperatures.

Cole and Dorsey [71] investigated the retention behaviour of PAHs. Like Sander and Wise they used the selectivity index $\alpha_{TBN/BaP}$ to classify their results. Sentell et al. investigated the effect of temperature on the selectivity of PAHs [74] and homologous series selectivity [75]. They observed better shape selectivity on high bonding density columns than on low bonding density columns. For both column types, the shape selectivity improved with column temperatures lower than 25 °C. This effect was more pronounced with stationary phases of higher carbon load.

Sander and Wise [76, 77] conclude in a review on selectivity that dramatic selectivity changes occur with temperature. Shape discrimination is enhanced at lower temperatures, such that polymeric like selectivity can be mimicked by monomeric C_{18} phases.

Poole et al. [78, 79] investigated the influence of temperature on retention and selectivity using the solvation parameter model proposed by Abraham et al. [80, 81]. It was reported [78] that the predominant influence of increasing the temperature was a decrease of retention. The formation of the cavity for each solute in the mobile phase was easier at elevated temperatures because of a reduction in cohesive energy in the mobile phase. The effect of temperature on selectivity was largest with compounds differing in size. The ability to change retention and selectivity through variation of the mobile phase composition was found to be much greater than through variation of the temperature.

However, the changes in selectivity accompanying the variation of mobile phase composition were quantitatively different from those found for the variation of the temperature [79]. For method development the use of elevated temperatures was suggested to be complementary to the change of organic modifier.

2.5 Separation Performance

The efficiency of a column can be described by the van Deemter equation (Equation 14). It assumes that the individual contributions to plate height are independent and additive:

Equation 14

$$HETP = A + \frac{B}{u} + C_s * u + C_m * u$$

where *HETP* is the height equivalent of a theoretical plate at a given linear flow velocity. *A* is a function of the particle size. *B* describes the longitudinal diffusion within the mobile phase. The *C* term is split into two parts. The resistance to mass transfer in the stationary phase C_s and in the mobile phase C_m. The velocity of the mobile phase is u.

The *A* term (Equation 15) is independent of the mobile phase velocity. It is proportional to the particle size and can be influenced by the column packing technique.

Equation 15

$$A = \lambda d_p$$

λ is a geometrical factor and for well packed beds it will be between 1.5 and 2, d_p denotes the particle size.

The *B* term (Equation 17) describes the molecular diffusion in the mobile phase. It is dependent on the time the analyte spends in the column and therefore is inversely dependent on the mobile phase velocity. The relationship of bandwidth and time is expressed through the Einstein equation (Equation 16):

Equation 16

$$\sigma^2 = 2Dt$$

Where σ^2 is the variance of the distribution (bandwidth), D is the diffusion coefficient and t is the time. The sample only diffuses when it is in the mobile phase. That means that t in the equation is the time the solute spent in the mobile phase and D is the diffusion coefficient of the solute in the mobile phase. Diffusion in the packed bed of a separation column is slower than in neat solvent. To account for the packed bed an obstruction factor is added to the Einstein equation (Equation 17).

Equation 17

$$B = 2\gamma \frac{D_m t}{L} = 2\gamma \frac{D_m}{u}$$

u is the linear velocity, γ the obstruction factor and D_m the diffusion coefficient of the solute in the mobile phase.

The C terms describe the resistance to mass transfer which can be divided into resistance to mass transfer in the mobile and in the stationary phases. This dispersion effect results from the time necessary for a solute to transfer from the mobile to the stationary phase and vice versa. Some molecules of the same solute will be stationary in the packing material while the molecules already transferred to the mobile phase will move with the pump flow along the column. Consequently a spreading effect occurs. Equation 18 A-B shows the two functions proposed by van Deemter to describe resistance to mass transfer,

Equation 18 A-B

$$C_m = \frac{f_1(k) d_p^2 u}{D_m}$$

A: resistance to mass transfer in the mobile phase

$$C_s = \frac{f_2(k) d_f^2 u}{D_s}$$

B: resistance to mass transfer in the stationary phase

where k is the retention factor, D_s is the diffusion coefficient of the solute in the stationary phase and d_f is the film thickness of the stationary phase.

For a normal packed bed with porous particles the van Deemter equation as a whole can be expressed as in Equation 19:

Equation 19

$$HETP = 1.5d_p + 2\gamma\frac{D_m}{u} + \frac{f_1(k)d_p^2 u}{D_m} + \frac{f_2(k)d_f^2 u}{D_s}$$

The relationship between H and u for a given column can be determined experimentally. There are a number of different methods to calculate the number of theoretical plates of a column from the peaks eluting from the column. The probably most common method is the half width method. Equation 20 shows the equation used for the calculation of the number of theoretical plates,

Equation 20

$$N = 5.54\left(\frac{t_r}{w_h}\right)^2$$

where N is the number of theoretical plates, t_r is the retention time and w_h is the peak width at half height.

The plate number per column can easily be translated into the height equivalent of a theoretical plate.

Equation 21

$$HETP = \frac{N}{L}$$

L is the length of the column.

Using the above equations it is possible to plot curves of HETP vs. u, which allows comparison of the separation performance of different columns and/or chromatographic systems.

2.5.1 Quality of column packing

The quality of the packed bed has a significant influence on the band spreading in chromatography. Knox and Parcher investigated the dispersion of un-sorbed solutes through a column packed with glass beads [82]. They report higher linear flow velocities close to the wall than in the centre of the packed bed. In a later paper, Knox et al. [83] proposed columns of infinite diameter to avoid solute reaching the zone of about 30 particle diameters from the wall. This "wall effect" describes the phenomenon of lower packing density close to the wall of a column compared to the centre of a column. When the column is packed the stationary phase material is pressed against the wall but cannot penetrate the wall. It cannot assume the closest packing density in the wall region hence the overall packing density is lower.

Farkas et al. [84, 85] investigated the radial inhomogeneity in HPLC columns. They inserted optical fibres perpendicularly into the column exit frit. This way they could measure the solute distribution over the whole width of the column at any one time. They found that in badly packed columns the solute close to the column walls reached the column end first. The mobile phase velocity at the walls was higher than in the centre of the column. In columns, which were well packed they found that the solute in the centre of the column reached the column end first. The mobile phase velocity in the middle of the column was higher than close to the walls. They measured differences in linear velocities of up to 10 % across the column diameter. On average the region of maximum velocity was found about 1/3 or 1/2 column radius off the column centre. The velocity in the column centre lagged behind that region by about 1 to 2%. The velocity close to the wall was 2-3% smaller than in the column centre. When the mobile phase flow rate was decreased the relative difference between the velocities at the centre and other local values, which were expected to remain constant, decreased as well. The differences

became negligible when the columns were operated at a flow rate of 0.2 ml/min or less, which is close to the optimum value for the minimum HETP they measured.

A number of researchers confirmed the differences in linear flow velocity and efficiency dependent on the radial position in the column using a number of different techniques, including NMR imaging [86-88], microvoltammetric electrodes [89], packed glass columns with mobile and stationary phases of matched refractive indices [90, 91] and numerical calculation of elution profiles [92-94].

Shalliker et al. distinguished three velocity zones [95]. From the column wall in radial direction the three zones were as such: zone 1, a small zone of high mobile phase velocity immediately against the wall followed by zone 2, a thicker zone where the mobile phase velocity was slightly lower than the average mobile phase velocity in the column and zone 3, a zone around the column axis where the mobile phase velocity is higher than its average in the column.

The second zone was thought to be caused due to wall friction increasing the compressive stress during the packing process of the column resulting in the packing density being higher in this region [96]. This is what Shalliker called the second wall effect [95] in order to distinguish it from the wall effect described by Knox [83].

In a more recent paper Shalliker et al. [97], investigate differences in diffusion for a solute dependent on the solutes radial and axial positions in the column. They reported a decrease of the solute's diffusion coefficient as it entered the wall region. This was thought to be caused by the increasing tortuosity of the packed bed from the centre of the column towards the wall.

In summary, the quality of the column packing has a significant impact on the column's performance. Not only does it influence the flow profile but impacts on the diffusion coefficient of an analyte i.e.

has repercussions for the rate of mass transfer between the stationary and the mobile phase.

2.6 Effect of temperature on efficiency

In addition to the impact that temperature has on retention and selectivity changes in separation efficiency were observed when the separation temperature was changed.

In 1971 Schmit et al. reported [57] a gain in efficiency with increasing temperature and ascribed the increased efficiency at higher temperatures to the drop in mobile phase viscosity and hence an increase in diffusion rate. They reported a twofold increase in efficiency; a similar increase in efficiency at ambient temperature was only achieved by increasing the column length fourfold.

Saner et al. [98] reported a loss in efficiency on a 5 µm dp RP18 column at a temperature of 60 °C compared to ambient. They attributed the loss in efficiency to a drop in diffusitivity within the stationary phase resulting in reduced mass transfer. In the same study an increase in efficiency for a 10 µm dp RP18 column was reported.

Horvath and Lin evaluated individual plate height contributions to the overall plate height [99]. They found evidence that kinetic resistance plays a significant role in band spreading, particularly for strongly retained solutes. The effect of the retention factor on the various plate height contributions at fixed flow velocity was reported as shown in Table 1. With increasing retention factor the increments of the resistance to mass transfer and of the kinetic contribution to the plate height at a given temperature increased and the contribution of extra column effects decreased. H_{disp} is the plate height increment due to axial dispersion, H_{diff} due to resistance at the particle boundary and the intraparticular diffusion resistance to mass transfer. H_{kin} expresses

the kinetic resistance for solute binding and $H_{extr\ col.}$ the plate height contribution of extra column band spreading.

Table 1: Effect of retention factor on different plate height contributions

solute	k	H_{disp}	H_{diff}	H_{kin}	$H_{ext\ col}$
3,4-dihydroxymandelic acid	0.5	1.9	1.7	3.8	7.5
4-hydroxymandelic acid	0.95	1.9	2.2	8.3	4.5
2,3,4-trihydroxybenzoic acid	1.87	1.9	2.7	15	2
3,4-dihydroxyphenylacetic acid	3.88	1.9	3.3	22	0
4-dihydroxyphenylacetic acid	7.19	1.9	3.6	27	0

Against all expectations based on theory Warren and Bidlingmeyer reported a loss in efficiency with increasing temperature [100]. They worked in the temperature range of 35 - 65 °C and used acenaphthene and dibutyl phthalate as solutes. Regardless of eluent, solute type and flow rate, a higher temperature led to higher H values.

Two different types of column and column heater were used. The first type of column was a steel column, 3.9 mm i.d., the second type a radial pack cartridge, 8 mm i.d.. The types of column heaters were a block heater and an air oven. When using the block heater a 21 inches length of steel capillary was used as the pre-heating coil for the incoming mobile phase. Employing the air oven a length of 48 inches of steel capillary was placed in the oven to pre-heat the incoming mobile phase. Warren and Bidlingmeyer [100] attributed the negative impact of temperature on efficiency to a radial thermal gradient, which exists for thermostated columns. Other researchers had earlier proposed thermal gradients as the reason for a loss in efficiency at

elevated temperatures [98]. Radial thermal gradients will be discussed in more detail later in this work.

Warren and Bidlingmeyer concluded that improvements in efficiency for reversed phase chromatography systems were not a guaranteed consequence of elevating the separation temperature [100].

The same year Horvath and Antia [101] performed a theoretical examination of the effect of temperature on the efficiency for the separations of large molecules.

Their assumptions for their theoretical analysis were:

- the analyte had a **constant retention factor** of $k = 3$ throughout the temperature range
- the column packing structure was invariant with temperature
- the mobile phase had the **properties of water** throughout the temperature range
- **slow sorption kinetics** for large molecules were assumed

A variation of the van Deemter equation published in an earlier paper [99] was used for the calculation of plate height, which comprised a term to account for the band spreading due to slow kinetics.

Under conditions where the column length, the inlet pressure and the particle size was set, the dependent variable analysis time decreased and efficiency increased with temperature. On increasing the temperature under constant analysis time conditions, the back-pressure in the theoretical system decreased and the efficiency increased.

All data was calculated for large molecular weight solutes with slow desorption kinetics and totally porous particles packed in a 3 cm column.

Horvath and Antia proposed an increase in efficiency with an increase in temperature because of enhanced diffusivity and faster sorption kinetics for large molecules at elevated temperatures.

In 1992 Liu et al. [102] reported an increase in efficiency at elevated temperatures for open tubular capillary LC. They found that the mobile phase had to be pre-heated to column temperature to achieve the best efficiency. Like Horvath and Antia [101] they explained the increase in efficiency as being due to an improved solute diffusivity at elevated temperatures.

In 1993 Chen and Horvath [21] published experimental data on protein separations, which supported the results of the theoretical analysis by Horvath and Antia [101]. It was proposed that the main advantages of high column temperatures derived from lower mobile phase viscosity and the concomitantly increased solute diffusivity, reduced column back pressure, and accelerated sorption kinetics. Furthermore elevated temperatures brought an enhanced solubility for substances, which were not soluble under ambient conditions.

A group of researchers at the University of Oslo [103, 104] generated a high temperature method to separate heavy, relatively polar compounds with low water solubility, which were not adequately separated by conventional HPLC. They found that elevated temperatures decreased the analysis time and back-pressure but did not find the expected increase in efficiency. The mobile phase composition (90% acetonitrile, 10% DMF) was not changed when temperature was increased which meant that k values for the test solutes were not kept constant. They ascribed the absence of an increase in separation efficiency, to the increased contribution of extra column band broadening to the overall efficiency because of significantly decreasing k values. Furthermore, they observed lower

efficiencies using low flow rates at elevated temperatures [104]. This was explained by the increase in axial dispersion. At below optimum flow rates, band broadening is primarily controlled by axial dispersion, which increases with temperature [105].

In a more recent study, Yan et al. [106] found that the reduction of the C term at elevated temperatures was more significant for more highly retained solutes. This indicated that the resistance to mass transfer was reduced at higher temperatures. They showed that for less retained solutes or if the mobile phase was not adjusted to keep the retention factor constant there was a smaller improvement in the C term. On elevating the temperature, they found that the optimum linear velocity was moved to a higher velocity than at ambient temperatures. The conclusions from the study were that it was beneficial to operate a HPLC separation at high temperatures and flow rates to improve efficiency and shorten analysis time.

2.6.1 Radial thermal gradients

As mentioned earlier, radial thermal gradients are a concern regarding separation efficiency [100]. However, this is not only the case due to inefficient temperature control when working at elevated temperatures [98] but also at ambient temperatures [107].

Halasz and co-workers [108] and Poppe et al. [107] reported radial thermal gradients in chromatographic columns due to frictional heating.

They showed that under ambient HPLC conditions the inner core of the separation column is warmer than the wall region [107]. Depending on the mobile phase and the pressure drop the temperature difference was found to be from 0.5 °C to up several °C. This was proposed to be a reason for additional band broadening, firstly through a viscosity gradient and secondly through a retention factor gradient. Assuming the pressure drop over the cross section of the column is constant the

viscosity gradient causes a higher linear flow velocity for the mobile phase in the centre of the column. The retention factor gradient is caused through a temperature dependence of the retention factor and could cause a non-uniformity in the migration of retained compounds.

In order to measure the effect of the proposed thermal gradient Poppe and Kraak measured the peak width at 0.6 and 0.1 maximum peak height of un-retained and retained compounds [109]. A 31% aqueous ethanol mobile phase was used to magnify the effect of the expected viscosity gradient. The plate heights for the different solutes (uracil, nitrobenzene, dinitrophenyl) were plotted as a function of the mobile phase feed temperature at different flow rates.

Higher efficiencies were found by using a mobile phase inlet that was slightly lower in temperature than the column temperature. The severity of this effect was dependent on the flow rate. With a less viscous mobile phase such as aqueous acetonitrile the effect was not as pronounced. This indicated a compensation effect of viscous heat dissipation through lowering the feed temperature of the mobile phase.

They suggested the formation of an inverted flow profile, which negated the band broadening effect of the normal parabolic flow caused by frictional heating (Figure 3).

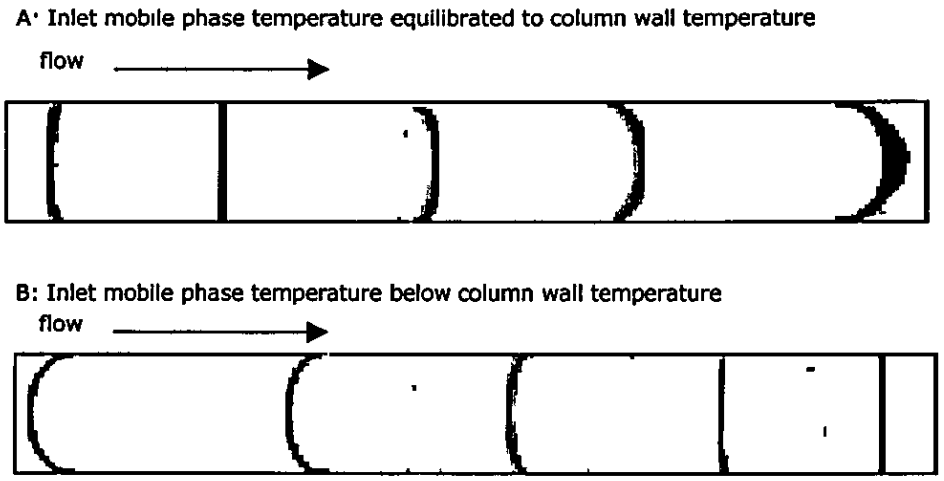

Figure 3: Band broadening in separation column due to frictional heating. A: mobile phase temperature is equilibrated to the column wall temperature. The centre of the column is at a higher temperature than the wall region due to the frictional heating and poor heat transfer in the packed column. B: mobile phase temperature is below column wall temperature. The centre of the column is cooler than the wall region. The temperature in the centre catches up with wall region due to frictional heating.

An optimum temperature differential between mobile phase inlet and column was proposed, just enough to "relax" the temperature gradient caused by frictional heating [110].

Welsch and co-workers [111] supported the findings of Poppe and Kraak. They examined non-porous and porous reversed phase and normal phase column materials at 40 °C column temperature and reported that improved efficiency could be obtained by reducing the inlet temperature of the mobile phase [112]. They attributed the effect to the compensation of thermal gradients caused by frictional heating in the column and suggested that different inlet temperatures might be required for each column to compensate for the different resistances to flow. It was proposed that there is an optimum feed temperature for a specific column. Lowering the eluent pre-cooling below this optimum temperature or identical temperatures of eluent and column resulted in increased plate heights. Furthermore, they claimed their results were independent of flow rate because at high

rates there was an internal compensating feature, as reduced contact time in the preheating coil automatically lowered the inlet temperature.

Wolcott and Dolan found that heating the mobile phase to the same temperature as the column for gradient elution brought best efficiencies and peak shapes [113, 114].

In a different paper [115] Wolcott et al. clarified that preheating the mobile phase to the same temperature as the column was preferable if frictional heat effects are negligible and supported the findings by Poppe and Kraak and of Mayr and Welsch that deliberate cooling of the incoming solvent can cancel out the band broadening effects of viscous heat dissipation.

2.7 Applications of elevated temperature chromatography

Elevating the separation temperature appears to be established as a tool to improve separation efficiency [116] despite some of the observations mentioned in the previous section. A number of papers by Zhu et al. [117-120]were published proposing the combined use of solvent strength and temperature to optimise reversed phase gradient elution. The use of temperature as an optimisation parameter for retention and selectivity was even included in method development software tools [121-127].

Several researchers propose temperature gradients as an alternative and/or in addition to solvent gradients [128-131]. Two comprehensive reviews on the use of elevated temperature in liquid chromatography were recently published [58, 132].

Mao and Carr [133] proposed the "thermally tuned tandem column concept" (T^3C) to increase separation selectivity. Two columns with distinctly different chromatographic selectivities are serially coupled. The temperature for each column is controlled independently. The

selectivity is "tuned" by adjusting the individual temperatures of the two columns.

When applying elevated temperatures it is important to control the column temperature efficiently [132, 134]. Furthermore, the temperature of the mobile phase entering the column has to be controlled [114, 115]. However, there is some debate as to whether the mobile phase should enter the column equilibrated to column temperature [114, 115, 135] or should be adjusted to a fixed value below column temperature [111, 112] to achieve the optimum separation efficiency (see chapter 2, section 2.6.1).

2.8 Aims of the present study

This study set out to investigate the capabilities of reversed phase HPLC at elevated temperatures. Analytical methods are regularly developed in one laboratory but then after validation employed in a number of laboratories. In order to present a viable complementary and/or alternative method the transferability of elevated temperature methods has to be ensured. The intention was to define critical variables for successful method transfer. The study was thus designed to give answers to a number of questions concerning the capability for day-to-day applications. Because contradicting results regarding the benefits of elevated temperature chromatography were reported over a number of years, the question of first and foremost importance was, how important are system variables like dead volume, mobile phase composition, different stationary phases, and temperature control of column and eluent. The effects of different eluents and different means of temperature control on the separation selectivity and efficiency were investigated and results were compared.

The effect of the mobile phase inlet temperature was then investigated. In most cases the earlier papers on the effect of mobile

phase inlet temperature on column efficiency have been based on the examination of a single column brand or stationary phase. The present study therefore set out to examine in detail the influence of the inlet temperature of the mobile phase on the column efficiency at different flow rates, using a range of different commercial stationary phase materials, a range of column dimensions and a standard test mixture. The intention was to determine if generalised recommendations could be formulated for the optimisation of a separation system.

This work lead to a number of applications of elevated temperature and superheated water separations.

3 EXPERIMENTAL

In this chapter general experimental details and chemicals are described for studies on the effect of temperature on reversed phase chromatography.

3.1 Materials

Methanol, acetonitrile and toluene were HPLC grade (Fisher, Loughborough) and water was deionised and purified (ELGA Ltd. High Wycombe, UK). Uracil, butylbenzene, o-terphenyl, pentylbenzene and triphenylene, propranolol HCl, alkylbenzoic acids and glacial acetic acid were laboratory reagent grade from Sigma-Aldrich, Poole, UK. The ammonium acetate analytical grade was purchased from Fisons, UK.

3.1.1 Columns

3.1.1.1 Preliminary studies

The retention behaviour tests were performed on: 5 µm Hypersil HiPurity Advance (150 x 4.6 mm, 100 x 3.0 mm, Thermo Separations, Runcorn, UK); 5 µm XTerra C18, 3.5 µm XTerra C18, 2.5 µm XTerra C18 (50 x 3.0 mm, Waters, Milford, USA)

3.1.1.2 Tanaka test columns

Columns used for the Tanaka test were packed with: 6 µm EU C18 (150 x 4.0 mm) and 5 µm Prontosil C18 (150 x 4.0 mm, Bischoff, Leonberg, Germany); 5 µm Hypersil HiPurity C18 (150 x 4.6 mm , Thermo Separations, Runcorn, UK); Kromasil ODS (150 x 4.6 mm, Eka Nobel, Sweden), 5 µm Symmetry C18 (150 x 3.9 mm) and 5 µm Novapak (150 x 2.0 mm, Waters, Milford, USA); 5 µm Luna C18 (150 x 2.0 mm, Phenomenex, Macclesfield, UK), 5 µm Purospher RP-18 (125 x 4.0 mm, 150 x 3.0 mm, 150 x 2.0 mm), and 5 µm Purospher

RP-18e, (150 x 4.6 mm, 150 x 3.0 mm, 150 x 2.0 mm, 150 x 1.0 mm) and Chromolith Performance RP-18e, (100 x 4.6 mm, Merck, Darmstadt, Germany).

3.1.2 Equipment

3.1.2.1 Preliminary studies

The separations of the alkylbenzoic acids were performed on a Kontron HPLC system (Kontron Instruments, Watford, UK) comprising a Kontron 320 pump, a Kontron HPLC 332 detector and a Kontron HPLC 360 auto sampler linked up to a MT2 data evaluation system. A Pye 104 GC oven (Pye Unicam, Cambridge, UK) was used as column oven. The mobile phase was equilibrated to column temperature by placing 45 cm of stainless steel capillary, 0.018 mm I.D. in the oven between the injector and column.

3.1.2.2 Tanaka test

The Tanaka test separations were conducted on both Hewlett Packard 1100 series and 1090 series liquid chromatographs (Palo Alto, CA, USA) equipped with auto injectors and diode array detectors. The inlet tubing to the column was 0.018 mm (0.007") I.D., 20 cm x 1.6 mm (1/16 ") OD stainless steel of which the last 15 cm was placed in a water jacket. The column was placed in a separately controlled water jacket (Figure 4). The jackets were supplied with water from thermostated tanks (SU6, Grant Instruments, Cambridge) and (Techne, Tempette TE-8A, Techne, Refrigerated Bath, RB-5) which were calibrated to ± 0.1°C against a standard thermometer.

The integration of peak areas and calculation of theoretical plate numbers was performed with data acquisition software (Hewlett Packard Chemstation® revision A.06.03).

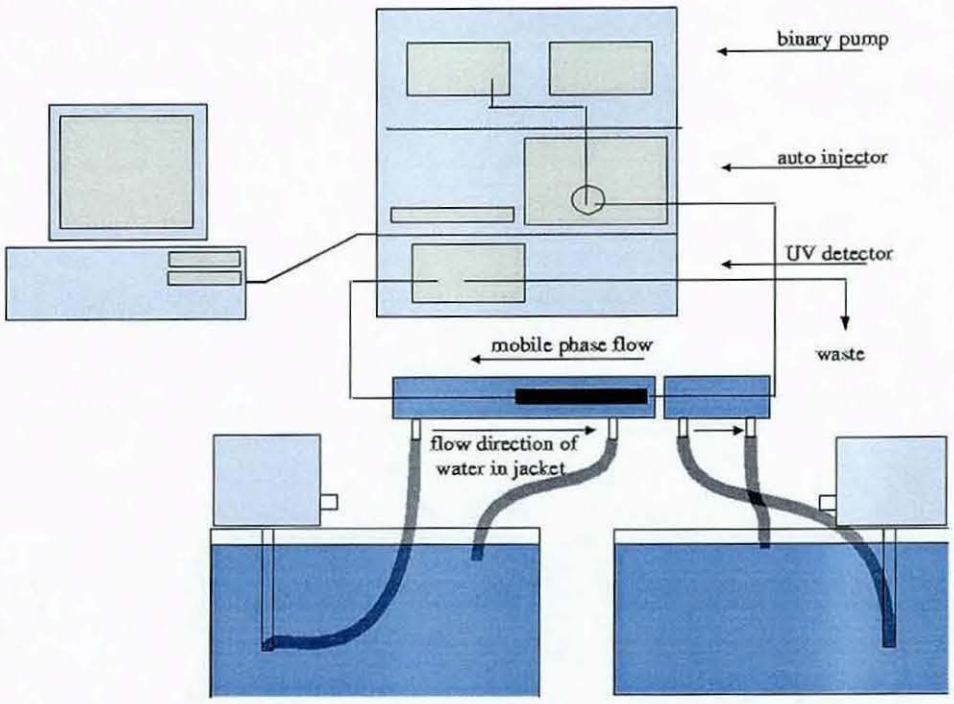

Figure 4: Instrumental set up for Tanaka test separations to investigate the impact of mobile phase inlet temperature.

3.2 Preparation of buffers and solutions

3.2.1 Preliminary studies

3.2.1.1 Ammonium acetate buffer

Ammonium acetate 3.85 g was weighed and transferred into a 1 litre volumetric flask. The salt was dissolved in about 600 ml deionised water. The pH of the solution was adjusted to 4.1 or 3.3 depending on the application, using acetic acid. Subsequently the volumetric flask was filled up to the mark with deionised water. The solution was mixed well. The concentration of the buffer was 50 mM.

3.2.1.2 Mobile phase

The mobile phase for the retention behaviour studies was prepared by mixing acetonitrile or methanol and ammonium acetate buffer. The compositions ranged from 60 % (v/v) to 85 % (v/v) buffer. The mobile phase was premixed and degassed by sonication for 10 minutes.

3.2.1.3 Uracil solution

Uracil (0.02 g) was weighed into a 100 ml volumetric flask. The volumetric flask was made up to volume with mobile phase. 10 ml of the stock solution was pipetted into a 100 ml volumetric flask and made up to volume. A sample of 10 µl of the uracil solution was injected to determine the void volume of the chromatographic system.

3.2.1.4 Alkylbenzoic acids solution

A standard of eight alkylbenzoic acids (o-toluic acid, 4-ethylbenzoic acid, 4-propylbenzoic acid, 4-butylbenzoic acid, 4-pentylbenzoic acid, 4-hexylbenzoic acid, 4-heptylbenzoic acid and 4-octylbenzoic acid) was used in retention studies. Stock solutions at 100 mg of each acid were weighed into separate 100 ml volumetric flasks. The volumetric flask was made up to volume with mobile phase containing 60 % ammonium acetate buffer and mixed well. 10 ml of each of the alkyl benzoic acid stock solutions was pipetted into a 100ml volumetric flask. The solution was made up to volume with ammonium acetate buffer and mixed well.

3.2.1.5 Propranolol, toluene, isopropylbenzoic acid mixture

To prepare the standard solutions 200 mg propranolol, 100 mg toluene and 100 mg 4-isopropylbenzoic acid were weighed into 100 ml volumetric flasks, respectively. The volumetric flasks were made up to volume with premixed 50 % (v/v) ammonium acetate buffer and acetonitrile and mixed well. 10 ml of each of the three standard solutions were pipetted in to a 100 ml volumetric flask. The solution was made up to volume with premixed 50 % (v/v) ammonium acetate buffer (see 3.2.1.1) and 50 % acetonitrile (v/v) and mixed.

3.2.2 Tanaka test method

3.2.2.1 Mobile phase

The mobile phase employed for the Tanaka test consisted of 75 parts methanol and 25 parts (w/w) deionised water. The mixture was prepared weighing 750 g methanol and 250 g water, mixing the solvents in an appropriate container and degassing the mixture by sonication for 10 minutes.

3.2.2.2 Test mix

0.02 g of uracil, 1.0 g butylbenzene, 0.02 g o-terphenyl, 1.5 g pentylbenzene and 0.03 g triphenylene were each weighed into separate 100 ml volumetric flasks. The volumetric flasks were made up to volume with mobile phase and sonicated for about 5 minutes. To prepare the test mixture, 10 ml of each standard was pipetted into a 100 ml volumetric flask. The volumetric flask was made up to volume with mobile phase and the solution was mixed well.

3.3 Methods

3.3.1 Preliminary studies

The system was equilibrated for 1 hour before every experiment. The percentage of organic modifier was adjusted in some instances to ensure constant retention times at different temperatures. The separation efficiencies of the columns at different temperatures were calculated for conditions with constant retention times (varying mobile phase composition) and constant mobile phase conditions (varying retention times). The test mix was injected in triplicate onto the columns. Uracil was used as the void volume marker.

3.3.2 Tanaka Test

The Tanaka test mixture was injected in triplicate. Uracil was used as the void volume marker for the calculations of shape selectivity and hydrophobicity (Equation 22) [136].

Equation 22: Calculations for shape selectivity and hydrophobicity employing the Tanaka test mix and uracil as the void volume marker.

$$shape\ selectivity = \frac{(retention\ time\ triphenylene - retention\ time\ uracil)}{(retention\ time\ o\text{-}terphenyl - retention\ time\ uracil)}$$

$$hydrophobicity = \frac{(retention\ time\ pentylbenzene - retention\ time\ uracil)}{(retention\ time\ butylbenzene - retention\ time\ uracil)}$$

3.3.3 Calculation of performance parameters

If not stated otherwise the performance parameter peak width, peak asymmetry and skew and the number of theoretical plates for a separation were calculated using the default calculations of the Agilent Chemstation® software [137].

The Chemstation® default method to calculate the number of theoretical plates is the ASTM/USP method. The calculation is performed following Equation 23 [138, 139],

Equation 23

$$N = 16\left(\frac{t_r}{w_b}\right)^2$$

where w_b is the peak width at the base of the peak.

The USP tailing is calculated following Equation 24 [139],

Equation 24

$$t = \frac{w_5}{t_W * 2}$$

where w_5 is the peak width at 5 % of its height and t_W is the distance between the peak front at 5 % peak height and the peak apex (retention time).

However, the default Chemstation® calculation is using the moments equations below (Equation 26 A-D) [137].

Equation 25

$$peak-symmetry=\sqrt{\frac{m_1+m_2}{m_3+m_4}}$$

Equation 26 A-D

$$m_1=a_1\left(t_2+\frac{a_1}{1.5H_f}\right) \quad \text{A}$$

$$m_2=\frac{a_2^2}{0.5H_f+1.5H} \quad \text{B}$$

$$m_3=\frac{a_3^2}{0.5H_r+1.5H} \quad \text{C}$$

$$m_4=a_4\left(t_3+\frac{a_4}{1.5H_r}\right) \quad \text{D}$$

Where $m_{1\text{-}4}$ are the pseudomoments of the observed peak, $a_{1\text{-}4}$ the area of the slice, $t_{1\text{-}4}$ the time of the slice, H_f the height of the front inflection point, H_r the height of the rear inflection point and H the peak height at its apex (Figure 5).

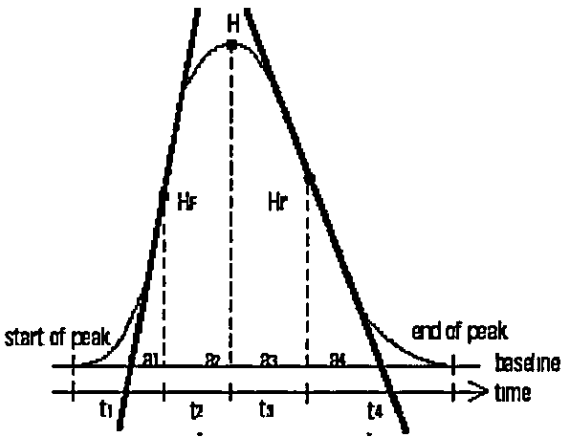

Figure 5: Area slices of peak as used in symmetry calculation in Agilent Chemstation® [137].

The first moment is the mean retention time measured at the centre of gravity of the peak. It is different from the chromatographic retention time, which is measured at the peak maximum, unless the peak is symmetrical.

The second moment is the peak variance, which is a measure of lateral spreading. It is the sum of the variance contributions of the different parts of the instrument.

The third moment describes the vertical symmetry or skew of a peak. A symmetrical peak has the skew of zero. Tailing peaks have a positive skew and fronting peaks have negative skew.

The fourth moment, the excess is a measure of the compression or stretching of the peak along a vertical axis and how it compares to a Gaussian peak. If the peak is squashed down in comparison to the Gaussian peak its excess is negative, if it is taller its excess is positive.

4 EFFECT OF COLUMN TEMPERATURE ON RETENTION, SELECTIVITY, AND EFFICIENCY

4.1 Introduction

The shorter analysis times obtainable by working at elevated temperatures can potentially match the requirements of today's high through-put laboratories and this has lead to a renewed interest in liquid chromatography at above-ambient temperatures. These conditions potentially offer a number of advantages. The lowered viscosity and the resulting reduced inlet pressure [57] enable small stationary phase particles to be used [140]. Furthermore, elevated temperatures offer increased separation efficiency due to increased diffusion between the mobile and stationary phases [37] [99]. A prerequisite for elevated temperature chromatography is reproducible and accurate temperature control. Furthermore the impact of the temperature parameter on the chromatography needs to be understood and controlled in order to develop reliable, reproducible and transferable methods. This chapter describes work investigating retention and selectivity at elevated temperatures.

4.2 Retention

A simple experiment was set up to trace the retention behaviour of compounds. Eight homologous alkylbenzoic acids were separated on a Hypersil HiPurity Advance column using 70 % ammonium acetate buffer pH 3.3 and 30 % acetonitrile. The separation was performed at four different temperatures across the range of 40–70 °C. The column temperature was controlled using a fan oven. The retention of each compound was dependent on the length of the alkyl side chain and temperature. The shorter the chain the shorter is the compound's

retention time and the higher the temperature the shorter the retention time [141, 142]. This behaviour was observed over the whole temperature range studied (Figure 6).

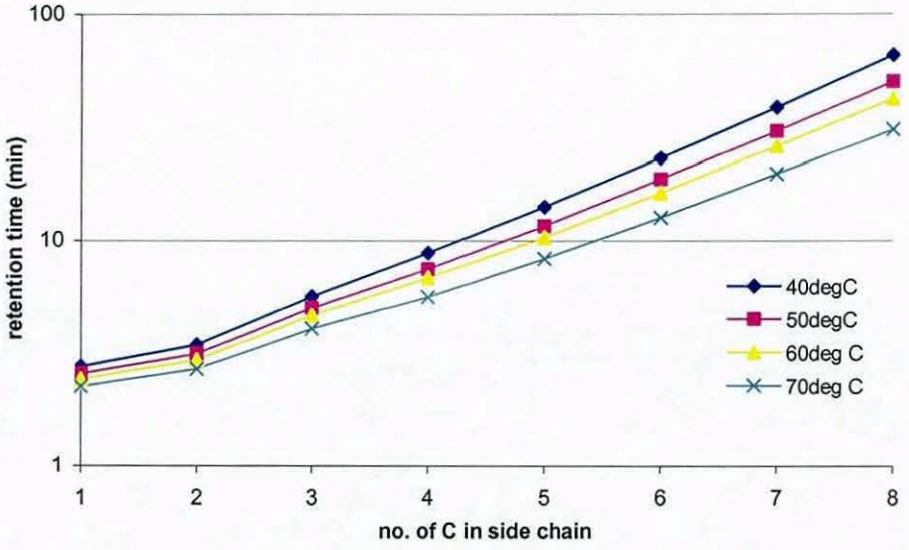

Figure 6: Retention time (log scale) vs the chain length of the side chain of 8 alkyl benzoic acids observed across the temperature range of 40 °C to 70 °C on Hypersil HiPurity Advance 150 x 4.6 mm, mobile phase 70 % ammonium acetate pH 3.3, 30 % acetonitrile, flow 1.0 ml/min. 1 = o-toluic acid, 2 = 4-ethylbenzoic acid, 3 = 4-propylbenzoic acid, 4 = 4-butylbenzoic acid, 5 = 4-pentylbenzoic acid, 6 = 4-hexylbenzoic acid, 7 = 4-heptylbenzoic acid, 8 = 4-octylbenzoic acid.

A van't Hoff plot of the natural logarithm of retention factor verses 1/T can be used to illustrate potential changes in standard enthalpy of separation. If compounds follow the same retention mechanism over the observed temperature range, the plot is expected to be linear [64]. For the compounds employed in this study the relationship was found to be linear over the temperature range investigated (Figure 7). The curves for the alkyl benzoic acids with different chain length did not cross over i.e. there was no change in retention order when the separation temperature was increased. Previously structurally similar compounds have shown comparable decreases in retention time with temperature [117]. However, the distance between the curves was smaller at higher temperatures indicating a reduction in selectivity [75].

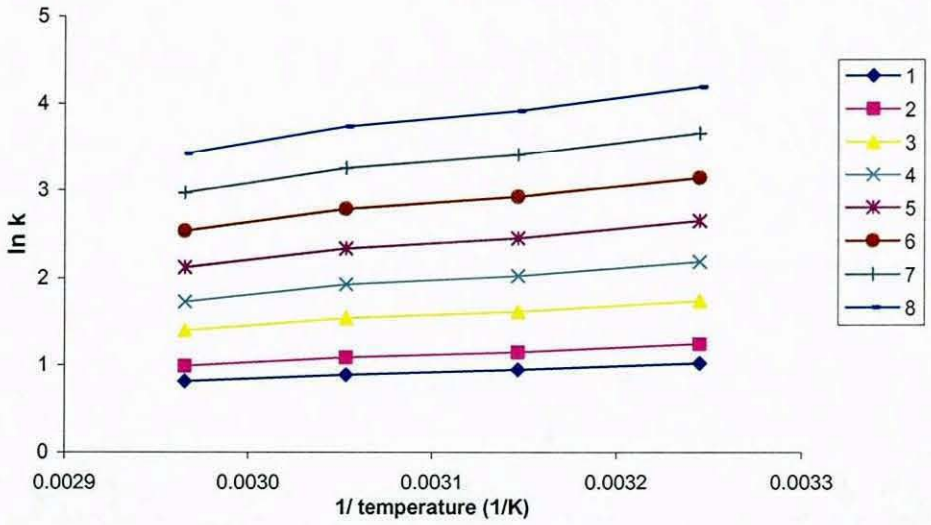

Figure 7: van't Hoff plot of 8 alkyl benzoic acids across the temperature range of 40 °C to 70 °C on Hypersil HiPurity Advance 150 x 4.6 mm, mobile phase 70 % ammonium acetate pH 3.3, 30 % acetonitrile, flow 1.0 ml/min; 1 = o-toluic acid, 2 = 4-ethylbenzoic acid, 3 = 4-propylbenzoic acid, 4 = 4-butylbenzoic acid, 5 = 4-pentylbenzoic acid, 6 = 4-hexylbenzoic acid, 7 = 4-heptylbenzoic acid, 8 = 4-octylbenzoic acid.

Using the same column and eluent a mix of propranolol, toluene and 4-isopropylbenzoic acid was employed to investigate the influence of temperature on structurally different test compounds (Figure 8).

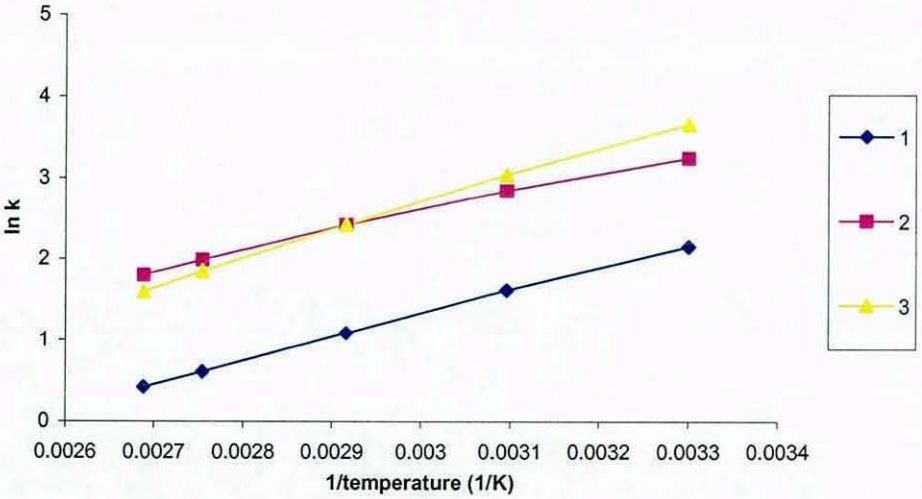

Figure 8: van't Hoff plot of three structurally different compounds across the temperature range of 40 °C to 100 °C on Hypersil HiPurity Advance 150 x 4.6 mm, mobile phase 70 % ammonium acetate pH 3.3, 30 % acetonitrile, flow 1.0 ml/min; 1 = propranolol, 2 = toluene, 3 = 4-isopropylbenzoic acid

All three compounds showed a linear relationship between the reciprocal of the absolute temperature and ln *k* indicating that the retention mechanism is unchanged with temperature. However, the curves for toluene and 4-isopropylbenzoic acid crossed over. This denotes a change of retention order over the temperature range examined indicating a difference in interaction with phases for structurally different compounds as found previously [118-120].

4.3 Selectivity and hydrophobicity

It was noted earlier that the selectivity of a separation column is dependent on temperature [127, 143]. Hence, the selectivity of a separation column can be applied as a means to determine the effective column temperature [72, 76, 144]. Furthermore, the hydrophobicity as measured applying the Tanaka test mix [136] is dependent on the column temperature [145]. In order to use selectivity and hydrophobicity as an "internal thermometer" it is necessary to determine a calibration curve for the selectivity and hydrophobicity of a separation column in a strictly controlled environment. The water bath is less sensitive in comparison to an air bath to fluctuations in room temperature because of its large thermal mass. Furthermore, the rate of heat transfer between water and the column is significantly higher than between air and the column [146]. As a result the temperature of the column in a water bath will be much closer to the temperature of the bath than the temperature of a column in an air bath [76]. Therefore the shape selectivity measured with the column thermostated employing a water bath was used to yield a calibration curve for the change of shape selectivity with temperature.

The Tanaka test [136] of the ratio of the retention of triphenylene and o-terphenyl was applied to measure the shape selectivity and the ratio of retention of pentylbenzene and butylbenzene to measure hydrophobicity of the tested columns. Each data point represents the

mean of three injections. The average RSD was below 0.5 %. The temperature of the mobile phase entering the column was adjusted to the column temperature by placing 15 cm length of the inlet capillary into a water jacket. The water jacket was fed by a water bath of the same temperature as the column water bath. To illustrate the change in selectivity with temperature the shape selectivity calculated for the column was plotted against the reciprocal of the set temperature of the water bath between 40 °C and 60 °C for three columns (Figure 9). The results were curve fitted. The quadratic coefficients were small, in the range of $1*10^{-4}$ to $2*10^{-4}$. Therefore a linear fit was applied as a reasonable approximation over a small temperature range. The different columns demonstrated different sensitivity to temperature change. The shape selectivity of the Purospher RP18 column, for example, changed twice as fast with temperature than the shape selectivity of the Purospher RP18e and more than twice as fast as the Prontosil column (Figure 9).

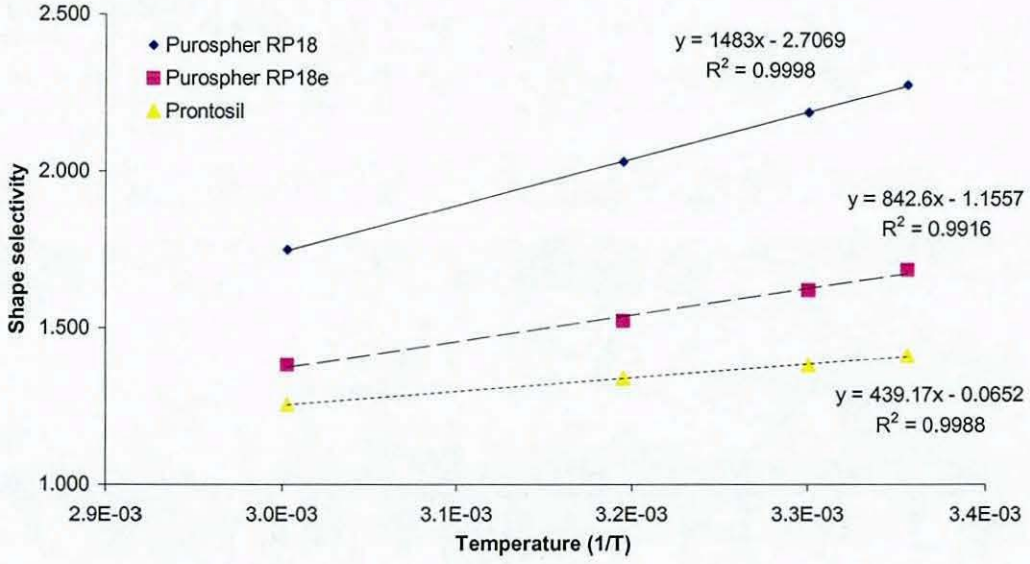

Figure 9: Reciprocal of the absolute temperature vs. the shape selectivity measured applying the Tanaka test; mobile phase 75% methanol, 25% water (w/w), temperatures 25 to 60 °C controlled in water bath; columns used were: Purospher RP18 125 x 4.0 mm i.d.,. Purospher RP18e 150 x 4.6 mm i.d., Prontosil 150 x 4.0 mm i.d..

The fitted equation for the linear relationship of 1/T and shape selectivity can be used to calculate the reciprocal of the absolute

temperature and thus the average temperature of the respective column.

The above equations (Figure 9) were used to compare the impact of the mode of temperature control on the average column temperature for these three columns. The same calibration was performed for the dependence of the hydrophobicity on temperature.

4.3.1 Temperature control

Differences in selectivity and retention indicate a difference in effective column temperature, as the selectivity of a separation is very sensitive to temperature [76]. There are several different methods to control temperature in liquid chromatography. Often all of these methods are deemed to be equivalent.

The block heater is the most commonly used heater in HPLC. It consists of a heated metal block in a confined space. The column is fixed in front of the metal block and the heat is transferred via convection from the metal block to the separation column. In some cases the mobile phase entering the column is equilibrated to column temperature by threading the inlet capillary through the heated metal block.

It is very easy to use, is maintenance free and does not take up much space. These are definite advantages of the block heater. Ideally the column should not touch the heated metal block. If the column is in contact with the metal block the heat is transferred via conduction as well as convection. This can lead to non-uniform heating of the column and can cause a loss in separation efficiency [107, 109]. The majority of HPLC instruments come with a block heater as standard column oven. These heaters usually cover the temperature range of 30 °C to 70 °C.

The use of fan ovens is not very widespread in liquid chromatography. Most HPLC fan ovens are capable of temperatures of up to 80 °C to 100 °C. They consist of an insulated oven cavity where the column is fixed in place. The oven cavity is heated indirectly. A fan is forcing air across an electrical heater. The air warms up and is directed into the oven cavity. It can circulate in the oven cavity and around the column. This way distribution of heat around the column is more homogeneous than in a block heater.

A water bath is less convenient to use but it is not very sensitive to variations in room temperature, hence temperature control is more robust because of the high thermal mass of the liquid. However, if a water jacket is used and the water is pumped through the jacket from a thermostated reservoir the tubing and the water jacket should be insulated to minimize thermal loss. The rate of heat transfer is significantly higher in a water bath [146] than in a fan oven or block heater. Ideally the thermostat of the water bath should be accurate to +/- 0.1 °C.

In order to test the impact of the type of heater the columns were used in three variations of instrument set up which were the block heater, fan oven and water bath. The test compound mix, the Tanaka test mix, contained a dead volume marker to account for differences in dead volume of the different set ups. The assumption was that the same nominal temperature should result in the same retention times and relative retention times regardless of the means of temperature control.

The initial experiments investigated the variation of temperature over a period of 6 hours using different means of temperature control. The different temperature control devices were set to be at the same measured temperature, 60 °C. The temperature was measured with

the same calibrated thermocouple and checked before the first injection of the experiment. Each system was equilibrated to temperature for a minimum of one hour before the first injection was performed. The Tanaka test mix was injected every three hours and the retention times for the five compounds were measured. The fan oven and the water bath performed very well. There were no significant variations in retention time over time. However, retention time variations were more significant when the block heater was used. Table 2 shows the results obtained for a period of 6 hours (three injections).

Table 2: Variation of retention time over a period of 6 hours, measured on Purospher RP18e in water bath, fan oven and block heater, mobile phase 75 % (w/w) methanol, 25 % (w/w) water, nominal temperature 60.0 °C

	water bath		fan oven		block heater	
	RT (min)	RSD (%)	RT (min)	RSD (%)	RT (min)	RSD (%)
uracil	1.49	0.07	1 49	0.04	1.48	0.07
butylbenzene	7.81	0.01	7.87	0.05	9.38	2.26
o-terphenyl	9.72	0.01	9.81	0.08	10.52	2.33
pentylbenzene	10.52	0 01	10 62	0.08	11.48	3.02
triphenylene	12.82	0 01	13 07	0.11	14.06	2 29

The retention times of the compounds shortened when the laboratory warmed up during the day. The block heater was not very well insulated hence the temperature inside the column cavity varied with room temperature. Figure 10 show two chromatograms, one from the beginning of the day and one run in the afternoon. The retention time for the last peak, triphenylene shifted by more than half a minute during the course of the experiment.

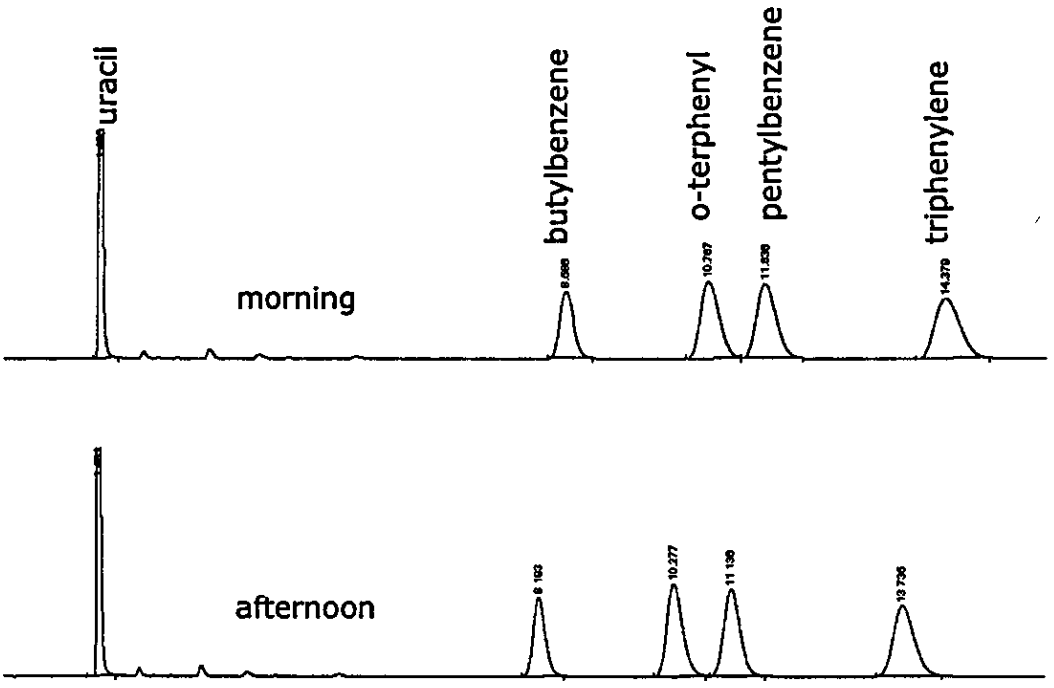

Figure 10: Change of retention time over the period of a day. Separation of the Tanaka mix on Purospher RP18e 150 x 4.6 mm i.d., mobile phase 75% methanol, 25% water (w/w), temperature 60.0 °C in block heater. Chromatograms acquired in the morning and in the afternoon of a warm day.

If experiments were performed in an air-conditioned laboratory the change in retention time may be negligible. However, unluckily the University laboratory was not air-conditioned and the block heater could not be used for further investigations, as the temperature control was not reproducible enough.

The retention times of the individual compounds changed when the mode of temperature control was changed (Table 2). The column temperature appeared to be higher in the water bath because retention times of the test compounds were shorter. This indicates a lower effective column temperature in the fan oven than in the water bath.

In order to determine the effective column temperature of the column thermostated in the fan oven further separations of the Tanaka test

mix were performed. For each column the selectivity was calculated and the results were compared to the results obtained when a water bath was used (see section 4.3, Figure 9). The average column temperatures for each of the columns in the fan oven were calculated employing the calibration curve for the shape selectivity (Figure 9). 1/T was converted to °C. Table 3 shows the results of these calculations.

Table 3: Shape selectivity for different columns in water bath and air oven, calculations assume a linear fit in the temperature range of 50 to 60 °C.

column	column i.d. (mm)	°C water bath measured	Δ selectivity per °C	selectivity water bath	**fan oven**	°C of column in water bath calculated	°C of column in fan oven calculated	ΔT water bath - fan oven
Purospher RP18e	4.6	59.9	0.007	1.382	1.392	59.0	57.7	Δ 1.3
Purospher RP18	4	60.0	0.013	1.747	1.757	60.0	59.2	Δ 0.8
Prontosil	4	60.0	0.004	1.254	1.261	59.9	58.1	Δ 1.9

Thus the apparent column temperatures of columns in the fan oven were generally lower than in a water bath (Table 3). These data were initially surprising. The temperature of the column in the fan oven was expected to be above that in the water bath because the rate of heat transfer in a fan oven is lower than in a water bath, hence it was assumed that it would be more difficult to remove the heat generated by frictional heating [147, 148] and the column would be above the set temperature. However, the average temperatures of the columns in the fan oven appeared to be below those in the water bath. The temperature of a column in a fan oven must be considerably lower than expected in order to firstly compensate for the occurring frictional heating and secondly for the overall column temperature to remain below that in the water bath.

4.3.2 Effective temperature and permeability

The apparent temperature of the Purospher RP18 column in the fan oven was higher than the apparent temperatures of the Purospher RP18e and the Prontosil columns. The difference in internal column diameter is one possible explanation. The Purospher RP18e has a slightly larger internal diameter (4.6 instead of 4.0 mm). The inlet pressures measured at flow rates across the range of 0.2 to 1.5 ml/min are listed in Table 4.

Table 4: Inlet pressure measured for Purospher RP18, 4.0 mm i.d.; Purospher RP18e, 4.6 mm i.d. and Prontosil, 4.0 mm i.d., at various flow rates. The column temperature was controlled using a water bath adjusted to 60 °C.

pump flow rate (ml/min)	*pressure (bar)* Purospher RP18 4 0 mm i d.	Purospher RP18e 4 6 mm i.d.	Prontosil 4.0 mm i.d.
0 2	21	20	20
0 5	53	48	49
0 7	73	67	69
1	104	96	99
1.2	124	116	118
1 5	155	145	149

The same volumetric pump rate causes a higher back-pressure and a higher linear flow velocity of the mobile phase in the 4 mm i.d. column compared to the 4.6 mm i.d. column. The lower mobile phase velocity in the wider bore column causes less frictional heating [107, 109, 147] and thus results in a lower average column temperature.

The observed lower temperature of the 4.6 mm i.d. column supports the proposed explanation. However, the column i.d. of the Prontosil column and the Purospher RP-18 is identical but the temperature difference between air oven and water bath for the Prontosil column is 1.9 °C as opposed to only 0.8 °C for the Purospher RP-18 column.

Darcy's law (Equation 27) describes the flow of fluids through a packed bed. It governs the flow through a liquid chromatography column [149]. Equation 27 gives Darcy's law [150]

Equation 27

$$u = \frac{B_0}{\eta} * \frac{\Delta P}{L}$$

where u is the fluid linear velocity, B_0 the specific permeability of the bed, η the viscosity, ΔP the inlet pressure and L the column length. According to Darcy's law the linear velocity of the mobile phase is proportional to the back-pressure and the permeability of the packed bed. The ratio of the column back-pressure and viscosity of the mobile phase can be considered constant for a given system. Furthermore, the length is constant for a specified column. Therefore the slope of the graph of linear velocity versus back-pressure is the permeability B_0 of a column.

Figure 11 shows the linear velocity versus the inlet pressure curves for the three columns listed in Table 4.

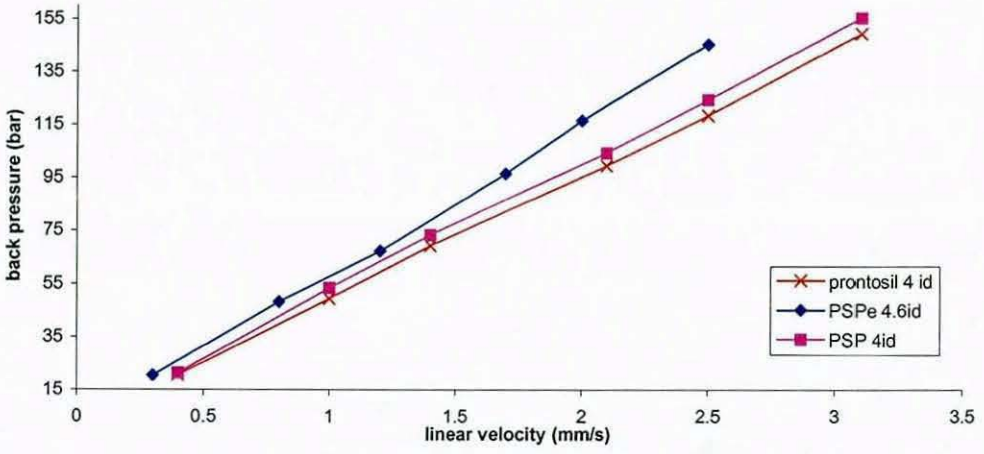

Figure 11: Linear velocity versus inlet pressure for three different columns: Prontosil 4.0 mm i.d., 5 µm dp; Purospher RP18 4.0 mm i.d., 5 µm dp; Purospher RP18e 4.6 mm i.d., 5 µm dp; water bath temperature 60 °C,

The Prontosil column shows a lower column back-pressure than the other two columns at similar mobile phase linear velocities. This indicates that the permeability for this column is higher than for the Purospher RP18 and the Purospher RP18e columns. Differences in

permeability of the columns cause differences in frictional heating in the columns [107, 109, 147, 148].

Figure 12 shows the calculated permeability (using Equation 27) for seven different columns with comparable internal diameters. To calculate the permeability of each column their inlet pressures were recorded at 1 ml/min flow rate (Table 5).

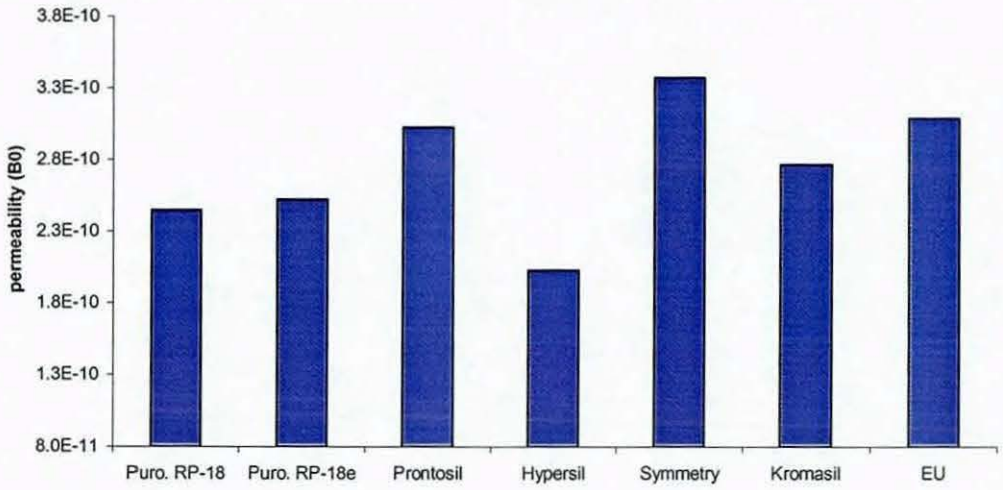

Figure 12: B_0 calculated for seven columns tested at 1ml/min flow rate.

The calculated permeability values fit in with the proposed lower temperature and lower back-pressure for the Prontosil column. This reduction of resistance to flow results in reduction of frictional heating in the Prontosil column.

In summary, the internal temperature of a column depends on a number of parameters. The type of temperature control i.e. water bath or fan oven, the linear flow velocity of the mobile phase, the back-pressure of the column and the permeability. At the same volumetric flow rate columns of the same dimensions but a different permeability will produce a different back-pressures and hence a difference in frictional heating. Furthermore, a difference in average

temperature will impact on the diffusion rate of the solute, which in turn influences the efficiency of a column.

4.4 Efficiency

4.4.1 Instrumental considerations

Working at elevated temperatures the mobile phase inlet temperature needs to be controlled to prevent temperature gradients between mobile phase and column [114]. In the fan oven the temperature control of the inlet can be realized by a length of narrow bore stainless steel capillary in front of the column to heat up the mobile phase. The temperature of the mobile phase leaving the capillary was measured to ensure that the mobile phase temperature was equilibrated to oven temperature. A length of one metre stainless steel capillary inside the oven was found to be sufficient to equilibrate the incoming mobile phase to the temperature of the oven at all flow rates used during the study. Temperature fluctuations at the outlet of the column can influence the reproducibility and stability of detection e.g. when a UV/VIS or RI detection is used [151]. Therefore, a metre length of stainless steel capillary was placed between the oven and detector to cool down the mobile phase. These controls are important for good performance but can cause a large dead volume in the system. For compounds with small retention factors the contribution of extra column band spreading to their plate height can be large [99]. Hence, the efficiency for these compounds can be reduced.

4.4.2 Retention factor

A mixture of compounds, propranolol, toluene and 4-isopropyl benzoic acid was separated in order to study the influence of extra column band broadening and shortening of retention times on the efficiency of a separation.

The retention factor for toluene on X-terra MS, 50 x 3 mm, 5 µm dp column using a mobile phase of 35% methanol and 65 % ammonium

acetate buffer 50 mM, pH 4.1 was 7.6 at 30 °C and 2.9 at 70 °C. Due to the large retention factor at 30 °C the impact of extra column dead volume on plate height should be small in relation to dispersion, diffusion and kinetic effects. However, at higher temperatures with smaller retention factor the contribution of extra column dead volume increases [99]. Figure 13 shows the van Deemter curves measured at the three different column temperatures.

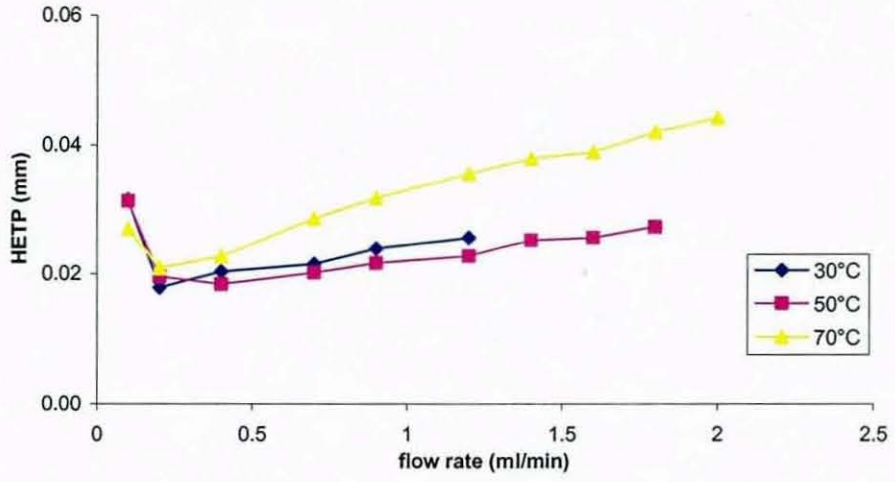

Figure 13: Van Deemter plot at three different column temperatures of toluene on X-terra MS, 50 x 3 mm, 5µm dp, flow 1 ml/min, 35 (v/v)% methanol, 65 % (v/v) ammonium acetate buffer pH 4.1, mobile phase composition constant over the temperature range.

The plate heights measured at 50 °C column temperature were smaller than the plate heights measured at 30 °C. However, when the retention factor was reduced to 2.9 at 70 °C the plate height increased due to the increased impact of extra column band broadening.

To counteract this effect a study was carried out in which the mobile phase composition was adjusted to provide a constant retention factor for propranolol the first eluting analyte in the compound mixture. At higher temperatures a lower percentage of organic modifier was necessary to achieve similar retention times as the dielectric constant of water is reduced as temperature is increased [152].

The mobile phase composition was changed in the following way to keep the retention factor constant at:

30 °C 65 % buffer pH 4.1, 35 % methanol

50 °C 70 % buffer pH 4.1, 30 % methanol

70 °C 75 % buffer pH 4.1, 25 % methanol

Under constant retention factor conditions, as the separation temperature increased the separation efficiency was also found to increase despite the large dead volume (Figure 14). However, the mobile phase composition can only be adjusted correctly for one compound of the mixture. The retention factors for the other compounds in the mixture varied slightly (Figure 15).

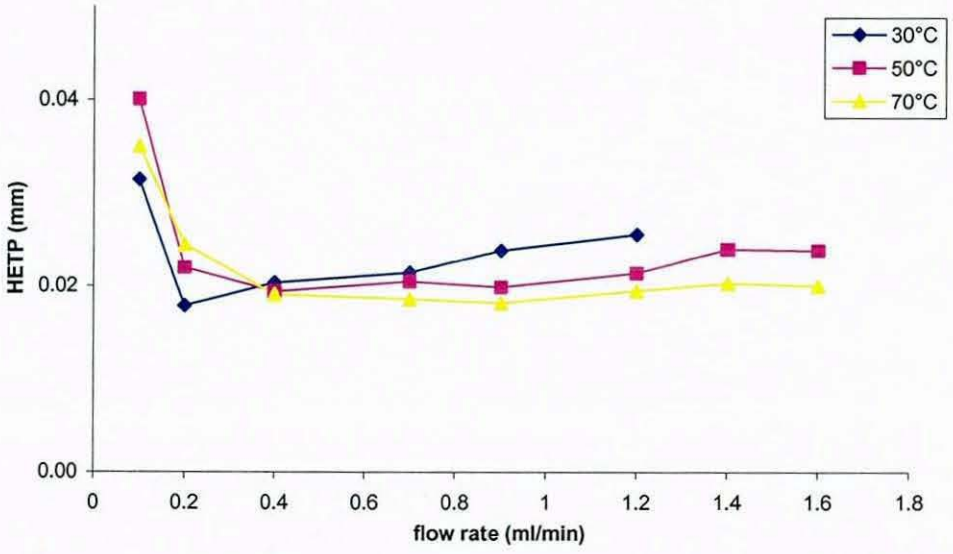

Figure 14: Van Deemter plot for toluene on X-terra MS, 50 x 3 mm, 5µm dp, flow 1 ml/min, 35% to 25% MeOH, 65% to 75% buffer pH 4.1 (as text), mobile phase composition adjusted to provide constant retention factor for propranolol

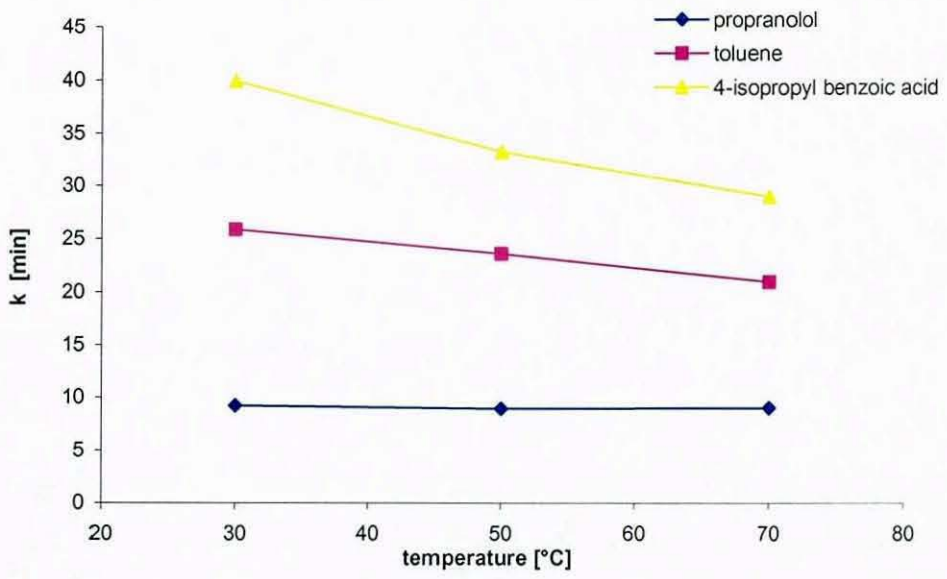

Figure 15: Change of retention factor with temperature, on X-terra MS, 50 x 3 mm, 5µm dp, flow 1 ml/min, 35% to 25% MeOH, 65% to 75% buffer pH 4.1 (as text), mobile phase composition adjusted to provide constant retention factor k = 9 for propranolol.

Furthermore, changes of the mobile phase composition also alter the viscosity of the mobile phase and the diffusion of the solutes in the mobile phase. The changes in selectivity as a function of temperature are not identical to changes in selectivity as a result of composition changes of the mobile phase [153].

The experiment was repeated employing acetonitrile as the organic modifier in the mobile phase in order to investigate the influence of the type of organic modifier. The change in efficiency with increasing temperature was again measured under constant retention factor conditions.

The change in efficiency with temperature was different from the change observed when methanol was used as organic modifier in the mobile phase (Figure 16 compare with Figure 14). The van Deemter curves seem to be flatter and closer to one another. By changing the mobile phase's organic component and the composition the viscosity of the mobile phase is also changed. At a temperature of 30 °C a

mobile phase containing 35% methanol will have a viscosity of about 1.4 cP. A mobile phase containing 20% methanol will show a lower viscosity of about 1.2 cP [23]. The viscosity of a mobile phase containing acetonitrile is significantly lower than that of a mobile phase containing methanol. Its viscosity slightly increases from 0.8 to 0.85 cP when the percentage acetonitrile is reduced from 35% to 20 %, however, it is still lower than the viscosity of the mobile phase containing methanol [154].

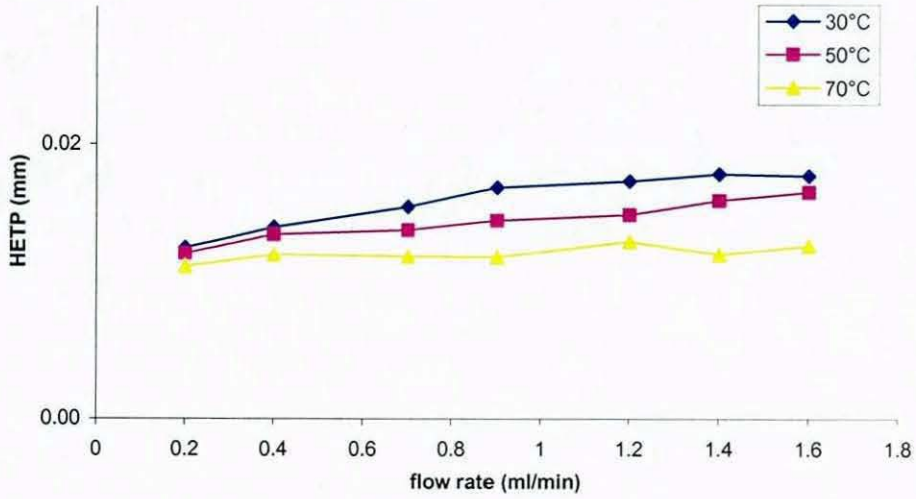

Figure 16: Van Deemter plot for toluene on XTerra MS, 50 x 3 mm, 5µm dp, 25 (v/v)% - 15 (v/v)% acetonitrile, 75 (v/v) % - 85 (v/v) % buffer pH 4.1, mobile phase composition adjusted to provide constant retention factor

Furthermore, the viscosity of a mobile phase containing 35 % methanol will drop from 1.4 cP to below 0.7 cP when the composition is changed to 25 % methanol and the separation temperature is increased from 30 °C to 70 °C [16, 23]. The viscosity of the mobile phase has a direct impact on the diffusion coefficient of solutes in the mobile phase hence an impact on efficiency [21]. The results of the comparison between methanol/water and acetonitrile/water mobile phases were in agreement with results published by Li and Carr [23]. They measured the diffusion coefficient for a number of compounds including toluene in acetonitrile/water and methanol/water mixtures at

different temperatures. They found that the diffusion coefficient for toluene is higher in acetonitrile/water mixtures than in methanol water mixtures. Higher diffusion rates result in a flatter C term of the van Deemter equation i.e. improved efficiency at high linear flow velocities. The differences in diffusion rate of toluene in acetonitrile/water and methanol/water are likely to be the reason for the differences in efficiency measured employing the two different organic modifiers (see Figure 16 and Figure 14).

4.4.2.1 System optimisation

The HPLC system was then optimised in order to minimize its dead volume by using narrow bore stainless steel tubing running through a water jacket in order to equilibrate the mobile phase temperature to the temperature of the column. Due to the higher rate of heat transfer in water than in air, the capillary can be relatively shorter to achieve the same mobile phase temperature. Wolcott [115] has shown that the stainless steel capillary should have a narrow internal diameter but not be thin walled. They found that heat transfer is more efficient with larger outer diameter capillaries (OD 1/16") as they expose a larger surface area to the heated medium. In this study experiments were performed to measure the minimum length of capillary required to attain temperature equilibration at flow rates over the range of 0.1 to 2.0 ml/min and temperatures of 40 °C to 80 °C. The temperature of the liquid was measured with a calibrated thermocouple at the outlet of the capillary. A length of 15 cm of stainless steel tubing with an outer diameter of 1/16" (1.59 mm) and an inner diameter of 0.007" (0.18 mm) was sufficient to equilibrate the temperature of the incoming mobile phase to column temperature.

In order to check the performance of the system and columns the Tanaka mix was run at flow rates from 0.1 to 1.8 ml/min, at 40 °C and 60 °C. The mobile phase composition was not adjusted to provide constant retention factor, however, the retention factors for all

compounds were above 2, which should minimize the dead volume contribution to the plate height [99]. The temperature of the water jacket controlling the mobile phase inlet was adjusted to the same temperature as the column water jacket. The van Deemter curves for the two temperatures were plotted and a typical example is shown in Figure 17 [see Appendix A for data].

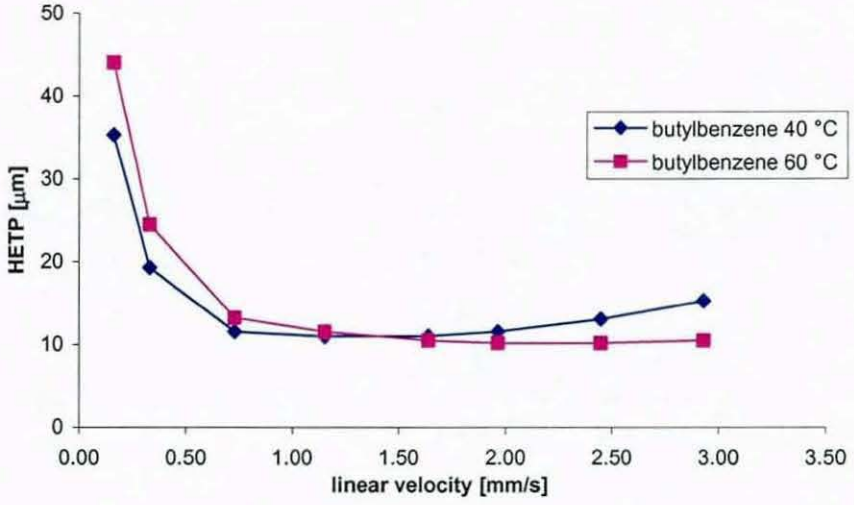

Figure 17: The effect of reduced dead volume on efficiency, van Deemter curves for butylbenzene on Purospher RP18e 150 x 4.6 mm i.d., mobile phase 75% methanol, 25% water (w/w), temperatures 40 to 60 °C controlled in water bath.

At higher linear flow velocities improved column efficiency was observed at 60 °C compared to 40 °C but at lower flow rates the efficiency was decreased at 60 °C compared to 40 °C. The flow rate giving the optimum efficiency increased with temperature. Similar changes were seen for all compounds contained in the Tanaka mix. The changes at higher flow rates (1 ml/min = 1.8 mm/s) are in agreement with the commonly accepted report that column efficiency improves when temperature is increased, which is attributed to increased diffusion rates in the mobile phase [21, 155]. At low flow rates increased molecular diffusion at 60 °C could be responsible for a larger value of the B term of the van Deemter equation, hence causing the observed decrease in efficiency at low flow rates.

4.4.3 Temperature control

The initial assumption was that the efficiency of a separation column is independent of the means of temperature control but differences in shape selectivity dependent on the type of temperature control were observed earlier in this study (see section 4.3.1). In order to test this assumption the efficiencies of seven separation columns were measured at 60 °C using the Tanaka test mix, consisting of uracil, butylbenzene, o-terphenyl, pentylbenzene and triphenylene. The separation temperature was controlled in two ways, A) using a water bath and B) using a fan oven. The following columns were employed, uncapped C18 material (EU material) and Prontosil RP18 packed into identical column hardware, 150 x 4 mm i.d. Hypersil HiPurity ODS 150 x 4.6 mm, Kromasil ODS 150 x 4.6 mm, Purospher RP 18 125 x 4.0 mm, Purospher RP18e 150 x 4.6 mm and the monolithic Chromolith material in a 100 x 4.6 mm cladding. In order to obtain data to plot van Deemter curves the separation was carried out across a range of flow rates from 0.1 ml/min to 1.8 ml/min. The flow rates were translated into the respective linear flow velocities for each column to facilitate a comparison of columns of different internal diameters. The mobile phase temperature was controlled as described in section 4.4.2.1 and adjusted to the same temperature as the column for all experiments in this section. Identical connecting tubing was used with both ovens.

The comparison of the effect of fan oven and water bath on column efficiency showed that the efficiency of a column could change when the column temperature control is changed. Figure 18 shows the changes in efficiency observed on the EU column. Figure 19 shows the changes observed for the Prontosil column. The same column packer into identical hardware packed both columns. However, the efficiency of the EU column significantly increased using the air oven while using either air oven or water bath did not have a significant impact on the efficiency of the Prontosil column. The plate height for butylbenzene

marginally increased at high linear velocities when using an air oven as opposed to a water bath.

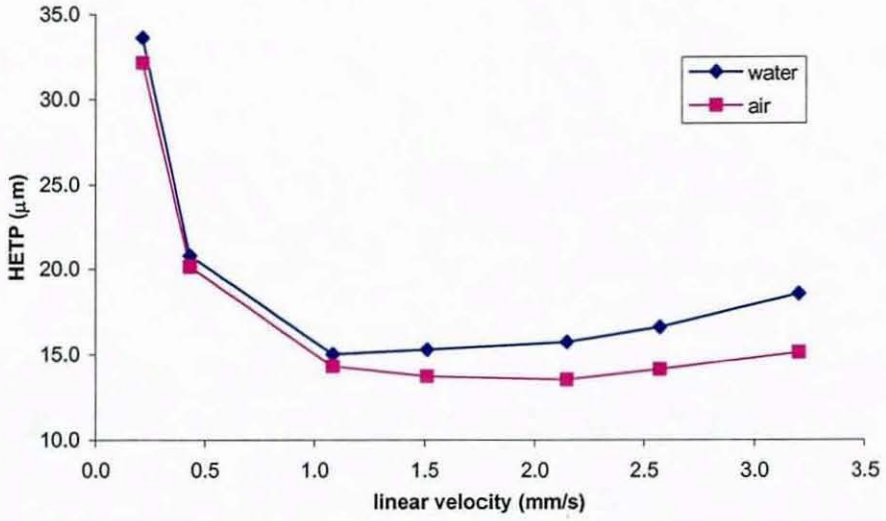

Figure 18: van Deemter curve for butylbenzene using water bath and fan oven to control the column temperature, mobile phase 70% methanol, 25% water (w/w), EU column, 150 x 4 mm i.d., temperature 60 °C; water = water bath, air = fan oven.

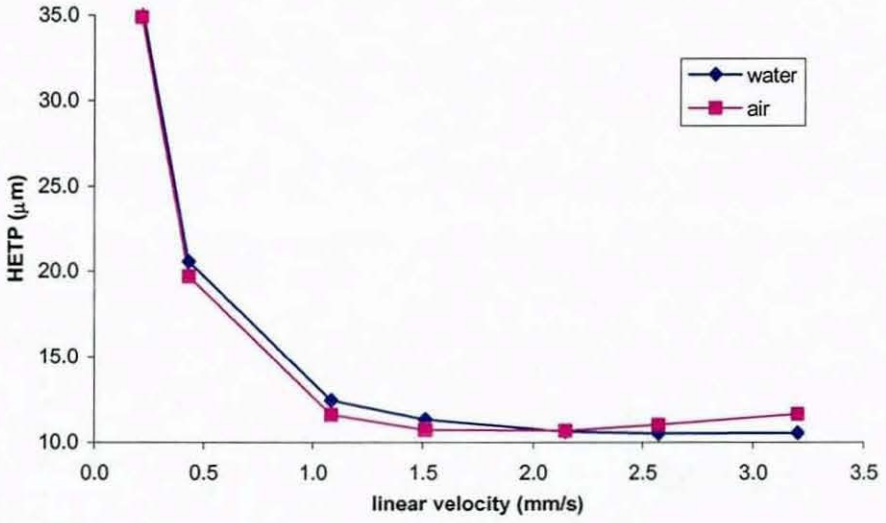

Figure 19: van Deemter curve for butylbenzene using water bath and fan oven to control the column temperature, mobile phase 70% methanol, 25% water (w/w), Prontosil C18 material, 150 x 4 mm i.d., temperature 60 °C; water = water bath, air = fan oven.

Butylbenzene is the earliest eluting compound of the Tanaka mix and was used as representative example. All other retained compounds in

the Tanaka mix behaved in a similar fashion. The full data is compiled in Appendices B to D.

The observed changes in column efficiency were different with different packing materials. Figure 20 and Figure 21 show the changes in efficiency when the mode of temperature control was changed for seven different columns at linear velocities of 1 mm/s and 2 mm/s respectively.

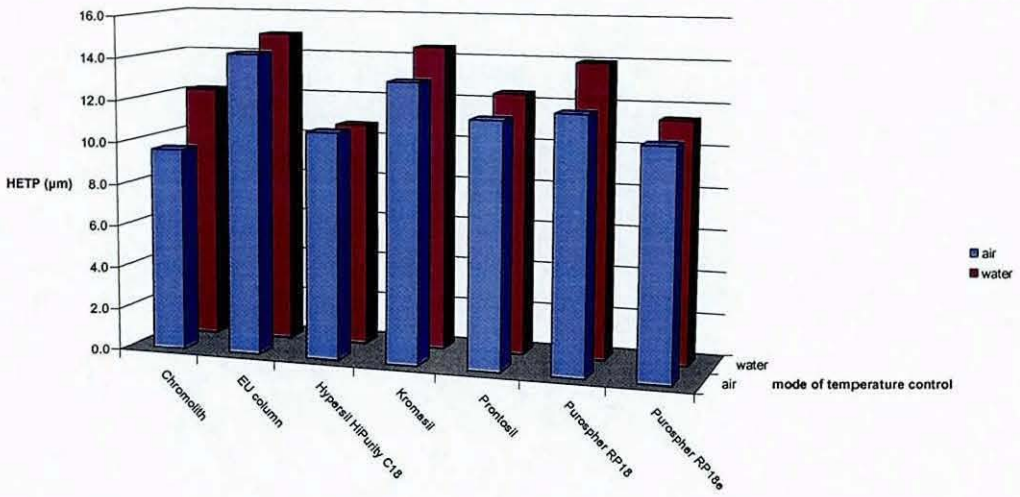

Figure 20: Effect of temperature control on efficiency of butylbenzene, at 1 mm/s linear velocity, 60 °C column temperature, blue bars: fan oven, red bars: water bath; columns tested were Chromolith, EU column, Hypersil HiPurity C18, Kromasil, Prontosil, Purospher RP18 and Purospher RP18e.

At 1 mm/s linear velocity the efficiency measured for the columns in the water bath was generally lower than in the air oven. However, a more significant impact on efficiency was observed for a higher linear flow velocity. The largest changes were observed on the EU column and the Hypersil HiPurity column. For both columns the efficiency was significantly lower when the column temperature was controlled using the water bath (Figure 21).

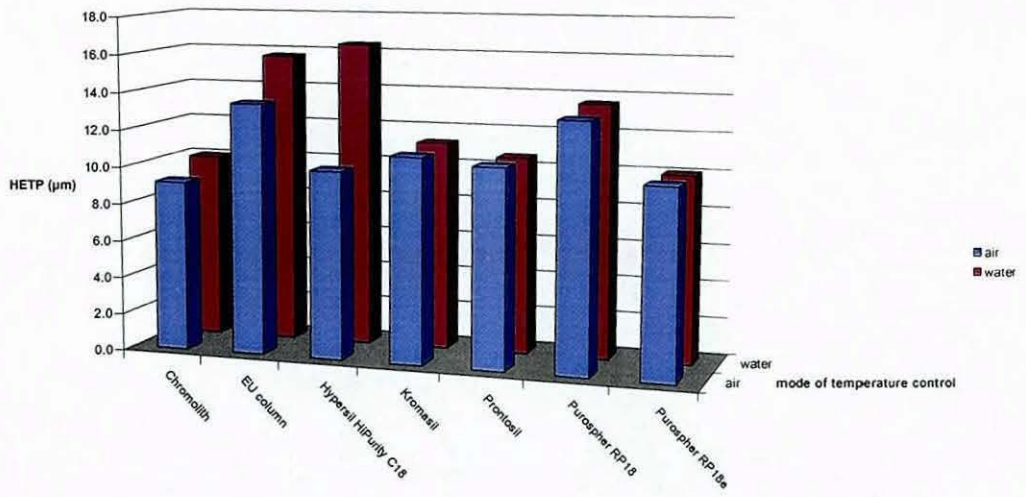

Figure 21: Effect of temperature control on efficiency of butylbenzene, at 2 mm/s linear velocity, 60 °C column temperature, blue bars: fan oven, red bars: water bath; columns tested were Chromolith, EU column, Hypersil HiPurity C18, Kromasil, Prontosil, Purospher RP18 and Purospher RP18e.

It is not clear why the efficiency of the EU column and the Hypersil HiPurity are more sensitive to the mode of temperature control than other separation columns.

5 MOBILE PHASE TEMPERATURE

The effect of introducing a temperature differential between the incoming mobile phase and the column was examined because previously published papers did not give a clear indication whether to it was preferable to equilibrate the mobile phase temperature to column temperature before it enters the column, contradicting results had been published [109, 111, 114, 135].

The performance of a number of different columns was therefore investigated. Four columns were tested at 40 °C column wall temperature while the mobile phase inlet temperature was changed. A larger set of columns was tested at 60 °C column wall temperature.

The Tanaka test mix was again employed but unless stated otherwise the efficiencies reported in this chapter are for butylbenzene. The other components gave comparable trends and results.

5.1 Stationary phase materials

In the first set of experiments the efficiencies of two columns, *Prontosil* RP18, and the EU column (*EU column, taken from 1st Round Robin study*) [145], packed into identical 150 x 4.0 mm i.d. column hardware were measured at column temperatures of 40 °C and 60 °C. The temperature of the incoming mobile phase was varied while the temperature of the column was kept constant. Van Deemter curves were plotted for each setting.

5.1.1 EU column

The column temperature and the mobile phase inlet temperature were kept at 40 °C. Flow rates from 0.2 to 1.5 ml/min were employed. At each flow rate three injections of the Tanaka test mix were performed. The mean plate number of the three injections for each compound was

determined and used to calculate the height equivalent of a theoretical plate (HETP). The results were plotted against the linear velocity of the mobile phase. The resulting van Deemter plot for this experiment was used as the reference point for the EU material at 40 °C.

The effect of changing the mobile phase inlet temperature was then investigated over the range of temperature differences between column wall and mobile phase of 0 to - 40 °. Results were plotted against the mobile phase linear velocity and compared with the van Deemter curve obtained at equilibrated conditions (Figure 22).

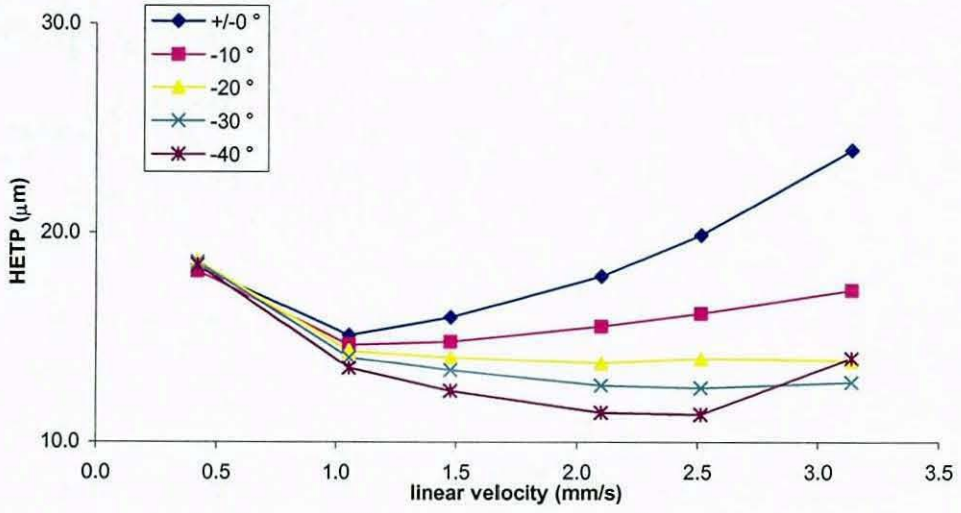

Figure 22: van Deemter plot of butylbenzene on EU column 150 x 4.0 mm i.d. at 40 °C column temperature, with different temperature differences between incoming mobile phase and column wall across the range of 0 to -40 °.

The efficiency of the separation improved when the mobile phase inlet temperature was dropped in relation to the column wall temperature. These results were in line with findings by other researchers [109, 111] although in the present study the number of plates increased steadily with ΔT. The lowered temperature of the incoming mobile phase was thought to counteract the band broadening caused by frictional heating. Furthermore, the optimum flow velocity moved to a higher linear flow velocity. The highest efficiency was achieved at a mobile phase linear velocity of 2.5 mm/s and a temperature

differential of -40 ° between column wall temperature and incoming mobile phase. However, at this temperature above the linear flow velocity of 2.5 mm/s the plate height suddenly increased above the optimum level achieved with a -20 ° temperature differential.

Further experiments employing the same column were performed after adjusting the column wall temperature to 60 °C. A similar pattern of improved efficiency was anticipated when a temperature differential was introduced into the system. However, because of the lower mobile phase viscosity and therefore lower inlet pressure and reduced frictional heating at the higher column temperature the effect on the van Deemter curves for the different mobile phase inlet temperatures were expected to be smaller than at 40 °C column wall temperature.

The results showed that the van Deemter curves plotted for the separations of the Tanaka test mix at 60 °C were similar to those at 40 °C column wall temperature and showed the same trends (Figure 23). The overall column efficiency improved due to the higher column temperature. Optimum efficiencies for the compounds in the test mix were observed at 2.5 mm/s linear flow velocity and -40 ° temperature difference between incoming mobile phase and the column wall. When the linear flow velocity exceeded 2.5 mm/s at a temperature differential of -40 ° the same sudden drop in efficiency as seen at 40 °C column wall temperature was observed.

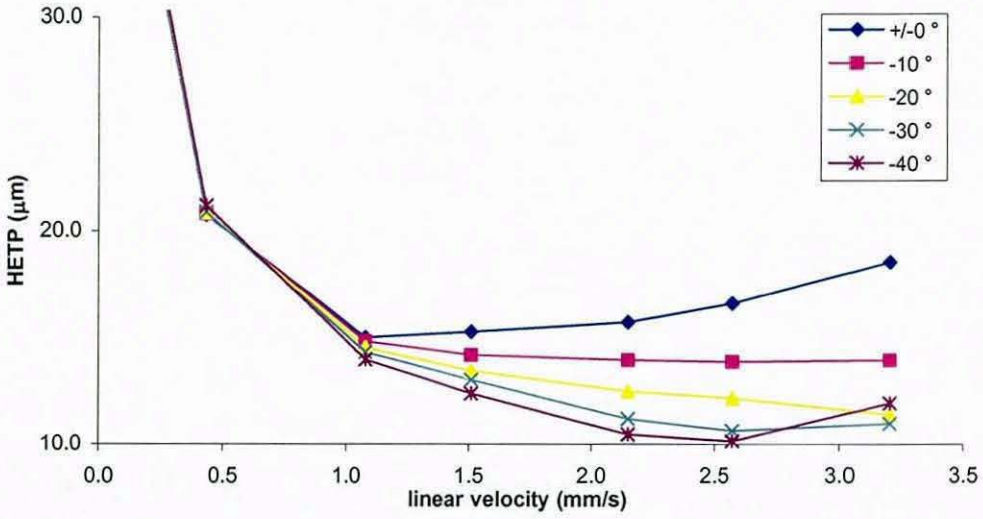

Figure 23: van Deemter plot of butylbenzene on EU column 150 x 4.0 mm i.d. at 60 °C column temperature, with different temperature differences between incoming mobile phase and column wall across the range of 0 to -40 °.

Contrary to expectations the changes in HETP because of the different inlet temperature was similar at 60 °C and 40 °C column wall temperature (Figure 24 A-B).

If anything the impact of the temperature differential seemed to increase at 60 °C column wall temperature when the flow rate was equal to or above 1 ml/min. Only the distance between the curves obtained for -30 ° and -40 ° temperature differential appeared to be reduced. Averaged over the different flow rates, the inlet temperature of the mobile phase seemed to have the same impact on the overall efficiency at higher temperatures.

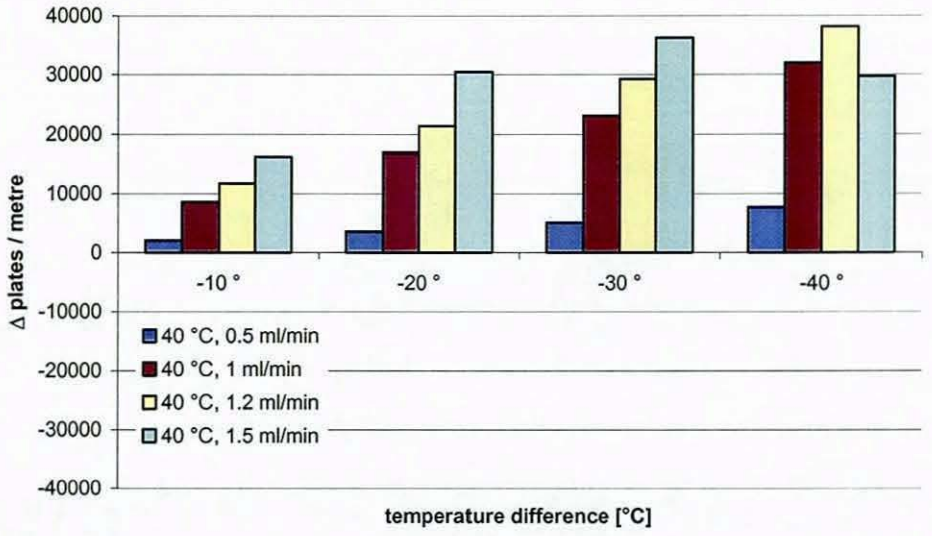

Figure 24 A: 40 °C column wall temperature

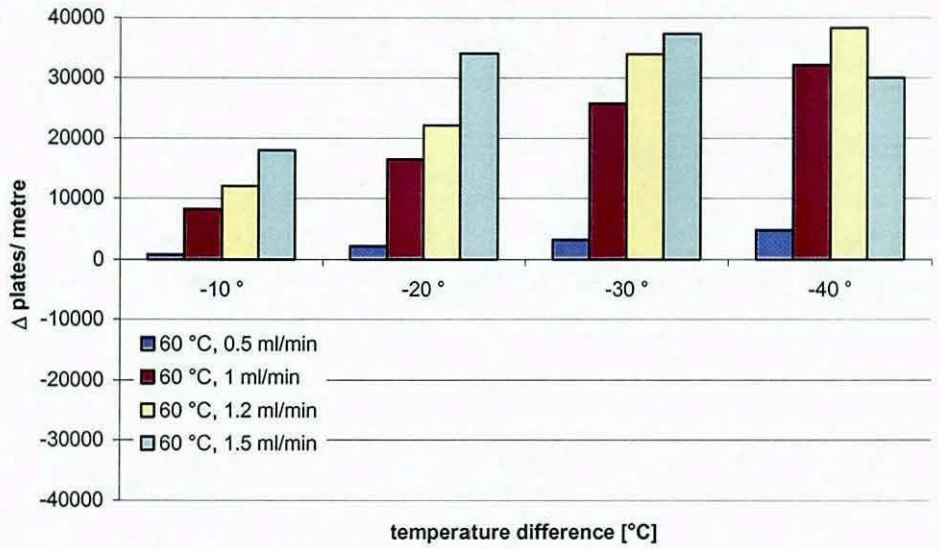

Figure 24 B: 60 °C column wall temperature

Figure 24 A-B: Difference in plates per metre between equilibrated mobile phase conditions and four mobile phase inlet temperature differentials at (A) 40 °C and (B) 60 °C column wall temperature for butylbenzene on EU C18 column 150 x 4.0 mm i.d. at four different flow rates..

The shape selectivity for the EU column was calculated for both column temperatures, 40 °C and 60 °C at the different mobile phase inlet temperatures. The change in shape selectivity dependant on temperature was estimated as (calculation see section 4.3) 0.007 per ° C temperature change in the column.

In order to estimate the change of average column temperature when the mobile phase inlet temperature was changed, the shape selectivity was plotted vs. the linear flow velocity for all the different mobile phase inlet temperatures. Figure 25 shows the dependence of selectivity on the mobile phase linear velocity at 40 °C column wall temperature. The blue line on the left hand side of the graph indicates the change of shape selectivity caused by a change in column wall temperature of 1 °C with an equilibrated inlet at 1 ml/min flow rate (equivalent to 2.1 mm/s linear velocity).

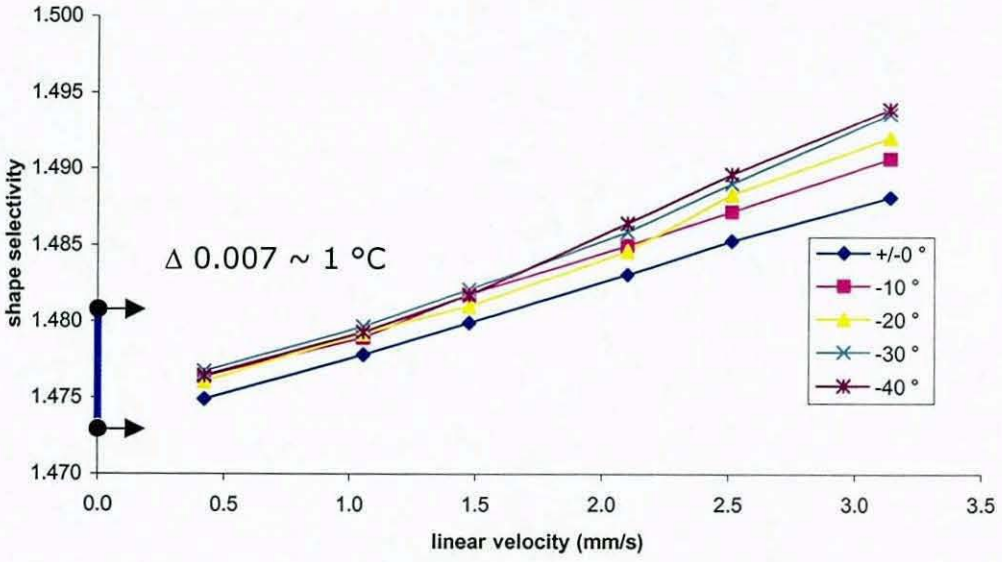

Figure 25: Change of shape selectivity with linear velocity and mobile phase inlet temperature on EU column at 40 °C column wall temperature.

Figure 25 shows that there is a change in shape selectivity when the linear velocity of the mobile phase is changed. Interestingly, the shape selectivity increased, which could lead to the conclusion that the average column temperature decreased when the linear flow velocity was increased. However, it is more likely that the pressure dependence of the retention factor and the method of void volume measurement were responsible for the observed increase in shape selectivity with increasing flow rate.

The column void volume was measured employing uracil as the void volume marker. Small organic compounds show a small degree of

retention thus the void volume measured, using uracil as the marker was most likely greater than the "true" void volume [156]. Furthermore, the column inlet pressure increases with the flow rate. Hence, the retention factor of all test compounds increases due to the pressure dependence of the retention factor [157, 158]. Figure 26 shows the dependence of the results of the void volume calculation on flow rate (i.e. pressure) using uracil as the void volume marker.

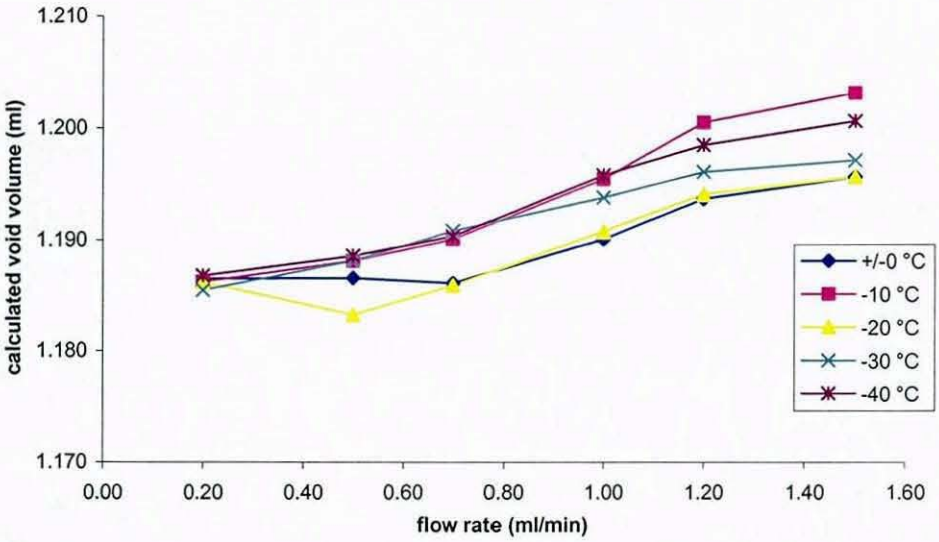

Figure 26: Volumetric flow rate vs. void volume calculated using uracil as the void volume marker. Uracil has small degree of retention, hence the void volume increases as the flow rate and thus the column pressure increases.

The calculated void volume increased with increasing flow rate, i.e. pressure. Figure 27 and Figure 28 show the dependence of the retention factor on flow rate and temperature differential for the first eluting compound (butylbenzene) and the last eluting compound (triphenylene). The retention factor for both compounds increased with increasing flow rate and temperature differential. However, the retention factor of the later eluting triphenylene (change of k in the range of 2 and 3.6 %) was more significantly affected than the retention factor of the earlier eluting butylbenzene (change of k in the range of 0.7 and 2 %). This has an impact on the retention factor ratio.

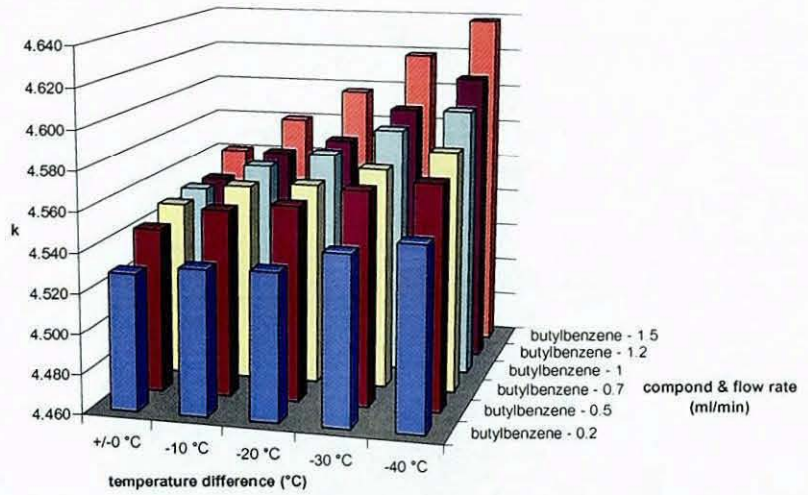

	+/-0 °C	-10 °C	-20 °C	-30 °C	-40 °C
butylbenzene - 0.2	4.529	4.533	4.534	4.545	4.551
butylbenzene - 0.5	4.543	4.555	4.559	4.568	4.573
butylbenzene - 0.7	4.549	4.560	4.563	4.573	4.583
butylbenzene - 1	4.551	4.565	4.573	4.587	4.598
butylbenzene - 1.2	4.550	4.566	4.575	4.593	4.610
butylbenzene - 1.5	4.560	4.580	4.597	4.618	4.638

Figure 27: Change of retention factor with volumetric flow rate and inlet temperature differential for butylbenzene.

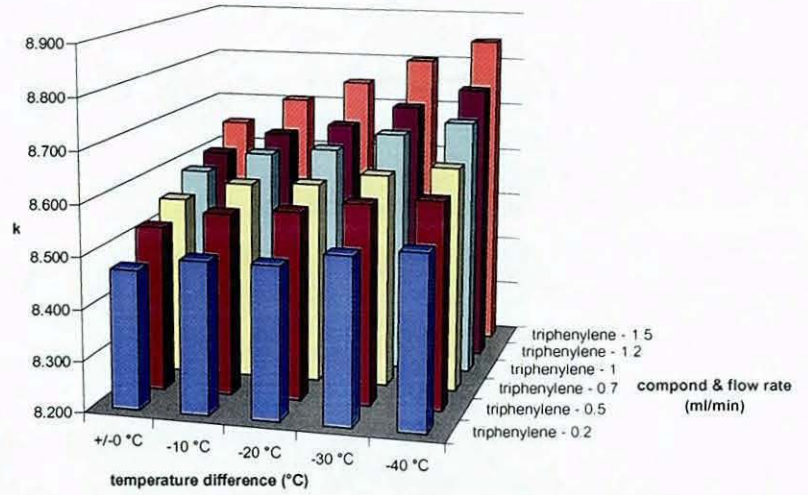

	+/-0 °C	-10 °C	-20 °C	-30 °C	-40 °C
triphenylene - 0.2	8.471	8.497	8.497	8.524	8.538
triphenylene - 0.5	8.525	8.560	8.571	8.593	8.606
triphenylene - 0.7	8.555	8.592	8.599	8.623	8.644
triphenylene - 1	8.588	8.631	8.645	8.682	8.710
triphenylene - 1.2	8.604	8.651	8.674	8.718	8.758
triphenylene - 1.5	8.650	8.706	8.748	8.801	8.845

Figure 28: Change of retention factor with volumetric flow rate and inlet temperature differential for triphenylene.

The shape selectivity and hydrophobicity of a separation column are defined as the retention factor ratio of pentylbenzene/butylbenzene

and triphenylene/o-terphenyl respectively, thus the increase in shape selectivity and hydrophobicity with flow rate was due to the pressure dependence of the retention factor and not due to a decrease in average column temperature. However, when the mobile phase inlet temperature was decreased at a set flow rate (e.g. 0.5 ml/min equivalent to 1.1 mm/s) the shape selectivity increased compared to the shape selectivity measured at equilibrated temperature conditions. This indicated that there was a real change in average column temperature when the temperature differential between mobile phase inlet and column wall was increased.

It can therefore be concluded that changes in shape selectivity and hydrophobicity with increasing flow rate were due to the pressure dependence of the retention factor. Furthermore, changes in shape selectivity and hydrophobicity at one flow rate (i.e. constant pressure) and varying inlet temperature differential were due to the temperature dependence of the shape selectivity and hydrophobicity and thus reflect a change in average column temperature.

Figure 29 shows the plot of linear flow velocity vs. shape selectivity at different mobile phase inlet temperatures at 60 °C column wall temperature.

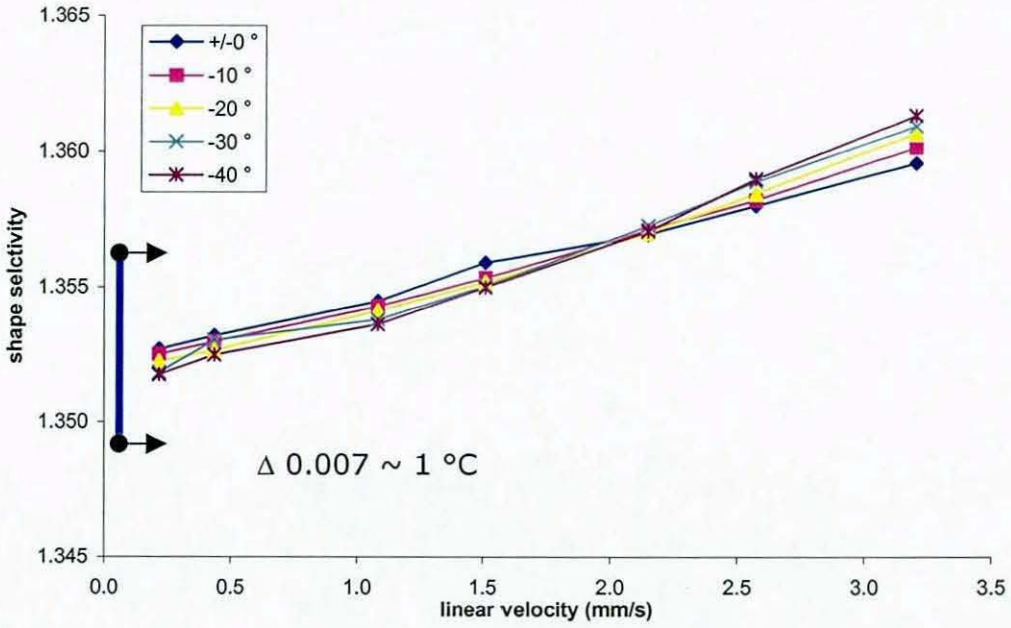

Figure 29: Change of shape selectivity with linear velocity and mobile phase inlet temperature on EU column at 60 °C column wall temperature.

The change of shape selectivity with decrease in mobile phase inlet temperature observed at 3.1 mm/s linear velocity and 40 °C column wall temperature represented a change in average column temperature of about 1 °C. However, the change in shape selectivity at 3.1 mm/s linear velocity and different mobile phase inlet temperatures was significantly smaller at 60 °C column wall temperature. It represented a change in average column temperature of less than 0.5 °C.

Similarly to the shape selectivity the results of the hydrophobicity estimation were plotted vs. the linear flow velocity in order to confirm the link between the changes in shape selectivity and average column temperature. Figure 30 and Figure 31 show the change in hydrophobicity of the EU column in relation to the mobile phase inlet temperature and linear flow velocity.

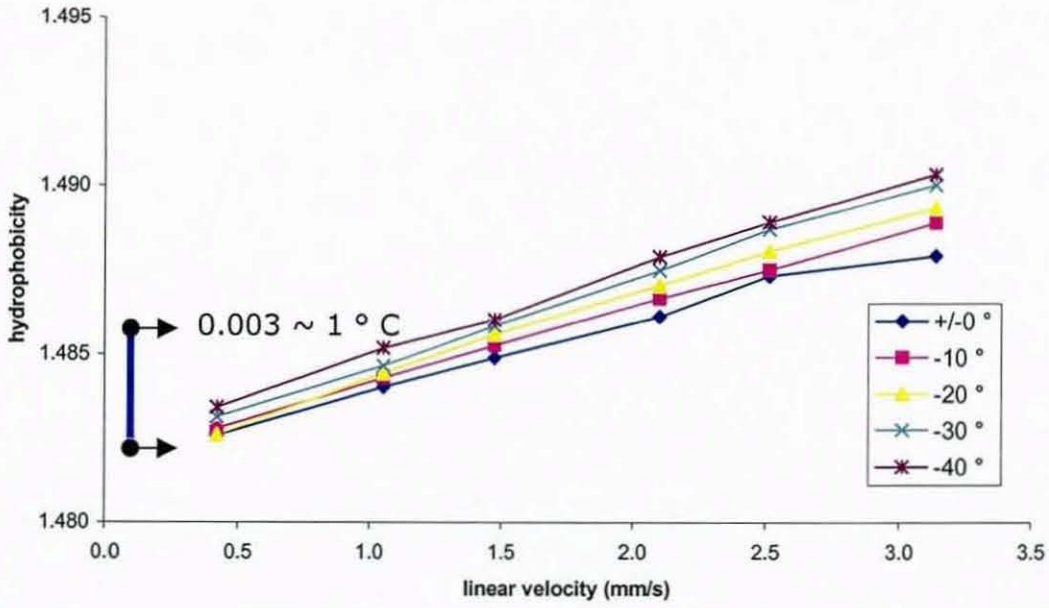

Figure 30: Change of hydrophobicity with linear velocity and mobile phase inlet temperature on EU column at 40 °C column wall temperature.

The hydrophobicity values for 40 °C column wall temperature confirm a significant difference between the average column temperatures at equilibrated mobile phase inlet temperature compared to different mobile phase inlet temperature differentials.

Figure 31 shows the change in hydrophobicity with linear flow velocity and mobile phase inlet temperature at 60 °C column wall temperature.

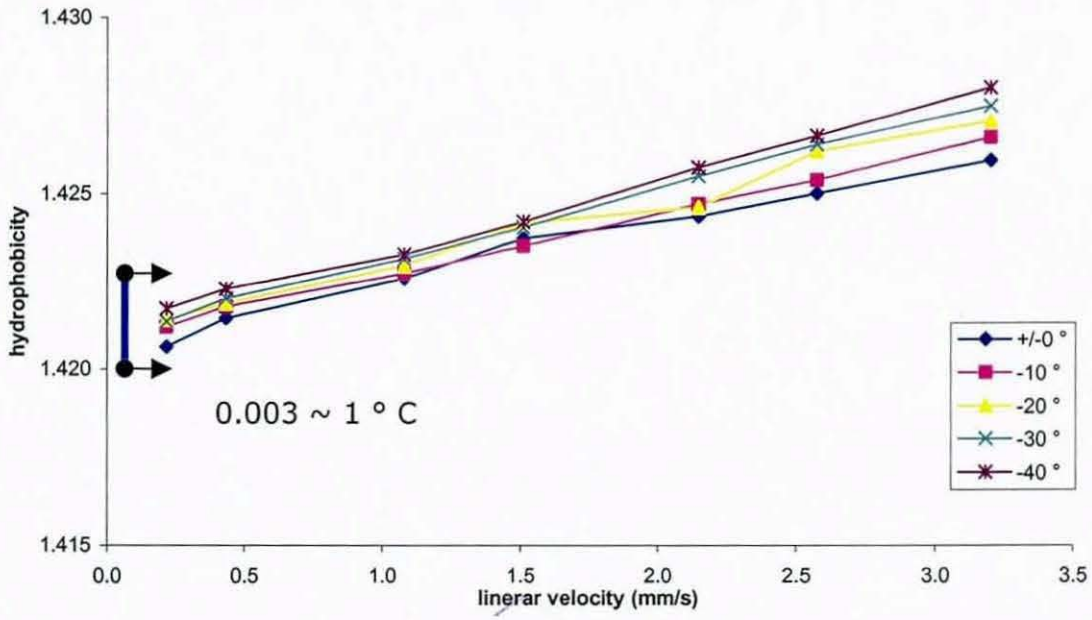

Figure 31: Change of hydrophobicity with linear velocity and mobile phase inlet temperature on EU column at 60 °C column wall temperature.

The change in average column temperature dependant on the mobile phase inlet temperature was calculated via the hydrophobicity as well as via the shape selectivity. At 40 °C column wall temperature both methods gave similar estimates. The calculation via shape selectivity estimated a change in average column temperature of about 0.9 °C for a change in mobile phase inlet temperature of –40 °C. The same change was estimated via the hydrophobicity to result in a change of 0.7 °C average column temperature. However, at 60 °C column wall temperature the difference in average column temperature estimated via the shape selectivity and the hydrophobicity was more significant. Using the shape selectivity the average column temperature was estimated to change by only about 0.2 °C. When the hydrophobicity was used the change in average column temperature was estimated about 0.7 °C, similar to the change observed at 40 °C column wall temperature.

5.1.2 Prontosil

The behaviour of a different stationary phase material was then studied in order to determine if these effects were common to all stationary phases and thus if generic recommendations could be developed to improve separation efficiency by lowering the mobile phase inlet temperature. The same column packer (Bischoff) packed the Prontosil C_{18} material into identical hardware as the EU column material. The set of experiments as described above was performed at 40 °C and 60 °C column wall temperatures. However, the results on this column were very different. Firstly the Prontosil ODS column was overall more efficient at 40 °C than the EU column. The temperature of the incoming mobile phase also seemed to have significantly less influence on efficiency (Figure 32), which didn't show a steady increase with increasing temperature differential.

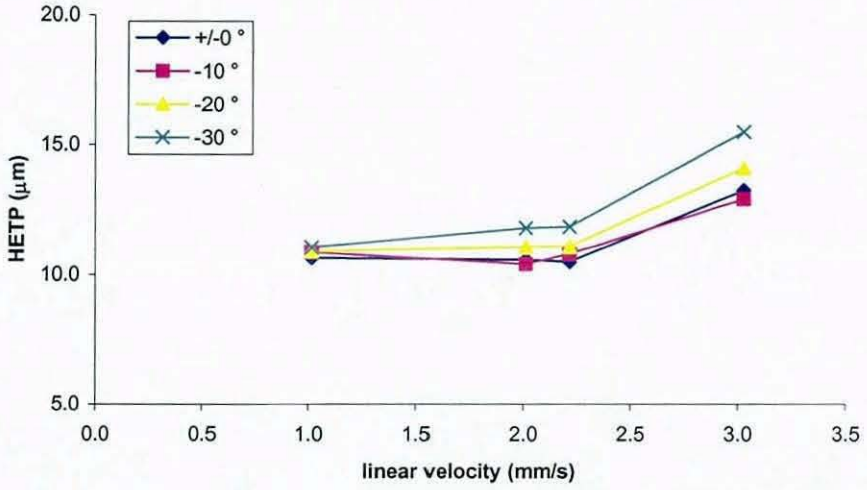

Figure 32: van Deemter plot of butylbenzene on Prontosil column 150 x 4.0 mm i.d. at 40 °C column temperature and four different mobile phase inlet temperature differentials.

The column's optimum efficiency was achieved at 2.2 mm/s linear velocity and the HETP for equilibrated conditions. The efficiency was only improved marginally by dropping the mobile phase inlet temperature and on further increasing the differential more than –10 ° the efficiency decreased (Figure 33).

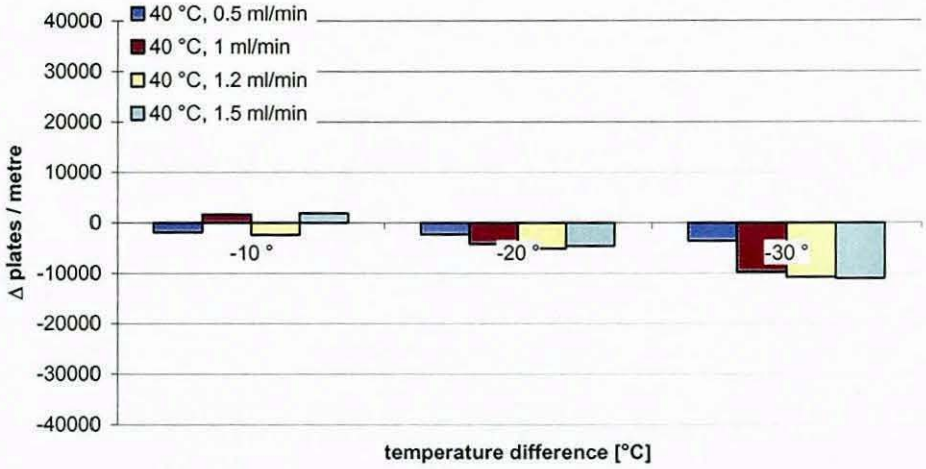

Figure 33: Difference in plates per metre between equilibrated mobile phase conditions and three mobile phase inlet temperature differentials at 40 °C column wall temperature for butylbenzene on Prontosil C18 column 150 x 4.0 mm i.d. at four different flow rates.

When the column wall temperature was changed to 60 °C a significant change in the effect of mobile phase inlet temperature was observed. As expected, when the mobile phase temperature was equilibrated to the same temperature as the column wall the efficiency increased due to the higher column wall temperature. However, in thus case the efficiency of the Prontosil column was significantly reduced when the mobile phase inlet temperature was dropped below the column wall temperature (Figure 34). The column efficiency degraded with increasing temperature difference, particularly at higher linear velocities. At and above -30 ° temperature differential and linear velocities above 2.0 mm/s, the van Deemter curve showed an extreme curvature.

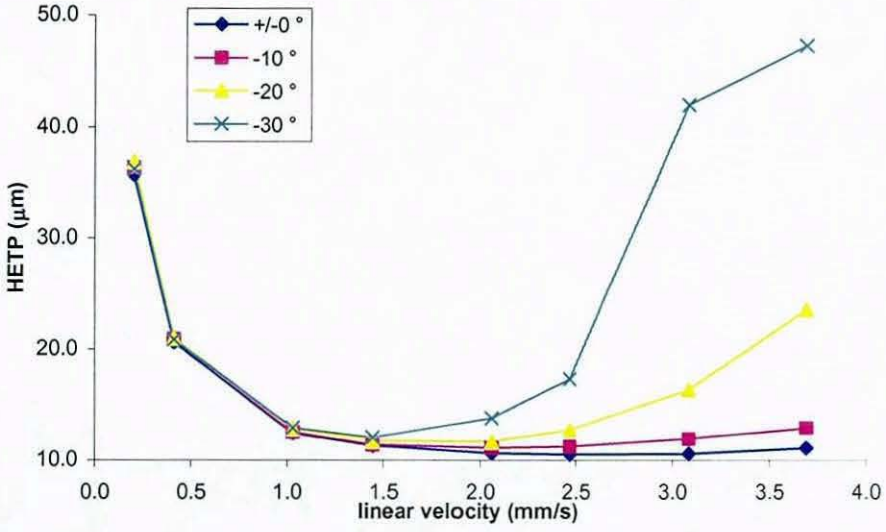

Figure 34: van Deemter plot of butylbenzene on Prontosil column 150 x 4.0 mm i.d. at 60 °C column temperature and four different mobile phase inlet temperature differentials.

The drop in efficiency was more significant for the Prontosil column than for the EU column. The higher the observed flow rate the more significant was the impact of the temperature differential on the column efficiency (Figure 35).

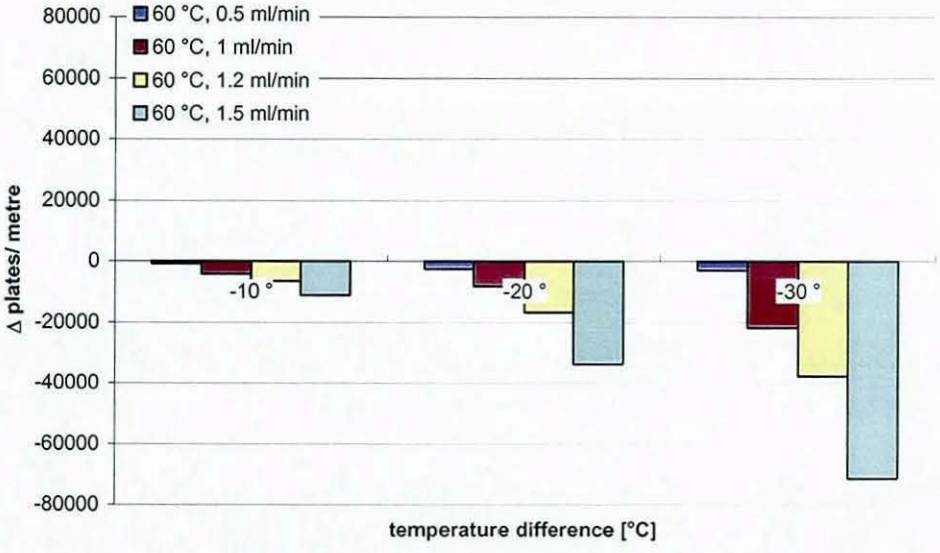

Figure 35: Difference in plates per metre between equilibrated mobile phase and three mobile phase inlet temperature differentials at 60 °C column wall temperature for butylbenzene on Prontosil C18 column 150 x 4.0 mm i.d. at four different flow rates.

The EU column and the Prontosil column were both packed by the same column packer into identical column hardware. Therefore, the column design and configuration and extra column effects due to frits should be the same. However, the behaviour of the two columns towards a temperature differential between column wall and incoming mobile phase at 60 °C column wall temperature was significantly different. In particular only decreases in plate number could be observed. It was therefore concluded that stationary phase properties were responsible for the difference in behaviour towards the introduction of a temperature differential between mobile phase and column wall.

No significant differences in average column temperature could be detected when comparing the shape selectivity at different mobile phase inlet temperature differentials (Figure 36).

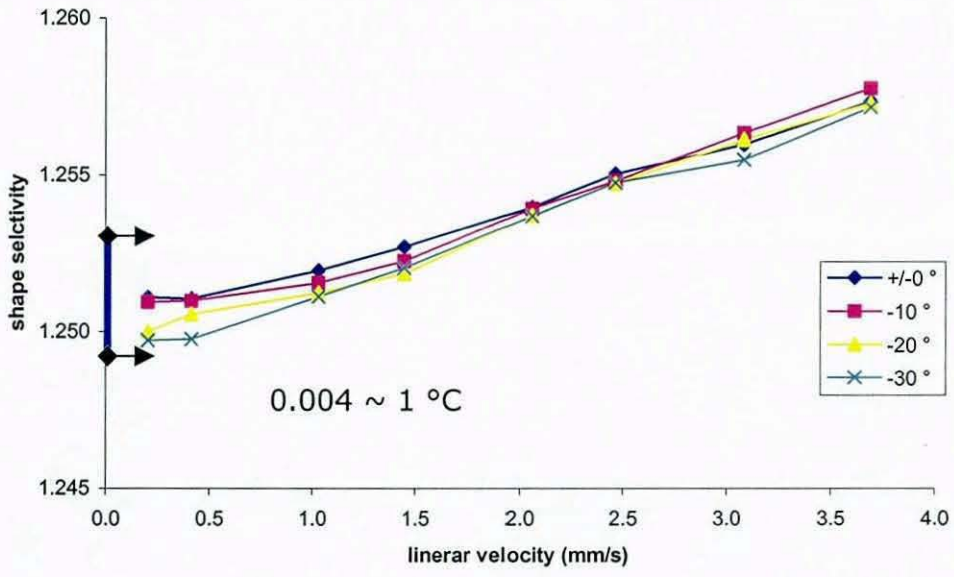

Figure 36: Change of shape selectivity with linear velocity and mobile phase inlet temperature on Prontosil C_{18} column at 60 °C column wall temperature.

The change in hydrophobicity with mobile phase inlet temperature differential was larger than the difference in shape selectivity (Figure 37).

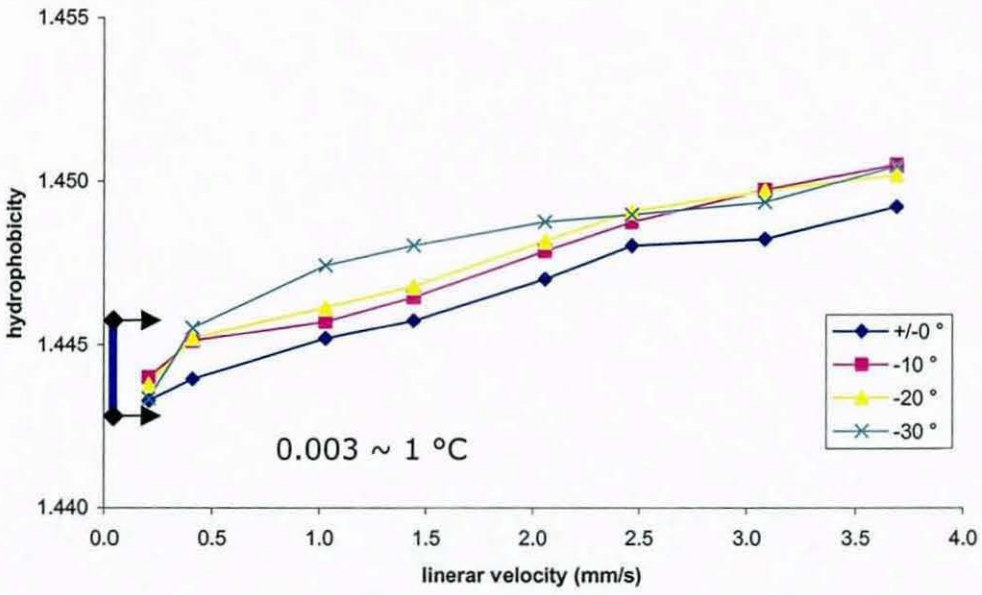

Figure 37: Change of hydrophobicity with linear velocity and mobile phase inlet temperature on Prontosil column at 60 °C column wall temperature.

However, the difference in hydrophobicity indicated a change in average column temperature of less than 1 °C.

In the light of these findings further experiments with a variety of stationary phase materials were performed at 60 °C column wall temperature. The aim was to identify if a feature of a column or stationary phase material could be related to the behaviour on introducing a temperature differential between the incoming mobile phase and column wall. With the results of this study it was hoped to be in a position to recommend optimum conditions for a specified stationary phase material. Table 5 give a comprehensive list of the columns used for the study and their stationary phase properties.

Table 5: List of columns employed for temperature study, part 1

	Purospher RP-18	Purospher. RP-18	Purospher. RP-18	Purospher. RP-18e	Purospher. RP-18e	Purospher. RP-18e	Purospher. RP-18e
column length (cm)	12.5	12.5	12.5	15	12.5	12.5	12.5
column ID (cm)	0.4	0.3	0.2	0.46	0.3	0.2	0.1
particle size (cm)	0.0005	0.0005	0.0005	0.0005	0.0005	0.0005	0.0005
pore size (Å)	80	80	80	80	80	80	80
surface area (sqm/g)	500	500	500	500	500	500	500
carbon load (%)	18	18	18	18	18	18	18
endcapping	polar	polar	polar	y	y	y	y
pressure (bar)	93	72	130	106	73	126	208
lin. Velocity (cm/s)	0.2	0.3	0.4	0.2	0.2	0.4	0.3
flow rate (ml/min)	1.0	0.5	0.5	1.0	0.5	0.5	0.18

y := yes

n := no

List of columns employed for temperature study, part 2

	Hypersil	Kromasil	EU	Chromolith	Symmetry	Luna	Novapak	Prontosil
column length (cm)	15	15	15	10	15	15	15	15
column ID (cm)	0.46	0.46	0.4	0.46	0.39	0.2	0.2	0.4
particle size (cm)	0.0005	0.0005	0.0006		0.0005	0.0005	0.0004	0.0005
pore size (Å)	115	100		2 um	125	100	60	124
surface area (sqm/g)	250	340		300	330	440	120	323
carbon load (%)	15	19	17	17	18	19	7	17
endcapping	y	y	n	y	y	y	y	y
pressure (bar)	94	93	106	47	109	136	113	106
lin. Velocity (cm/s)	0.1	0.2	0.2	0.1	0.3	0.3	0.4	0.2
flow rate (ml/min)	1.0	1.0	1.0	1.0	1.0	0.5	0.5	1.0

y := yes

n := no

The full sets of data for selected columns at 40 °C are compiled in Appendix F and the full list of data from the columns listed in Table 5 at 60 °C are compiled in Appendix E.

The results of two stationary phase materials Purospher RP 18 and Purospher RP18e are reported in detail. Both materials were packed at Merck in Merck cartridge systems. The silica material for both packing materials is similar. The Purospher RP18e material has the standard trimethylsilane end-capping while the Purospher RP18 has a polar aminopropyldimethylsilane end-capping. Both materials are commercially available

5.1.3 Purospher RP18 and RP18e

For the Purospher RP18e column with column water bath at 40 °C as the temperature of the incoming mobile phase was reduced to 30 °C (ΔT = -10°), there was a small increase in the column's efficiency at the optimum linear velocity of 1.6 mm/s (which corresponds to a volume flow rate of 1.0 ml/min) from 92107 plates/m to 94980 plates/m (Figure 38).

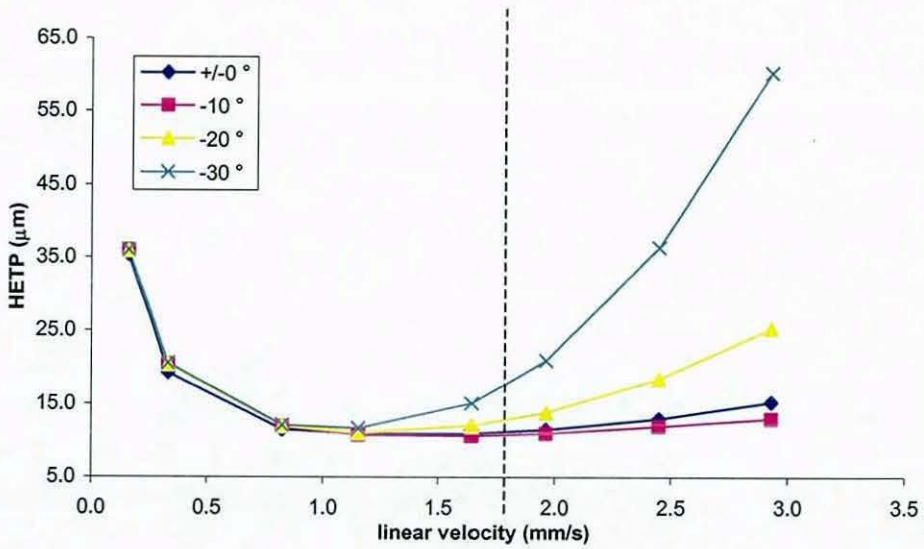

Figure 38: van Deemter curves for butylbenzene at four different mobile phase inlet temperature differentials. Purospher RP18e 150 x 4.6 mm i.d., mobile phase 75% methanol, 25% water (w/w), column temperature 40 °C controlled in water bath.

However, a further decrease in mobile phase inlet temperature to 20 °C (ΔT -20°) and 10 °C (ΔT -30°) resulted in a significant drop in separation efficiency down to 66753 plates /m at ΔT = -30°.

As the temperature difference increased the optimum linear velocity decreased from about 1.6 mm/s to 1.2 mm/s (Figure 38), and the optimum efficiency changed from 94980 plates /m to 86591 plates /m. Thus with a large temperature differential and high linear velocities, the van Deemter relationship became markedly curved unlike the conventionally reported linear increases at equilibrated conditions.

With the Purospher RP18 column material, the same changes in mobile phase temperature caused distinctly different changes in column efficiency at similar linear flow velocities (Figure 39).

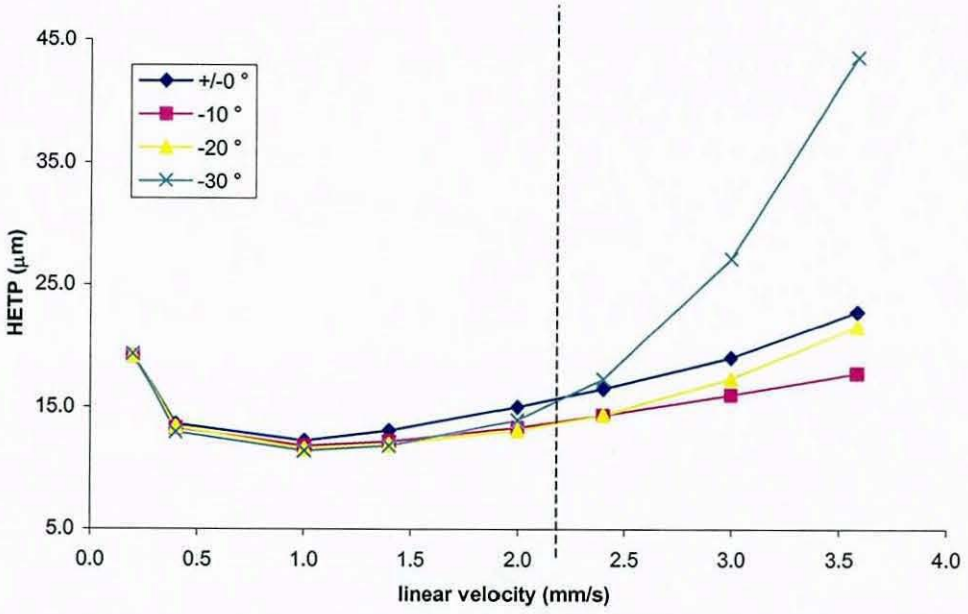

Figure 39: van Deemter curves for butylbenzene at four different mobile phase inlet temperature differentials. Purospher RP18 125 x 4.0 mm i.d., mobile phase 75% methanol, 25% water (w/w), column temperature 40 °C controlled in water bath.

At a linear velocity of 2.0 mm/s (flow rate of 1.0 ml/min), as the temperature difference increased to - 20 ° (inlet 20 °C) so did the column efficiency from an initial value of 66656 plates/m at ΔT = +/- 0 ° to 75611 plates/m at ΔT = -10 ° and 77075 plates/m at ΔT = -20

° (Figure 39). However, a further increase in temperature differential up to ΔT = -30 ° resulted in a sudden marked decrease in efficiency to 72269 plates/m which was still higher than the equilibrated temperature value. Only at higher linear velocities of 2.5 mm/s was there any significant decrease below the initial efficiencies. However, similar to the behaviour observed on the Purospher RP18e material, there was a pronounced curvature at higher flow rates suggesting an equilibration problem. The optimum linear velocity for the column remained almost constant. Thus this column not only showed an increase in efficiency when the inlet temperature was reduced but also was much more insensitive to flow rate changes. The marked drop in efficiency at high flow rates with increased temperature differential observed with the Purospher RP18e stationary phase (Figure 40) was now not apparent (Figure 41) until a temperature difference of -30 °C between column wall and mobile phase inlet was reached. However, at – 20 ° the van Deemter curve started to show a marked curvature. If the results at a linear flow of 0.5 ml/min on the two columns were compared the Purospher RP18e showed a steady decrease and the Purospher RP18 showed a steady increase in efficiency.

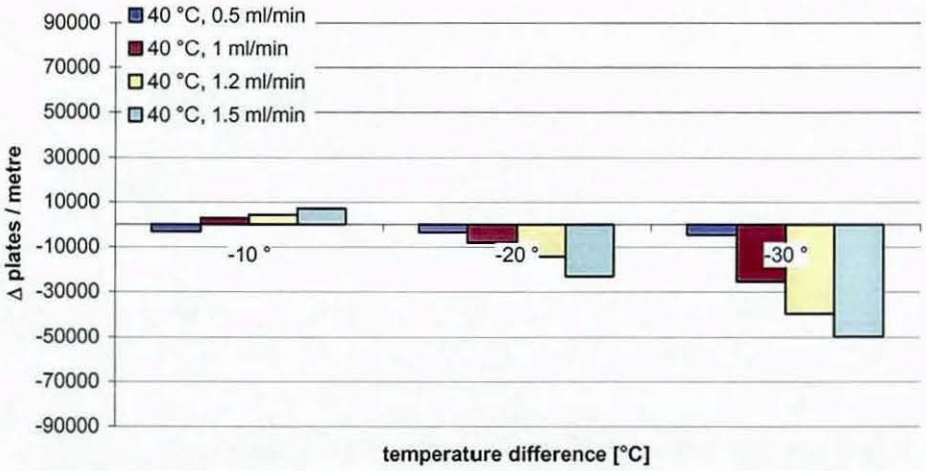

Figure 40: Difference in plates per metre between equilibrated mobile phase and three mobile phase inlet temperature differentials at 40 °C column wall temperature for butylbenzene on Purospher RP18e column 150 x 4.6 mm i.d. at four different flow rates.

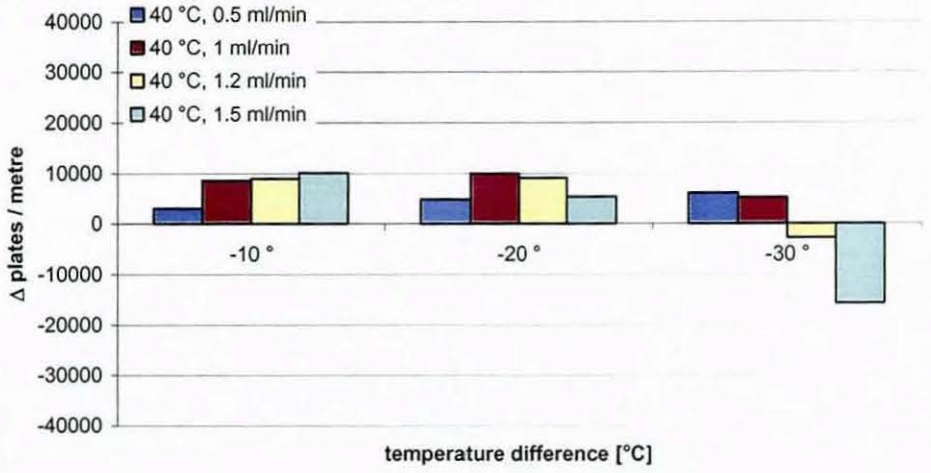

Figure 41: Difference in plates per metre between equilibrated mobile phase and three mobile phase inlet temperature differentials at 40 °C column wall temperature for butylbenzene on Purospher RP18 column 125 x 4.0 mm i.d. at four different flow rates.

The shape selectivity for the separations on the Purospher RP18e and the Purospher RP18 column were determined for each mobile phase inlet temperature differential and plotted against the linear flow velocity of the mobile phase (Figure 42 A-B). The change in selectivity per 1°C for both the Purospher RP18 and the Purospher RP18e was determined earlier in this work. For the Purospher RP18e a change in average column temperature of 1 °C caused a change of ~ 0.006 in shape selectivity of the column. The Purospher R18 column was more sensitive to temperature and a change in column temperature by 1 °C caused a change in shape selectivity of ~ 0.013.

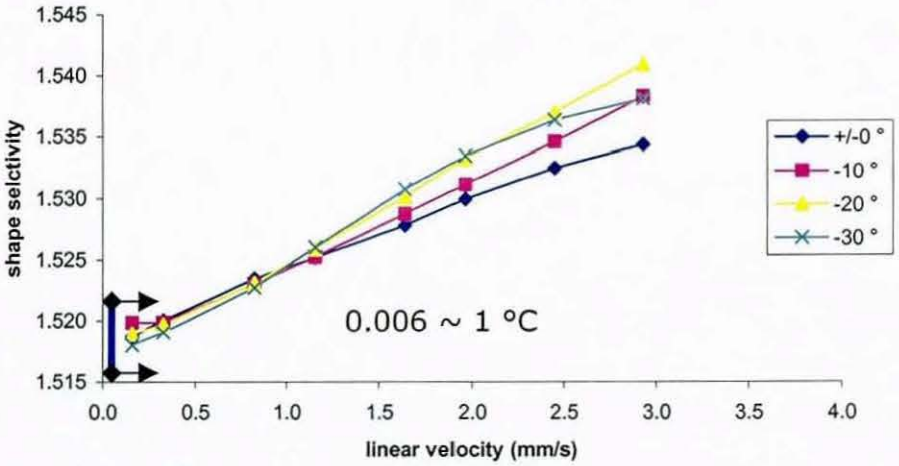

A: Purospher RP18e

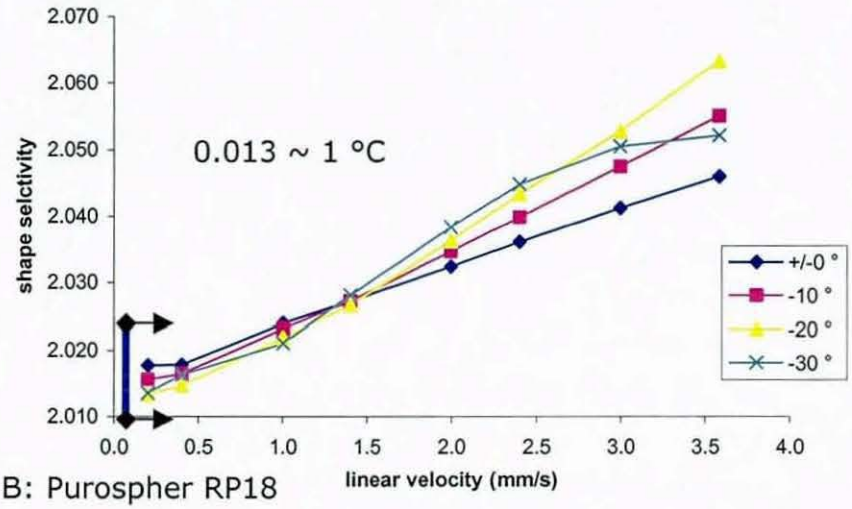

B: Purospher RP18

Figure 42 A-B: Change of shape selectivity vs. linear flow velocity at four temperature differentials between, column wall and incoming mobile phase on A: Purospher RP18e B: Purospher RP18 at 40 °C column wall temperature, change of selectivity per 1°C on Purospher RP18e = 0.006; change of selectivity per 1°C on Purospher RP18 = 0.013.

Both columns showed changes in shape selectivity with mobile phase inlet temperature differential. The largest change in selectivity for the Purospher RP18e was observed between 0 and –20 ° temperature differential at 3.0 mm/s linear velocity and was equivalent to a change in average column temperature of about 1 °C. Similarly, the largest difference in selectivity for the Purospher RP18 column was observed at 3.6 mm/s linear velocity between 0 and –20°C temperature differential and was equivalent to a change in average column temperature of about 1.3 °C. The selectivity recorded for both

columns at a temperature differential of -30 °C and high linear velocities were different from the changes observed for the EU column or the Prontosil column. The selectivity graph showed a curvature not observed before. This in combination with the marked curvature of the van Deemter plots for ΔT = -30 °C temperature differential for these two materials suggests a significantly different temperature profile. It appeared that the average column temperature increased at high linear velocities in spite of the large inlet temperature differential.

The change of the hydrophobicity was plotted versus the linear flow velocity of the mobile phase at different temperature differentials to ascertain that the changes in shape selectivity were not caused by configuration changes of the bonded phase. Figure 43 shows the hydrophobicity vs. linear velocity plot for the Purospher RP18e column. The curve for -30 ° temperature differential between mobile phase inlet and column wall temperature showed the same curvature at high linear velocities as the curve for the shape selectivity.

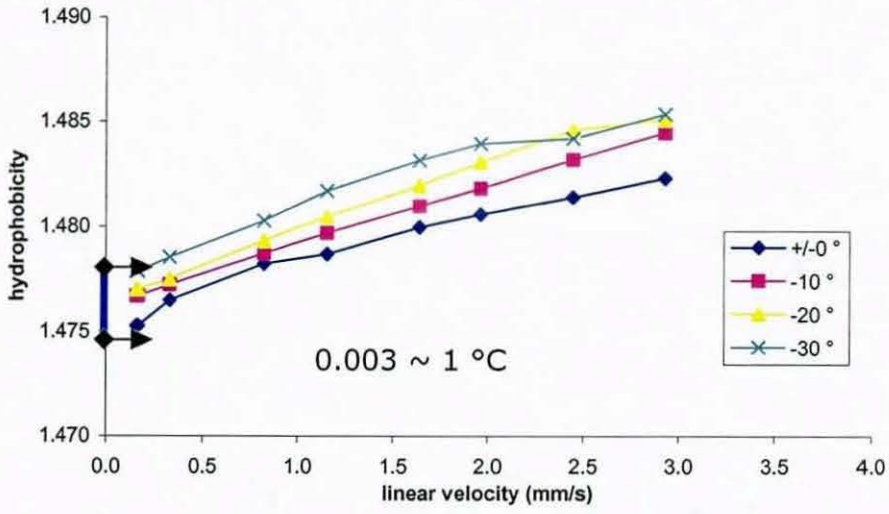

Figure 43: Change of hydrophobicity vs. linear flow velocity at four temperature differentials between, column wall and incoming mobile phase on Purospher RP18e, column wall temperature 40 °C.

However, the hydrophobicity curve for the Purospher RP18 column above 3 mm/s linear velocity and ΔT = −30 °C temperature differential was different from the curve observed for the shape selectivity. The

value for the hydrophobicity still increased at high linear velocities indicating lower average column temperature (Figure 44).

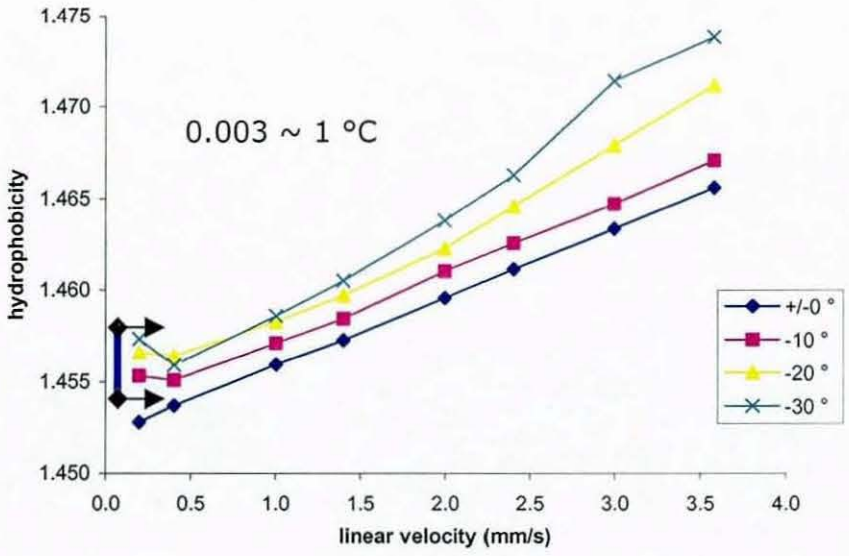

Figure 44: Change of hydrophobicity vs. linear flow velocity at four temperature differentials between, column wall and incoming mobile phase on Purospher RP18, column wall temperature 40 °C.

In order to investigate if these effects were dependent on the external column wall temperature or would change as overall diffusion rates increased and viscosity of the mobile phase dropped, the column wall temperature was raised to 60 °C by increasing the temperature of the column water bath. The effect of a mobile phase temperature difference on the Purospher RP18e column now showed a decrease in column efficiency as the mobile phase inlet temperature was reduced (Figure 45). Unlike the results at 40 °C there was no optimum differential in the inlet temperature.

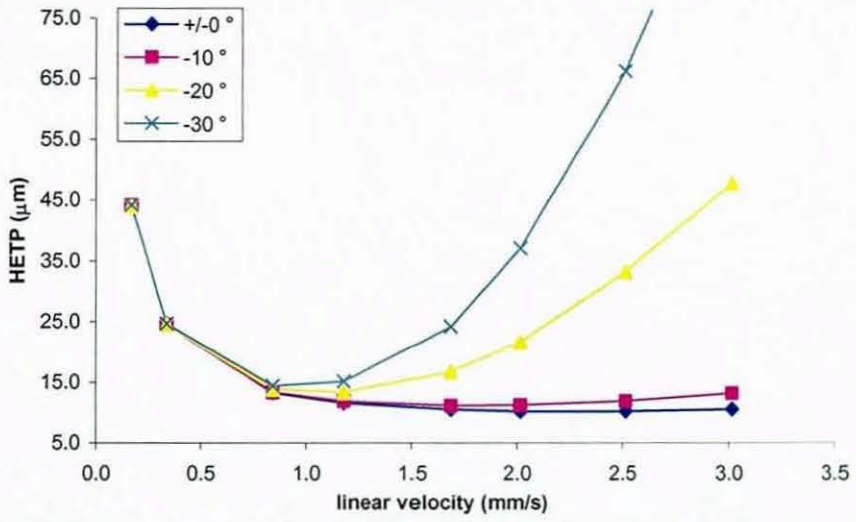

Figure 45: van Deemter curves for butylbenzene at four different mobile phase inlet temperatures, Purospher RP18e 150 x 4.6 mm i.d., mobile phase 75% methanol, 25% water (w/w),column temperature 60 °C controlled in water bath.

The best results for the column efficiency were achieved when the mobile phase inlet and the column wall were equilibrated to the same temperature (Figure 46). The benefit was most apparent at flow rates higher than the conventional 1 ml/min.

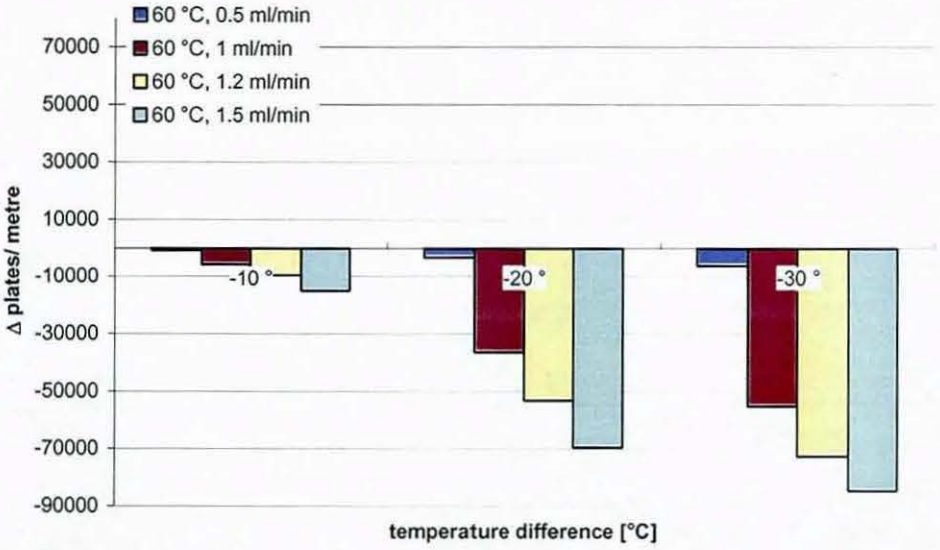

Figure 46: Difference in plates per metre between equilibrated mobile phase and three mobile phase inlet temperature differentials at 60 °C column wall temperature for butylbenzene on Purospher RP18e column 150 x 4.6 mm i.d. at four different flow rates.

The curves for the shape selectivity vs. linear velocity were closer to one another at 60 °C column wall temperature than at 40 °C (Figure 47).

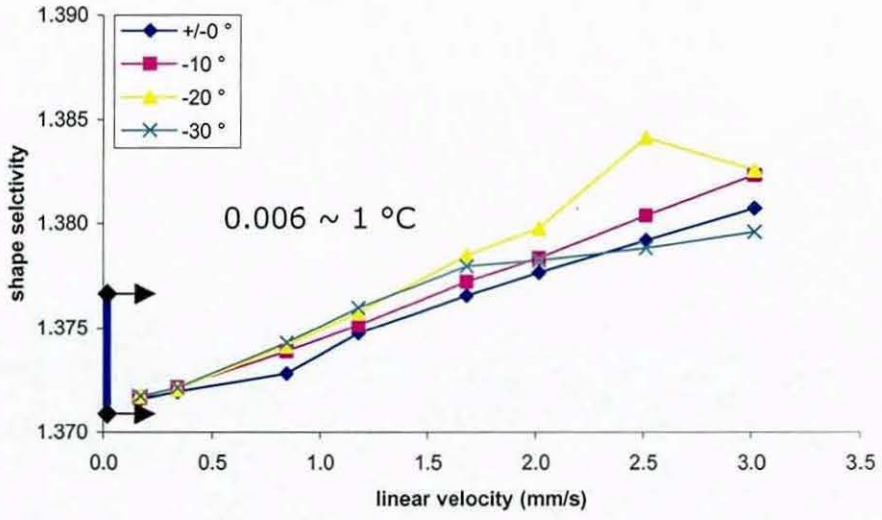

Figure 47: Change of shape selectivity vs. linear flow velocity at four temperature differentials between, column wall and incoming mobile phase on Purospher RP18e, column wall temperature 60 °C.

The maximum difference in shape selectivity 0.005 was measured at 2.5 mm/s linear flow velocity between the curves measured for +/-0 ° and the −20° temperature differential. A difference in shape selectivity of 0.005 was indicative of a difference in average column temperature of less than 1 °C. Furthermore, the curve for -30 ° temperature differential dropped off towards lower shape selectivity. The shape selectivity measured for −30° temperature differential dropped even below the value measured for equilibrated conditions.

Similar observations were made measuring the hydrophobicity. A change in hydrophobicity of 0.03 was calculated to be equivalent to a change in average column temperature of 1 °C. The dependence of the hydrophobicity on the mobile phase inlet temperature differential was 0.01 at 2.5 mm/s linear flow velocity between +/- 0 ° and - 20° inlet temperature differential. This was indicative of a change in average column temperature of less than 0.5 °C (Figure 48). The hydrophobicity difference measured at 40 °C column wall temperature at the same linear flow velocity and inlet temperature differential was

0.04 indicating a change in average column temperature of about 1.3 °C.

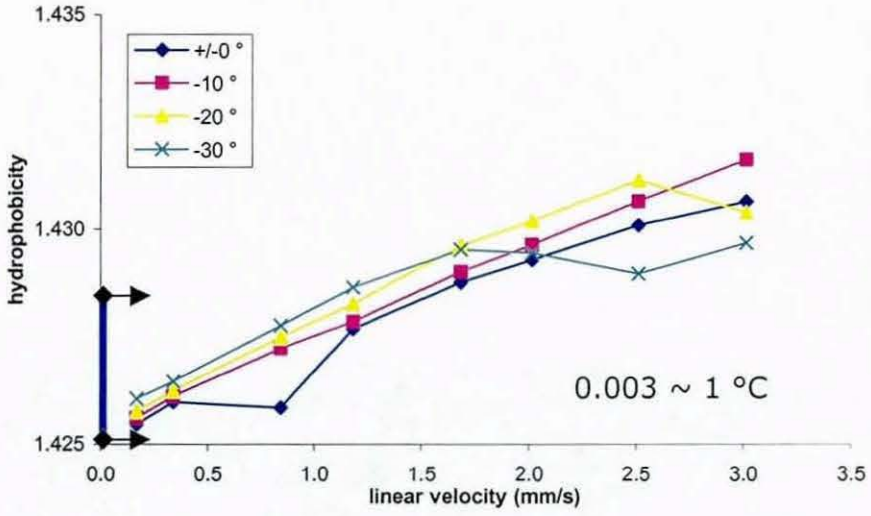

Figure 48: Change of hydrophobicity vs. linear flow velocity at four temperature differentials between, column wall and incoming mobile phase on Purospher RP18e, column wall temperature 60 °C.

At higher linear flow velocities there was a significant change in slope for the curve representing the hydrophobicity at −30 °C inlet temperature differential. This change in slope for the hydrophobicity curve was observed at the same linear velocity as for the shape selectivity curve, 1.7 mm/s (= 1.0 ml/min).

The behaviour of the Purospher RP18 column material at a column wall temperature of 60 °C was again noticeably different (Figure 49). At a temperature differential of −10 °C all velocities showed improved efficiency but the system altered at higher temperature differentials. At a linear velocity of 1.5 mm/s (flow 0.7 ml/min) the efficiency increased with temperature differential from 72805 plates/m to 83579 plates/m at ΔT = -30 °. However, at higher flow rates the situation was partially reversed and the efficiency decreased at the higher temperature differentials (Figure 50).

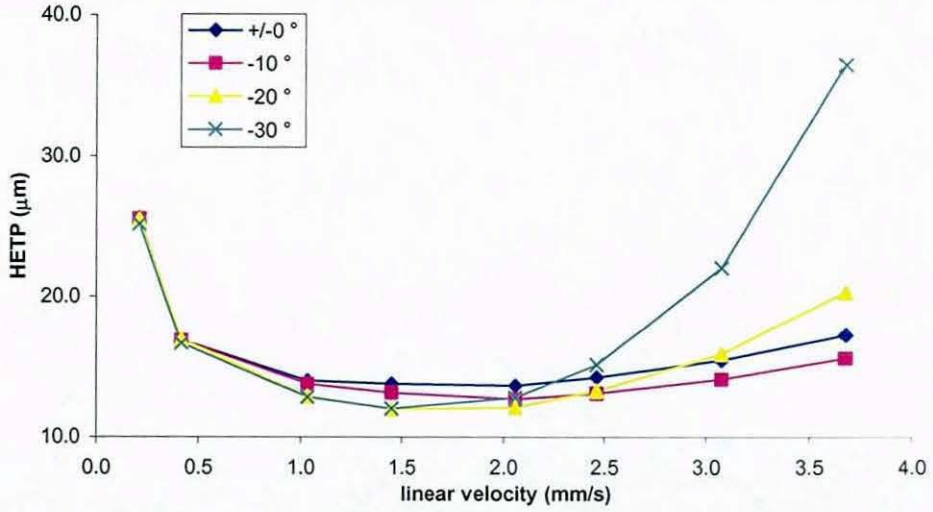

S0

Figure 49: van Deemter curves for butylbenzene at four different mobile phase inlet temperatures, Purospher RP18 125 x 4.0 mm i.d., mobile phase 75% methanol, 25% water (w/w),column temperature 60 °C controlled in water bath.

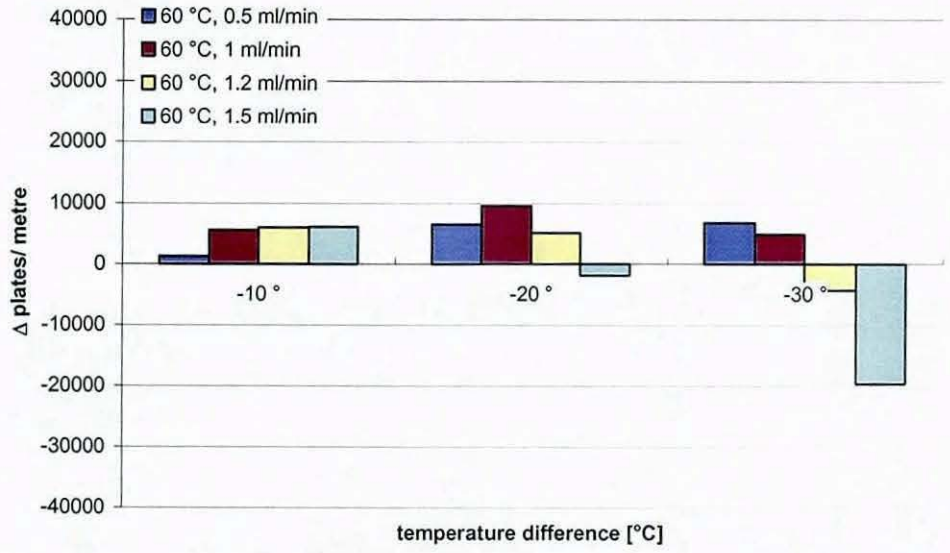

Figure 50: Difference in plates per metre between equilibrated mobile phase and three mobile phase inlet temperature differentials at 60 °C column wall temperature for butylbenzene on Purospher RP18 column 125 x 4.0 mm i.d. at four different flow rates.

For this column the van Deemter curves at higher temperature differentials became much more curved and resembled those on the RP18e column. The extreme curvature of the efficiency curve could be indicative of an inversion of the band profile. There was also a

decrease in the optimum linear velocity from 2.0 to 1.5 mm/s but the effect was much smaller than seen for the RP18e column.

The changes in shape selectivity with mobile phase inlet temperature at 60 °C column wall (Figure 51) temperature were very similar to the changes observed at 40 °C column wall temperature (Figure 42). The largest difference in shape selectivity was 0.012 between equilibrated conditions and −30 °C mobile phase temperature differential at 3.1 mm/s (1.5 ml/min) linear flow velocity indicative of a difference in average column temperature of just under 1 °C.

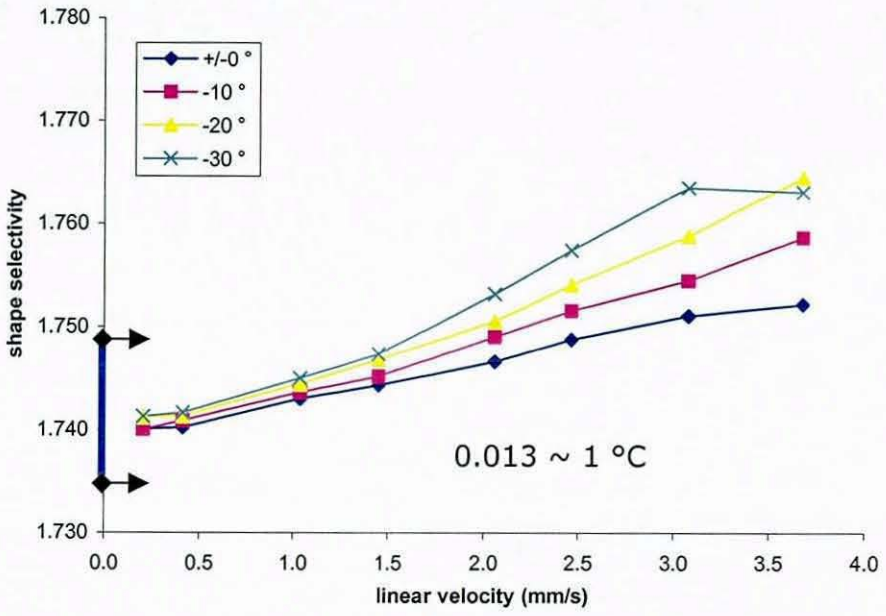

Figure 51: Change of shape selectivity vs. linear flow velocity at four temperature differentials between, column wall and incoming mobile phase on Purospher RP18, column wall temperature 60 °C.

The maximum change in shape selectivity was the same as measured at 40 °C column wall temperature. However, the −30 °C inlet temperature differential curve showed a change in slope only at 3.1 mm/s (1.5 ml/min) and not at 2.0 mm/s (1.0 mm/min) as it did at 40 °C column wall temperature.

The changes in hydrophobicity observed at 60 °C column wall temperature were distinctly different from those observed at 40 °C column wall temperature (Figure 52).

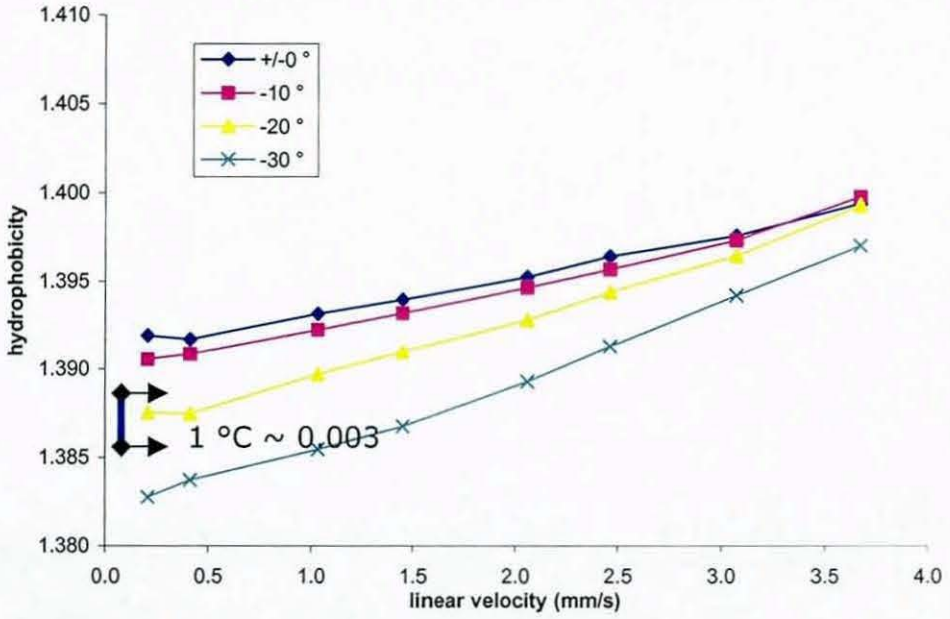

Figure 52: Change of hydrophobicity vs. linear flow velocity at four temperature differentials between, column wall and incoming mobile phase on Purospher RP18, column wall temperature 60 °C.

The curves at 60 °C column wall temperature appeared to be reversed compared to 40 °C column wall temperature. The distance between the curves was largest at low linear velocities and the hydrophobicity values measured for the largest temperature differential at the lowest linear velocity suggested a higher average column temperature at large temperature differentials. The shape selectivity data suggested the opposite.

In order to resolve this paradox the retention times measured at the different inlet temperature differentials at 2.1 mm/s linear flow velocity were plotted versus the temperature differential. Figure 53 shows the changes in retention time with increasing temperature differential. The retention data supported the conclusions drawn from the hydrophobicity data, higher average column temperature when the temperature differential was largest. The retention times decreased at larger temperature differentials.

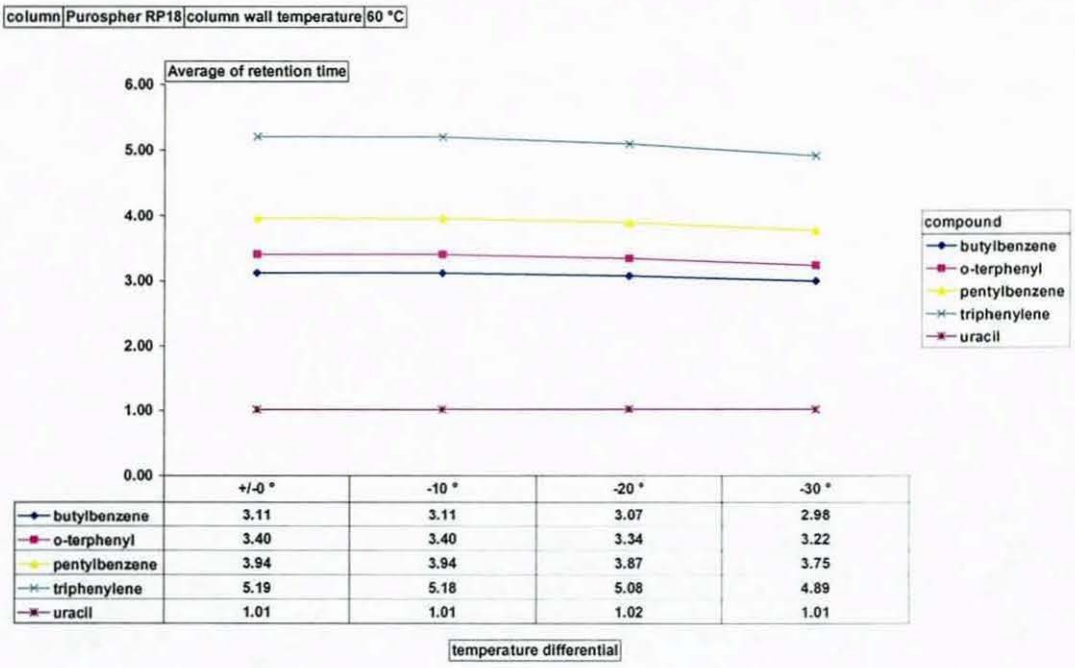

	+/-0 °	-10 °	-20 °	-30 °
butylbenzene	3.11	3.11	3.07	2.98
o-terphenyl	3.40	3.40	3.34	3.22
pentylbenzene	3.94	3.94	3.87	3.75
triphenylene	5.19	5.18	5.08	4.89
uracil	1.01	1.01	1.02	1.01

Figure 53: Change of retention time with different inlet temperature differentials at 60 °C column wall temperature and 2.1 mm/s linear flow velocity (1.0 ml/min) on Purospher RP18.

It is unclear why the retention times decreased. Initially a change in linear velocity caused by an unstable pump flow rate was suspected. However, the constant retention times measured for uracil across the range of temperature differentials suggested a constant linear velocity throughout the experiment.

5.1.4 Other stationary phase materials

The van Deemter curves of a number of other columns (Table 5) were then examined at 60 °C (Appendix E) with different mobile phase inlet temperatures and the results were compared to determine if the effect was related to a specific type of column material or could be correlated with properties, such as end-capping which differentiated the Purospher RP18 and RP18e columns. The responses fell into three groups depending on the nature of the changes and these can be illustrated by examining the changes at a flow rate of 1 ml/min (Figure 54). For 4.6 mm i.d. 4.0 mm i.d. and 3.9 mm i.d. columns the flow rate of 1 ml/min results in comparable linear velocities of 1.7 mm/s and 2.1 mm/s respectively.

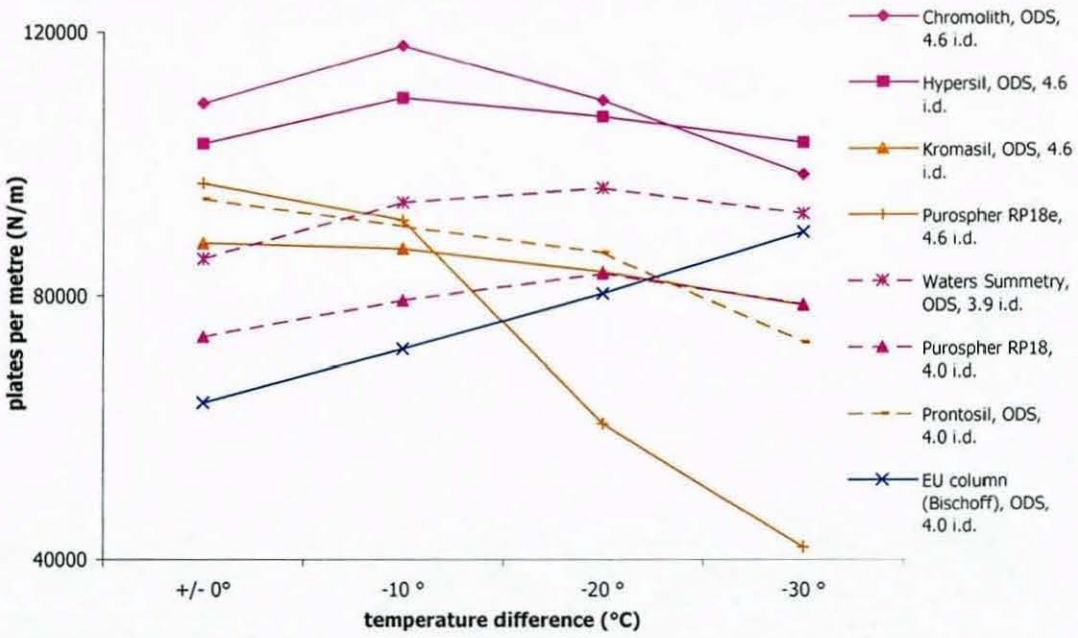

Figure 54: Comparison of the change of efficiency with inlet temperature differential for eight different columns at 1 ml/min flow rate, mobile phase inlet temperature difference +/-0 to -30 °C, at 60 °C column temperature.

The respective exact linear velocities are listed in Table 5. Three column materials, Purospher RP-18e, Prontosil C18, and ODS Kromasil (orange lines) all showed a steady decline in efficiency with increasing temperature difference at similar flow rates. In these cases, when the mobile phase and the column were at the same temperature high eluent flow rates had little effect on efficiency (see Appendix E). Thus these columns were robust to flow rate changes but were adversely affected by increasing temperature differentials.

In contrast, Hypersil ODS HiPurity, ODS Symmetry, and the monolithic Chromolith column material all behaved in a similar way to the Purospher RP18 column. In each case the column efficiency initially increased with small temperature differential (purple lines Figure 54) and then declined at higher temperature differentials. However, the optimum differential varied from -10 °C for the Chromolith and HiPurity columns to -20 °C for the Symmetry and Purospher RP-18 columns. In each case at low linear velocities, the temperature differential improved efficiency, loss of efficiency only occurred at high

linear velocities. For the Purospher RP18 column a temperature differential of -10 °C was beneficial over the whole range of applied linear velocities.

The EU column appears to be a special case [145]. Its performance steadily improved with increasing temperature differential. This column is the only column without any type of end capping. Furthermore, the particle size distribution of the EU ODS material is wider than for commercially available material.

A similar comparison was performed at 1.8 ml/min flow rate equivalent to ~ 3.7 mm/s for a 4.0 mm i.d. column and ~ 3.0 mm/s for a 4.6 mm i.d. column (1.5 ml/min ~ 3.1 mm/s for EU column). Figure 55 illustrates the changes in efficiency at the higher flow rate. The number of columns showing improved efficiency when a temperature differential was introduced was reduced from five to three. Furthermore, the optimum temperature differential was now at −10 °C. Again the EU column showed a steady improvement in efficiency with a larger temperature difference between incoming mobile phase and column wall.

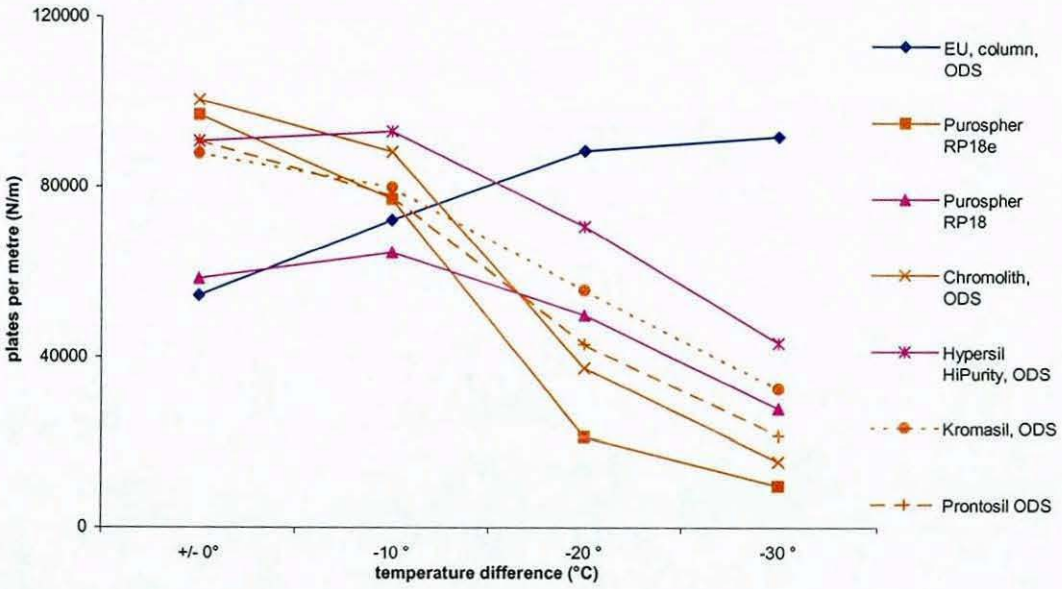

Figure 55: Comparison of the change of efficiency with inlet temperature differential for seven different columns at 1.8 ml/min flow rate (1.5 ml per min for the EU column), mobile phase inlet temperature difference +/-0 to -30 °C, at 60 °C column temperature.

No correlation between stationary phase end-capping and/or percentage of C_{18} coverage and the behaviour towards the introduction of a temperature differential between mobile phase and column wall temperature was clearly identified.

5.2 Column internal diameter

The effect that the internal diameter had on the behaviour towards the introduction of a temperature differential between mobile phase and column wall temperature was then investigated as it seemed that the inversion of the flow profile could be responsible for changes in efficiency on introducing a temperature differential.

According to Poppe et al [109] the impact of the column wall temperature on the core temperature of the column is dependent on the inner diameter of the column and the linear velocity of the mobile phase [110]. Assuming that the retention factor gradient across a column is the consequence of a radial temperature gradient and a resulting viscosity gradient, one would predict that the beneficial effect of lowering the mobile phase inlet temperature should either be less pronounced or vanish when the column internal diameter is decreased.

In order to test the assumption that the influence of a temperature gradient between mobile phase and column wall should be reduced employing smaller bore columns, the same stationary phase materials, Purospher RP18e and Purospher RP18 were used but packed into smaller i.d. column hardware. All the Purospher columns had the same outer diameter and hence the wall thickness varied. It was assumed that the metal of the column wall had high temperature conductivity and the difference in wall thickness would have little effect.

As opposed to the Purospher RP18e, 150 x 4.6 mm i.d. (Figure 45), which did not show any improvement in efficiency when the mobile phase inlet temperature was lower than the column wall temperature at 60 °C column wall temperature, a Purospher RP18e, 125 x 3.0 mm i.d. column did show an improvement (Figure 56).

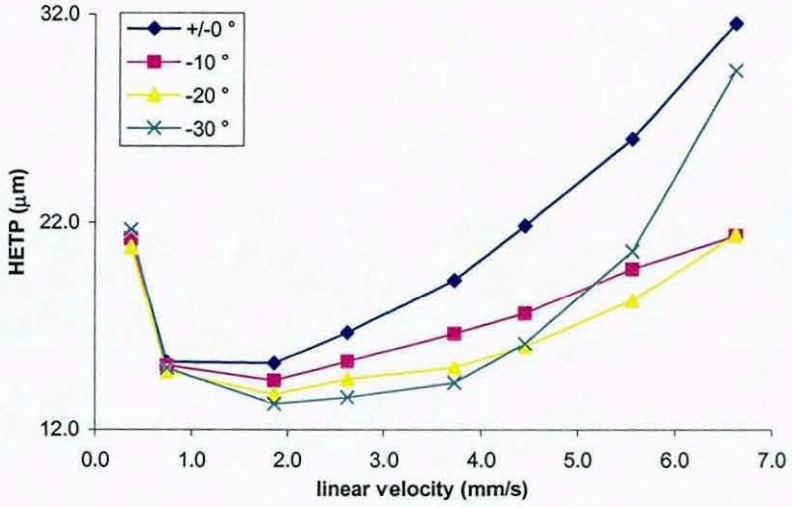

Figure 56: van Deemter curves for butylbenzene at four mobile phase inlet temperature differentials, Purospher RP18e 125 x 3.0 mm i.d., mobile phase 75% methanol, 25% water (w/w), temperature 60 °C controlled in water bath.

Again the curvature of the van Deemter curve recorded for –20°C and –30 °C temperature differential is far more pronounced at high linear flow rates in comparison to the curves for the other temperature differentials.

Similarly, the Purospher RP18, 125 x 3.0 mm i.d. did show an increase in efficiency when the mobile phase inlet temperature was dropped below the column wall temperature (Figure 57). Furthermore, as already observed for the Purospher RP18e column material the curvature for the –30°C temperature differential curve was more significant than for the other temperature differentials.

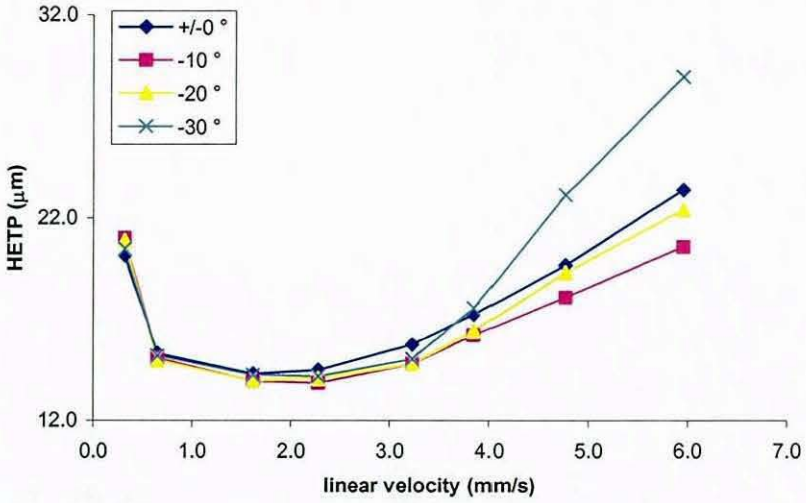

Figure 57: van Deemter curves for butylbenzene at four mobile phase inlet temperature differentials, Purospher RP18 125 x 3.0 mm i.d., mobile phase 75% methanol, 25% water (w/w), temperature 60 °C controlled in water bath.

For both 3 mm i.d. columns the highest efficiency was achieved with a larger temperature difference between inlet and column than for the columns with a wider diameter.

The change in selectivity with inlet temperature differential versus the linear velocity of the mobile phase was also recorded for both 3 mm i.d. columns (Figure 58 A-B). The results for the 3 mm i.d. Purospher RP18e column resembled the results for the 4.6 mm i.d. RP18e column. However, the curve for –30°C temperature differential did not drop down at higher linear velocities as it did on the 4.6 mm i.d. column. When running low linear velocities there was no change in selectivity with inlet temperature. At higher linear velocities the change in selectivity and hence the change in average column temperature, about 1 °C, was marginally higher than for the wider bore column.

The changes in selectivity for the Purospher RP18 column were different from the changes observed for the 4.0 mm i.d. column. The maximum change in selectivity for the Purospher RP18 at high flow

linear velocities was indicative of a change in average column temperature of about 1 °C.

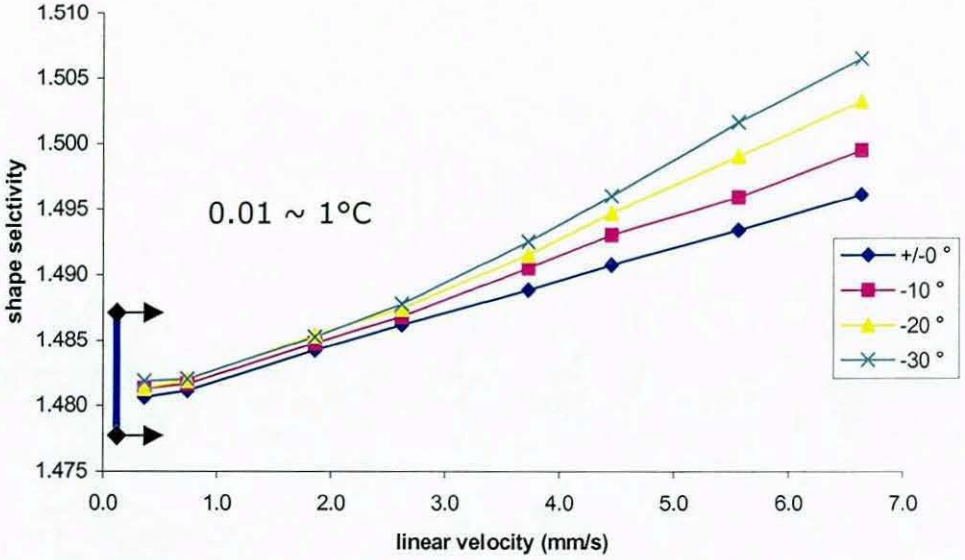

Figure 58A: Pursospher RP18e, 3.0 mm i.d., 60 °C column wall

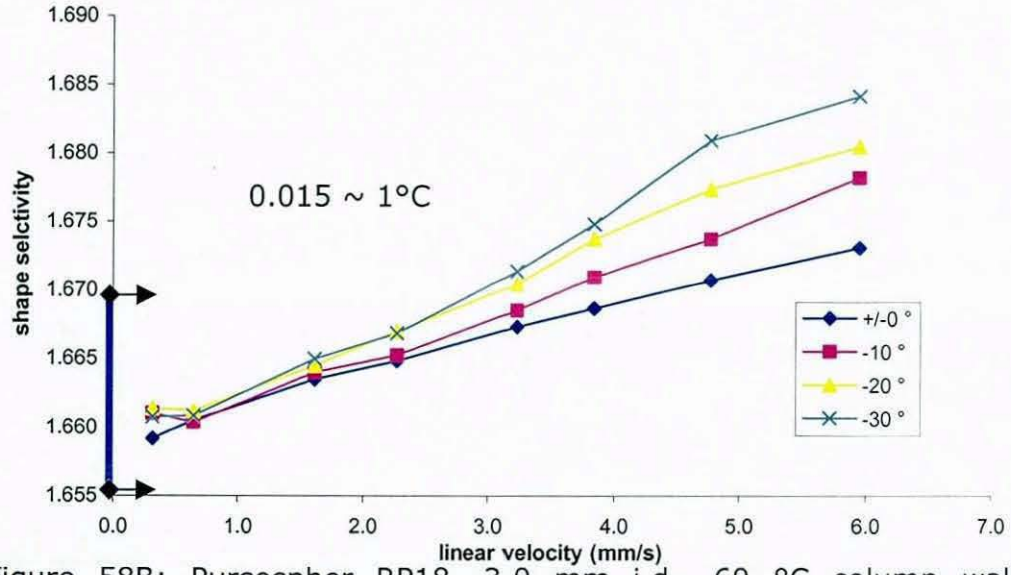

Figure 58B: Pursospher RP18, 3.0 mm i.d., 60 °C column wall

Figure 58 A-B: Change of shape selectivity with linear flow velocity at four temperature differentials between, column wall and incoming mobile phase on A: Purospher RP18e B: Purospher RP18 at 60 °C column wall temperature for 125 x 3.0 mm i.d.

These findings did not support the assumption that the effect of lowering the mobile phase inlet temperature on the average column temperature should either be less pronounced or vanish when the column internal diameter is decreased. However, the behaviour of the

average column temperature was closer to the expected result when the average column temperatures were estimated using the hydrophobicity change (Figure 59 and Figure 60).

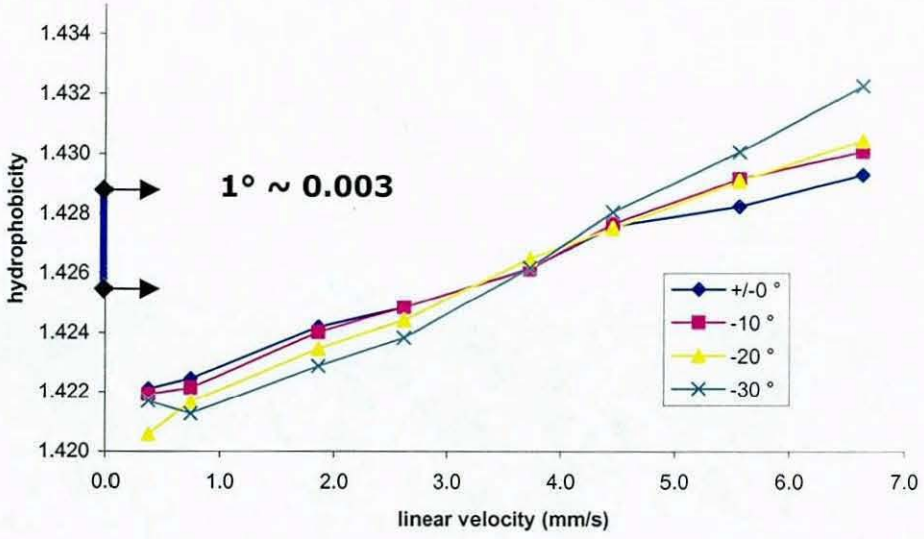

Figure 59: Change of hydrophobicity with linear flow velocity at four temperature differentials between, column wall and incoming mobile phase on Purospher RP18e, 125 x 3.0 mm i.d.

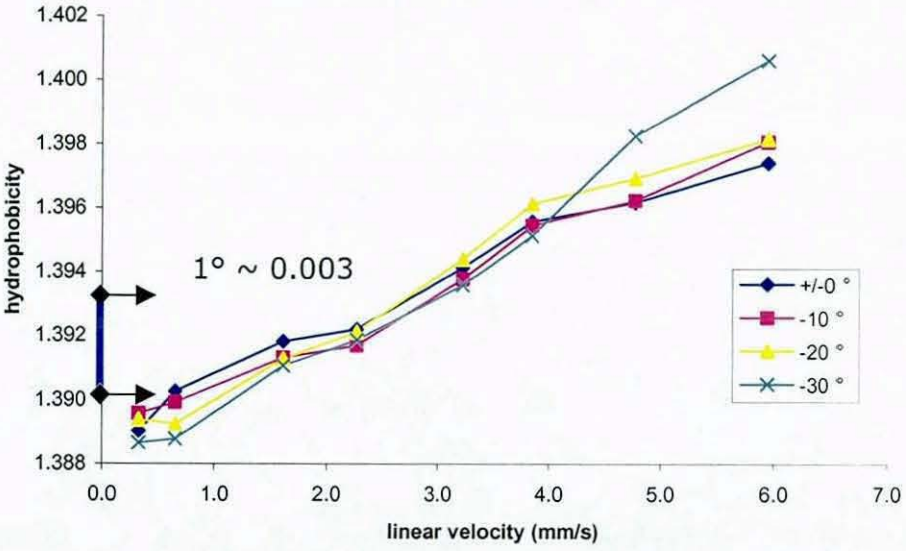

Figure 60: Change of hydrophobicity with linear flow velocity at four temperature differentials between, column wall and incoming mobile phase on Purospher RP18, 125 x 3.0 mm i.d.

The hydrophobicity dependence on the mobile phase inlet temperature difference was less significant up to a mobile phase linear velocity of 5 mm/s and above and a temperature difference of - 30°. For both columns the change in hydrophobicity at high mobile phase linear flow velocities and a temperature differential of -30 °C was indicative of a drop in average column temperature of about 1 °C.

A feasible explanation may be, when the mobile phase inlet temperature is lowered in relation to the column wall and pumped into the column with a fixed volumetric flow rate of e.g. 1.0 ml/min the proportion of the column affected by the colder mobile phase is far larger in a 3.0 mm i.d. column than in a 4.6 mm i.d. column. The resulting temperature of the incoming mobile phase mixed with the volume of mobile phase in the column will be lower in the 3.0 mm i.d. column, because there is a smaller volume of mobile phase in the column and equilibrated to the column wall temperature. However, if the internal diameter was reduced further there should be an internal diameter at which most of the mobile phase contained in the column is in contact with the column wall and therefore equilibration of a colder mobile phase to the column wall temperature should be nearly instantaneous.

In order to test these conclusions, further experiments employing 2 mm i.d. columns packed with Purospher RP18 and Purospher RP18e stationary phase material were performed. The van Deemter curves for both stationary phase materials were plotted (Figure 61).

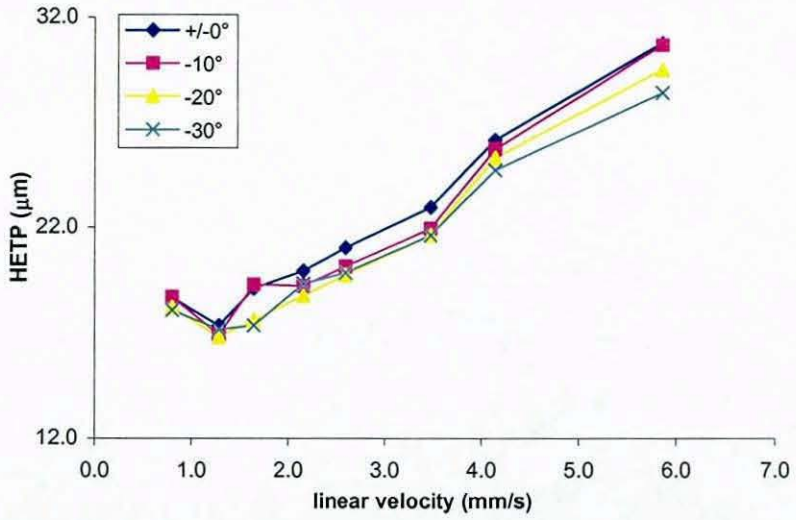

Figure 61A: Pursospher RP18e, 2mm i.d., 60 °C column wall

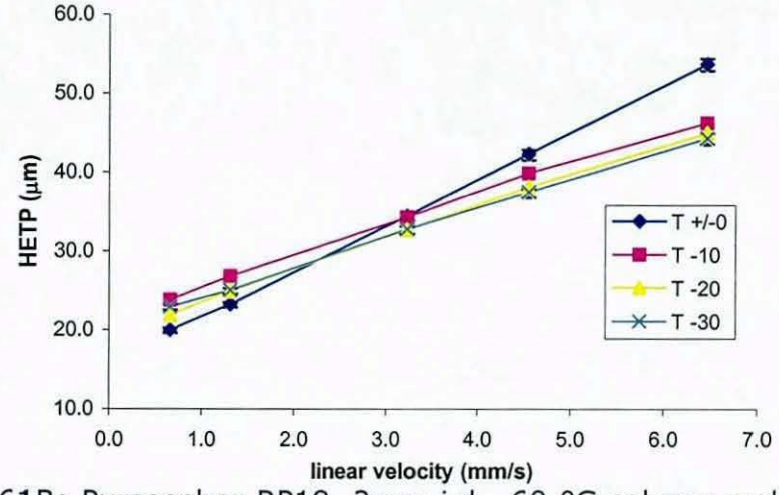

Figure 61B: Pursospher RP18, 2mm i.d., 60 °C column wall

Figure 61 A-B: van Deemter curves for butylbenzene at four mobile phase inlet temperature differentials, A: Purospher RP18e; B: Purospher RP18 125 x 2.0 mm i.d., mobile phase 75% methanol, 25% water (w/w), temperature 60 °C controlled in water bath.

There was still a small improvement of efficiency with introduction of the temperature differential. However, comparing the curves for the different temperature differential the difference in HETP were smaller than in the wider bore columns. Interestingly, both stationary phase materials showed an improvement in HETP with increasing temperature differential at high linear velocities. The extreme curvature observed in the van Deemter plots for the wider bore columns was not present any longer indicating radial equilibration.

Figure 62 A-B shows the change in selectivity with temperature differential. Similar to the wider bore columns the selectivity of the 2.0 mm i.d. columns changed with increasing linear flow. However, the difference in selectivity with inlet temperature differential at a given flow was insignificant in comparison to the 3.0, 4.0 and 4.6 mm i.d. columns.

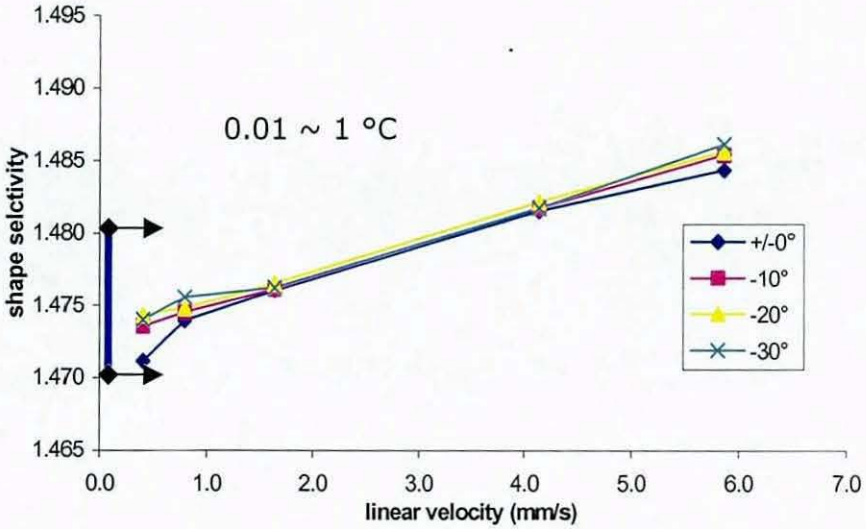

Figure 62A: Purospher RP18e, 2 mm i.d., 60 °C column wall

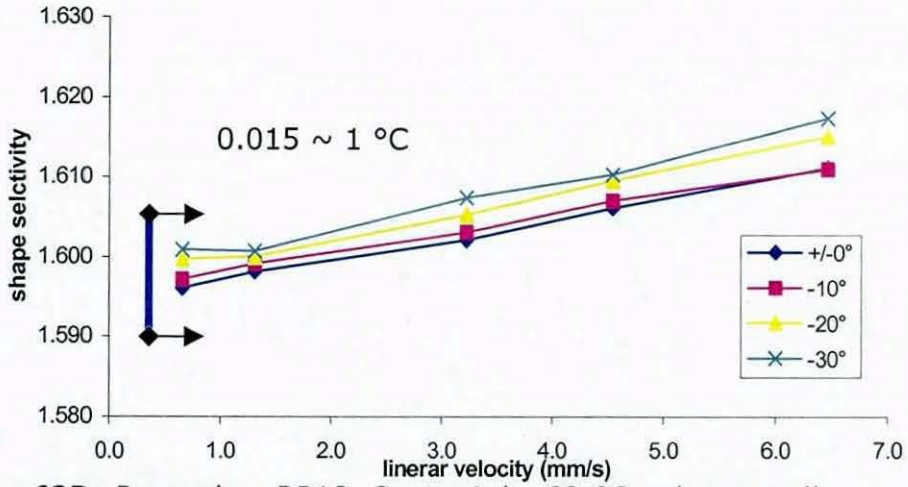

Figure 62B: Purospher RP18, 2 mm i.d., 60 °C column wall

Figure 62 A-B: Change of shape selectivity with linear flow velocity at four temperature differentials between, column wall and incoming mobile phase on A: Purospher RP18e B: Purospher RP18 at 60 °C column wall temperature for 125 x 2.0 mm i.d. columns.

The change in shape selectivity dependant on inlet temperature difference was indicative of a change in average column temperature of less than 0.5 °C.

Figure 63A-B illustrate the change of hydrophobicity with linear velocity at 4 different inlet temperature differentials.

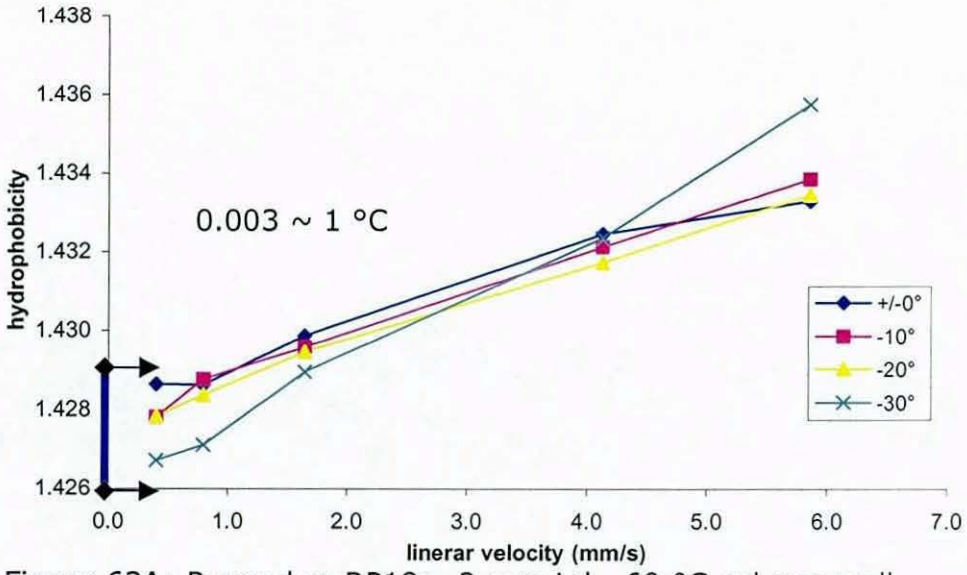

Figure 63A: Purospher RP18e, 2 mm i.d., 60 °C column wall

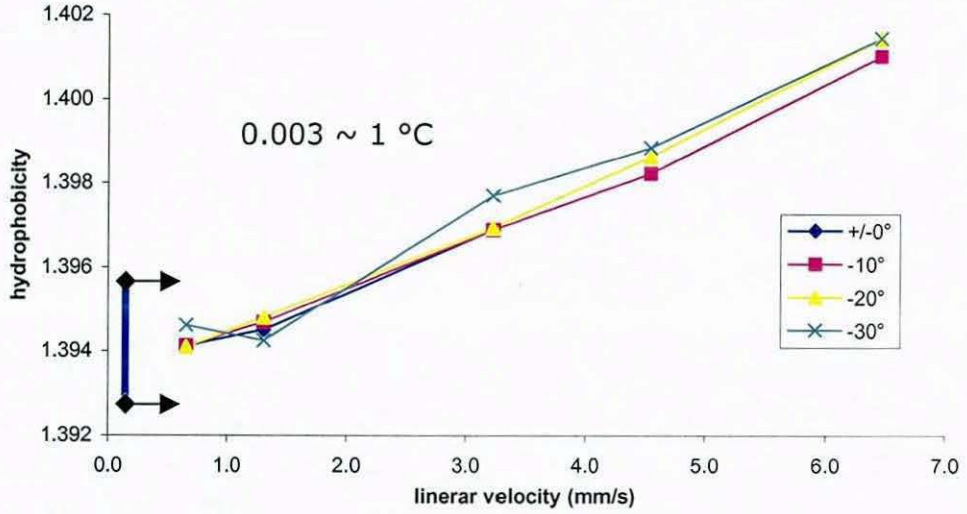

Figure 63B: Purospher RP18, 2 mm i.d., 60 °C column wall

Figure 63A-B: Change of hydrophobicity with linear flow velocity at four temperature differentials between, column wall and incoming mobile phase on A: Purospher RP18e B: Purospher RP18 at 60 °C column wall temperature for 125 x 2.0 mm i.d. columns.

The values calculated for the change in hydrophobicity at different inlet temperature differentials confirmed the results for the changes in shape selectivity. For the Purospher RP18e there was still a difference in hydrophobicity at high linear velocities indicating a change in average column temperature of about 1 °C. However, virtually no difference in hydrophobicity could be measured for the Purospher

RP18 2 mm i.d. column for all four mobile phase inlet temperature differentials.

A number of other narrow bore columns were examined (Figure 64) to give an overview of the change in plate number with inlet temperature differential for smaller bore separation columns.

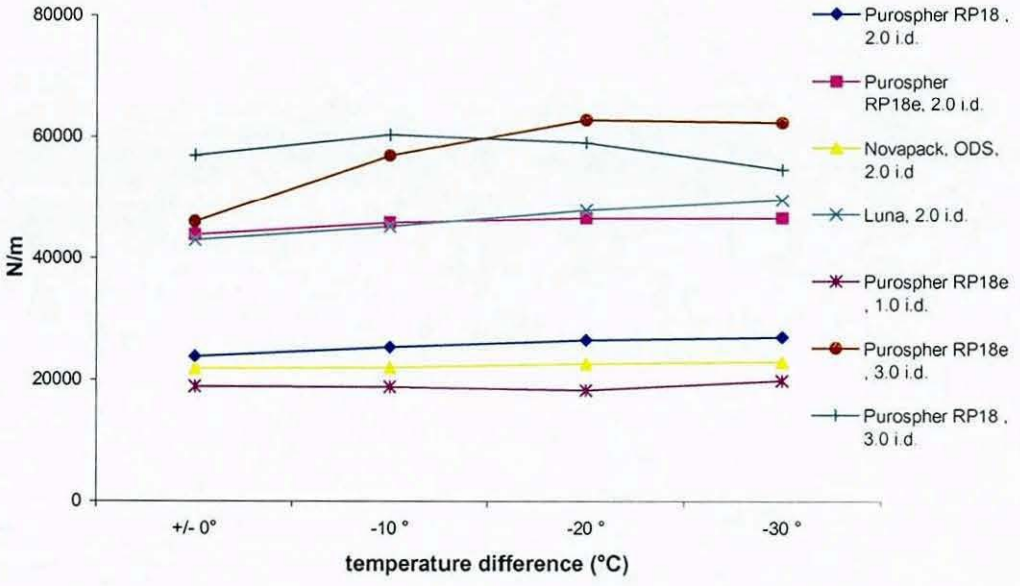

Figure 64: Comparison of plate numbers for butylbenzene on columns of different internal diameter at ~ 4 mm/s linear velocity, mobile phase inlet temperature difference +/-0 ° to -30 °, column temperature 60 °C.

A general but small trend of increasing plate numbers with increasing temperature differential could be observed. However, for the columns with an internal diameter less or equal to 2.0 mm the change in plate numbers was small. A significant change could only be observed at higher linear velocities.

Figure 65 shows a comparison of the Purospher RP18 and RP18e stationary phase materials packed in 2.0 and 3.0 mm i.d. columns at about ~ 6 mm/s linear velocity.

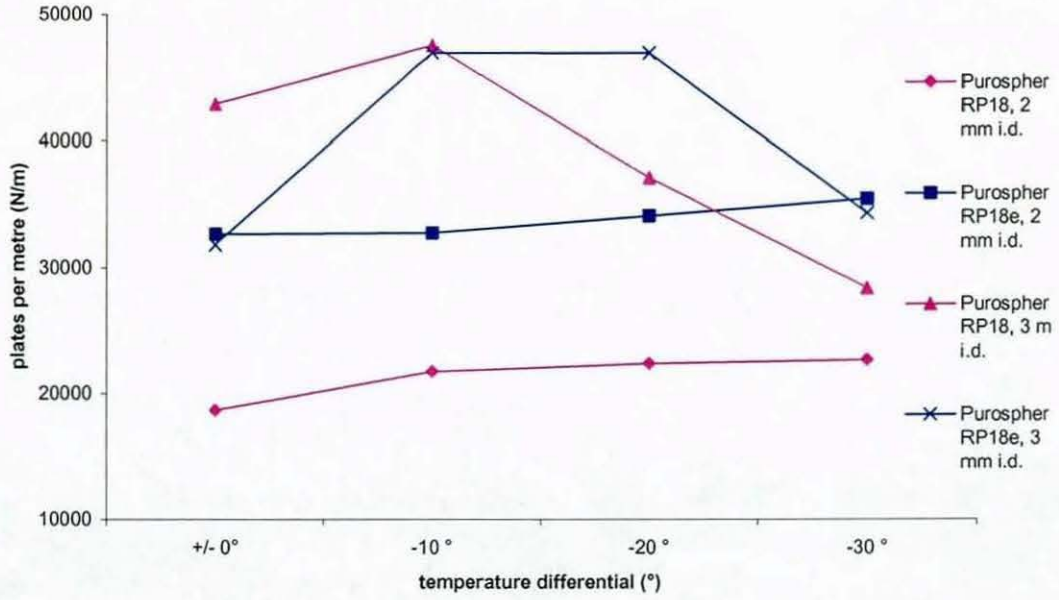

Figure 65: Comparison of plate numbers for butylbenzene on Purospher RP18 and RP18e columns, internal diameter 2.0 and 3.0 mm, at ~ 6mm/s linear velocity, mobile phase inlet temperature difference +/-0 ° to -30 °, column temperature 60 °C.

For the 3 mm i.d. columns at the higher mobile phase linear velocity there was initially an increase in plate numbers. However, after reaching an optimum at −10 °C temperature difference the plate number for the RP18e column reached a plateau and then decreased, the plate numbers for the RP18 column reached an optimum at −10 °C temperature differential and decreased without plateauing. On the other hand for the 2 mm i.d. columns a smaller but steady increase in plate numbers was observed with increasing temperature differential.

A second wall effect [95] is thought to affect a zone about 40 to 60 dp wide. For a column packed with 5 µm particle size stationary phase material this means that this zone could reach up to 0.3 mm into the bed. In a 4.6 mm i.d. column about 25% of the packed bed could be affected. For a narrower e.g. 3 mm i.d. column it could affect up to approximately 36% of the packed bed. This means that the proportion of the more densely packed zone is larger than in the wider bore column.

Taking into consideration the larger proportion of a more densely packed zone in a narrow bore column [95] and the higher inlet pressure (Table 5) when employing narrow bore columns the frictional heating in a smaller bore column is higher compared to a wider column. This could be the reason why the efficiency for both stationary phase materials, the Purospher RP18e and RP18 could be improved by introducing a temperature differential when smaller internal diameter columns were used.

5.3 Calculation of column efficiency

The number of theoretical plates for all the experiments above was calculated using the standard equation applied by the ASTM (American Society for Testing Materials) and in USP (United States Pharmacopoeia) and is the default method applied by the Chemstation® [137]. However, skewed peaks can show falsely high efficiencies when calculated with this method [159]. In order to make sure that the observed changes in efficiencies were not caused by an inappropriate calculation method, the statistical moments method was applied to a selected number of experiments. The statistical moments method is utilized to describe skewed peaks. It shows a smaller positive error in plate count when peaks are increasingly skewed [160, 161].

5.3.1 Comparison of ASTM/USP method and statistical moments method

The height equivalent of a theoretical plate was calculated for the EU C18 and the Prontosil columns via the statistical moments method and the ASTM/USP method. The values were compared to investigate whether the two methods resulted in significantly different plate height values (Figure 66 and Figure 67 A to D).

Each data point was calculated by averaging the data of three separate injections. The relative standard deviation of the calculated plate heights was determined. The standard deviation did not exceed 3% for any of the data points. The error bars indicate a relative standard deviation of 3%. The statistical moments method gave higher plate heights than the width at 50 % height method. However, the results for both calculation methods show the same trend. Both show a decrease in plate height with increasing temperature differential for the column packed with uncapped EU C18 material (Figure 66 A-D).

At equilibrated conditions the statistical moments method results in lower plate heights than the half width method. When a temperature differential is introduced the width at half height method results in lower plate heights than the statistical moments method. The differences in plate heights were larger with the early eluting peaks. However, the range of the coefficients of variation for all but one data point overlapped for all peaks. This leads to the conclusion that the difference in plate height caused by the choice of calculation method is not significant for this column.

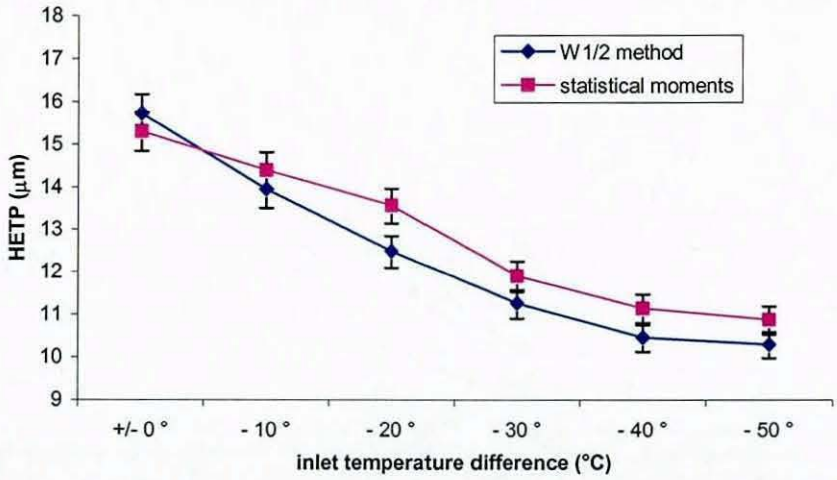

Figure 66 A: butylbenzene

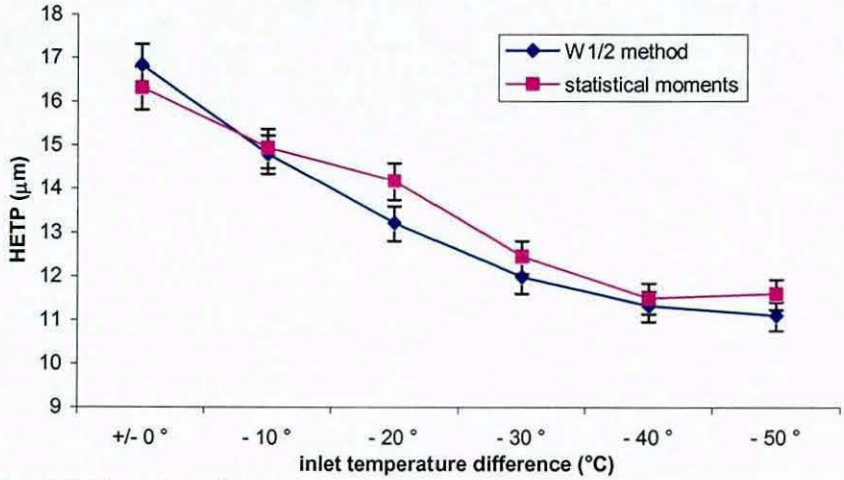

Figure 66 B: o-terphenyl

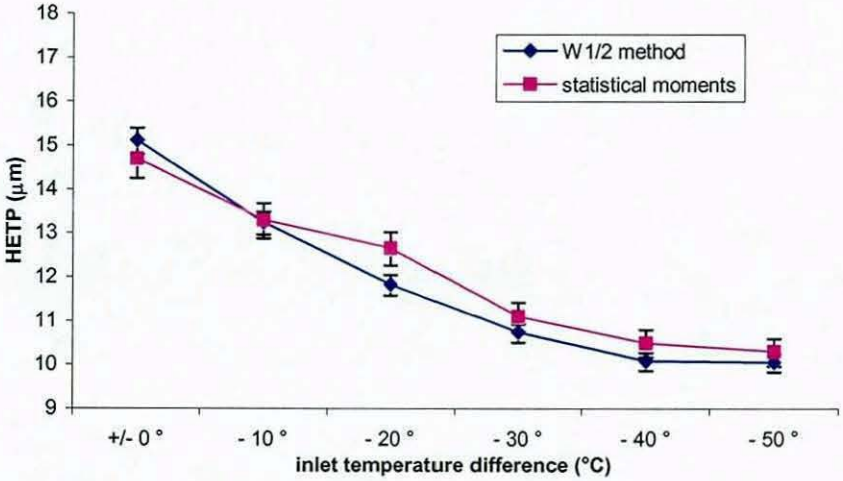

Figure 66 C: pentylbenzene

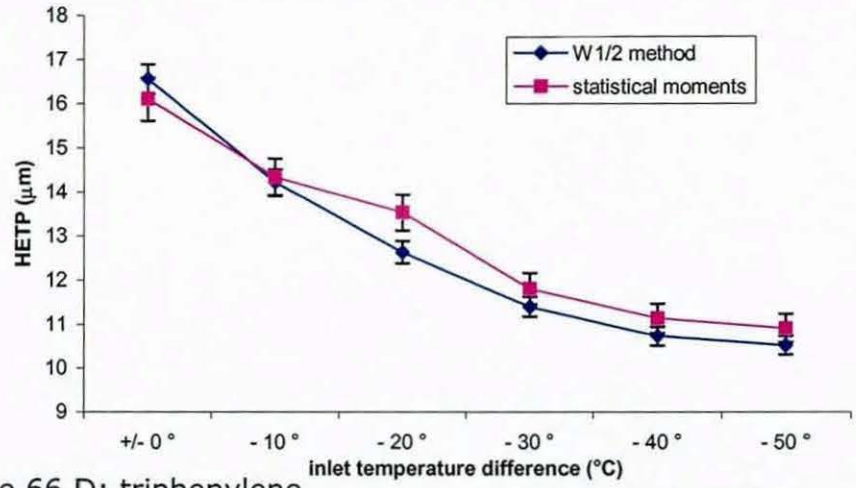

Figure 66 D: triphenylene

Figure 66 A-D: Height equivalent of a theoretical plate calculated applying the ASTM and the statistical moments method. Column C18 EU material, 150 x 4 mm i.d., column temperature 60 °C, mobile phase inlet temperature between 60 °C and 10 °C, flow rate 1.0 ml/min; error bars indicate 3% RSD.

The picture was different for the Prontosil column (Figure 67 A-D). There was a significant difference in plate height depending on the calculation method. Similarly to the results for the EU material the differences in plate heights were larger for the early eluting peaks. But in contrast to the EU column the plate heights increased when a temperature differential was introduced. The plate heights calculated applying the statistical moments method were significantly higher than the plate heights calculated utilizing the half height width method. However, the difference became less significant at larger temperature differentials. Furthermore, there was no significant difference between the results of the statistical moments method and the ASTM method for the late eluting peaks at large temperature differences between column temperature and mobile phase inlet temperature.

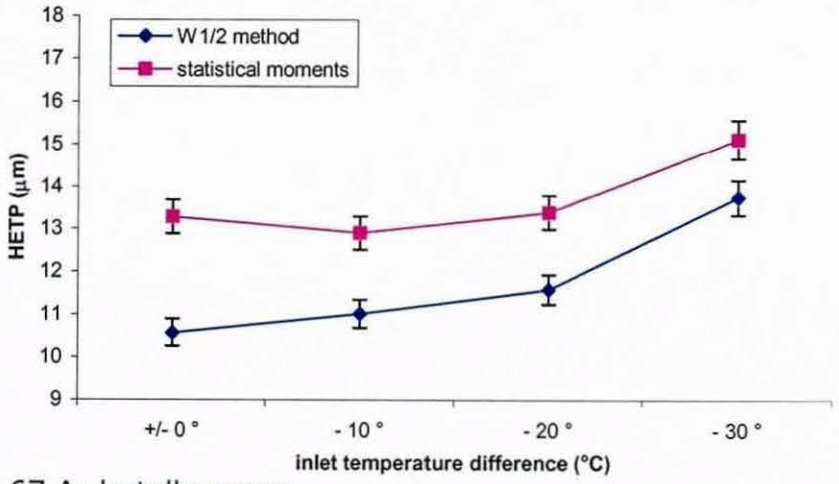

Figure 67 A: butylbenzene

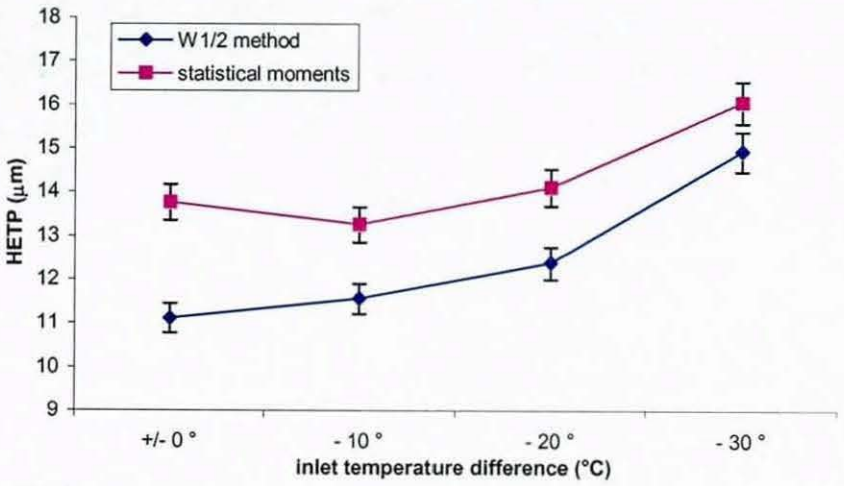

Figure 67 B: o-terphenyl

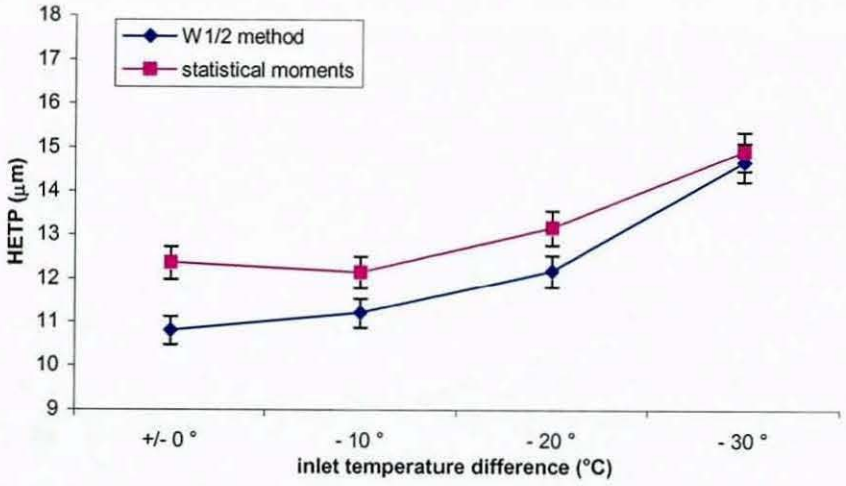

Figure 67 C: pentylbenzene

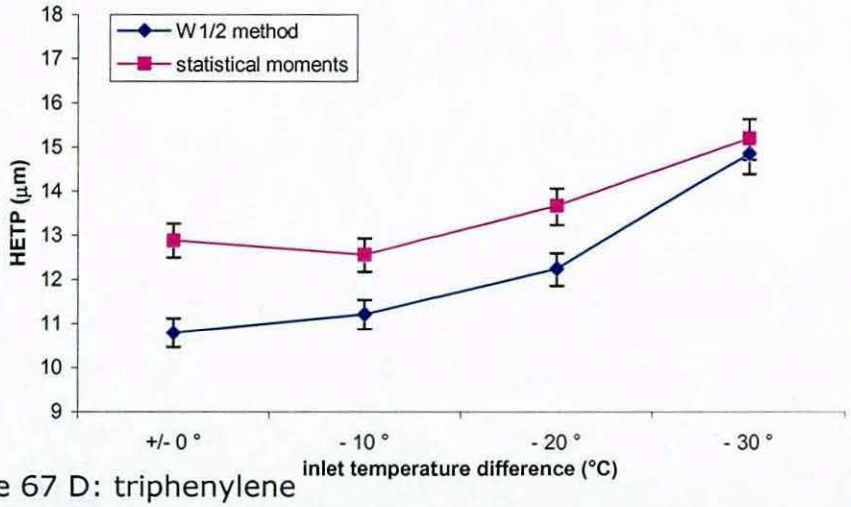

Figure 67 D: triphenylene

Figure 67 A-D: Height equivalent of a theoretical plate calculated applying the ASTM and the statistical moments method. Column Prontosil C18 material, 150 x 4 mm i.d., column temperature 60 °C, mobile phase inlet temperature between 60 °C and 30 °C, flow rate 1.0 ml/min; error bars indicate 3% RSD.

The assumption that peaks would be more skewed due to the introduction of a temperature differential between column and mobile phase, which should show up in higher moments could not be confirmed. The difference between plate heights calculated by applying the statistical moments method and the ASTM method was expected to increase with the introduction of a temperature differential values. However, the difference decreased (Figure 67 A-D). This points to an improvement in peak symmetry with the introduction of a temperature differential between column wall and mobile phase.

5.3.2 Peak symmetry

To investigate whether there was an improvement in peak symmetry when a temperature differential was introduced the USP tailing and the skew values of the first eluting peak and the last eluting peak of the test mix were plotted verses the temperature differential.

The peaks eluting from the EU column were tailing at equilibrated conditions. The tailing was slightly reduced when the temperature

differential between column and mobile phase inlet was increased (Figure 68A-B).

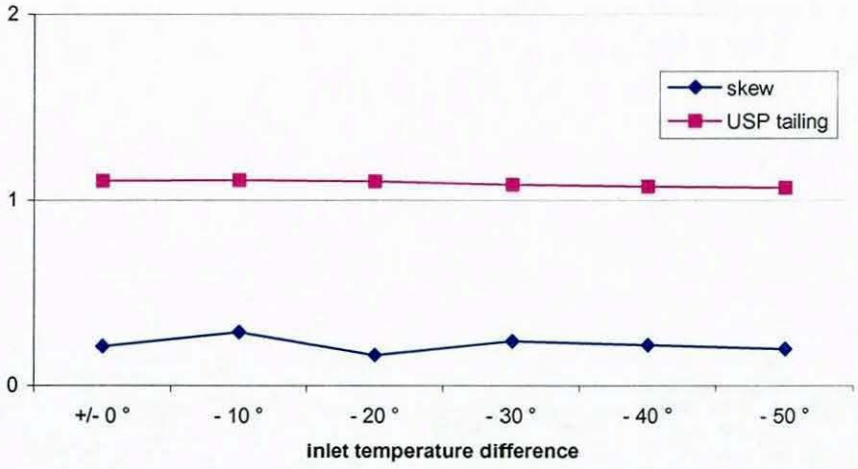

Figure 68A: butylbenzene

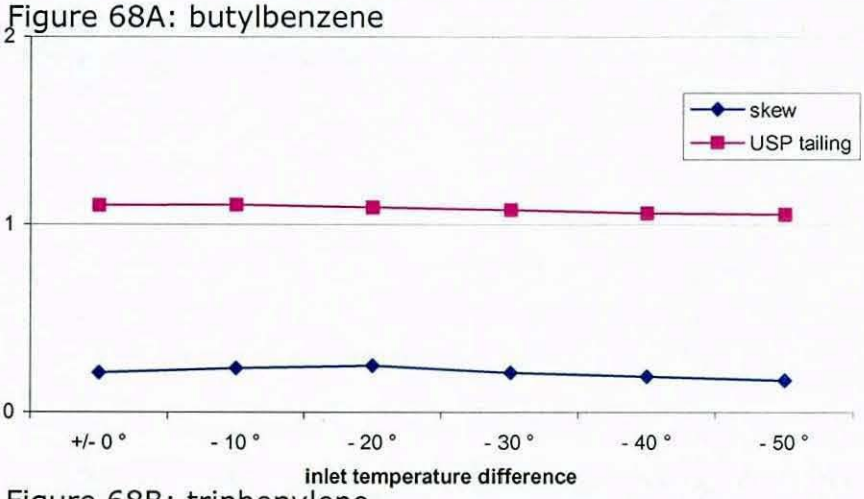

Figure 68B: triphenylene

Figure 68A-B: Peak skew and tailing (USP) of A butylbenzene and B triphenylene peak on EU column at different mobile phase inlet temperatures, column wall temperature 60 °C controlled in water bath, flow rate 1 ml/min.

Similarly on the Prontosil C18 column the peaks showed tailing at equilibrated conditions. However, the peak tailing was significantly reduced when the temperature of the incoming mobile phase was reduced (Figure 69). This change in peak tailing and skew confirms the changes in efficiency calculated employing the statistical moments equation. The difference between efficiency calculated using the ASTM/USP method and the statistical moments method was insignificant at large temperature differentials because the peaks were more symmetrical at higher temperature differentials, which results in

smaller positive error for the plate number calculated using the ASTM/USP method [159].

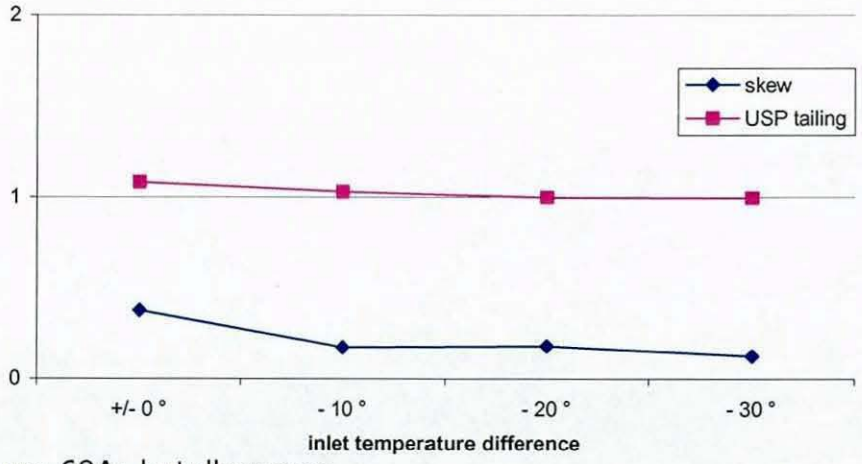

Figure 69A: butylbenzene

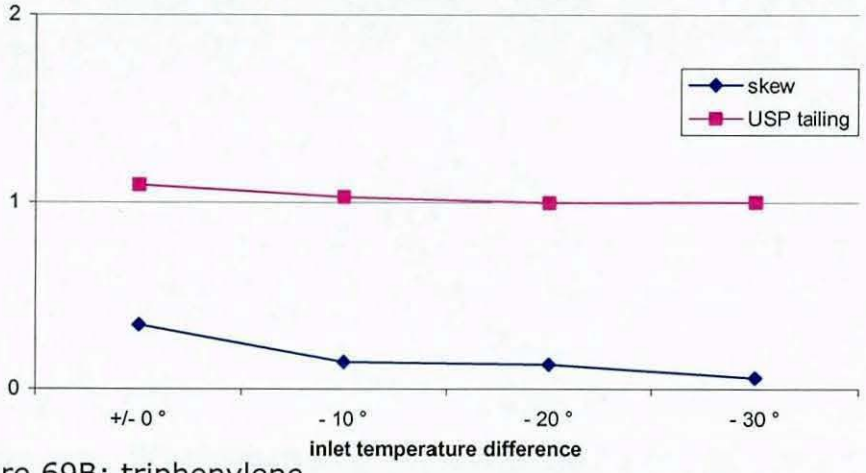

Figure 69B: triphenylene

Figure 69 A-B: Peak skew and tailing (USP) of A butylbenzene and B triphenylene peak on Prontosil column at different mobile phase inlet temperatures, column wall temperature 60 °C controlled in water bath, flow rate 1 ml/min.

Therefore, increasingly tailing or skewed peaks did not cause a significant positive error in the plate height calculations for the columns. The changes in efficiency observed during the investigation of the effect of the mobile phase inlet temperature were real and not caused by a positive error due to application of the ASTM equation.

The change in peak symmetry with the inlet temperature differential was recorded for all columns used for the study. For ease of

application, calculations were performed applying the Chemstation software package. The peak symmetry was calculated as a pseudo-moment as opposed to the USP method applied earlier in this work using the moments equations.

The two most efficient columns in the study, the Chromolith and the Hypersil HiPurity showed improved efficiency when the mobile phase inlet temperature was adjusted below column wall temperature. The peak symmetry steadily improved with increasing temperature differential between mobile phase and column (Figure 70).

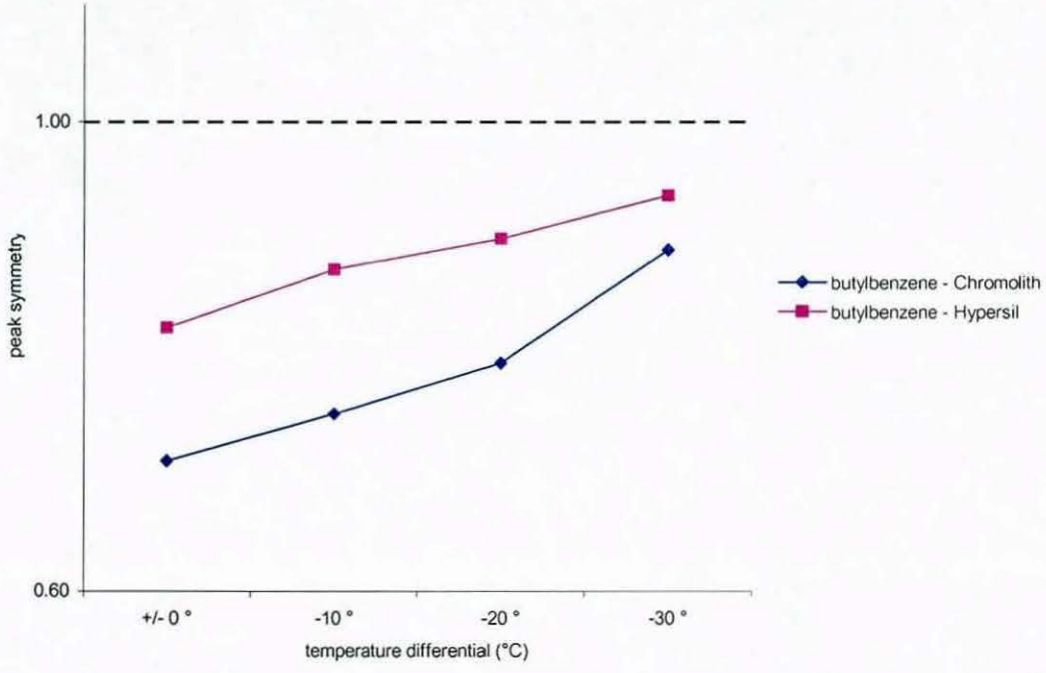

Figure 70: Peak symmetry on Hypersil HiPurity and Chromolith column at equilibrated conditions and temperature differential conditions.

Dropping the mobile phase inlet temperature relative to the column temperature steadily improved the peak symmetry, however, the overall efficiency of these two columns reached its optimum at a temperature differential of –10 °C (Appendix E).

The slightly less efficient Purospher RP18e did show an improvement in optimum column efficiency of about 2000 plates by introducing a

temperature difference when the column was held at 40 °C (Appendix F). However, this cannot be observed at 60 °C column temperature (Appendix E). Neither was there any improvement observed for the Prontosil and Kromasil columns. However, the initial peak symmetry calculated for butylbenzene on these columns (Figure 70) was significantly higher than the peak symmetry calculated for the Hypersil HiPurity and the Chromolith column (Figure 71). The slightly tailing butylbenzene peak at equilibrated conditions was turned into a fronting peak when the temperature differential was introduced. Comparison with the earlier calculated peak symmetry for the Prontosil column applying USP tailing and skew (chapter 4 Peak symmetry) shows that the results of all three methods are equivalent.

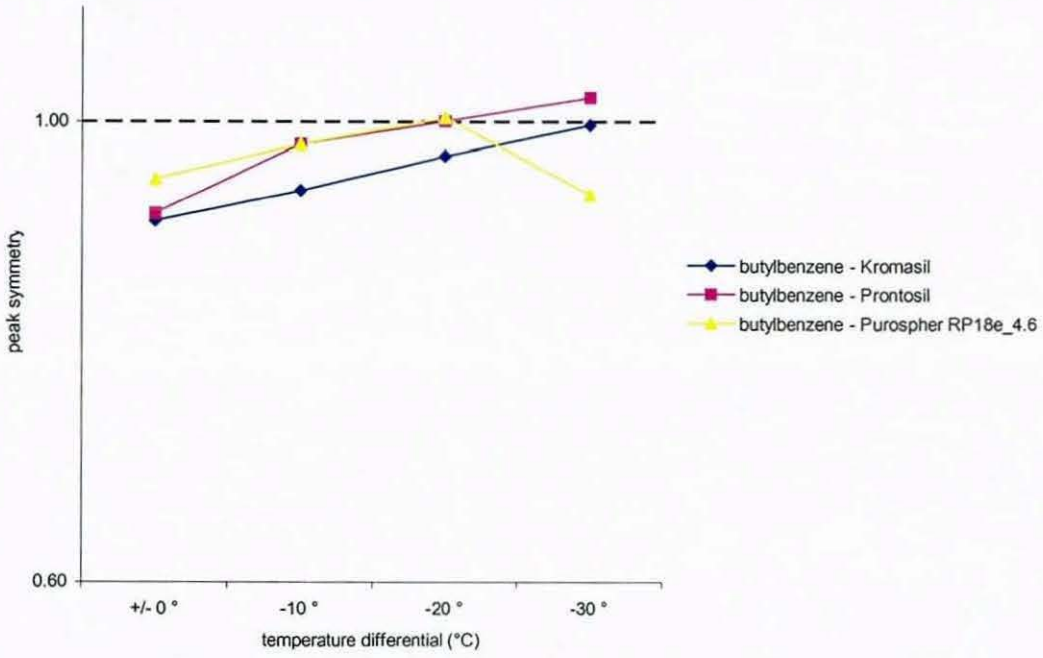

Figure 71: Peak symmetry on Prontosil, Kromasil and Purospher RP18e column at equilibrated conditions and temperature differential conditions.

The even less efficient Purospher RP18 and Symmetry columns did show improvement in column efficiency when introducing a temperature difference at both 40 °C and 60 °C column temperature (Appendix E). At 60 °C both columns reached an optimum in column

efficiency with a temperature difference of -20 °C between mobile phase and column. The initial peak symmetry for the butylbenzene peak on these columns was slightly higher than on the Hypersil HiPurity and the Chromolith columns (Figure 72).

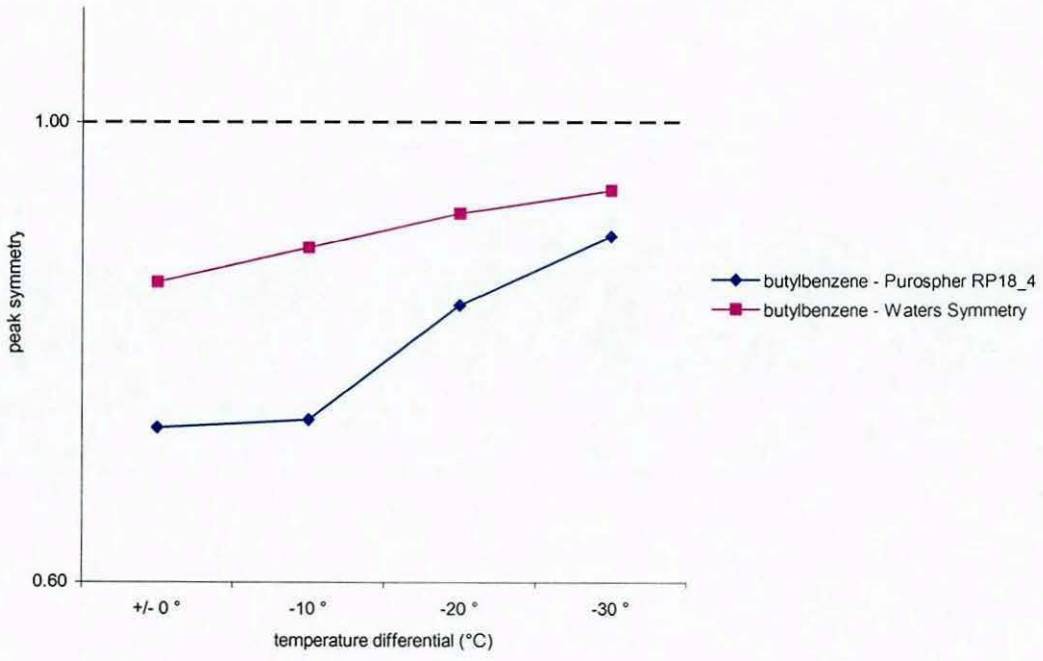

Figure 72: Peak symmetry on Waters Symmetry and Purospher RP18 column at equilibrated conditions and temperature differential conditions.

The least efficient column, the EU ODS column, showed constant increase in efficiency with increasing temperature difference. The observed change in peak symmetry for the butylbenzene peak eluting from the EU ODS column was less significant than for any of the other columns tested (Figure 73).

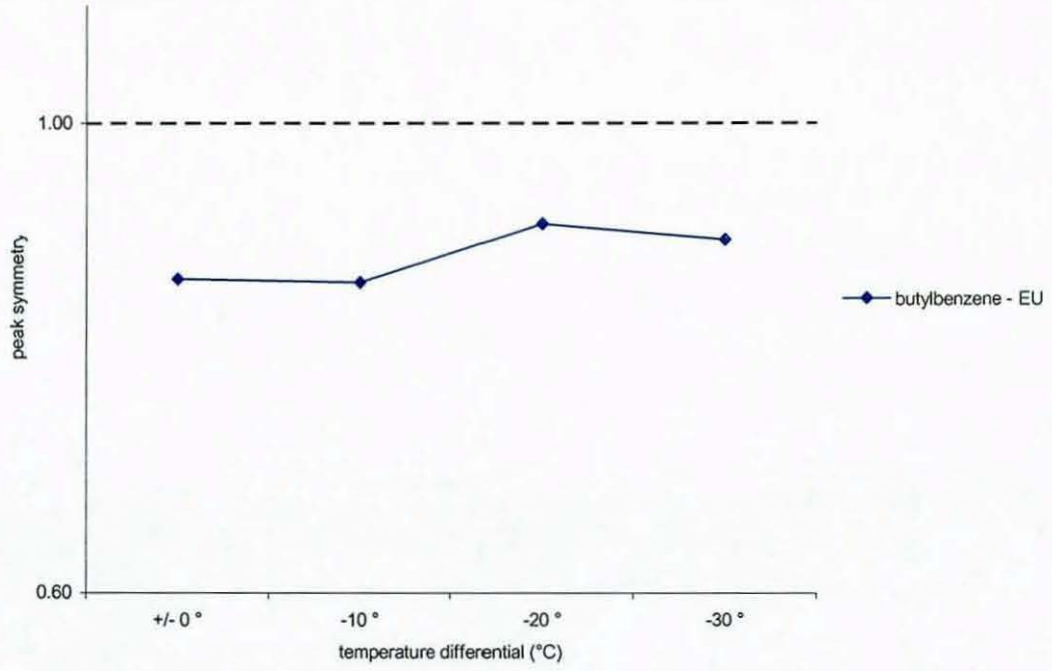

Figure 73: Peak symmetry on EU ODS column at equilibrated conditions and temperature differential conditions.

Comparing the changes in peak symmetry for all columns of around 4 mm internal diameter (Table 6) and linking it with the efficiency data (Appendix E) it appears that the optimum efficiency of a separation column is achieved when the peak symmetry approaches the value of 0.90.

Table 6: Overview of peak symmetry at equilibrated conditions and temperature differential conditions. All columns but Purospher RP18 are 150 mm long. Purospher RP-18 column length = 125 mm.

	Chromolith	EU	Hypersil	Kromasil	Prontosil	Purospher RP18	Purospher RP18e	Waters Symmetry
mm i.d.	4.0	4.0	4.6	4.6	4.0	4.0	4.6	3.9
+/- 0 °	0.71	0.87	0.82	0.91	0.92	0.73	0.95	0.86
-10 °	0.75	0.86	0.87	0.94	0.98	0.74	0.98	0.89
-20 °	0.79	0.91	0.90	0.97	**1.00**	0.84	**1.00**	0.92
-30 °	0.89	0.90	0.94	**1.00**	**1.02**	0.90	0.94	0.94

Looking at the changes in peak symmetry for butylbenzene on the smaller bore columns a significant change in peak symmetry was only observed for the Purospher RP18 column of 3 mm i.d. (Figure 74). The Purospher RP18 was the column showing the largest change in

peak symmetry for the wider bore columns as well (compare Table 6 and Table 7).

Table 7 Overview of peak symmetry at equilibrated conditions and temperature differential conditions. All columns but Luna and Novapack are 125 mm long. Luna and Novapack column length = 150 mm.

	Luna	Novapack	Purospher RP18	RP18	Purospher RP18e	RP18e	RP18e
mm i.d.	2.0	2.0	3.0	2.0	3.0	2.0	1.0
+/- 0 °	0.80	0.75	0.73	0.86	0.89	0.85	0.77
-10 °	0.81	0.76	0.77	0.84	0.87	0.86	0.77
-20 °	0.80	0.76	0.82	0.85	0.87	0.86	0.78
-30 °	0.81	0.76	0.86	0.86	0.88	0.85	0.77

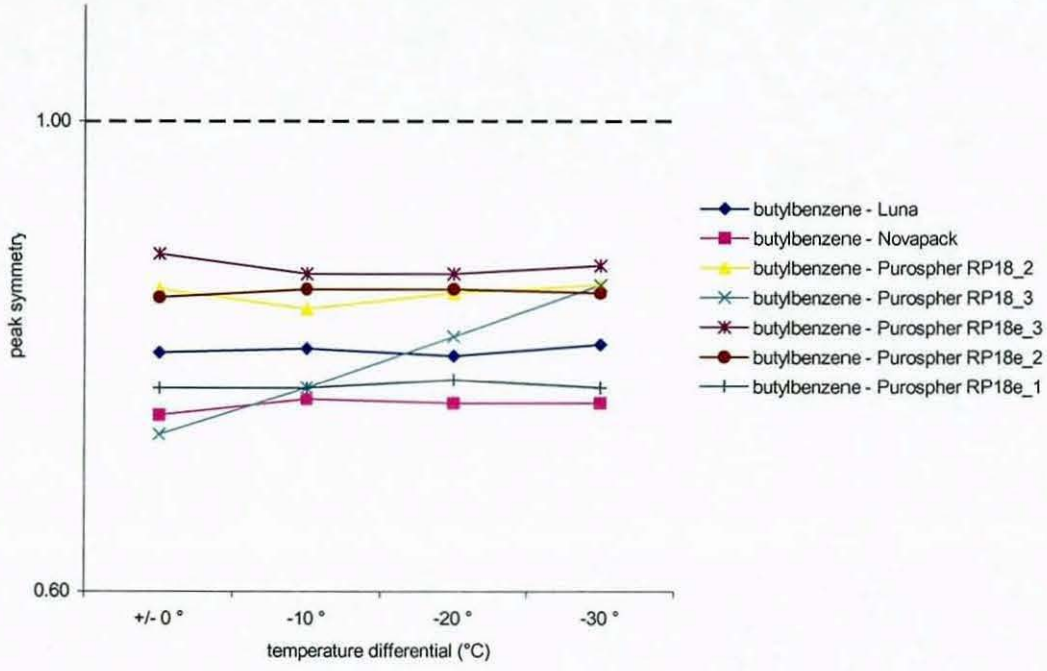

Figure 74: Change of peak symmetry for butylbenzene dependant on the temperature differential on various columns with internal diameters between 3.0 mm and 1.0 mm at ~ 0.4 cm/s linear velocity.

The peaks eluting from the 3 mm i.d. RP18e are less symmetrical compared to the RP18e 4.6 mm i.d. (Figure 71) and the plate count for the 3 mm i.d. column is not as high as for the 4.6 mm i.d. column (Appendix E). However, there is a significant improvement in efficiency for the 3 mm i.d. Purospher RP18e column with increasing temperature differential as opposed to the wider bore 4.6 mm i.d. RP18e column.

The results of this study confirm that it is feasible to improve the peak symmetry by lowering the mobile phase inlet temperature. However, an improvement in peak symmetry did not always result in improved overall column efficiency.

6 CONCLUSIONS AND FURTHER WORK

The capabilities of elevated temperature reversed phase chromatography have been investigated. It was shown that elevating the separation temperature could improve the separation efficiency and reduce analysis times. However, the dead volume of the chromatography system should be minimised as the impact of extra column band broadening on the overall efficiency is increased as retention times decrease.

The type of heater used for elevated temperature chromatography was shown to have an impact on the efficiency and selectivity of a separation column. Therefore, in method development and method transfer the type of heater used should always be stated.

When using a block heater or any sort of heater the actual temperature inside the oven and its variations over time should always be measured with a thermometer or a calibrated thermocouple. The shape selectivity and hydrophobicity at a defined flow rate (back-pressure), measured with the Tanaka test, of a separation column proved to be a good indicator for the effective average column temperature. However, the pressure dependence of k made it difficult to estimate the change of average column temperature with flow rate. Further work needs to be carried out to investigate the change of retention factor with pressure in order to be able to use the shape selectivity of a separation column to estimate the dependence of the average column temperature on flow rate.

The accuracy of the column temperature has a significant impact on the reproducibility of the separation. Therefore, in order to ensure successful method transfer between laboratories it is proposed that the shape selectivity and hydrophobicity of a column is compared when a method is transferred rather than the nominal temperature

adjustment. Ideally this comparison is performed using the same stationary phase material. The EU column used in this study was a trial column, which has now been developed into a reference material. This means that its properties like shape selectivity and hydrophobicity were measured under rigidly controlled conditions. It allows the comparison of the accuracy of the settings of different instruments and is a valuable tool for method transfer [145].

The causes of the changes in column efficiency when lowering the mobile phase inlet temperature below the column wall temperature are not entirely clear. Generalised recommendations for the optimisation of separation performance could not be formulated. The earlier suggestion of formation of an inverted flow profile [109, 111], negating the band broadening effect of a parabolic flow profile caused by frictional heating does not fully explain the observed phenomena.

The band shape of compounds eluting from a separation column depends on various factors. Frictional heating [111] and radial and axial dispersion influence the band shape [89]. Axial dispersion [89], flow velocity [85, 88], packing density [84, 87] and packing quality [82, 83] vary with radial position of the injected compound in the column. The conclusions drawn from this work are as such; rather the in-homogeneity of column beds than the type of stationary phase material may be responsible for the observed changes in column efficiency when lowering the mobile phase inlet temperature below the column wall temperature. The inlet system (column frits) and analytes may also play an important part in the distribution of the sample plug [162, 163].

We normally consider a more efficient column to be more homogenously packed. Therefore the radial variation of packing density should be less significant while the viscosity gradient due to frictional heat dissipation will remain unchanged. Hence for very efficient columns only the frictional heat dissipation has to be counter-balanced with the introduction of a small temperature differential.

This results in improved peak symmetry. If the column is not homogenously packed the effect of a gradient of the packing density adds to the viscosity gradient due to frictional heating. Furthermore, the increased packing density has a detrimental effect on the diffusion rate of the solutes, which can cause peak tailing [93, 94]. Hence a larger temperature gradient between mobile phase inlet temperature and column wall temperature is required to counter balance the distortion of the elution profile.

The effect of the introduction of a temperature gradient between mobile phase inlet and column wall may be a good indication of the homogeneity of the column bed. Further work needs to be carried out to quantify the interrelationship of the packing in-homogeneity and the temperature differential. However, if this relationship can be quantified the temperature differential required to optimise the elution profile of solutes can potentially be applied as an inexpensive means to investigate reproducibility of a column packing process.

7 ELEVATED TEMPERATURE AND SUPERHEATED WATER CHROMATOGRAPHY

7.1 Introduction

As mentioned earlier in this work, a number of elevated temperature chromatography methods have been developed in recent years and their drawbacks and advantages have been investigated and reviewed [58].

A special variation of elevated temperature chromatography is the superheated water chromatography [14, 15]. Superheated water chromatography makes use of the lower dielectric constant of water at higher temperatures [10], which makes it possible to run reversed phase separations with 100 % aqueous mobile phase. A number of applications have been developed in recent years [13, 18, 152], including the separation of pharmaceuticals [34, 164, 165], natural product separations [166] and extractions with superheated water [19, 167]. A comprehensive review on superheated water extractions has recently been published [168].

This chapter gives an overview of previously conducted and ongoing studies on superheated water and elevated temperature chromatography and advances in instrumentation.

7.2 Chromatographic Hardware

7.2.1 Tubing, fittings and frits

In conventional chromatography, little care needs to be taken whether the hardware is stable at high temperatures, as usually temperatures range from ambient to about 40 °C. Because of its ease of use the

application of polyetheretherketone (PEEK) tubing and PEEK finger tight fittings is widespread. However, the application of temperatures of up to 250 °C puts higher demands on the temperature stability of the tubing and fittings. Furthermore, the mobile phase entering the column needs to be controlled to avoid band broadening due to temperature mismatch. PEEK is a very poor heat conductor and is not stable above 150 °C. It is therefore not suitable for high temperature chromatography.

Stainless steel tubing, ferrules and nuts should be employed instead of PEEK. The thermal conductivity and stability of stainless steel are considerably higher. As an alternative for the PEEK finger tight fittings, stainless steel capillaries with stainless steel finger tight nuts and graphitised ferrules such as Secure-Fit™ specialist high temperature HPLC fittings could be used [169]. Furthermore, the use of Slipfree™ connectors usually used in SFC is possible.

Furthermore, the actual column hardware can create problems at elevated temperatures. E.g. the polymeric cladding of a Chromolith silica monolith is only stable up to about 60 °C. Moreover, sometimes PEEK encapsulated frits are used even for columns packed with temperature stable materials. PEEK encapsulated frits can also be found in a range of pre-columns and pre-column filters. Ideally the frits should be made of stainless steel and not be PEEK encapsulated. However, because of the high porosity and therefore large surface area of the frits even stainless steel frits can be oxidised in superheated water [170]. Particles of rust can contaminate the column bed. Titanium frits could be used as an alternative to stainless steel.

7.2.2 Column ovens

Most commercially available HPLC ovens are not capable of being heated to temperatures above 80 °C. Some Peltier elements possess inadequate insulation and therefore poor temperature control or do not facilitate temperature control of the mobile phase. Furthermore, for temperature programming the oven needs to be capable of rapidly returning to the starting conditions of a program. This is impossible with a Peltier element and commercially available HPLC fan ovens rarely possess cooling capability.

For high temperature liquid chromatography a GC oven seems the ideal alternative to a standard HPLC oven [130]. A GC oven, a fan driven circulating air bath has a good distribution of heat in the oven cavity, can be heated to temperatures well above 250 °C and is capable of running temperature gradients, and rapidly returning to the programme's starting conditions.

A specialised high temperature HPLC oven is the Series 8000 HPLC oven (Selerity Technologies, Salt Lake City, USA). It can run temperature isothermally or gradients up to 200 °C [171]. This type of temperature programme could also be run using a GC oven [172]. However, the advantage of specialised equipment like the Series 8000 HPLC oven is the minimised extra column dead volume. To equilibrate the incoming mobile phase to column temperature a low-volume, low thermal mass solvent pre-heater is used [Figure 75]. At the column outlet a Peltier element cools the effluent to a constant temperature. This set-up allows the use of most HPLC detectors [151].

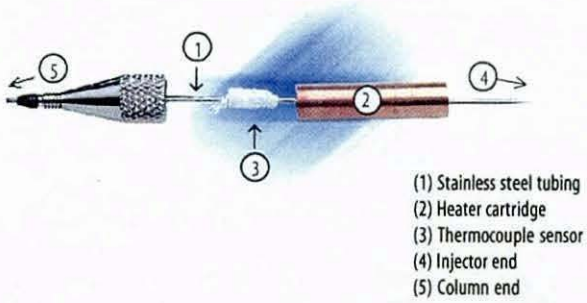

Figure 75: Design of the Selerity Technologies solvent pre-heater. Picture taken from reference [173].

7.2.3 Detectors

Virtually all HPLC detectors can be employed with superheated water chromatography. With efficient temperature control for the effluent in place even refractive index detection could be utilized. Superheated water chromatography lends itself to the application of flame ionisation detection (FID) in liquid chromatography. Among only a few other compounds, water does not create a significant FID detector response [174]. Using superheated water as the mobile phase facilitates therefore the use of the most popular universal GC detector in HPLC and several researchers have worked on its realisation [14, 172, 175-177]. Extensive effort has been put into the development of the HPLC-detector interface and a patent on this interface is pending [178].

Furthermore, the use of superheated water chromatography is advantageous in LC-NMR. Water can be substituted by deuterium oxide. As deuterium oxide does not generate an H-NMR response it is not necessary to perform any solvent suppression procedures. The whole spectrum can be used for compound characterisation as opposed to ordinary LC-NMR where part of the spectrum is swamped by the solvent's signals. A number of applications have been developed and published [166, 179-182] and further examples are given in this thesis.

7.2.4 Columns for high temperature RP-LC

At elevated temperatures special attention has to be paid to the stationary phase materials employed. Bonded phases are very susceptible to hydrolytic cleavage of the Si-OR bonds [183].

In addition to the cleavage of the bonded phase from the support the silica backbone can be easily degraded at higher temperatures. The solubility of silica increases linearly with temperature and increases exponentially with pH [184]. For monosilicic acid $Si(OH)_4$ it is about 100 ppm at room temperature in a pH range of 1-9 [185]. At the pH range above 9 the solubility increases exponentially due to the formation of silicate ions in addition to monosilicic acid. At basic pH hydroxyl ions are chemisorbed onto the silica surface. This weakens the oxygen bonds to the underlying silicon and silicon goes into solution as silicate ion [186][Figure 76].

$$SiO_2 + H_2O \xleftarrow{OH^-} Si(OH)_4$$
$$Si(OH)_4 + OH^- \leftrightarrow [Si(OH)_5]^-$$

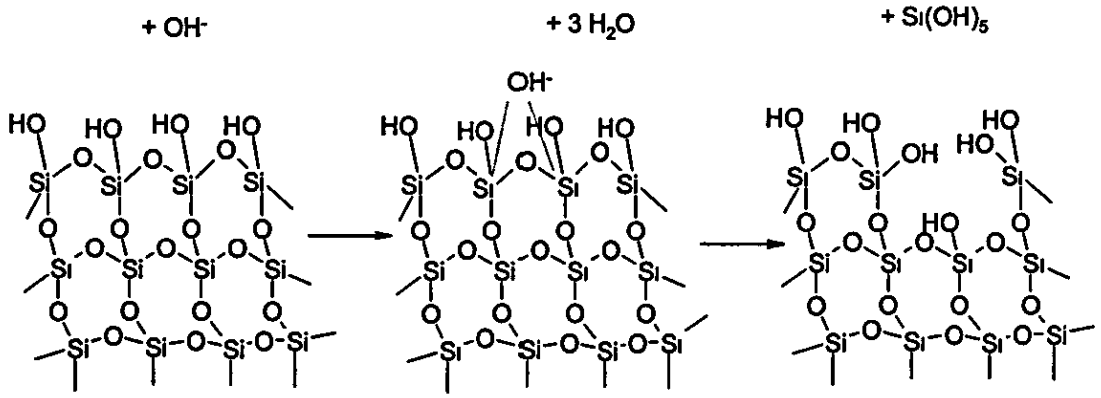

Figure 76: Mechanism of silica dissolution as proposed by Iler [186].

Furthermore, the rate of hydrolysis increases with decreasing silica particle size [187]. Hence, the performance of silica based stationary phase material with small particle size may degrade very quickly at elevated temperatures.

A variety of stationary phase materials with improved temperature stability have been developed over recent years [188]. Stablebond stationary phases [140] and polydentate bonded stationary phases [189], which are sterically protected silica based column materials were reported to be stable up to 100 °C and extreme pH for extended periods of time. About 30 % of silanol groups are replaced by methyl groups during synthesis of the XTerra phase [190] resulting in a hybrid (inorganic/organic) particle, which can be operated at elevated temperature and pH. Furthermore, zirconia based stationary phase materials offer significantly improved temperature stability [191]. Li and Carr performed several studies to investigate the selectivity and stability of polybutadiene coated Zirconia in comparison to silica based reversed phase materials [192-195].

Reversed phase material will often exhibit decreasing solute retention when highly aqueous mobile phases are employed. The loss in retention is often attributed to a chain collapse of the bonded phase [196]. However, recent studies point to a de-wetting of the pores of the stationary phase as the reason for loss of retention [197]. It was found that retention on a column, which had been used with 100% aqueous mobile phase, could be regenerated by washing the column with high percentage of organic modifier [198].

A different concept of tuning selectivity with temperature has been realised with temperature responsive stationary phases. Silica based phases have been coated with poly(N-isopropylacrylamide) (PIPAAm) to develop these temperature responsive stationary phases [199, 200]. They show hydrophilic properties at lower temperatures and are increasingly hydrophobic at higher temperatures. The retention of hydrophobic compounds on these temperature responsive stationary phases increases when the separation temperature is increased.

Another temperature stable alternative to silica based reversed phase stationary phase materials are polymer stationary phases like the polystyrene divinylbenzene phase (such as PLRP-S). However, extremely high retention times and broad, tailing peaks due to sorption into the polymer matrix have been reported for these stationary phase materials [201].

7.3 Compound stability

Liquid chromatography at elevated temperatures and superheated water chromatography does not only put the demand for increased temperature stability on the chromatographic hardware but also on the analytes. Analytes have to be stable at elevated temperatures and should not be susceptible to hydrolysis and oxidation. A number of compounds, e.g. anilines, phenols and ketones [202] have been found to oxidise under superheated water conditions. However, even temperature labile compounds can potentially be analysed at elevated temperatures if the analysis is fast and hence residence time for the compounds on column is short [203, 204]. Thomson and Carr [205] investigated criteria for the analyte stability in elevated temperature chromatography. They employed the Damkoehler number as a measure as to whether a compound can be analysed at elevated temperatures. The Damkoehler number is the ratio of the compound's residence time on column and the reaction time of the respective reaction (Equation 28),

Equation 28

$$Da = \frac{kL(1+k_R)}{u_0}$$

where k is the reaction rate, L is the length of the column, k_R is the retention time and u_0 the linear velocity of the mobile phase. If there is no reaction (Da <<1) or very fast reaction (Da > 50) single peaks are expected. At intermediate Damkoehler numbers a distortion of the peak profile or even the presence of two peaks is expected.

A good example for the relationship of reaction rate and residence time is the decomposition of dicumyl peroxide (Figure 77) [204].

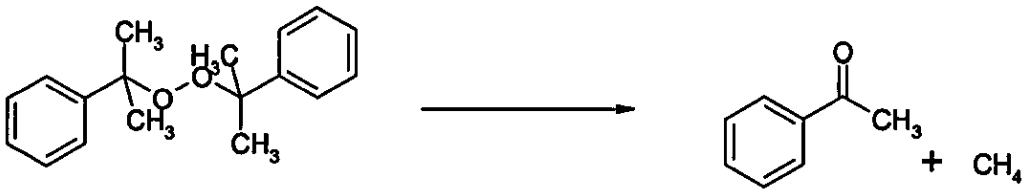

Figure 77: Decomposition of dicumylperoxide to acetophenone and methane.

Only one peak, dicumylperoxide, is detected when the compound is not decomposed on the column. Two peaks, one for dicumylperoxide and one for acetophenone, are detected when the residence time is too long and/or the temperature of the separation column is too high.

7.4 Aim of the present study

A number of elevated temperature liquid chromatography methods were developed to prove the concept of the application of temperature as an optimisation parameter in reversed phase liquid chromatography. Examples are given for the optimisation of the separation selectivity using temperature as the optimisation parameter and for employing high temperature to substitute organic solvent.

Furthermore, to show the feasibility of hyphenation of high temperature liquid chromatography with spectroscopic techniques such as, mass spectroscopy (MS) and nuclear magnetic resonance (NMR).

8 EXPERIMENTAL

In this chapter general experimental detail, equipment and chemicals are described for elevated temperature and superheated water reversed phase chromatography applications.

8.1 Materials

Water was deionised and purified (ELGA Ltd. High Wycombe, UK). Methanol HPLC grade was purchased from Fisher Scientific. Loughborough, UK. The beta-blockers used were acebutalol, pindolol, metoprolol, oxprenolol alprenolol propranolol HCl. Methylated xanthines applied were theobromine, theophylline and caffeine. The phenolic acid standards used were 3,4-dihydroxy benzoic acid, 3,4-dihydroxy cinnamic acid, vanillic acid, ferulic acid and chlorogenic acid. All were laboratory reagent grade from Sigma-Aldrich, Poole, UK, as were formic acid and glacial acetic acid. Furthermore, following steroids were purchased from Sigma Aldrich, 1,4-androstadiene-3,11,17-trione, 19-nortestosterone, testosterone, dehydro-isoandrosterone and trans-androstadiene. Ammonium acetate was purchased from Fisons, UK. Echinacea plant extract capsules were purchased from Holland's and Barrett's.

The Tanaka test mix was applied as in the column stability studies (see section 3.1.2.2)

8.2 Solutions

8.2.1 Uracil solution

Some of the injected samples were spiked with a uracil solution to determine the dead time of the HPLC systems. The uracil solution was prepared weighing 10 mg uracil into a 100 ml volumetric flask. The uracil was dissolved using about 30 ml of methanol/water (50/50, v/v). The volumetric was made up to volume with methanol/water (50/50, v/v).

8.2.2 Beta-blocker solutions

10mg of each of the beta-blockers acebutalol, pindolol, metoprolol, oxprenolol, alprenolol, propranolol HCl were weighed into separate 20 ml volumetric flasks. 5 ml acetonitrile and 5ml water was added and mixed well. After all solids were dissolved the volumetric flasks were filled to the mark with water. These were the beta-blocker standard solutions.

To prepare the mix 100 µl was taken from the propranolol and the pindolol standard solutions and 600 µl of each of the other standard solutions and pipetted into a 10 ml vial. 3 ml of deionised water was added to this mix. This was the chromatographic test mix.

8.2.3 Steroid solutions

Separate steroid standards containing 1 mg/ml steroid were prepared. To prepare the solutions 10 mg of each of the steroids 1,4-androstadiene-3,11,17-trione, 19-nortestosterone, testosterone, trans-androsterone and dehydro-isoandrosterone were weighed into separate 10 ml volumetric flasks and dissolved with about 5 ml of 50/50 (v/v) methanol/water. After all solids were dissolved the volumetric flasks were made up to volume.

To prepare the mixed standards 2 ml of 1,4-androstadiene-3,11,17-trione, 2 ml 19-nortestosterone and 2 ml testosterone solutions were

mixed in a 10 ml volumetric flask and made up to volume with methanol/water (50/50, v/v).

This is steroid mix A.

A mixed standard of 5 steroids was prepared mixing 2 ml of 1,4-androstadiene-3,11,17-trione, 2 ml 19-nortestosterone, 2 ml testosterone, 2 ml trans-androsterone and 2 ml dehydro-isoandrosterone solutions.

This is steroid mix B.

8.2.4 Phenolics and methylated xanthines solutions

For development of the extraction and separation method separate standards of chlorogenic acid, 3,4-dihydroxy cinnamic acid and 3,4-dihydroxy benzoic acid at 1 mg/ml concentration were prepared. A 50% methanol and 50% water diluent (v/v) was used for these stock standards.

10 ml of each stock standard was transferred into a 100 ml volumetric flask and made up to volume with water. This is phenolic acids mixed standard 1.

8.3 Equipment

The superheated water methods were developed on a HP-1090 series liquid chromatograph (Palo Alto, CA, USA) equipped with an auto injector and diode array detector. The inlet tubing to the column was 0.018 mm (0.007") I.D., 1.6 mm (1/16 ") OD stainless steel. 50 cm was placed as a preheating coil into the column oven. The column oven was a Pye 104 GC oven. As a second set-up a Hewlett Packard 1100 series liquid chromatograph with a HP 5890 GC was used as the column oven (Hewlett Packard, Palo Alto, CA, USA). The column was placed in the oven and the outlet tubing was lead through a water jacket to cool down the column effluent. A circulating pump (Techne, Tempette TE-8A) supplied the jacket with coolant from a tank filled

with cold water. The set up of the superheated water system is shown in Figure 78.

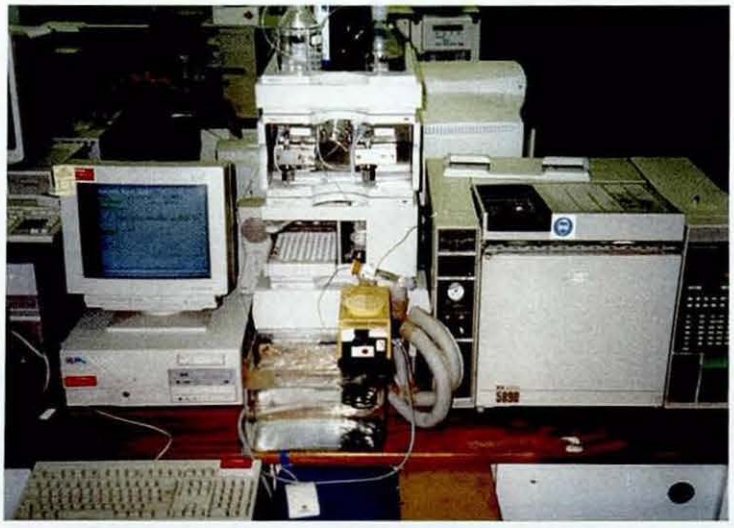

Figure 78: Superheated water chromatograph from left to right: Computer running Chemstation software, 1100 series Hewlett Packard liquid chromatograph, Hewlett Packard 5890 series gas chromatograph, front: water tank with Techne TE-8A thermostat connected to water jacket.

LC-MS experiments were run courtesy of AstraZeneca in their laboratories at Macclesfield on a Hewlett Packard 1100 system with diode array detection (Palo Alto, CA, USA) and a quadrupole mass spectrometer (Micromass Manchester, UK). The LC flow was split after the DAD detector MS: waste, 1:5.

NMR experiments were performed on a Bruker 250 MHz and 400 MHz spectrometer (Karlsruhe, Germany) at AstraZeneca, Alderly Park. A Bruker LC pump, DAD detector and a 600 MHz spectrometer were used for part of the LC-NMR experiments. For the majority of LC-NMR experiments a Varian HPLC instrument with DAD detector and a 500 MHz Varian spectrometer were used at Syngenta at their Jealott's Hill Research Station.

8.4 Columns

The following columns were employed with superheated water chromatography:

5 µm Hypersil HiPurity Advance (150 x 4.6 mm, Thermo Separations, Runcorn), 5 µm Aqua and 5µm Luna C18 (250 x 2.0 mm, Phenomenex, Macclesfield, UK), 5 µm PLRP-S, spherical polystyrene-divinylbenzene (150 x 4.6 mm, Polymer Labs, Church Stretton, Shropshire, UK), 5 µm Zirchrom PBD (150 x 4.6 mm, Zirchrom, Anoka, Minnesota, USA).

9 APPLICATIONS OF ELEVATED TEMPERATURE AND SUPERHEATED WATER CHROMATOGRAPHY

A number of applications were developed to show how standard reversed phase HPLC methods could be translated to elevated temperature and/or superheated water chromatography methods. The following chapter summarises the application development for four example applications and gives guidance on how to approach an elevated temperature RP-HPLC method development.

9.1 How to develop elevated temperature and superheated water applications?

Two effects were investigated, firstly the effect of changing the mobile phase composition on retention time of the solutes and secondly the effect of changing the separation temperature on retention time of the solutes. By plotting volume fraction of organic modifier (in %) versus ln k or ln RT (RT := retention time) the effect of mobile phase composition on retention time can be estimated. From the plot a regression line can be fitted. Applying the resulting linear equation retention times can be extrapolated.

The effect of temperature on retention is given by the equation Equation 29

Equation 29

$$\ln k = -\frac{\Delta H^0}{R\mathrm{T}} + \frac{\Delta S^0}{R} + \ln \beta$$

If the retention mechanism does not change with temperature a linear plot is obtained when *ln k* is plotted versus 1/T (van't Hoff plot). The slope of the line is $-\Delta H^0/R$ and the intercept $\Delta S^0/R + \ln \beta$. This plot

can be used to estimate the changes in retention time when the temperature is altered. Furthermore, it is possible to predict if the order of elution will change. For ease of use and if no thermodynamic data is to be calculated it is possible to plot temperature versus ln RT. This also yields a nearly linear plot. The fitted equation can be applied to extrapolate compound retention for different temperatures. It is feasible to extrapolate retention behaviour for changes in mobile phase composition and temperature if the temperature dependent change of retention was measured with different volume fractions of organic modifier in the mobile phase.

9.2 Examples

Separations for four different compound groups, beta-blockers, steroids, phenolic acids and methylated xanthines have been performed using temperature as the optimisation parameter. These separations are described in the following.

9.2.1 Separation of selected beta-blockers

One example for the application of elevated temperature and superheated water chromatography is the separation of β-blockers. For the preparation of the chromatographic test mix see Experimental.

9.2.1.1 Elevated temperature chromatography

The separation was performed employing a Phenomenex Aqua column. The mobile phase contained 20% acetonitrile and 80% ammonium acetate buffer pH 4.5 (v/v). The separation was initially performed at 40 °C column temperature. A typical chromatogram is shown in Figure 79. The last eluting compound, alprenolol, eluted at 22.85 minutes. When the percentage of acetonitrile in the mobile phase was increased by 10 % the retention time of alprenolol decreased to 5.65 minutes, 75% shorter than the retention time with 20% acetonitrile in the mobile phase.

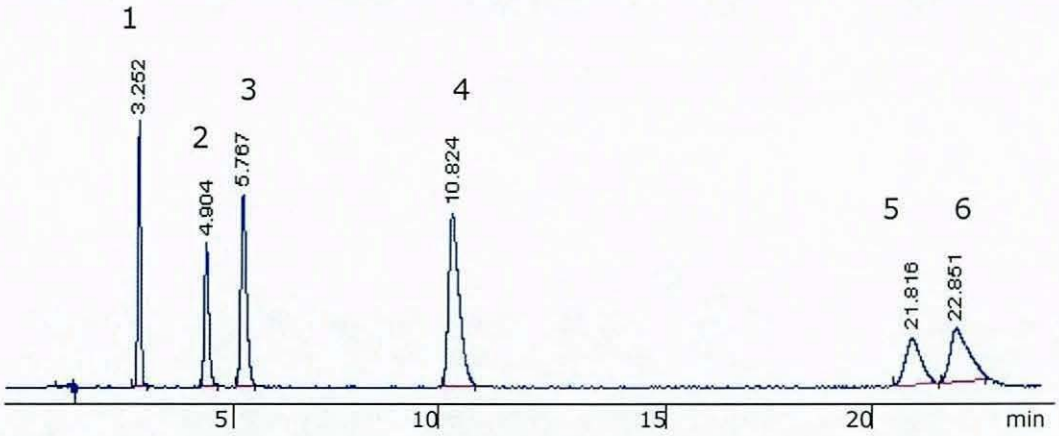

Figure 79: Separation of selected beta-blockers, in order of elution (1) pindolol, (2) acebutalol, (3) metoprolol, (4) oxprenolol, (5) propranolol and (6) alprenolol on Phenomenex Aqua, 250 x 2.0 mm, 40 °C, flow 1.0 ml/min, mobile phase 20% acetonitrile, 80% ammonium acetate buffer pH 4.5.

Figure 80 shows a chromatogram of the separation performed with 30% acetonitrile. The change in mobile phase composition significantly shortened the analysis time. However, the separation of the critical pair remains virtually unchanged whether the run time is 7 minutes or 25 minutes. A change in selectivity for these two compounds cannot be achieved by a change in mobile phase composition.

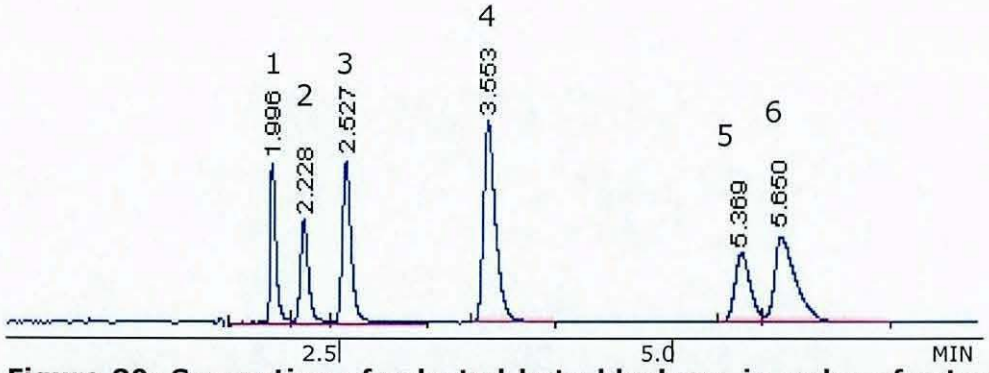

Figure 80: Separation of selected beta-blockers, in order of retention (1) pindolol, (2) acebutalol, (3) metoprolol, (4) oxprenolol, (5) propranolol and (6) alprenolol on Phenomenex Aqua, 250 x 2.0 mm, 40 °C, flow 1.0 ml/min, mobile phase 30% acetonitrile, 70% ammonium acetate buffer pH 4.5.

Figure 81 shows the change in retention with increasing acetonitrile fraction in the mobile phase. The % organic modifier is plotted versus ln RT to arrive at a nearly linear relationship. It is obvious from Figure 81 that there is no change in retention order of the peaks. There is a

81 that there is no change in retention order of the peaks. There is a negligible loss in resolution of the critical pair propranolol and alprenolol.

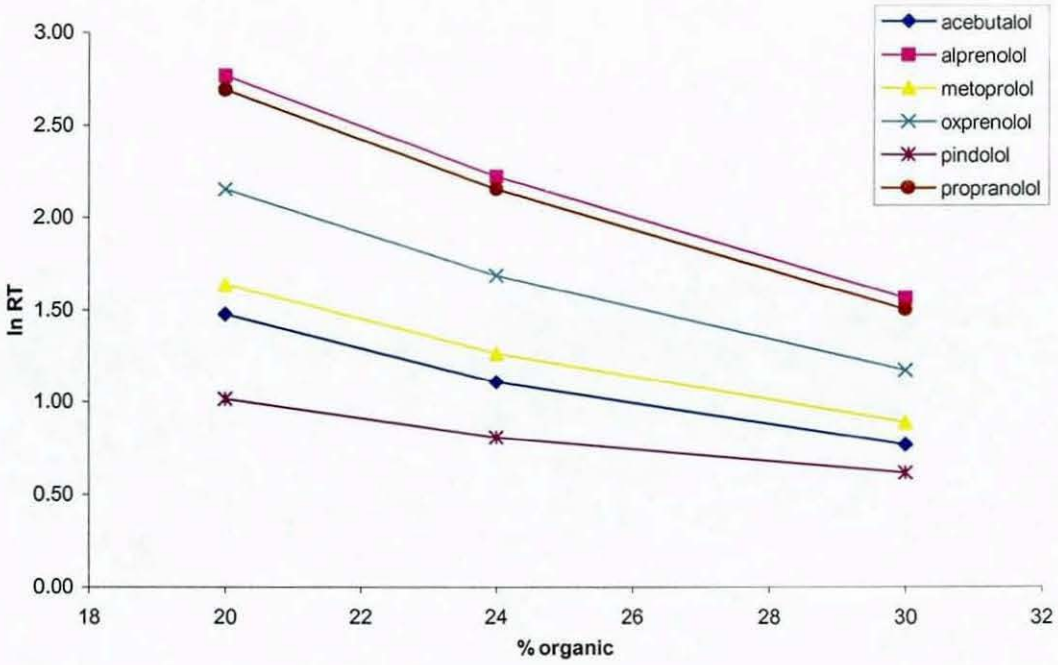

Figure 81: Change in retention of beta-blockers versus change of percentage acetonitrile in the mobile phase on Phenomenex Aqua 250 x 2.0 mm, flow 1.0 ml/min, column temperature 40 °C.

An alternative approach to alter analysis time and selectivity in reversed phase chromatography is to change the separation temperature. The separation of beta-blockers was then performed at higher column temperatures. As a result of the temperature increase the retention times for all the compounds dropped. In this case the resolution for the critical pair propranolol/alprenolol increased from 1.0 at 40 °C (Figure 79) to 2.2 at 80 °C (Figure 82).

As with increasing the percentage of organic modifier increasing the temperature caused a general decrease in retention time. However, manipulating the temperature of the separation offers a change in separation selectivity different from the changes due to manipulating the percentage of organic modifier [153].

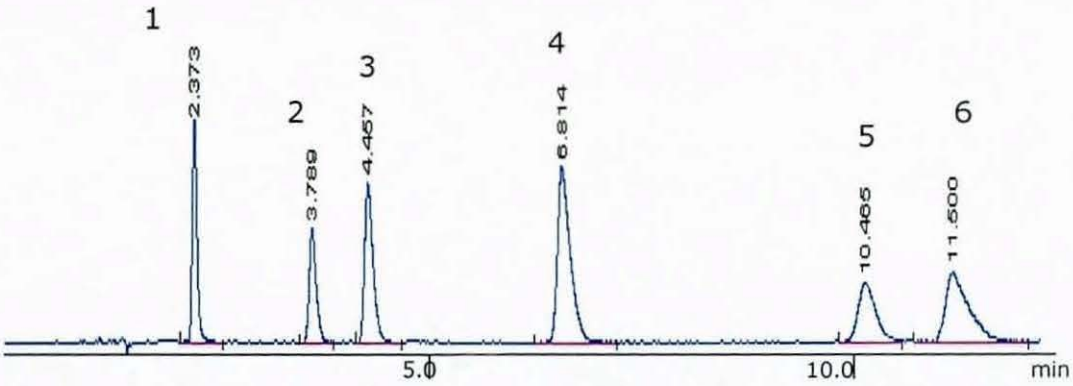

Figure 82: Separation of selected beta-blockers, in order of retention (1) pindolol, (2) acebutalol, (3) metoprolol, (4) oxprenolol, (5) propranolol and (6) alprenolol on Phenomenex Aqua, 250 x 2.0 mm, 80 °C, flow 1.0 ml/min, mobile phase 20% acetonitrile, 80% ammonium acetate buffer pH 4.5.

Figure 83 show the van't Hoff plot of the beta-blocker separation in the temperature range of 40 to 80 °C. The slopes of the calculated trend lines are lower than for the trend lines calculated for a change in mobile phase composition vs ln k.

The change in retention time was dependent on the volume fraction of organic modifier and the change in temperature. The change per 1°C and per 1 % organic modifier was calculated applying the fitted linear equations. The results are listed in Table 8.

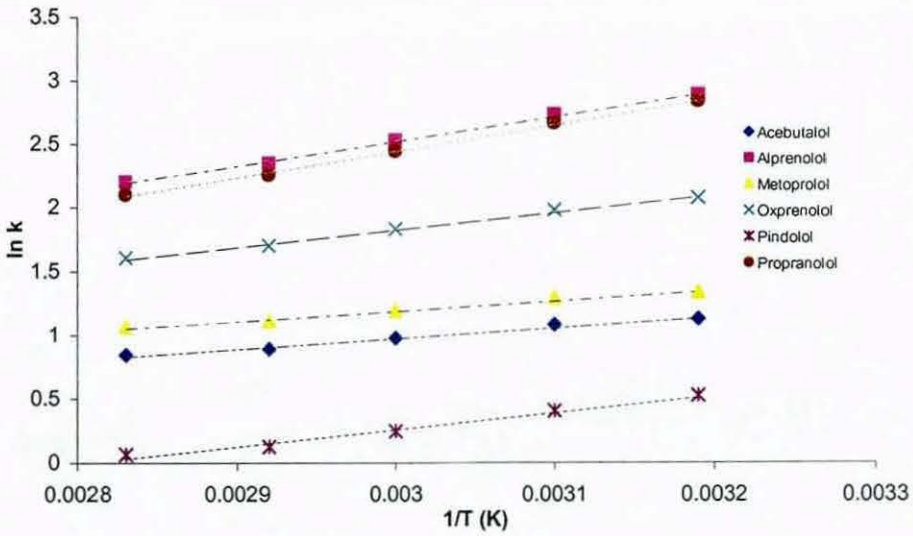

Figure 83: Van't Hoff plot for change in retention of beta-blockers versus 1/temperature ° Kelvin on Phenomenex Aqua 250 x 2.0 mm, flow 1.0 ml/min, 20% acetonitrile, column temperature range 40 to 80 °C.

Table 8: Calculated change in retention time for one % increment change in % organic modifier at 40 °C and change in one temperature increment, for mobile phase containing 20 % acetonitrile.

change of retention time when organic modifier is changed by 1%

	% org (A)	% org (B)	RT (A)	RT (B)	RT change	intercept	slope
Pindolol	20	21	1.57	1.43	**0.14**	2.324	-0.094
Acebutalol	20	21	2.95	2.59	**0.36**	3.651	-0.129
Metoprolol	20	21	3.66	3.23	**0.43**	3.776	-0.124
Oxprenolol	20	21	7.73	6.71	**1.02**	4.865	-0.141
Propranolol	20	21	16.54	14.10	**2.44**	6.000	-0.160
Alprenolol	20	21	17.39	14.85	**2.54**	6.016	-0.158

change of retention time when temperature is changed by 1 °C

	1/T (A)	1/T (B)	RT (A)	RT (B)	RT change	intercept	slope
Pindolol	0.003663004	0.0036496	3.14	3.09	**0.06**	-3.759	1339.000
Acebutalol	0.003663004	0.0036496	6.54	6.47	**0.07**	-1.153	827.310
Metoprolol	0.003663004	0.0036496	5.55	5.49	**0.06**	-1.210	798.190
Oxprenolol	0.003663004	0.0036496	15.35	15.07	**0.28**	-2.292	1371.200
Propranolol	0.003663004	0.0036496	46.18	44.90	**1.28**	-3.852	2098.000
Alprenolol	0.003663004	0.0036496	45.06	43.91	**1.15**	-3.300	1940.600

Analysing the figures in Table 8 the impact of 2 °C temperature change on retention is similar to the impact of changing the fraction of organic modifier by 1 %.

The separation shown in Figure 82 with 20 % acetonitrile took 13 minutes while the separation with 30% acetonitrile took just 7 minutes. In order to further shorten analysis time the same separation was then run with 30% acetonitrile in the mobile phase at 80 °C. Figure 84 shows a chromatogram of the separation at elevated temperature. The total run time was reduced to 4.5 minutes.

The resolution of the critical pair was 1.5 when the separation was performed at 80 °C and 30% acetonitrile in the mobile phase.

With optimisation of both organic modifier and temperature it was possible to run an isocratic separation, shorten analysis time and improve resolution of the critical pair alprenolol and propranolol.

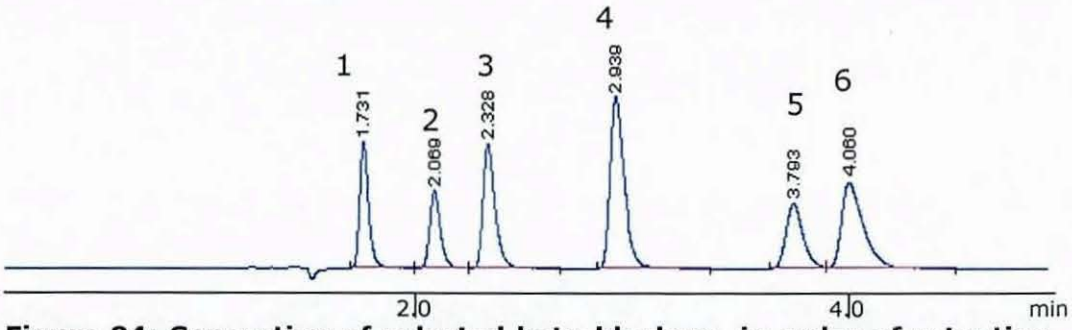

Figure 84: Separation of selected beta-blockers, in order of retention (1) pindolol, (2) acebutalol, (3) metoprolol, (4) oxprenolol, (5) propranolol and (6) alprenolol on Phenomenex Aqua, 250 x 2.0 mm, 80 °C, flow 1.0 ml/min, mobile phase 30% acetonitrile, 70% ammonium acetate buffer pH 4.5.

9.2.1.2 Superheated water chromatography

The retention data collected in the temperature range of 40 to 80 °C and 20 to 30 % acetonitrile can be utilised to estimate retention at higher or lower temperatures and varying concentrations of acetonitrile. It is feasible to either apply the van't Hoff plot to estimate the change of retention with temperature or to plot temperature versus the logarithm of retention time. If the retention mechanism is unchanged with temperature both plots yield a linear response. The plot of temperature (°C) versus ln RT can be used as an practical estimation if no thermodynamic data needs to be calculated.

Looking at a plot of temperature versus ln retention time for different concentrations of acetonitrile in the mobile phase (Figure 85) one can observe that the slopes of the curves vary with the percentage of organic in the mobile phase. The higher the content of organic in the mobile phase the smaller the change of retention per °C change in column temperature.

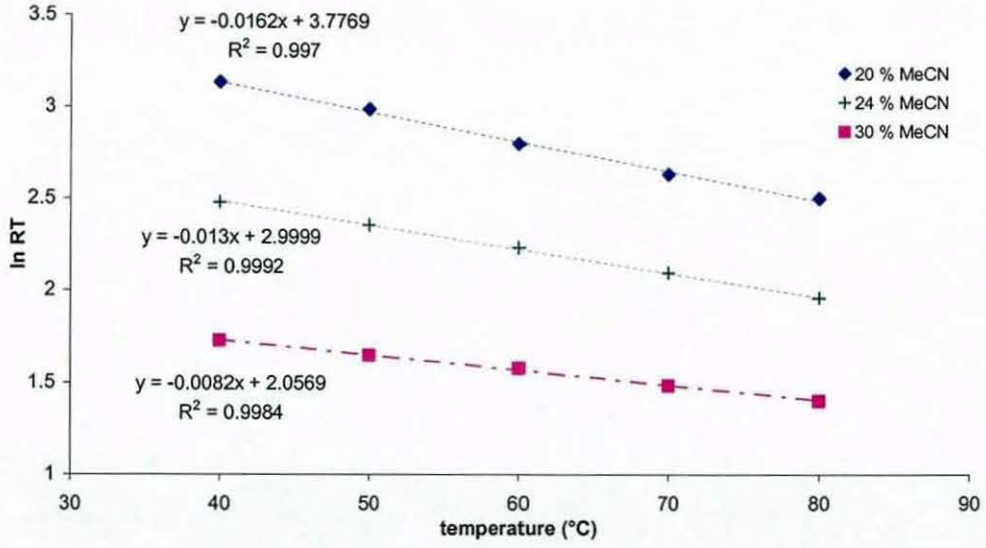

Figure 85: Temperature versus ln retention time for alprenolol on Phenomenex Aqua 250 x 2.0 mm, flow 1.0, mobile phase containing 20%, 24% and 30% acetonitrile respectively.

Thus the impact of temperature on retention, changes with the content of organic modifier in the mobile phase. This needs to be taken into account when performing any extrapolation of compound retention time for higher temperature or a 100% water mobile phase. The slope indicates how much the retention will change with temperature. The intercept reflects the retention of a compound at a given mobile phase composition at 0 °C. The slopes and the intercepts of the curves in Figure 85 were plotted versus the percentage organic modifier to investigate the relationship describing the changes in slope (Figure 86) and intercept (Figure 87) of the temperature versus ln retention time curves in Figure 85.

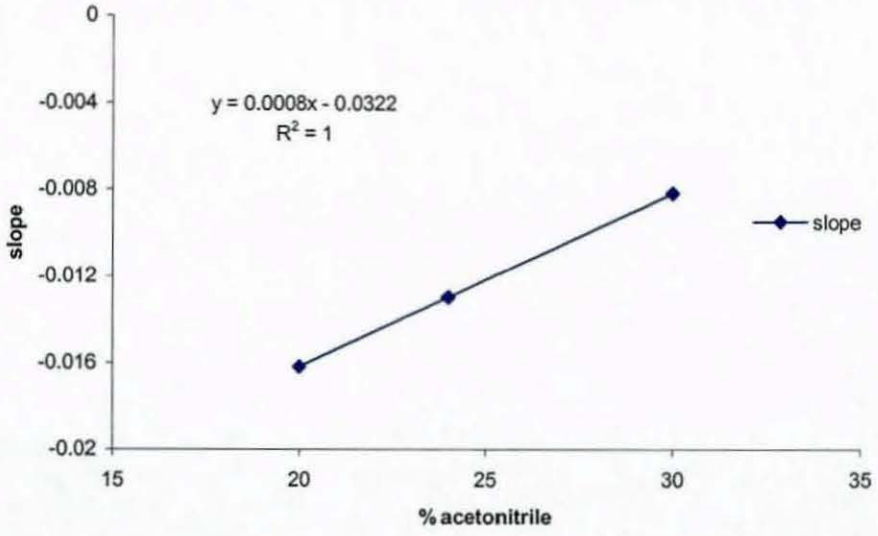

Figure 86: Percent organic modifier versus slope of temperature dependency curve (Figure 85) for alprenolol on Phenomenex Aqua 250 x 2.0 mm, flow 1.0.

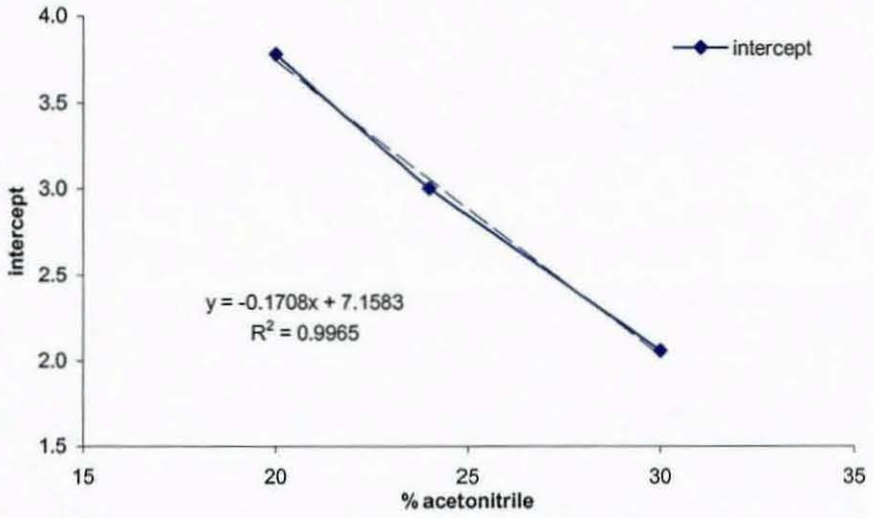

Figure 87: Percent organic modifier versus intercept of temperature dependency curve (Figure 85) for alprenolol on Phenomenex Aqua 250 x 2.0 mm, flow 1.0.

From Figure 86 and Figure 87 and the calculated regression it is obvious that there is a nearly linear relationship between the change in slope and intercept of the temperature versus retention curves (Figure 85) and the volume fraction of organic modifier in the mobile phase. An extrapolation to conditions of higher temperature and 0 % organic modifier is possible, when substituting the slope of the

temperature versus ln retention time curve with the linear relationship for the change in slope with the mobile phase composition (Figure 86) and intercept of the same curve with the relationship for the change in intercept with mobile phase composition (Figure 87). The necessary substitutions into the linear equation were performed as follows:

To substitute in Equation 30:

Equation 30

$$y = m * x + b$$

the variables where defined as such: y is ln retention time, m is the slope, x is the temperature of the column and b the intercept.

The slope m is dependent on the volume fraction of organic modifier. The dependency is described through Equation 31

Equation 31

$$m = 0.0008z - 0.0322$$

where z is the volume fraction of organic modifier in % v/v.

The intercept b is dependent on the volume fraction of organic modifier as well. Equation 32 describes the dependency of the intercept

Equation 32

$$b = -0.1708z + 7.1583$$

where z is the volume fraction of organic modifier in % v/v.

When m and b in Equation 30 are substituted with Equation 31 and Equation 32 respectively one arrives at Equation 33 describing the change in ln retention time dependent on temperature and volume fraction of organic modifier for alprenolol on a Phenomenex Aqua 250 x 2.0 mm column.

Equation 33

$$y = (0.008z - 0.0322) * x + (-0.1708z + 7.1583)$$

It is important to note that this empirical equation is applicable to help estimating the retention time of the observed compound at extrapolated condition but that it has no thermodynamic relevance.

Table 9 shows estimated retention times for alprenolol applying Equation 33. The estimated retention times have been calculated based on a relatively small amount of retention data and will by no means be accurate predictions. These values are rather a guide as to whether or not it would be feasible to apply pure water as a mobile phase when the separation of the compound concerned is run at elevated temperature.

Table 9: Extrapolation results to 0% acetonitrile, column temperature 40 °C to 180 °C, for alprenolol retention on Phenomenx Aqua 250 x 2.0 mm, flow 1.0 ml/min, retention calculated applying Equation 33.

% ACN	T (°C)	RT (min)	ln RT calc.
0	40	354.36	5.87
0	50	256.80	5.55
0	60	186.10	5.23
0	70	134.87	4.90
0	80	97.74	4.58
0	90	70.83	4.26
0	100	51.33	3.94
0	110	37.20	3.62
0	120	26.96	3.29
0	130	19.54	2.97
0	140	14.16	2.65
0	150	10.26	2.33
0	160	7.44	2.01
0	170	5.39	1.68
0	180	3.91	1.36

The predicted retention time for alprenolol at 150 °C and pure water as mobile phase (Table 9) was comparable to the retention time at 80 °C and 20 % organic modifier in the mobile phase (Figure 82).

A separation of six beta blockers was performed in the temperature range of 160 °C to 180 °C (Figure 88) applying pure water as the mobile phase to investigate the quality of the extrapolation shown in Table 9. Table 10 contains the retention times yielded from the experiments.

Table 10: Measured retention times for six beta blockers applying pure water as the mobile phase, separation temperature 160 °C to 180 °C, Phenomenex Aqua 250 x 2.0 mm, flow 1.0.

temperature °C	acebutalol	alprenolol	metoprolol	oxprenolol	pindolol	propranolol
160	3 67	6 77	3 93	5.05	1.47	5.93
170	2 80	5.08	3 08	3.84	1 32	4.47
180	2 56	4.73	2.92	3.58	1 28	4.13

The predicted retention times for alprenolol were shorter than experimental but comparable to the measured retention times. This shows that it is feasible to extrapolate with reasonable accuracy to pure water mobile phase conditions by applying retention data obtained at lower temperatures with eluent containing organic modifier in the mobile phase.

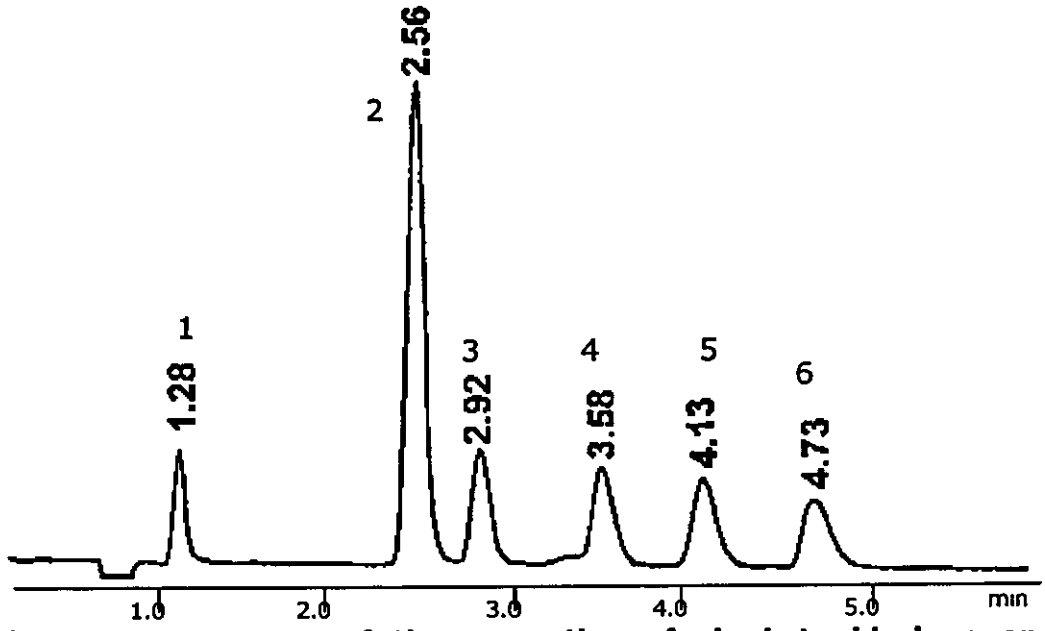

Figure 88: UV trace of the separation of six beta blockers on Phenomenex Aqua 250 x 2.0 mm, 100% water mobile phase + formic acid. Beta-blockers in order of retention (1) pindolol, (2) acebutalol, (3) metoprolol, (4) oxprenolol, (5) propranolol and (6) alprenolol.

9.2.1.3 Superheated water chromatography – MS

The effluent of the separation column was split into a DAD detector (trace shown in Figure 88) and an MS detector. The MS trace is shown in Figure 89. The MS spectra shown in Figure 90 A to F confirm that the order of retention has not changed and that none of the compounds were degraded at the higher temperature.

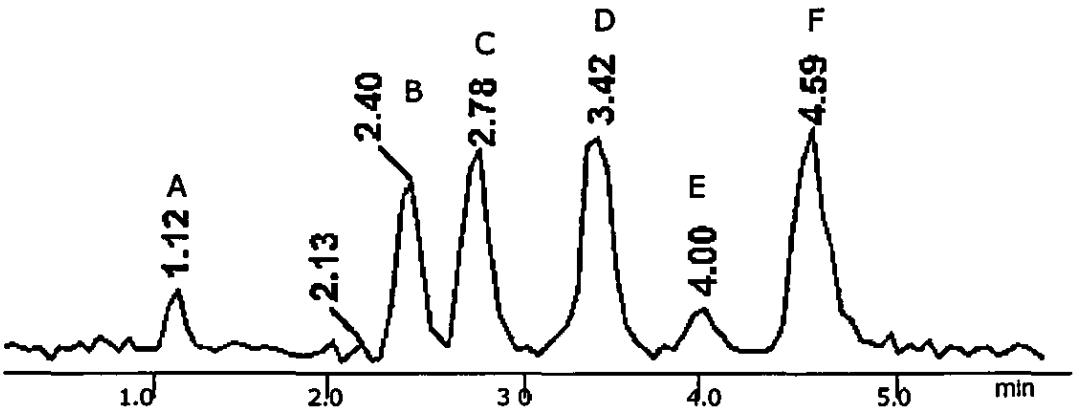

Figure 89: MS traces of the six separated beta-blockers on Phenomenex Aqua 250 x 2.0 mm, 100% water mobile phase. Beta-blockers in order of retention (A) pindolol, (B) acebutalol, (C) metoprolol, (D) oxprenolol, (E) propranolol and (F) alprenolol.

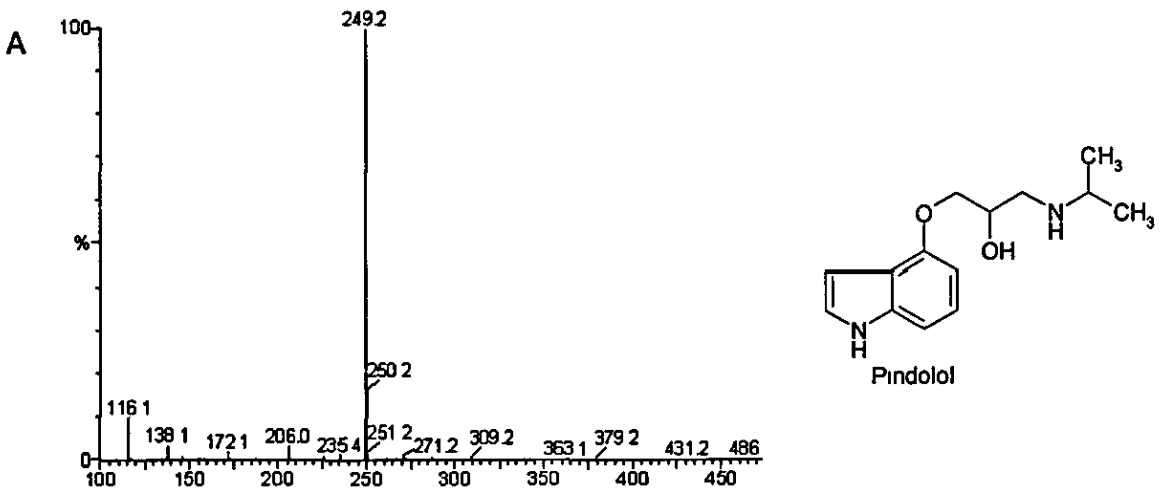

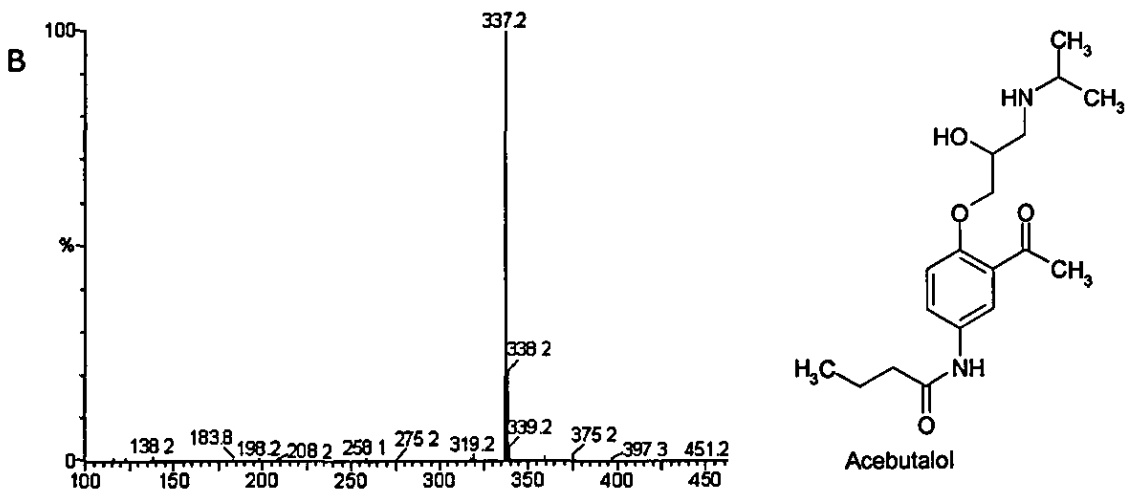

C

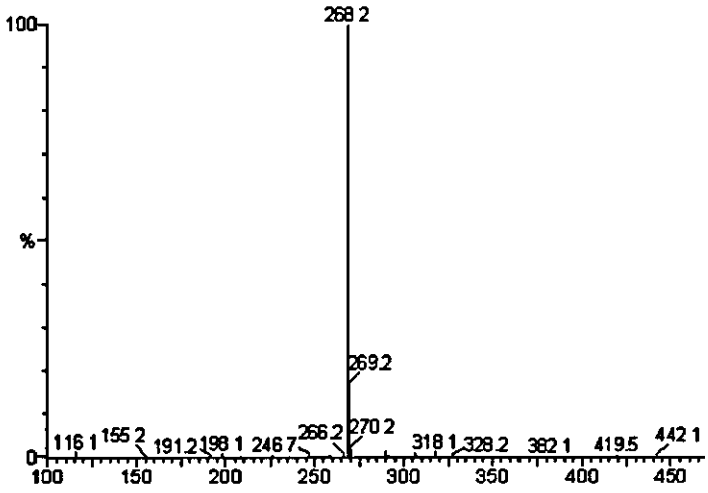

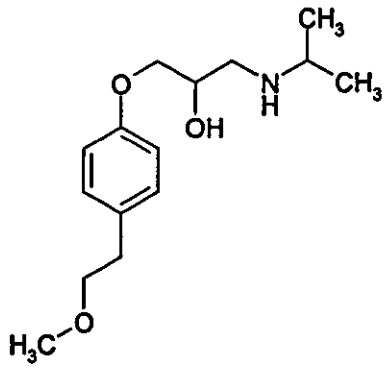

Metoprolol

D

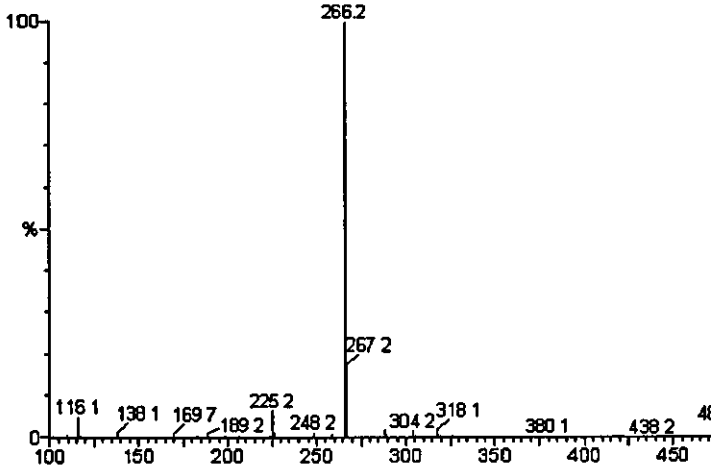

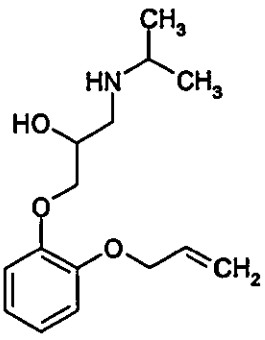

Oxprenolol

E

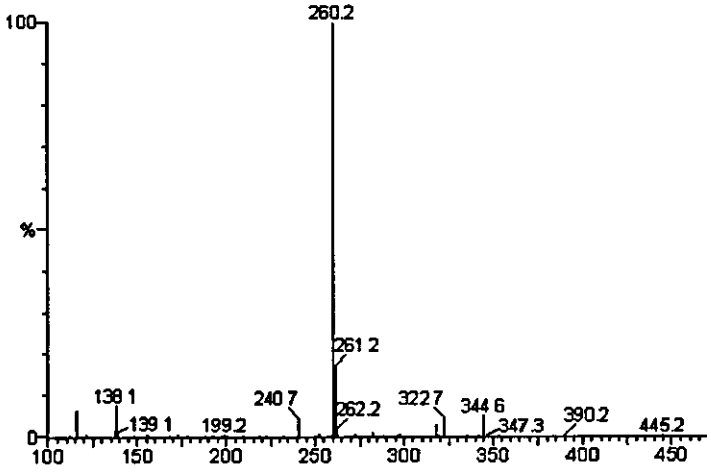

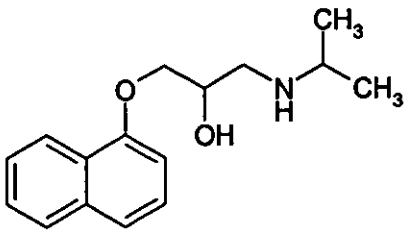

Propranolol

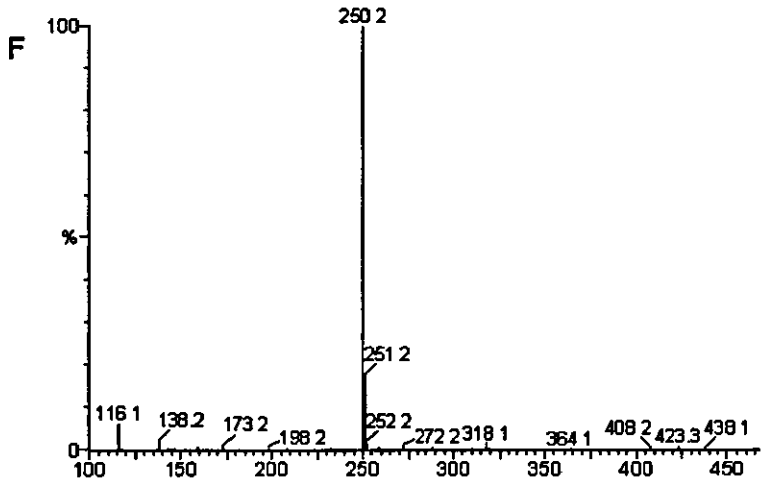

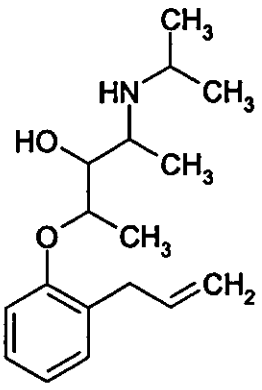

Alprenolol

Figure 90 A-F : Mass spectrum and structures for six beta blockers. In order of retention: pindolol, acebutalol, metoprolol, oxprenolol, propranolol, alprenolol.

The performance of the Aqua column degraded significantly after about 12 hours. Therefore as an alternative the separation of beta-blockers was performed on a more temperature stable zirconia PBDcolumn. However, the separation on the zirconia column resulted in very poor resolution for the individual components of the mix and was therefore not examined further. Another more temperature stable alternative is the polystyrene divinylbenzene (PLRP-S) column. Figure 91 shows a chromatogram of the beta-blocker mix separated applying a PLRP-S column.

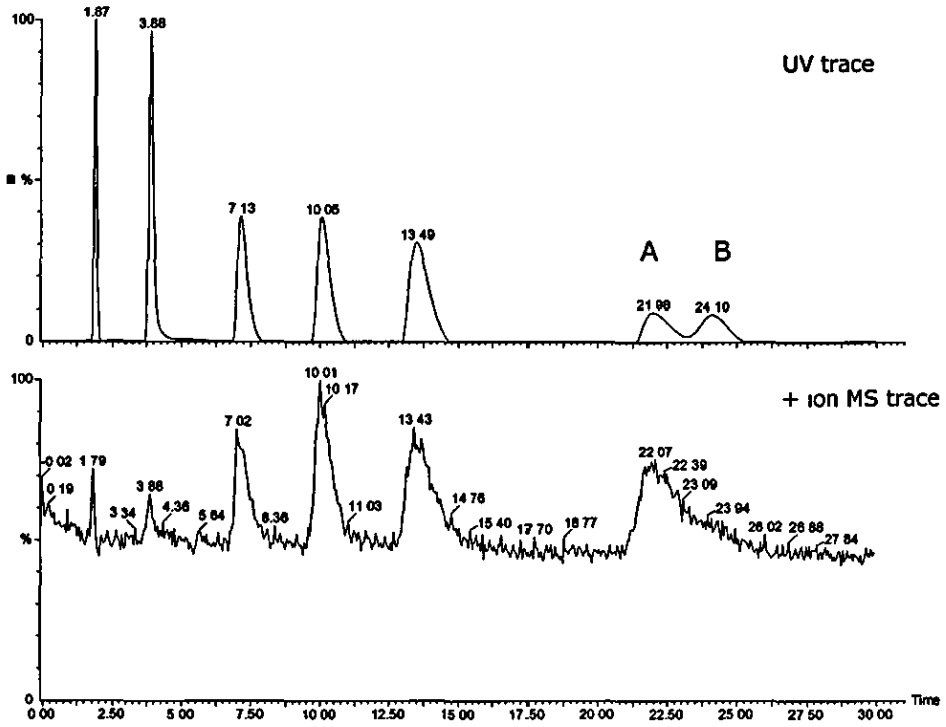

Figure 91: UV trace and positive ion MS trace of the separation of six beta blockers on PolymerLabs PLRP-S, 150 x 4.6 mm column, temperature 180 °C, mobile phase water + 0.01 % formic acid. Beta blockers in order of retention uracil, pindolol, acebutalol, metoprolol, oxprenolol, alprenolol and propranolol.

The separation of the mix employing the Polymerlabs PLRP-S (polystyrene divinyl benzene) column appeared to be equivalent to the separation on the silica based column. However, the polymer column was more retentive than the C18 column at the same temperature. On analysing the mass spectra it became obvious that the order of retention had changed. Alprenolol now eluted in front of propranolol. Figure 92 A-B show the mass spectra collected from the last two peaks. From the mass spectrum in Figure 92 B it is clear that alprenolol and propranolol were not fully separated.

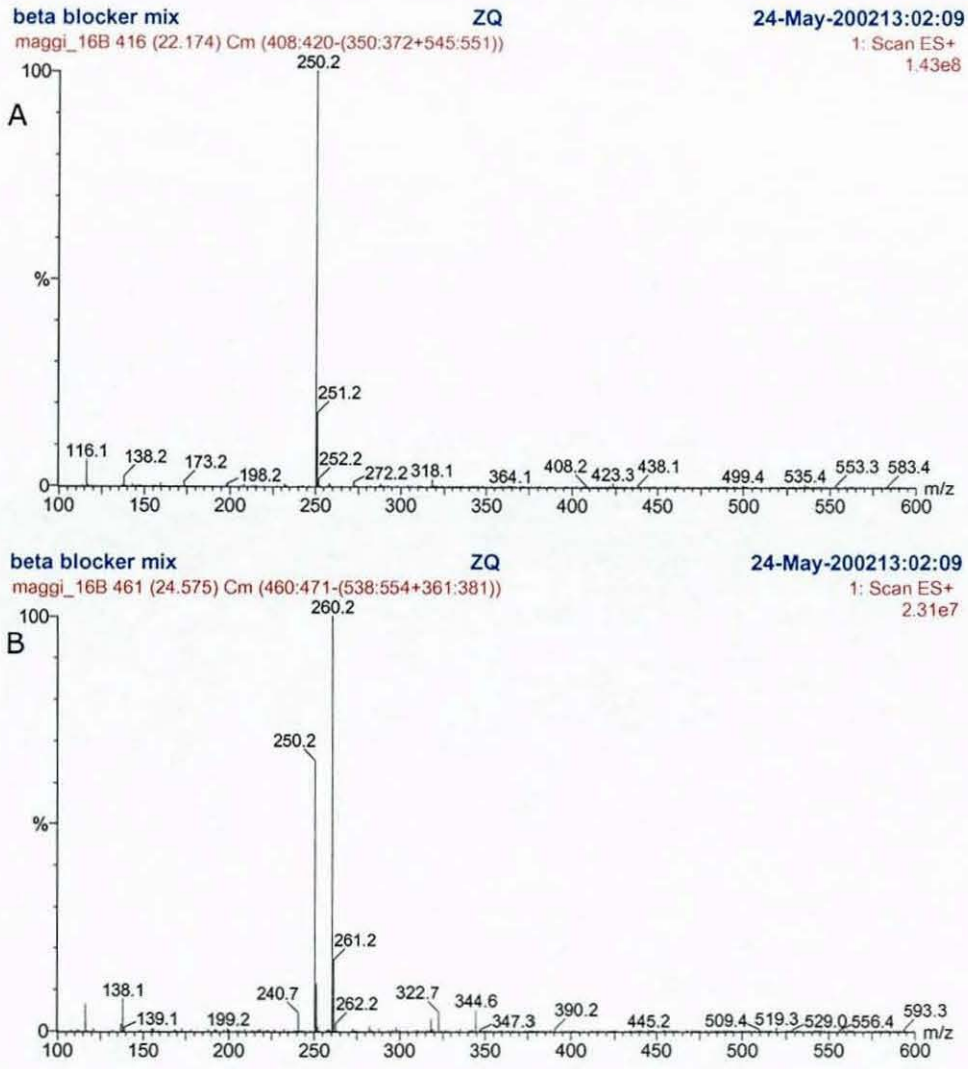

Figure 92 A-B: MS peaks A and B from Figure 91; (A) mass spectrum alprenolol M+ 250, (B) mass spectrum Propranolol M+ 260, containing traces of Alprenolol. Separation performed on PolymerLabs PLRP-S 150 x 4.6 mm, 180 °C, mobile phase water + 0.01 % formic acid.

The polymeric stationary phase is highly retentive for non-polar compounds. The double ring system of propranolol appears to have a higher affinity to the PLRP-S stationary phase than to the C18 stationary phase at elevated temperature conditions.

9.2.2 Separation of Steroids

A separation of a mixture of steroids was developed as a further example for the application of elevated temperatures in reversed phase chromatography.

The initial separation of steroid mix A spiked with uracil solution was performed employing a Hypersil HiPurity C18 column. The mobile phase contained 30 % methanol and 70 % water. The steroid mix A consisted of three steroids, 1,4-androstadiene-3,11,17-trione, nortestosterone and testosterone (see Experimental).

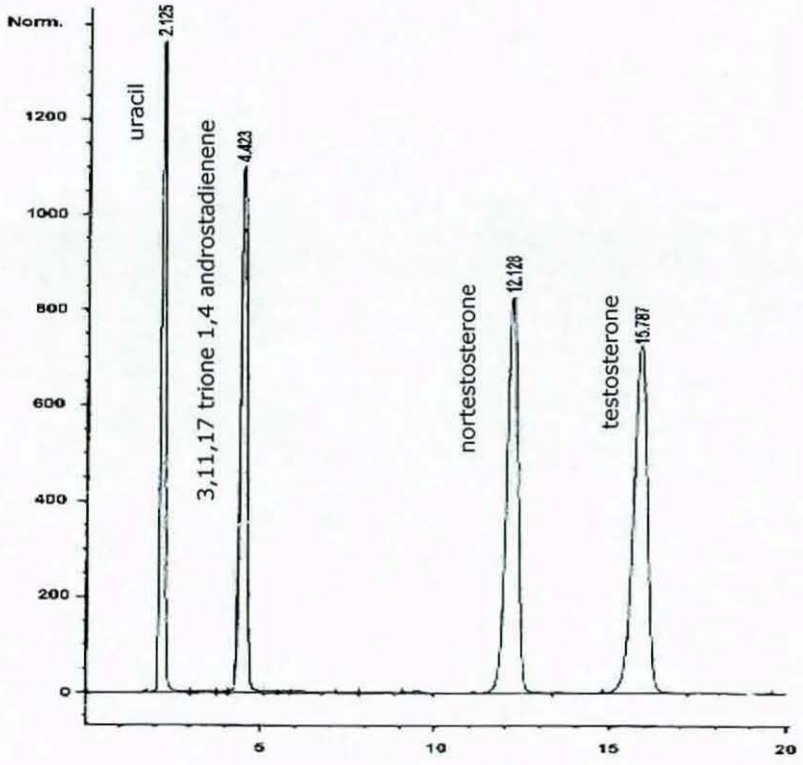

Figure 93: Separation of 1,4-androstadiene-3,11,17-trione, 19-nortestosterone and testosterone, uracil employed as a void volume marker, separation column Hypersil HiPurity C18, 150 x 4.6 mm, mobile phase 30 % methanol, 70 % water, column temperature 60 °C, flow 1.0 ml/min

All the steroids were well separated. The temperature was increased to 60 °C to shorten analysis time similar to the beta blocker separation. The latest eluting compound was testosterone eluting at about 16 minutes. A typical separation is shown in Figure 93.

9.2.2.1 Superheated water chromatography

The mobile phase composition was changed to 20 % methanol to ensure reasonable retention for the earliest eluting compound 1,4-androstadiene-3,11,17-trione when investigating the temperature

dependent change of retention over a wider temperature range. The temperature range between 60 °C and 120 °C was investigated. The change in retention time with temperature is listed in Table 11

Table 11: Change of retention time with temperature, mobile phase containing 20 % methanol, 80 water, on Hypersil HiPurity C18

	ret. time (min)		
temperature (°C)	androstadien	19-nortestosterone	testosterone
60	7.379	28.631	40.392
80	5.385	16.548	22.213
100	4.150	9.912	12.513
120	3.357	6.908	8.429

Figure 94 shows the van't Hoff plot for steroid mix A over the tested temperature range. From the van't Hoff plot it appears that the retention mechanism remains unchanged over the observed temperature range. A linear relationship is yielded for all three steroids. The curves do not crossover which means that the order of retention is unaffected and will most likely be unaffected when the separation is run at temperatures above the tested temperature range employing 100 % water as the mobile phase.

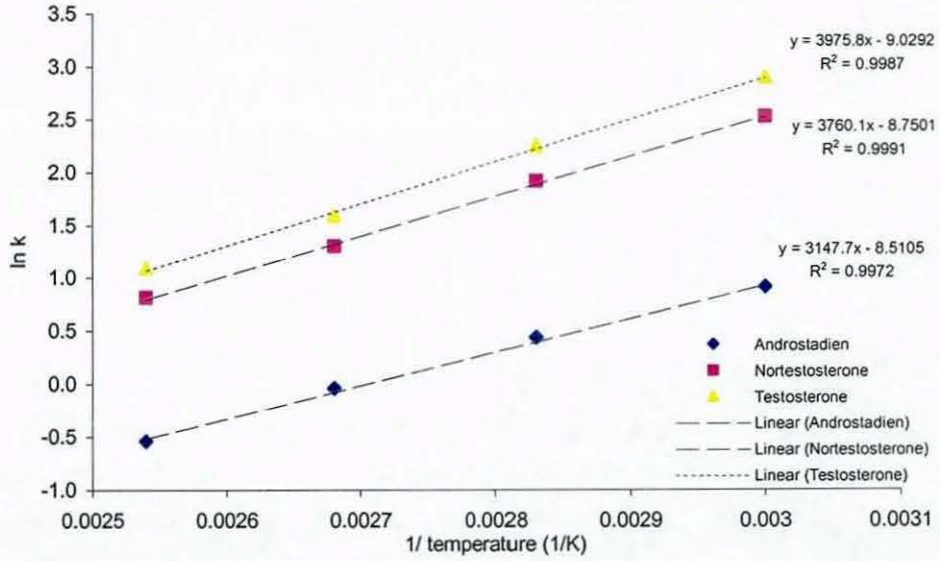

Figure 94: Van't Hoff plot of steroid mix A, 1,4,-androstadien-3,11,17-trione, 19-nortestosterone and testosterone. Separation run on Hypersil HiPurity C18, 150 x 4.6mm, 5 µm particle size, mobile phase 20 % methanol, 80 % water (v/v), temperature range 60 °C to 120 °C.

In order to estimate the retention time of the steroids for 100 % water mobile phase the same approach as for the beta-blockers was employed. Data generated for the van't Hoff plot with 20 % methanol in the mobile phase and retention data yielded with 30 % methanol in the mobile phase was employed to estimate the retention time at 100 % water conditions. The retention data, which was used for the extrapolation is listed in Table 12. The plotted data is shown in Figure 95 and the extrapolated data is shown in Table 13.

Table 12: Retention data for 1,4-androstadiene-3,11,17-trione, on Hypersil HiPurity C18, 150 x 4.6 mm, 5 µm particle size, flow 1.0 ml/min; data employed to estimate retention with 100 % water mobile phase

MeOH 20% temperature	androstadiene ln RT	MeOH 30% Temperature	androstadiene ln RT
60	1.999	40	1.323
80	1.684	50	1.246
100	1.423	60	1.193
120	1.211		

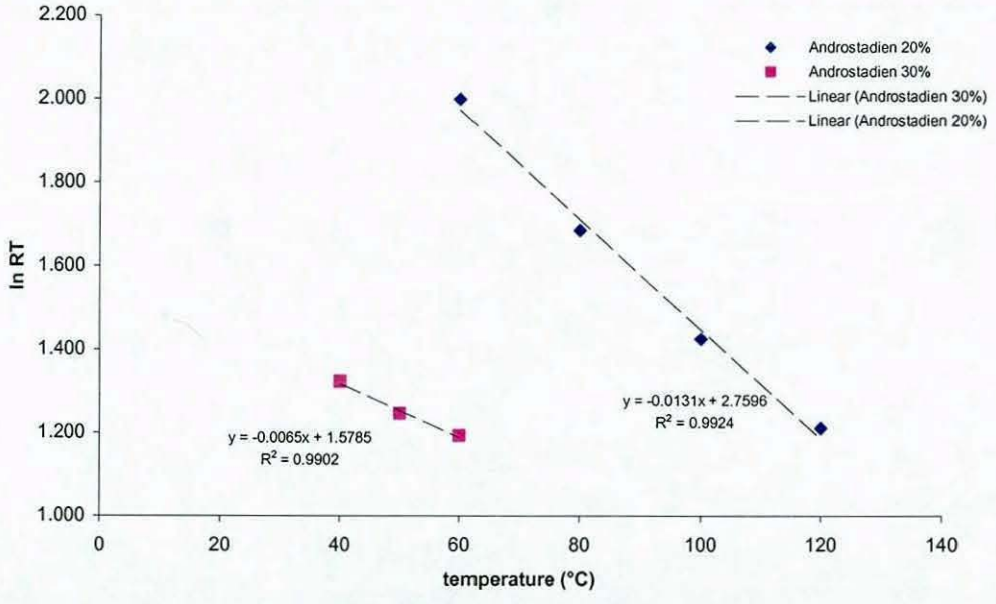

Figure 95: Temperature versus ln retention time for 1,4-androstadien-3,11,17-trione on Hypersil HiPurity C18, 150 x 4.6 mm, flow 1.0, mobile phase containing 20% and 30% methanol respectively.

Table 13: Prediction results for 0% methanol, column temperature 40 °C to 160 °C, 1,4-androstadiene-3,11,17-trione on Hypersil HiPurity C18, 150 x 4.6 mm, flow 1.0, retention calculated applying similar substitution principles as for Equation 33

% MeOH	Temp °C	RT (min)	ln RT
0	20	99.07	4.60
0	40	58.55	4.07
0	60	34.60	3.54
0	80	20.45	3.02
0	100	12.08	2.49
0	120	7.14	1.97
0	140	4.22	1.44
0	160	2.49	0.91
0	180	1.47	0.39

From the results of the prediction one can expect retention times for 1,4-androstadiene-3,11,17-trione when running 100 % water mobile phase at 140 °C column temperature to be comparable to the retention time at 60 °C and 30 % methanol (Figure 93). However, the assessment was performed using a very limited data set and therefore the extrapolated retention times can be only a rough guide as to whether the retention of the observed compounds can be brought into a reasonable retention window when using 100 % water as the mobile phase.

All measured retention times at superheated water conditions were longer than expected from the extrapolation results. Table 14 lists the measured retention times at 140 °C and 160 °C with 100 %water as the mobile phase.

Table 14: Measured retenion times for three steroids applying pure water as the mobile phase, separation temperature 140 °C to 160 °C, Hypersil HiPurity C18, 150 x 4.6 mm, flow 1.0.

	ret. time (min)		
temperature (°C)	1,4-androstadiene-3,11,17-trione	19-nortestosterone	testosterone
140	7.605	26.781	37.258
160	4.422	11.286	14.894

The retention of the compounds and efficiency of the column degraded very quickly when running at 160 °C. Figure 96 shows a chromatogram of the separation performed at 160 °C employing 100 % water as the mobile phase. The peaks are broad and tailing compared to the earlier separations.

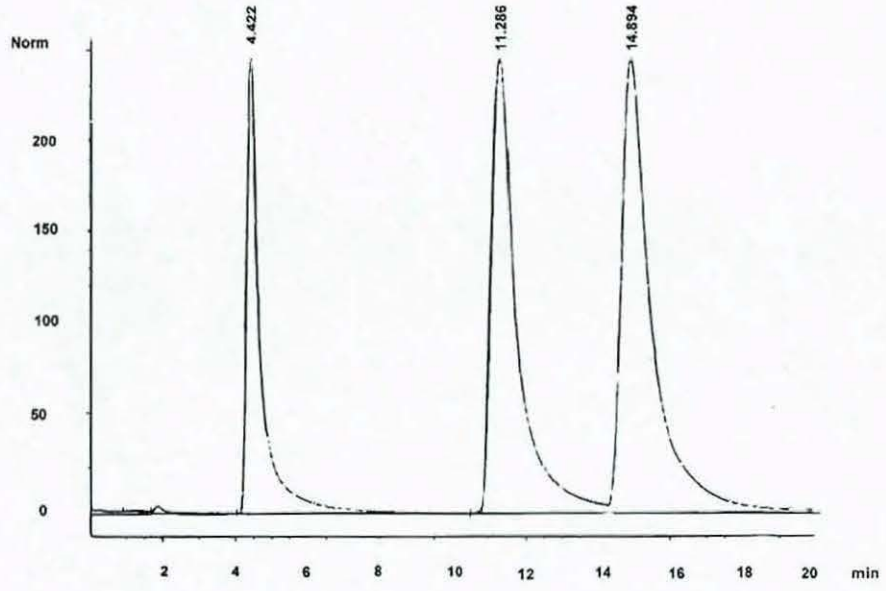

Figure 96: Steroid mix A, 1,4-androstadiene-3,11,17-trione, 19-nortestosterone and testosterone separated on Hypersil HiPurity C18, 150 x 4.6 mm, 160 °C, mobile phase 100 % water.

9.2.2.2 Superheated water - MS

A separation of steroid mix B, which also included dehydroisoandrosterone and trans-androsterone, adopting similar separation conditions as applied on the Hypersil column was performed at 150 °C employing a Zirconia PDB coated column (Figure 97). The Zirconia column was slightly less retentive than the C18 column. Hence the separation temperature was lowered by 10 °C. The effluent of the separation column was split into a DAD and an MS detector.

Comparing the UV trace and the ion trace in Figure 97 one can see that it was possible to pick up a signal for trans-androsterone employing the MS detector, which is absent from the UV trace as

expected for the saturated compound. Figure 98 A – E show the MS spectra and structures of the steroids contained in steroid mix B.

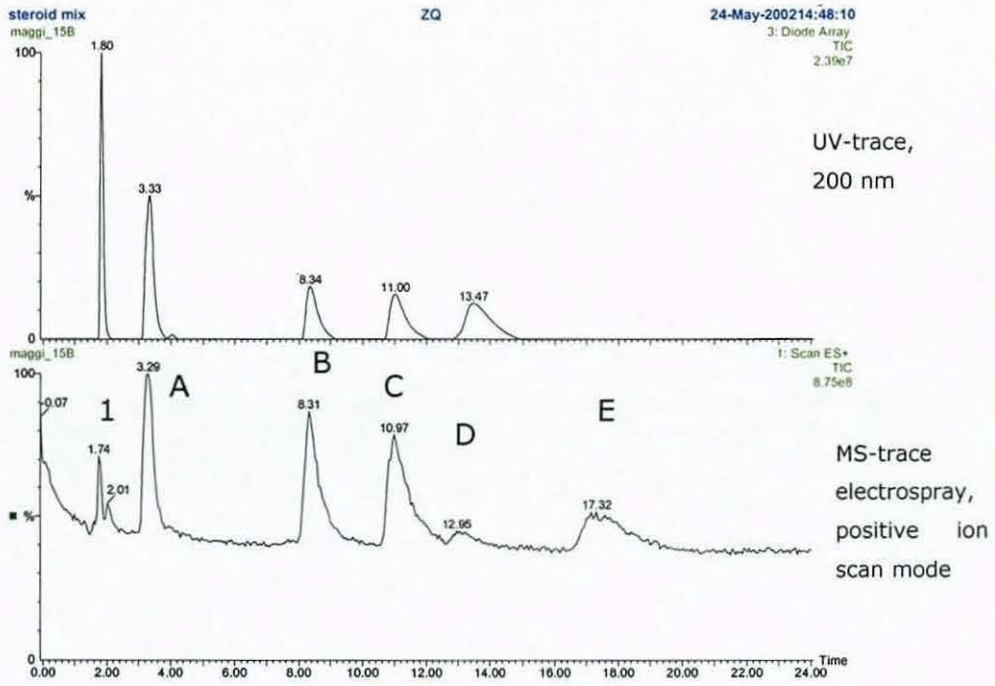

Figure 97: UV trace (top) and mass trace (bottom) of steroid mix B, (1) uracil, (A) 1,4-androstadien-3,11,17-trione, (B) 19-nortestosterone, (C) testosterone, (D) dehydroiso androsterone and (E) trans androsterone separated on Zirconia PDB, 150 x 4.6 mm, 150 °C, mobile phase 100 % water.

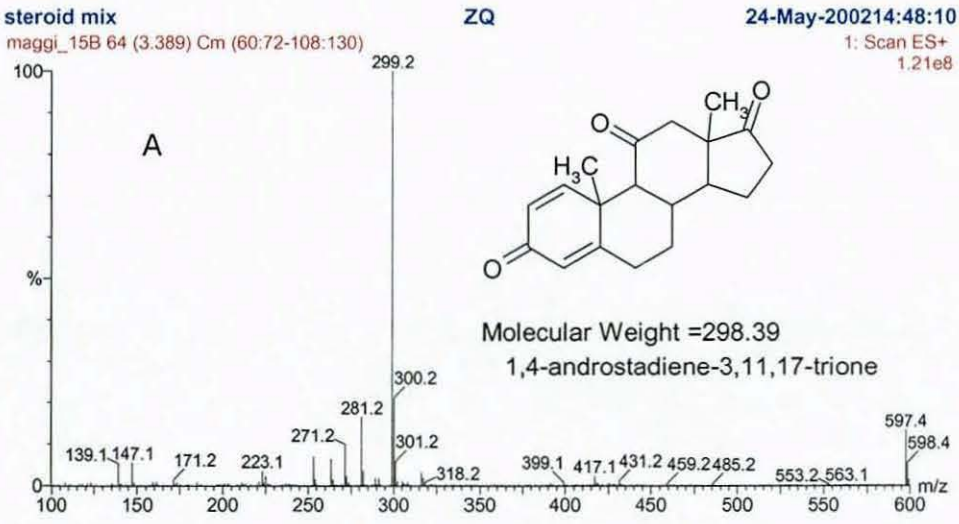

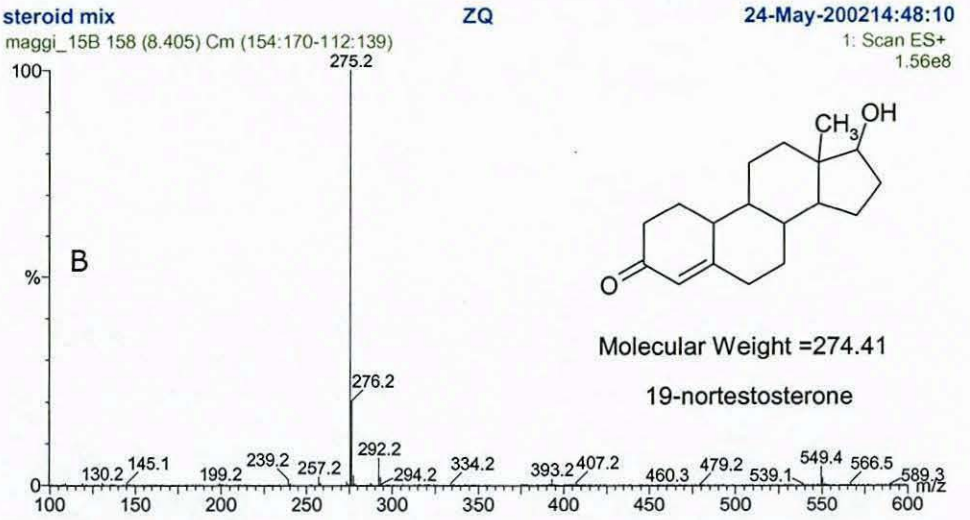
steroid mix
ZQ
24-May-200214:48:10
maggi_15B 158 (8.405) Cm (154:170-112:139)
1: Scan ES+
1.56e8
B
275.2
276.2
292.2
Molecular Weight =274.41
19-nortestosterone
m/z

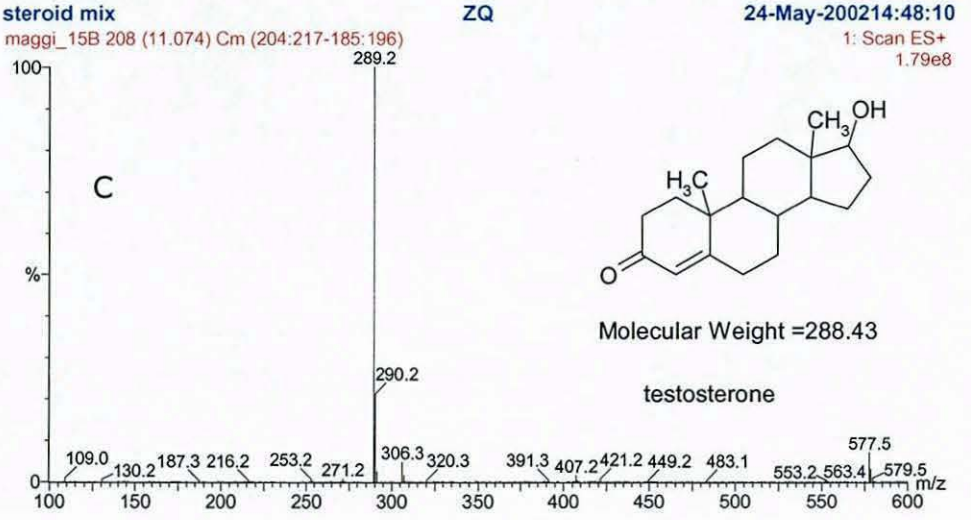
steroid mix
ZQ
24-May-200214:48:10
maggi_15B 208 (11.074) Cm (204:217-185:196)
1: Scan ES+
1.79e8
C
289.2
290.2
Molecular Weight =288.43
testosterone
m/z

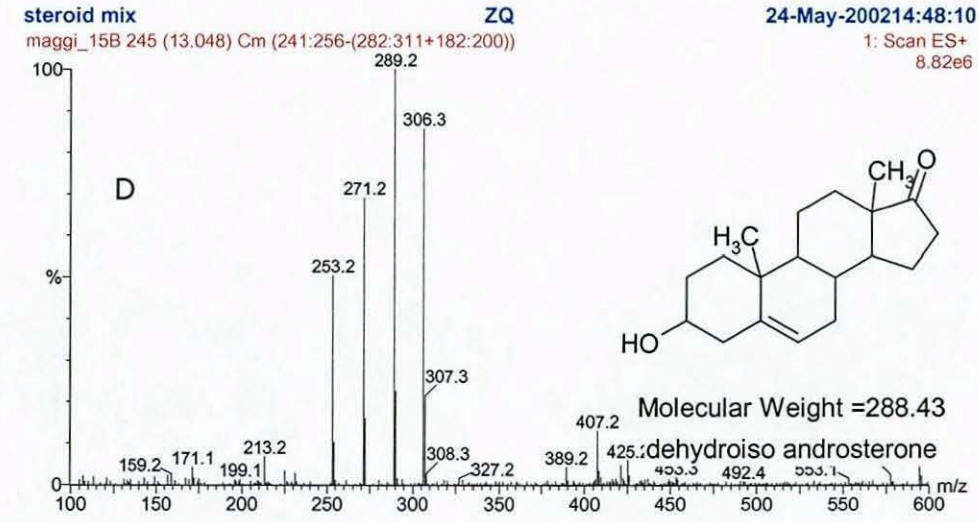
steroid mix
ZQ
24-May-200214:48:10
maggi_15B 245 (13.048) Cm (241:256-(282:311+182:200))
1: Scan ES+
8.82e6
D
289.2
306.3
271.2
253.2
307.3
Molecular Weight =288.43
dehydroiso androsterone
m/z

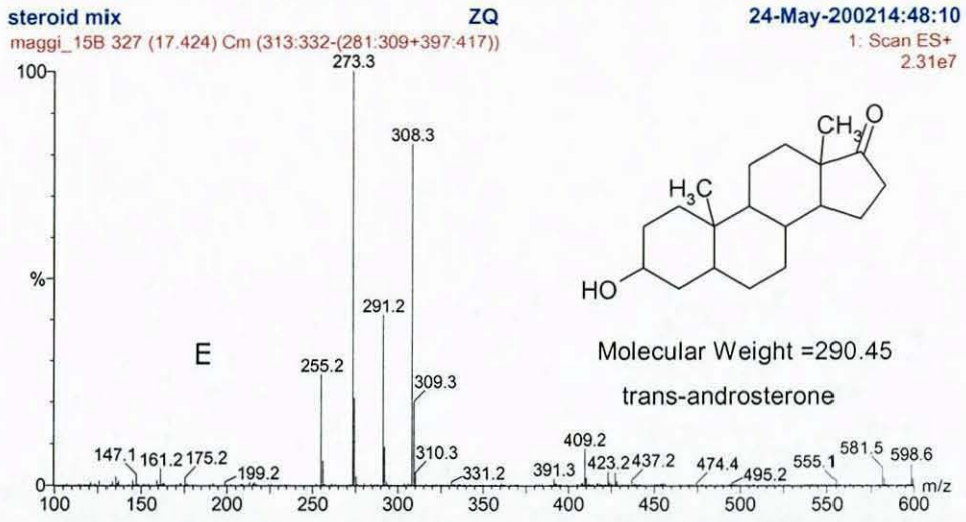

Figure 98 A – E: Mass spectra of 5 steroids, MS peaks A to E Figure 97 (A) 1,4,-androstadien-3,11,17-trione, (B) 19-nortestosteron, (C) testosterone, (D) dehydroiso androsterone, (E) trans androsterone

It was shown that it is possible to separate five steroids by superheated water chromatography. Furthermore, hyphenation with MS detection was shown to be feasible.

9.2.3 Separation and identification of phenolic acids in Echinacea nutraceuticals

Hydroxycinnamic acids, such as caffeic acid are ubiquitous constituents of higher plant cells. They occur naturally in a vast group of combined forms. Caffeic acid can occur in association with sugars, organic acids, amines, lipids and cyclohexane carboxylic acid [206]. In Echinacea purpurea it occurs in association with quinic acid as chlorogenic acid and in association with succinic acid as cichoric acid, which is known for its immunostimulatory properties [207]. Therefore, reliable methods for the identification and quantification of phenolic acids in plant extracts are of interest to the neutraceuticals industry.

9.2.3.1 Superheated water chromatography

The initial separation of three phenolic acids, 3,4-dihydroxy benzoic acid, caffeic acid (3,4-dihydroxy cinnamic acid) and chlorogenic acid

(phenolic acids mixed standard 1) was performed on a Hypersil HiPurity C18 column at 70 °C employing 100% water as the mobile phase. Figure 99 shows a chromatogram of the phenolic acid mix and the structures of the respective acids.

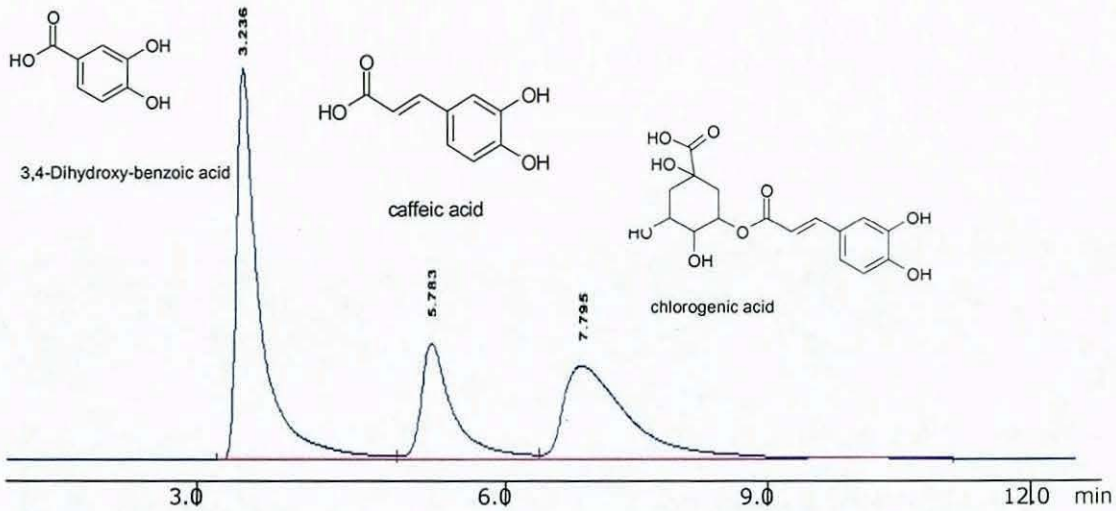

Figure 99: Phenolic acids mix in order of retention; 3,4-dihydroxy benzoic acid, caffeic acid (3,4 dihydroxy cinnamic acid) and chlorogenic acid separated on Hypersil HiPurity C18, 150 x 4.6 mm, 70 °C, mobile phase 100 % water plus 0.05% formic acid.

The peaks were very broad and the Hypersil column showed poor efficiency. This separation method was transferred to a PLRP-S column, which showed markedly higher retention and improved peak shape for the phenolic acids. In order to achieve acceptable retention times the separation temperature was increased to 150 °C. Figure 100 shows a chromatogram of the phenolic acids mix on the PLRP-S column at 150 °C employing 100 % water acidified with 0.05% formic acid as the mobile phase. This separation method was then employed to control the quality of various extraction methods for phenolic acids from commercially available Echinacea purpurea capsules.

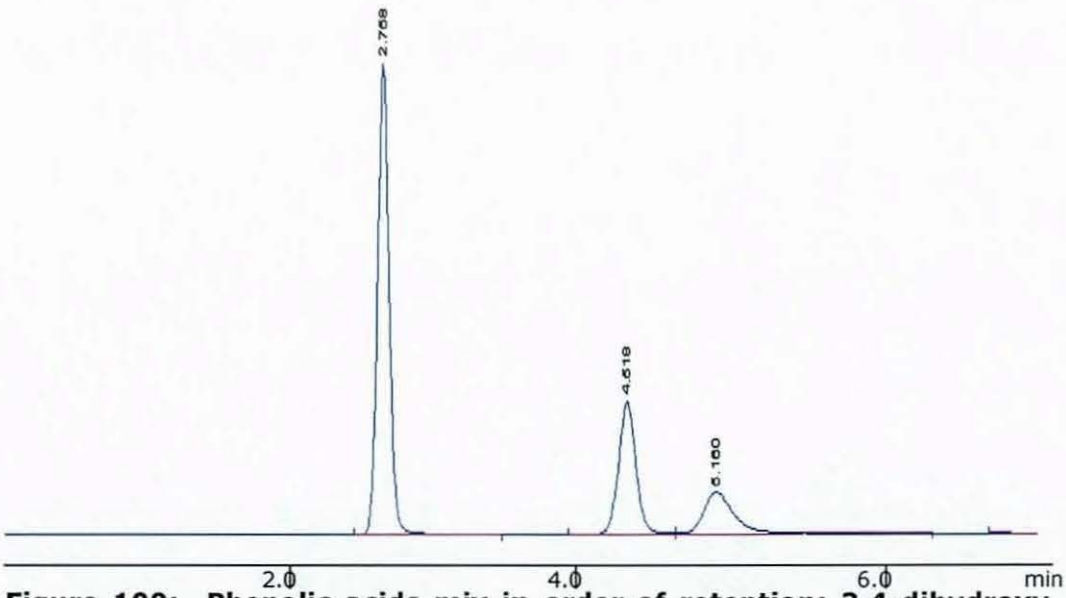

Figure 100: Phenolic acids mix in order of retention; 3,4-dihydroxy benzoic acid, caffeic acid (3,4-dihydroxy cinnamic acid) and chlorogenic acid separated on PLRP-S, 150 x 4.6 mm, 150 °C, mobile phase 100 % water plus 0.05% formic acid.

9.2.3.2 Extraction of phenolic acids

Four different extraction methods were tested regarding their performance for the extraction of phenolic acids from Echinacea capsules. The phenolic acids mix 1 was used in order to compare the recovery of the different extraction methods. The following extraction methods were investigated:

A: C_{18} SPE cartridge

B: NH_2 SPE cartridge

C: Si SPE cartridge

D: boiling methanol

Table 15 shows the equilibration steps, wash steps and elution steps for the different SPE cartridges. The effluent from the SPE cartridges from the different extraction steps (Table 15) was collected and injected into the HPLC system in order to trace whether material was lost during sample extraction or did not elute from the cartridge at all.

To test recovery of the liquid extraction method the liquid extraction was performed using 10 ml methanol and 1 ml of phenolic acids

standard mix 1. The methanol was boiled under reflux for 40 minutes. Subsequently the solvent was evaporated and the sample re-dissolved in 1 ml of 0.01 M NaOH. This solution was injected into the HPLC system.

Table 15: Equilibration, wash and elution steps for phenolic acids mix 1 from three different 1 ml SPE catridges. (A) C18 cartridge, (B) NH_2 cartridge, (C) Si cartridge.

	A C_{18}	B NH_2	C Si
equilibration	1 x methanol	1 x methanol	1 x methanol
	1 x water	1 x water	1 x methanol
sample application	1 ml phenolic acids mix 1	1 ml phenolic acids mix 1	1 ml phenolic acids mix 1
wash	1 x water + 0.005 % formic acid	1 ml acetonitrile	1 ml acetonitrile
elution I	1 ml 50 %methanol / 50 % water + 0.01 M NaOH	1 ml 50 %methanol / 50 % water + 0.01 M NaOH	1 ml 0.01 M NaOH
elution II	1 ml 50 %methanol / 50 % water + 0.01 M NaOH	1 ml 50 %methanol / 50 % water + 0.01 M NaOH	1 ml 0.01 M NaOH

The peak areas of a standard injection and injections of the effluent of the SPE cartridges were compared to calculate recovery. Table 16 shows the percentage recovery for the different steps and compounds for the three SPE cartridges.

The recovery for the methanol extraction was 96 %.

Analysing the data in Table 16 comparing the different SPE extractions the best extraction was achieved with the aminopropyl SPE cartridge.

The diluent of standard mix 1 was water. Because of the use of water as the solvent the phenolic acids were not retained on the Si cartridge.

The liquid extraction with boiling methanol (taken up in 1 ml 0.01 M NaOH) showed comparable recovery rates.

Table 16: percent recovery for (1) 3,4-dihydroxybenzoic acid, (2) caffeic acid and (3) chlorogenic acid from three different extraction cartridges, (A) C18 cartridge, (B) NH_2 cartridge, (C) Si cartridge.

	A C_{18}			B NH_2			C Si		
Compound	1	2	3	1	2	3	1	2	3
Sample application (unretained)	30 %	< 1 %	8 %	< 1 %	< 1 %	< 1 %	83 %	84 %	83 %
Wash	54 %	1 %	7 %	< 1 %	< 1 %	< 1 %	10 %	11 %	10 %
Elution I	9 %	71 %	62 %	80 %	95 %	95 %	< 1 %	< 1 %	< 1 %
Elution II	2 %	27 %	21 %	15 %	2 %	2 %	< 1 %	< 1 %	< 1 %
Total	95 %	99 %	98 %	95 %	97 %	97 %	93 %	95 %	93 %

Extractions were then performed using the dried plant material taken out of commercially available capsules. However, the SPE cartridges blocked very easily when the dried plant material was extracted. Therefore, it was decided to use the liquid extraction for the extraction of plant material.

For the analysis of the phenolics in Echinacea 10 capsules of Holland's and Barrett's Echinacea capsules were opened and the pulverised plant material was extracted under reflux in methanol. The yellow colour of the alkaline liquid confirmed the presence of phenolics in the extract [206]. However, injection into the HPLC (Figure 101 A-B) system showed that the concentration of phenolics in the extracted material was insufficient for easy analysis.

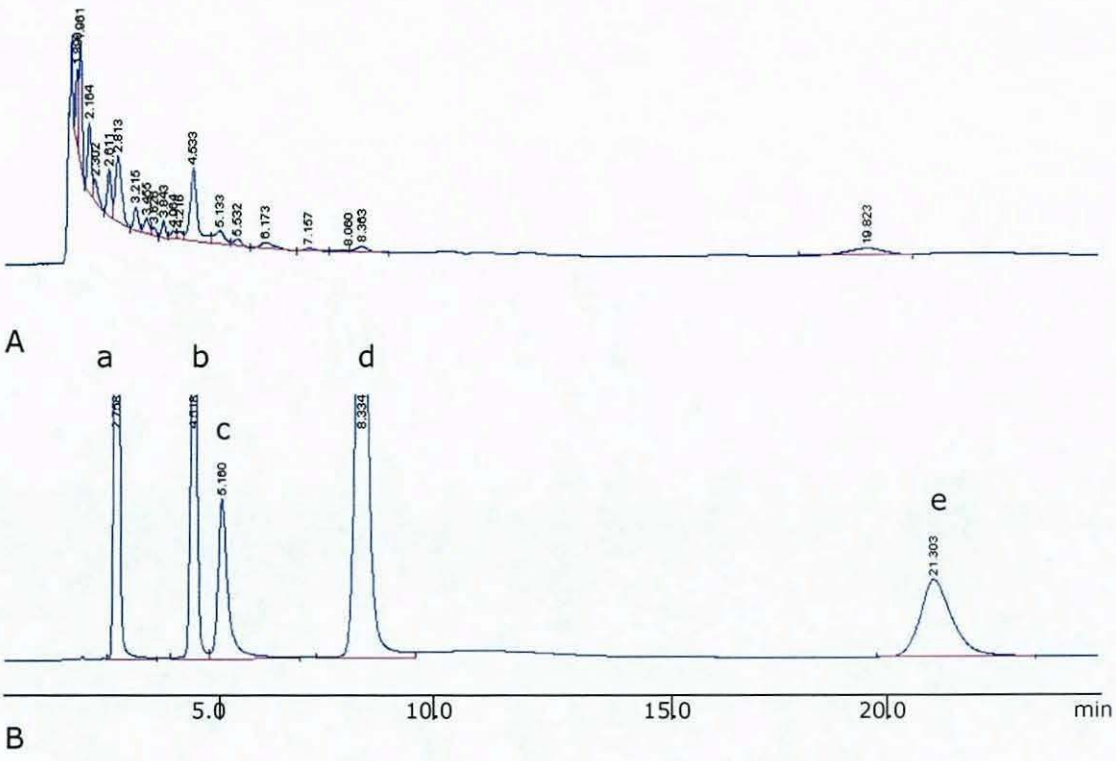

Figure 101 A - B: A: 20 µl Methanol extract of 10 Echinacea purpurea capsules; B: 20 µl, 1 mg/ml standard injection of 5 phenolic acids. Respective order of retention (a) 3,4-dihydroxy benzoic acid, (b) caffeic acid, (c) chlorogenic acid, (d) vanillic acid and (e) ferulic acid. Conditions: PLRP-S 150 x 4.6 mm id, mobile phase: 100 % water at 150 °C, UV 254 nm.

Furthermore, the early eluting phenolic acids were masked by impurities, which were extracted with the methanol extraction. As there were later eluting peaks in the extract two well retained phenolic acids potentially present in the plant extract, vanillic acid and ferrulic acid were added to the standard mix.

The extraction was repeated with the content of 50 capsules in order to increase the concentration of extracted phenolics. The pulverised plant material was boiled under reflux with methanol. Figure 102 shows a chromatogram of 20 µl extract injected into the HPLC system.

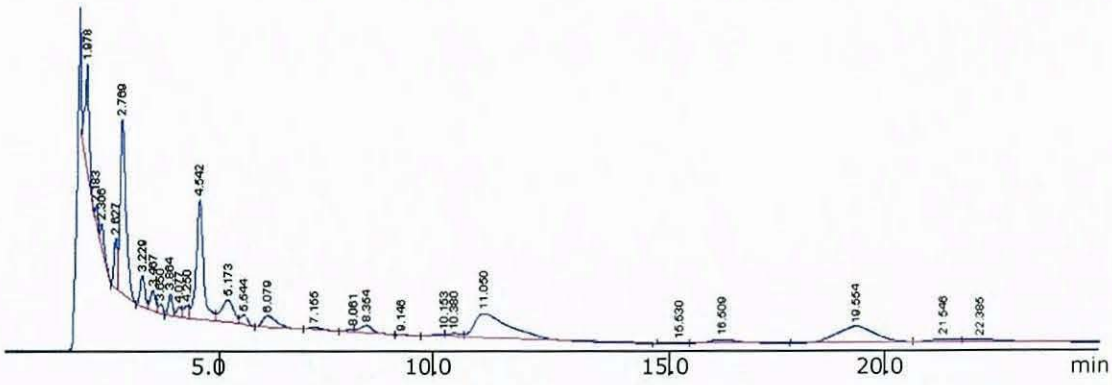

Figure 102: Methanol extract of 50 Echinacea purpurea capsules in 10 ml, PLRP-S 150 x 4.6 mm id, mobile phase water, 150 °C, UV 254 nm.

The concentration of the extract is considerably higher, however, the early eluting peaks still co-elute with early eluting impurities. A temperature gradient was developed in order to separate the early eluting phenolic acids from these extraction impurities. The initial separation temperature was 100 °C, after 10 minutes, temperature was increased by 4 °C/min up to 185 °C.

Figure 103 A and B show a chromatogram of the extract of 50 capsules and of the phenolic acid standards respectively under temperature gradient conditions.

All the peaks were well separated. When matching up retention times in the chromatogram of the standards with those in the chromatogram of the extract, it appeared that all five of the phenolics in the standard mix were also present in the extract. The levels of chlorogenic acid and vanillic acid were very low in the extract. However, because of extraction impurities it was not possible to identify the phenolic acids unambiguously. Furthermore, one additional peak at about 7 minutes and another larger peak at about 27 minutes were present in the extract. None of these could be seen in the standard.

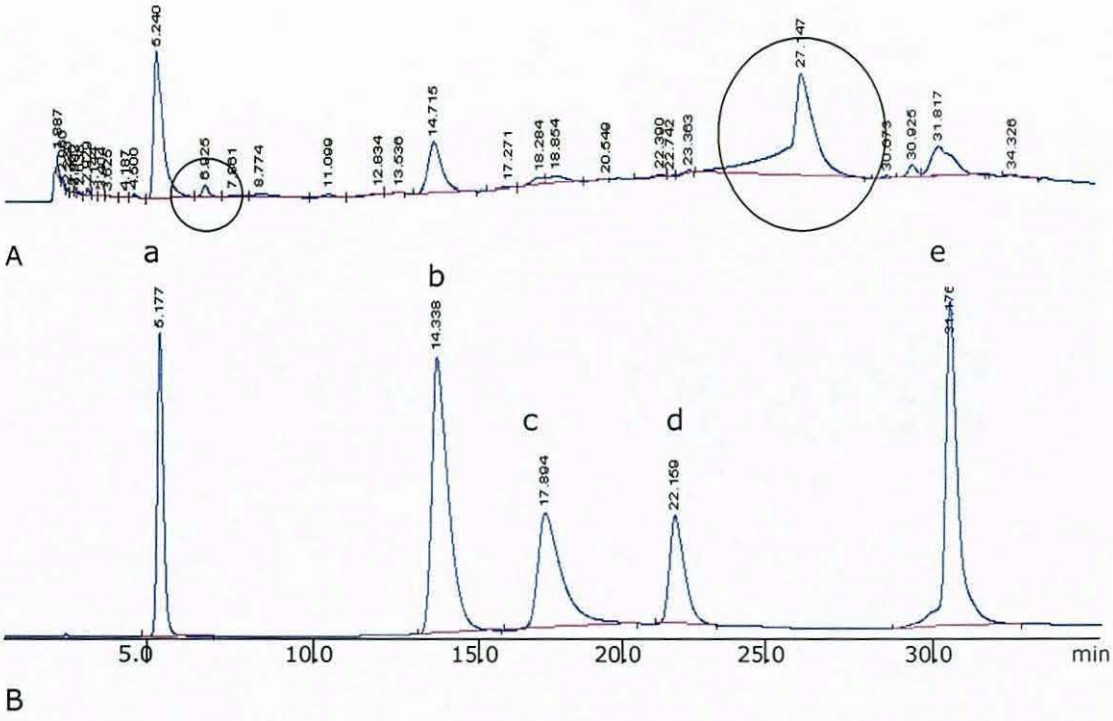

Figure 103 A - B: A: 20 µl Methanol extract of 50 Echinacea purpurea capsules; B: 20 µl, 1 mg.ml standard injection of 5 phenolic acids. In order of retention (a) 3,4-dihydroxy benzoic acid, (b) caffeic acid, (c) chlorogenic acid, (d) vanillic acid and (e) ferulic acid. PLRP-S 150 x 4.6 mm id, mobile phase water, temperature gradient 100 °C for 10 minutes, 4 °C/min up to 185 °C, hold 10 minutes, flow 1.0, UV 254 nm.

The peak at 27 minutes seemed to be co-eluting with a compound showing a very broad and flat peak.

9.2.3.3 Superheated water MS

In order to identify the phenolics extracted from the ground and dried plant material in the capsules, the above separation was hyphenated with mass spectroscopy. Figure 104 shows the UV and the negative ion trace for the standard mix. The retention times are slightly longer as a different HPLC system was used. Furthermore the transfer capillary to the MS instrument was longer than the capillary leading into the diode array detector.

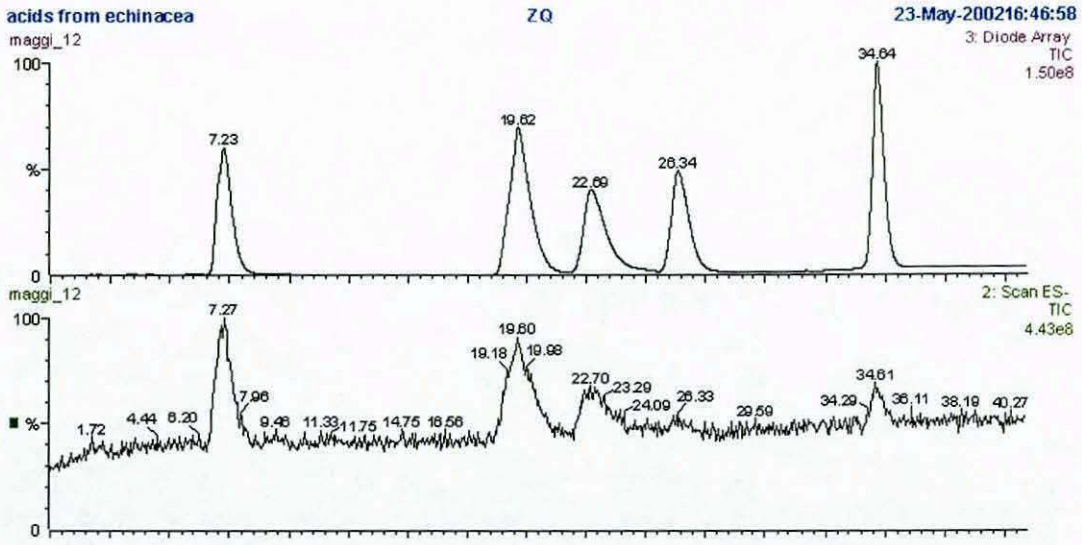

Figure 104: 20 µl, 1 mg.ml standard injection of 5 phenolic acids. In order of retention 3,4-dihydroxy benzoic acid, caffeic acid, chlorogenic acid, vanillic acid and ferrulic acid. PLRP-S 150 x 4.6 mm id, mobile phase water, temperature gradient 100 °C for 10 minutes, 4 °C/min up to 185 °C, hold 10 minutes, flow 1.0, UV 254 nm and negative ion trace.

The spectra for all acids present in the standard mix were collected. Figure 105 shows the spectra from the standard injection. A good spectrum could be achieved for all compounds of the mix. Subsequently the Echinacea extract was injected. The negative ion trace collected from the methanolic extract of 50 capsules was collected (Figure 106).

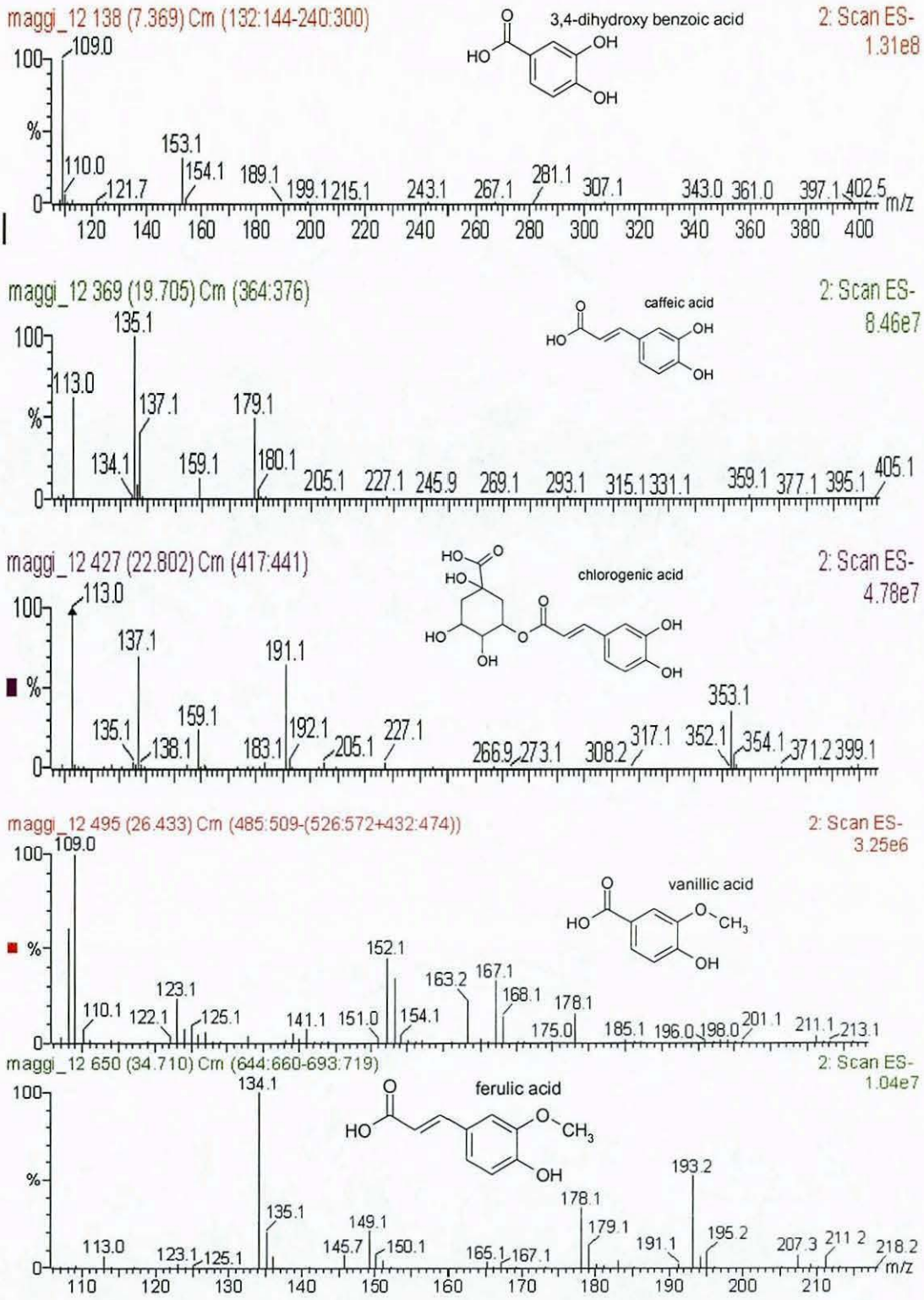

Figure 105: Negative ion spectra collected from phenolic acids standard, 3,4-dihydroxy benzoic acid (M = 154), caffeic acid/cinnamic acid (M = 180), chlorogenic acid (M = 354), vanillic acid (M = 168) and ferulic acid (M = 194)

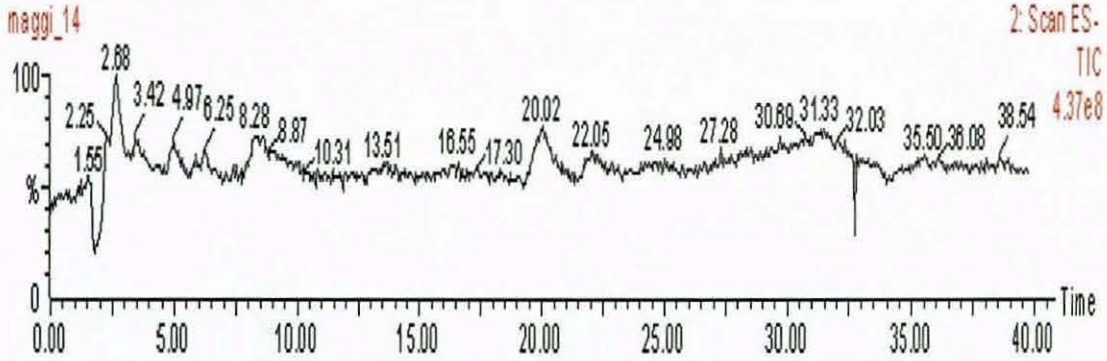

Figure 106: negative ion trace of methanolic extract of 50 capsules filled with dried and ground plant material of echinacea purpurea. PLRP-S 150 x 4.6 mm id, mobile phase water, temperature gradient 100 °C for 10 minutes, 4 °C/min up to 185 °C, hold 10 minutes, flow 1.0, 20 µl injection volume.

The negative ion peak for 3,4-dihydroxy benzoic acid was detected at 7.27 minutes in the standard chromatogram. No peak could be detected in the negative ion trace collected from the extract at that retention time. However, there was a peak at about 8.4 minutes, Figure 107 shows the spectrum extracted from the peak.

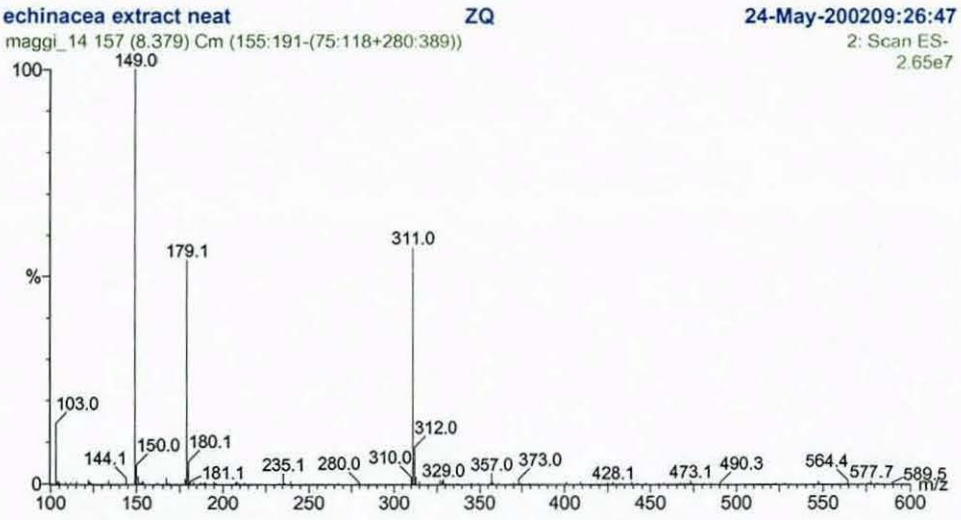

Figure 107: Mass spectrum extracted from peak at 8.379 minutes in chromatogram of Echinacea purpurea extract.

3,4-dihydroxy benzoic acid has a molecular mass of M = 154. The spectrum clearly does not reflect the molecular mass for 3,4-dihydroxy benzoic acid.

However, taking a spectrum from the front of the peak, at 8.058 minutes instead of the apex of the peak gave a different picture. Figure 108 shows the spectrum extracted from the front of the peak.

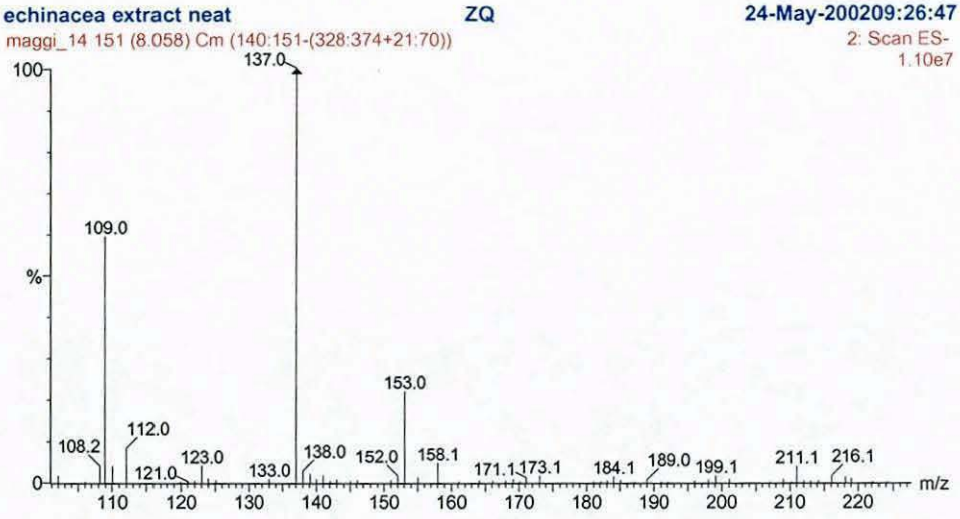

Figure 108: Mass spectrum extracted from peak at 8.058 minutes in chromatogram of Echinacea extract.

The spectrum confirmed the presence of 3,4-dihydroxy benzoic acid. The mass peak 137 can be ascribed to the presence of mono hydroxy benzoic acid. However, the hydroxy benzoic acids were obviously co-eluting with another unknown compound.

When Figure 106 is compared with Figure 104 one can see that the ionisation of chlorogenic acid and vanillic acid is not very good in the standard. Whereas the ionisation for caffeic acid was very good. The spectrum extracted from the peak at 20 minutes (Figure 106), which was assumed to be caffeic acid due to the retention time match, is shown in Figure 109. The spectrum extracted from the peak confirmed the peak as caffeic acid.

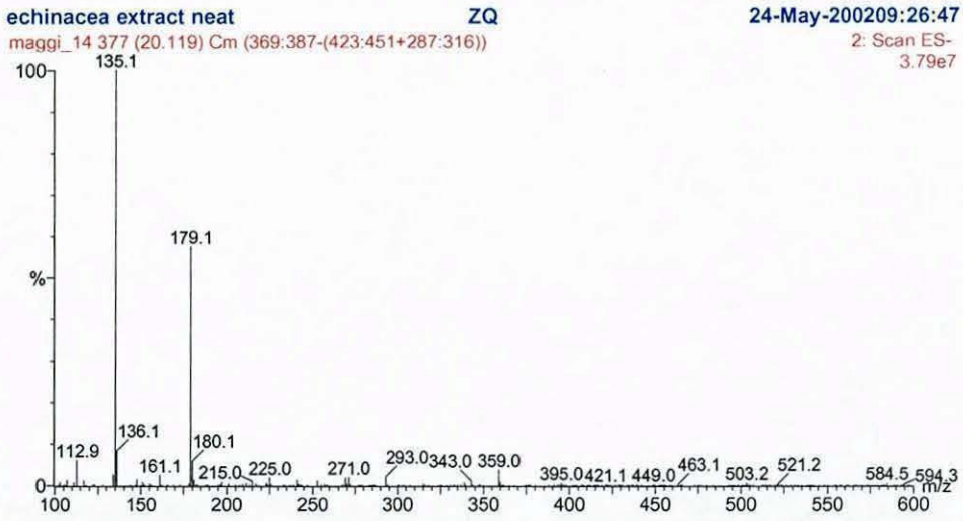

Figure 109: Spectrum extracted from peak at 20.119 minutes. Spectrum confirms caffeic acid M^{-1}.

Matching the retention time of standard and extract the next peak at about 22 - 23 minutes was expected to be chlorogenic acid. Similar to the standard negative ion trace the response was not very good. However, it was possible to extract a good spectrum from the peak. Figure 110 shows the spectrum extracted from the peak.

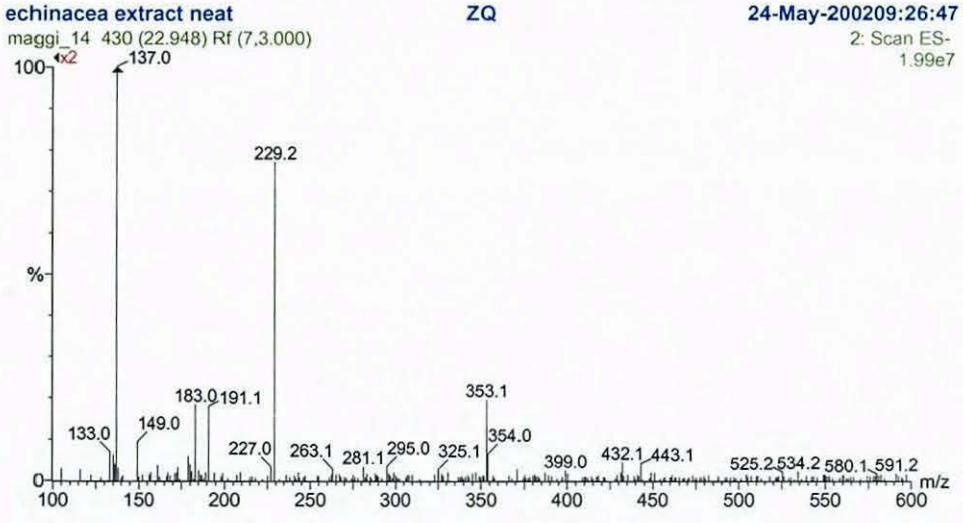

Figure 110: Spectrum extracted from peak at 22.948 minutes. Spectrum confirms chlorogenic acid M^{-1}.

The spectrum tied in with the retention time match that the peak eluting at about 22 - 23 minutes contained chlorogenic. However, the mass peak at 229 was not seen in the spectrum extracted from the standard for chlorogenic acid (Figure 105).

Spectra for vanilic acid, eluting in the standard chromatogram at about 26 minutes and for ferulic acid eluting at about 34.5 minutes could not be extracted from the chromatogram of the Echinacea extract.

A further peak was detected at 31.4 minutes. The peak could not be retention time matched with any of the peaks in the standard's chromatogram. Figure 111 shows the spectrum extracted from the peak eluting at 31.433 minutes.

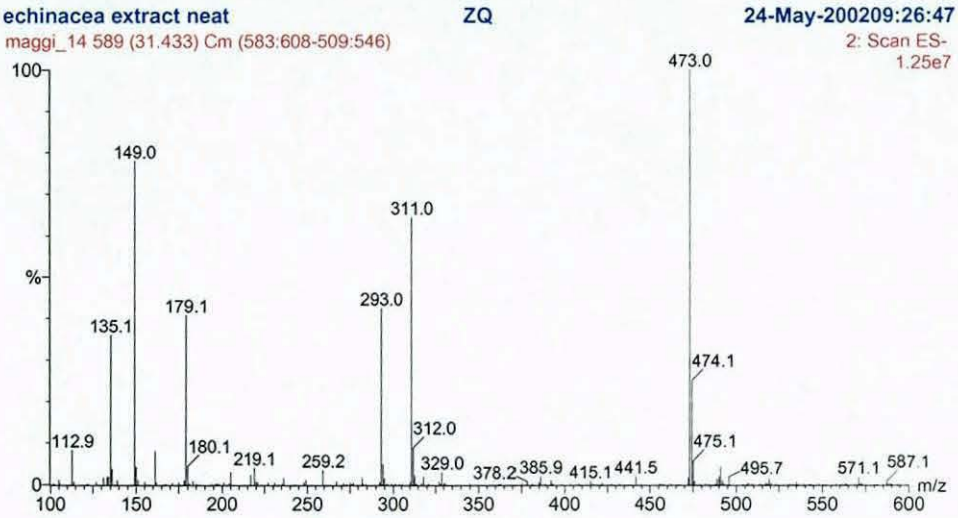

Figure 111: Spectrum extracted from peak at 31.433 minutes.

The presence of the masses M^{-1} = 135 and 179 in the spectrum of the peak pointed to caffeic acid being a likely building block for this compound. Further more, the mass M^{-1} = 311 had been found in the spectrum at 8.379 minutes (see Figure 107), a compound co-eluting with 3,4-dihydroxy benzoic acid. A selective ion scan for the masses M^{-1} = 473, 311 and 179 was performed in order to find out whether there was a link between caffeic acid, the early eluting unknown compound and the unknown compound eluting at 31.4 minutes. The retention times where the masses were found tied in with the idea that caffeic acid was likely to be a building block of the unknown compound. The spectra extracted from the peaks made it possible to

propose a structure for the two unknown compounds. Figure 112 shows the spectra and proposed structures.

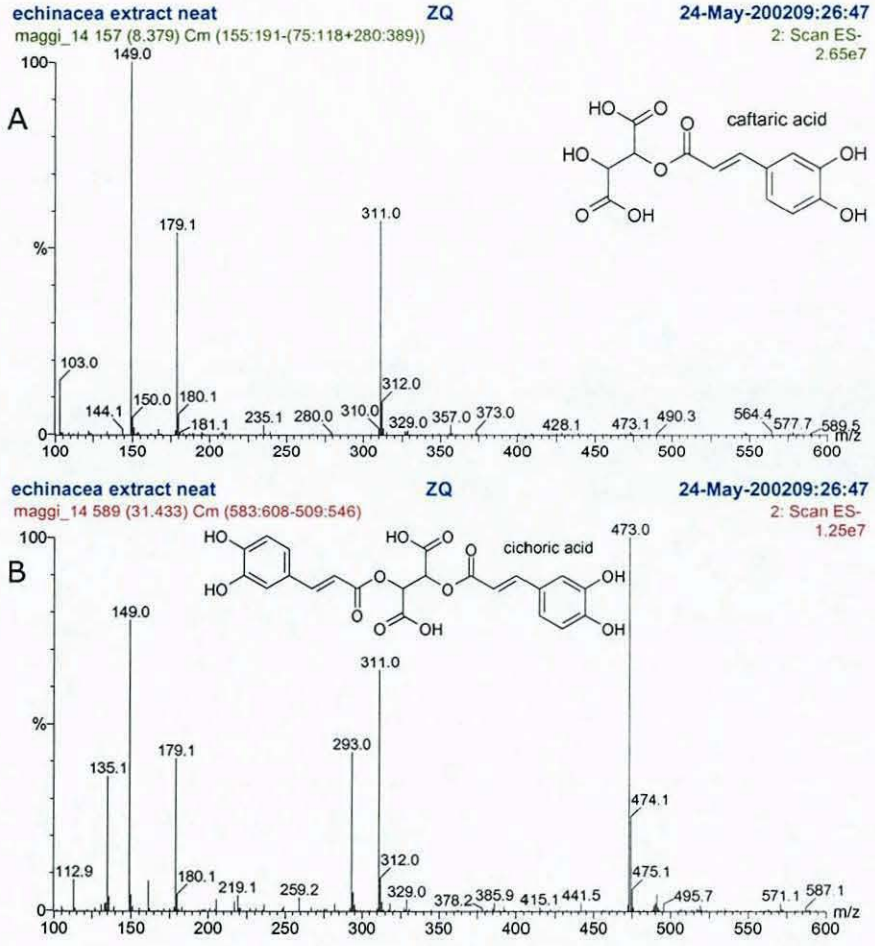

Figure 112: Mass spectra extracted from (A) the peak at 8.379 minutes and (B) the peak at 31.433 minutes and proposed structures.

Other researchers [207] have identified these compounds in Echinacea plant extract and nutraceuticals.

The following fragment pattern was suggested for the spectra in Figure 112 A: caftaric acid (M = 312), 3, 4-dihydroxy cinnamic acid fragment (caffeic acid) (M = 180), 2,3-dihydroxy-succinic acid fragment (tartaric acid, structure see Figure 113) (M = 150); for Figure 112 B: cichoric acid (M = 474), caftaric acid (M = 312), 2-[3-(3,4-dihydroxy-phenyl)-acroloyloxy]-but-2-enedioic acid fragment (structure see Figure 113) (M = 294) 3, 4-dihydroxy cinnamic acid (caffeic acid) (M = 180), 2,3-dihydroxy-succinic acid (tartaric acid) (M = 150), 4-vinyl-benzene-1,2-diol (structure see Figure 113) (M = 136).

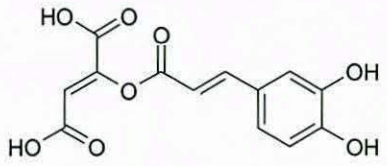

M = 294

2-[3-(3,4-Dihydroxy-phenyl)-acryloyloxy]-but-2-enedioic acid

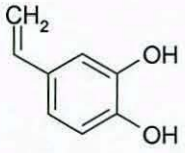

M = 136

4-Vinyl-benzene-1,2-diol

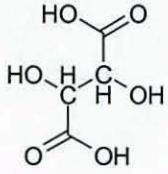

M = 150

2,3-Dihydroxy-succinic acid

Figure 113: Some of the proposed structures of fragments from caftaric acid and cichoric acid (see Figure 112) for remaining structures see Figure 105.

Standards for these compounds were unfortunately not available. Different means of structure identification will have to be applied to confirm these structures with any degree of certainty in a future study.

The hyphenation of superheated water chromatography and MS spectroscopy made it possible to identify phenolic acids in Echinacea neutraceuticals. However, elucidation of unknown structures can only be performed unambiguously employing NMR spectroscopy or standards.

9.2.4 Identification of methylated xanthines and caffeic acid

If co-eluting peaks or two different analytes possess the same molecular mass, it is impossible to identify them as two different

compounds by MS. One example for this happening is when theophylline, theobromine, caffeine and caffeic acid need to be distinguished.

9.2.4.1 Superheated water MS

The mixture of 3,4-dihydroxy benzoic acid, caffeic acid and methylated xanthines, theophyllin, theobromine and caffeine was separated at 150 °C on a PLRP-S column. Mobile phase was 100 % water. Figure 114 shows a typical separation of the standard mix.

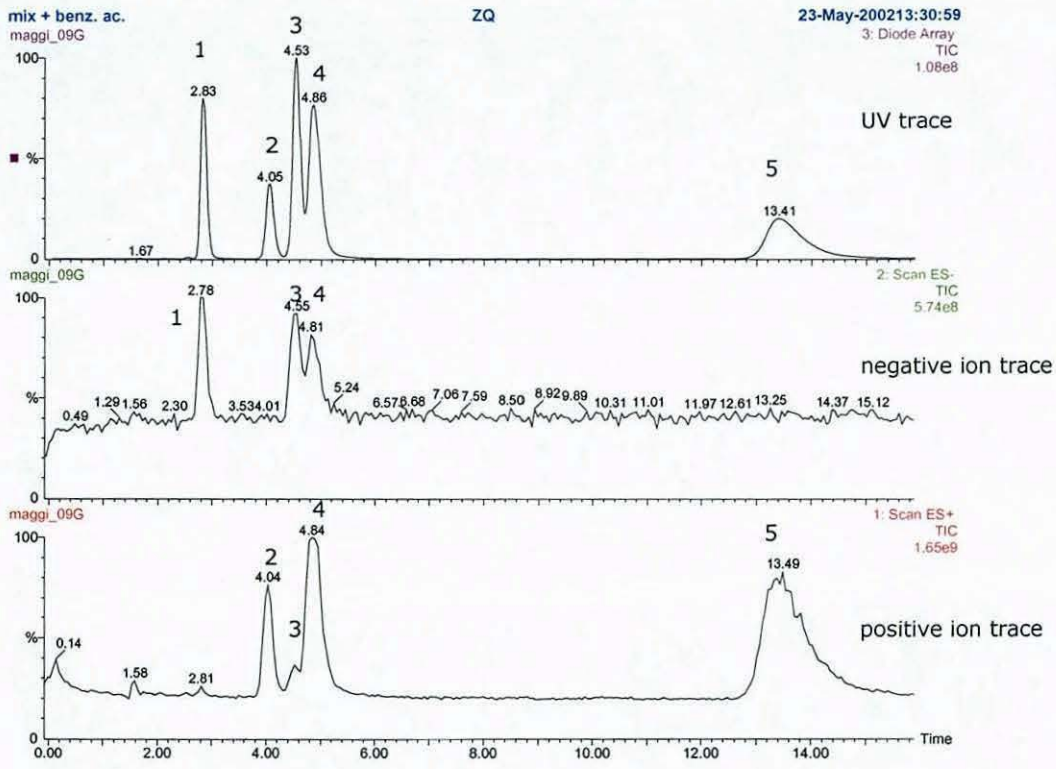

Figure 114: UV trace, positive ion and negative ion trace of a mixed standard on PRLP-S, 150 x 4.6 mm, flow 1.0 ml/min, mobile phase 100 % water + 0.01 % formic acid, 150 °C column temperature, compounds in order of retention, (1) 3,4-dihydroxy benzoic acid, (2) theobromine, (3) caffeic acid, (4) theophylline, (5) caffeine.

Theobromine, theophylline and caffeic acid all have the same molecular weight therefore it is not possible to distinguish these compounds on the grounds of the weight of the molecular ion only. Figure 115 shows the M^+ spectra and Figure 116 shows the M^- spectra extracted from the peaks in Figure 114. Caffeine, peak 5, has a higher molecular weight and is well separated. Therefore the MS

spectrum of peak 5 is not shown below. Note that theobromine was only seen in the positive ion trace and 3,4-dihydroxy benzoic acid was only seen in the negative ion trace, which can help in the identification of these compounds in a mixture.

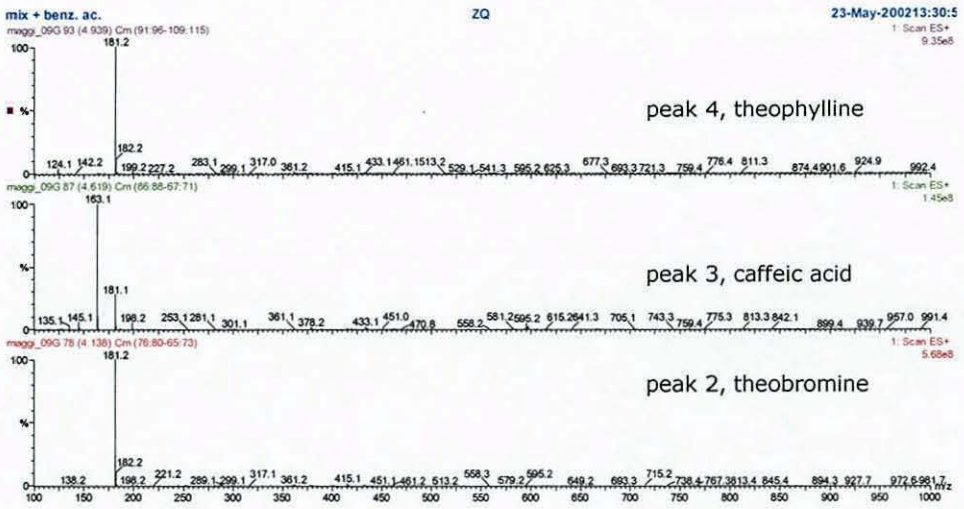

Figure 115: M^+ spectra of the three peaks at 4.1 (peak 2), 4.6 (peak 3) and 4.9 (peak 4) minutes.

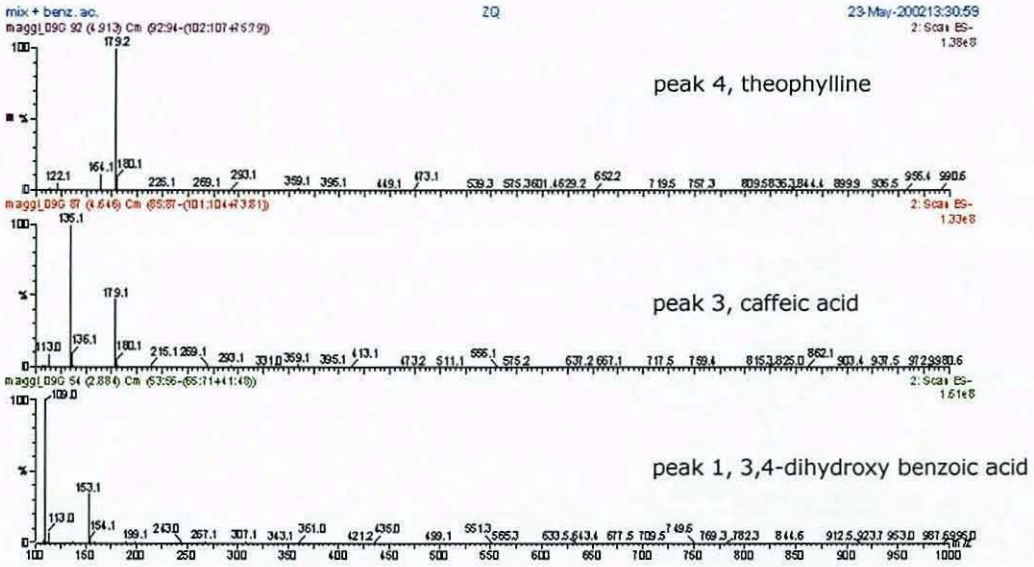

Figure 116: M^- spectra of the three peaks at 2.8 (peak 1), 4.6 (peak 3) and 4.9 (peak 4) minutes.

Theophylline and theobromine could not be distinguishable at all on the basis of the M^+ spectra while caffeic acid showed a fragment at the mass 163 in M^+. a fragment at 135 in M^-. However, it is not possible

to distinguish the three compounds unambiguously. NMR offers the capability to give the structural information required.

9.2.4.2 Superheated water chromatography – NMR

The major advantage of combining superheated water chromatography with NMR spectroscopy is that only one solvent is used, water. When water is replaced by deuterium oxide the whole spectral region is made available because the solvent signal vanishes. The biggest drawback of NMR is most certainly the lack in sensitivity. Samples of about 0.05 M concentration have to be injected in order to produce a signal sufficiently strong for on-flow spectral analysis. In the stop-flow mode the concentration can be slightly lower, however, a sample concentration of less than about 0.02 M is insufficient for either mode [208], however, the instrumentation is rapidly improving. Figure 117 shows the UV trace and the NMR trace of a standards mix of theobromine, theophylline and caffeine.

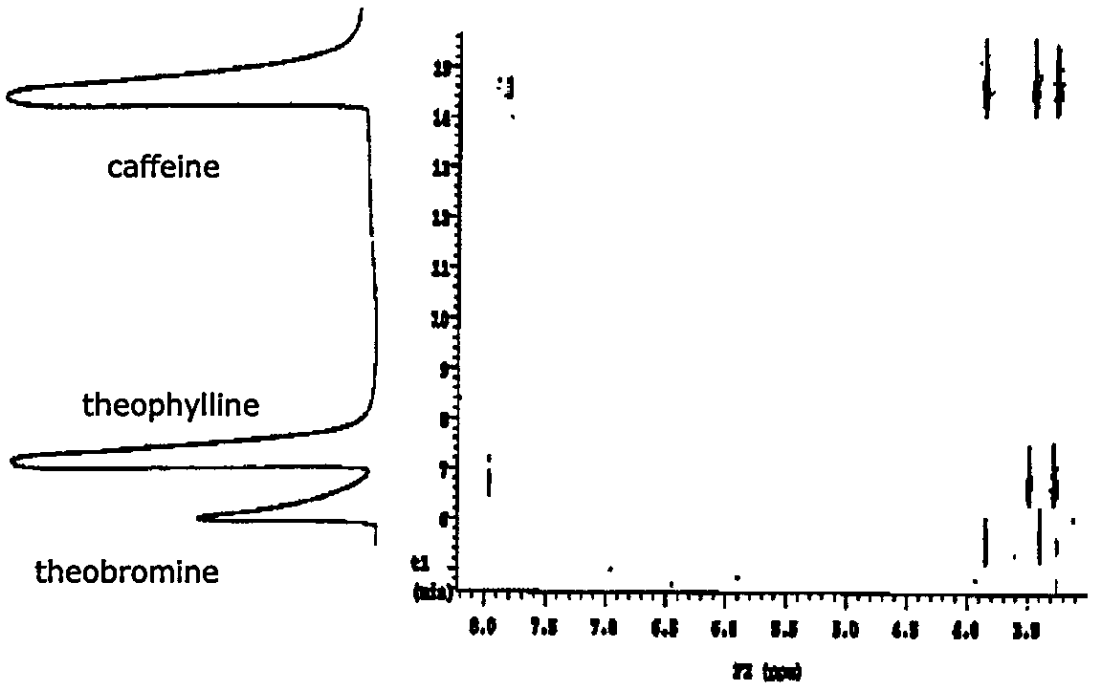

Figure 117: LC-NMR trace 400 MHz and UV trace of theobromine, theophylline and caffeine standard, separated on PLRP-S, 150 x 4.6 mm, 150 °C, mobile phase 100 % D_2O, flow rate 1.0 ml/min, 20 µl injection volume.

Each compound is present at a concentration of 0.05 M/l. The molecular mass of theobromine and theophylline is 180, for caffeine it is 194. A 0.05 M solution of theobromine, theophylline and caffeine is then equivalent to a concentration of about 10 mg/ml of each standard. The separation of the three compounds is sufficient to distinguish three peaks in the UV trace. However, the peak shape is not very good and the separation efficiency is low because the column was overloaded in order to obtain a good NMR on-flow signal. Figure 118 shows part of the spectra extracted from the separation. The distinguishing factor for the three methylated xanthines is the position of the methyl group. Therefore the chemical shifts between 2 and 6 were compared for the three compounds.

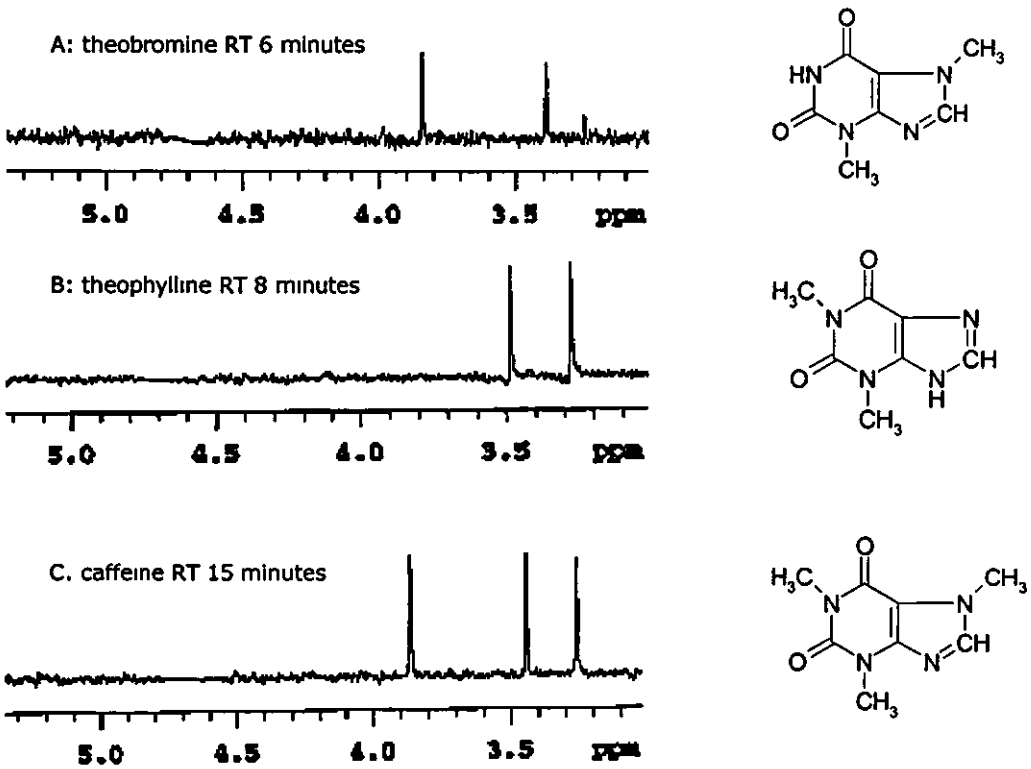

Figure 118 A - C: A: theobromine 400 MHz NMR spectrum, B: theophylline 400 MHz NMR spectrum, C: caffeine 400 MHZ NMR spectrum, spectra extracted from LC-NMR on-flow run of xanthine standard mix, separated on PLRP-S, mobile phase 100% D_2O, T = 150 °C, C = 0.05 M/l.

The masses of the first two molecules are identical but the NMR spectra make it possible to distinguish unambiguously between

theobromine and theophylline because of the chemical shifts of the methyl groups on the molecule.

Figure 119 shows the chromatogram (UV trace) and NMR trace of a standard mix of theobromine, theophylline, caffeic acid and caffeine. The concentration of each compound is 0.05 M/l. Theophylline and caffeic acid co-elute under the applied separation conditions.

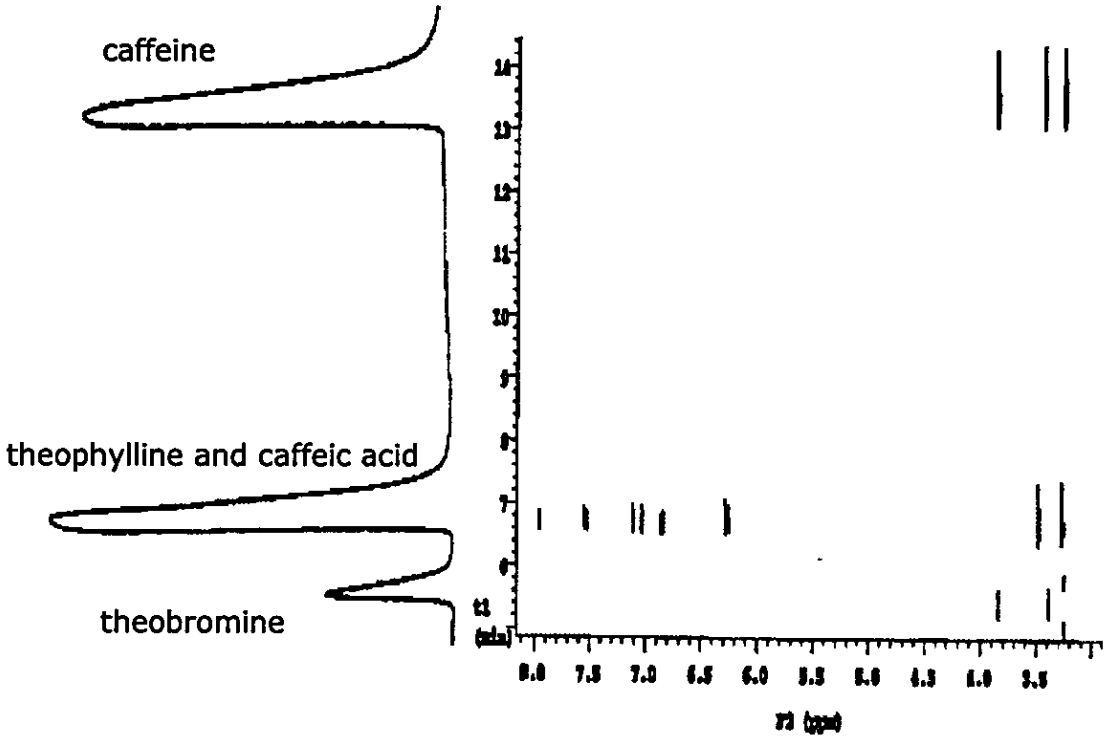

Figure 119: LC-NMR trace 400 MHz and UV trace of theobromine, theophylline, caffeic acid and caffeine standard, separated on PLRP-S, 150 x 4.6 mm, 150 °C, mobile phase 100 % D_2O, flow rate 1.0 ml/min, 20 µl injection volume.

The spectra for theobromine and caffeine were similar to those shown in Figure 118 A and C. The spectrum for the peak at 7.5 minutes is a mixture of the spectrum shown in Figure 118 B and the spectrum for caffeic acid. A slight difference in peak width compared to Figure 117 could be a possible indication of an extra component. However, the spectral data, additional chemical shifts in the spectrum give a clear indication of an extra component.

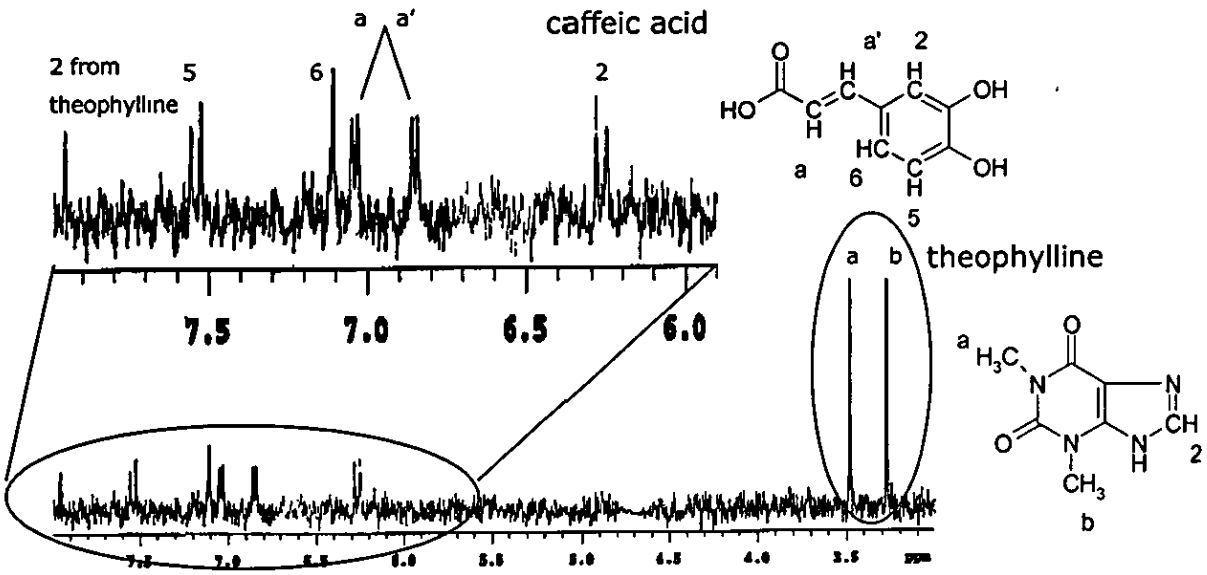

Figure 120: caffeic acid and theophylline co-eluting 400 MHZ NMR spectrum, spectra extracted from LC-NMR on-flow run of xanthine standard mix, separated on PLRP-S, mobile phase 100% D_2O, T = 150 °C, C = 0.05 M/l.

Without the information gained from the NMR spectrum it would have been impossible to know that the two compounds, theophylline and caffeic acid were coeluting. Only the NMR spectrum gives the clear indication that the peak does not only contain theophylline.

It was not possible to get good quality spectra from extracted coffee and tea samples because the concentration of the samples was too low.

10 CONCLUSIONS

The application of reversed phase elevated temperature chromatography showed to be advantageous for the separations carried out in this work. The analysis times could be reduced and improvements in separation selectivity (beta-blockers) were achieved.

It was shown that it is feasible to predict the retention times of compounds at elevated temperatures and under superheated water chromatography conditions. On the basis of a small number of experiments performed at lower temperatures and varying mobile phase compositions applying empirical equations the retention times were predicted with reasonable accuracy (+/-10% on average).

The application of MS as a detector for LC is fairly standard these days. It was therefore important that the hyphenation of elevated temperature reversed phase chromatography and superheated water chromatography with MS was easy to realise. Guiding the capillary connected to the column outlet through a water jacket cooled the effluent of the column sufficiently. The effluent could flow into the UV detection cell and the MS in the same way it does when running standard reversed phase chromatography.

The hyphenation of LC with NMR has gained in interest particularly for applications in drug metabolism and pharmaco-kinetics. The hyphenation of superheated deuterium oxide chromatography with NMR spectroscopy was demonstrated in this work. The major advantage of superheated deuterium oxide over the application of a solvent mix in LC-NMR is the possibility to use the full spectral bandwidth. However, the mass sensitivity of NMR spectroscopy is low in comparison to MS and UV spectroscopy. New developments in instrumentation promises improved

mass sensitivity for on-flow LC-NMR [209]. Furthermore, the hyphenation of SPE-NMR makes it possible to use "cheap" un-deuterated solvents and HPLC additives for the separation [209]. The sample is collected and dried on a SPE cartridge before it is transferred to the NMR system. Hence, it can be concentrated on the SPE cartridge and deuterated solvents only need to be used to elute the sample from the SPE cartridge. The application of superheated water chromatography could prove advantageous for the sample collection on SPE cartridges because the SPE cartridges are held at room temperature, where water is a very weak eluent.

References:

[1] B.L. Karger, L.R. Snyder and C. Horváth, An introduction to separation science, John Wiley & Sons, Inc., New York, 1973, pp. 63

[2] E.H. Smith and C. Davis, J. Environ. Sci. Health A, 32 (1997) 171

[3] E. Forgács and T. Cserháti, Molecular basis of chromatographic separation, CRC Press, Boca Raton; New York, 1997, pp. 118

[4] L.R. Snyder, J. Chromatogr. Sci., 16 (1978) 223

[5] L.R. Snyder, J. Chromatogr., 92 (1974) 223

[6] J. Wyman, Phys. Review, 35 (1930) 623

[7] G. Åkerlöf, J. Am. Chem. Soc., 54 (1932) 4125

[8] G.C. Akerlof and H.I. Oshry, J. Am. Chem. Soc., 720 (1950) 2844

[9] L.R. Snyder and J.J. Kirkland, Introduction to modern liquid chromatography, John Wiley & Sons, Inc., New York, 1979, pp. 248

[10] Y. Yang, A.D. Jones and C.D. Eaton, Anal. Chem., 71 (1999) 3808

[11] L.A. Cole, J.G. Dorsey and K.A. Dill, Anal. Chem., 64 (1992) 1324

[12] D.J. Miller and S.B. Hawthorne, Anal. Chem., 70 (1998) 1618

[13] Y. Yang, M. Belghazi, A. Lagadec, D.J. Miller and S.B. Hawthorne, J. Chromatogr. A, 810 (1998) 149

[14] D.J. Miller and S.B. Hawthorne, Anal. Chem., 69 (1997) 623

[15] R.M. Smith and R.J. Burgess, Anal. Communications, 33 (1996) 327

[16] T.E. Young, S.T. Ecker, R.E. Synovec, N.T. Hawley, J.P. Lomber and C.M. Wai, Talanta, 45 (1998) 1189

[17] W. Hu, K. Hasebe and P.R. Haddad, Anal. Communications, 34 (1997) 311

[18] Y. Yang, A.D. Jones and C.D. Eaton, Anal. Chem., 71 (1999) 3808

[19] J.R. Bone and R.M. Smith, Anal. Communications, 36 (1999) 375

[20] E.N.daC.Andrade, Nature, 125 (1930) 309

[21] H. Chen and C. Horváth, Anal. Methods and Instrumentation, 1 (1993) 213

[22] C. Horváth and W. Melander, J. Chromatogr. Sci., 15 (1977) 393

[23] J. Li and P.W. Carr, Anal. Chem., 69 (1997) 2530

[24] R.C.Reid, J.M.Prausnite and T.K.Sherwood, The properties of gases and liquids, McGraw-Hill, New York, 1997, pp. 457

[25] E. Scheibel, Ind. Eng. Chem, 46 (1954) 2007

[26] K.A.Reddy and L.K.Doraiswamy, Ind. Eng. Chem. Fundam., 6 (1967) 77

[27] M.A.Lusis and .A.Ratcliff, Can. J. Chem. Eng., 46 (1968) 385

[28] W.Hayduk and .Landie, AICHE J., 20 (1974) 611

[29] C.R.Wilke and .Chang, AICHE J., 1 (1955) 264

[30] K. Sudgen, G.B. Cox and C.R. Loscombe, J. Chromatogr., 149 (1978) 377

[31] G.B. Cox and ..W. Stout, J. Chromatogr., 384 (1987) 315

[32] W. Marshall and E. Franck, J. Phys. Chem. Ref. Data, 10 (1981) 295

[33] P. Kryukov and V. Perkvets, Izv. Sib. Otd. Akad. Nauk. SSSR, Ser. Khim. Nauk, 2 (1966) 29

[34] O. Chienthavorn and R.M. Smith, Chromatographia, 50 (1999) 485

[35] A. Albert and E.P. Serjeant, The determination of ionisation constants,Chapman and Hall, London, 1984

[36] D.V. McCalley, J. Chromatogr. A, 902 (2000) 311

[37] J.H. Knox and G. Vasvari, J. Chromatogr., 83 (1973) 181

[38] D. Morel and J. Serpinet, J. Chromatogr., 200 (1980) 95

[39] D. Morel and J. Serpinet, J. Chromatogr., 214 (1981) 202

[40] D. Morel and J. Serpinet, J. Chromatogr., 248 (1982) 231

[41] K. Jinno, T. Ibuki, N. Tanaka, M. Okamoto, J.C. Fetzer, W.R. Biggs, P.R. Griffiths and J.M. Olinger, J. Chromatogr., 461 (1989) 209

[42] K. Cabrera, D. Lubda, H.-M. Eggenweiler, H. Minakuchi and K. Nakanishi, J. High Resol. Chromatogr., 23 (2000) 93

[43] L.A. Cole and J.G. Dorsey, Anal. Chem., 64 (1992) 1317

[44] L.C. Sander, J.B. Callis and L.R. Field, Anal. Chem., 55 (1983) 1068

[45] W.R. Tompson and J.E. Pemberton, Anal. Chem., 66 (1994) 3362

[46] D. MOREL, J. SERPINET, J.M. LETOFFE and P. CLAUDY, Chromatographia, 22 (1986) 103

[47] M. Ho and J.E. Pemberton, Anal. Chem., 70 (1998) 4915

[48] J.F. Wheeler, T.L. Beck, S.J. Klatte, L.A. Cole and J.G. Dorsey, J. Chromatogr. A, 656 (1993) 317

[49] S.J. Hansen and J. Callis, J. Chrom. Sci, 21 (1983) 560

[50] C.A. Doyle, T.J. Vickers, C.K. Mann and J.G. Dorsey, J. Chromatogr. A, 877 (2000) 25

[51] C.A. Doyle, T.J. Vickers, C.K. Mann and J.G. Dorsey, J. Chromatogr. A, 877 (2000) 41

[52] A.I. Rosen and C.A. Rivet, Anal. Chem., 20 (1948) 1093

[53] H.S. Frank and ..W. Evans, J. Chem. Phys., 13 (1945) 507

[54] G. Nemethy and H.A. Scheraga, J.Phys.Chem., 66 (1962) 1773

[55] L.T. Chang, Anal. Chem., 25 (1953) 1235

[56] D.C. Locke and D.E. Martire, Anal. Chem., 39 (1967) 921

[57] J.A. Schmit, R.A. Henry, R.C. Williams and J.F. Dieckman, J. Chromatogr. Sci., 9 (1971) 645

[58] T. Greibrokk and T. Andersen, J. Chromatogr. A, 1000 (2003) 743

[59] D. Bolliet and C. F.Poole, Analyst, 123 (1998) 295

[60] J.V. Tran, P. Molander, T. Greibrokk and E. Lundanes, J. Sep. Sci., 24 (2001) 930

[61] C.M. Bell, L.C. Sander and S.A. Wise, J. Chromatogr. A, 757 (1997) 29

[62] V. Boehm, J. Sep. Sci., 24 (2001) 955

[63] C. Horváth, W. Melander and I. Molnár, J. Chromatogr., 125 (1976) 129

[64] W. Melander, D.E. Campbell and C. Horváth, J. Chromatogr., 158 (1978) 215

[65] J. Hine, Physical organic chemistry, McGraw-Hill, New York, 1972, pp. 81

[66] W.R. Melander, B.-K. Chen and C. Horváth, J. Chromatogr., 185 (1979) 99

[67] K.A.Dill, J. Phys. Chem, 91 (1987) 1980

[68] K.A.Dill and .G.Dorsey, Chem.Rev., 89 (1989) 331

[69] A. Tchapla, S. Heron, E. Lesellier and H. Colin, J. Chromatogr. A, 656 (1993) 81

[70] E. Forgács and T. Cserháti, Molecular basis of chromatographic separation, CRC Press, Boca Raton; New York, 1997, pp. 132

[71] S.R. Cole and J.G. Dorsey, J. Chromatogr., 635 (1993) 177

[72] L.C. Sander and S.A. Wise, Anal. Chem., 61 (1989) 1749

[73] L.C.Sander and S.A.Wise, J. High Res. Chrom. Chrom. Communications, 11 (1988) 383

[74] K.B. Sentell and A.N. Hemderson, Anal. Chem. Acta, 246 (1991) 139

[75] K.B. Sentell, N.I. Ryan and A.N. Henderson, Anal. Chem. Acta, 307 (1995) 203

[76] L.C. Sander and S.A. Wise, J. Sep. Sci., 24 (2001) 910

[77] L.C. Sander and S.A. Wise, J. Chromatogr., 656 (1993) 335

[78] D. Bolliet and C.F. Poole, Analyst, 123 (1998) 295

[79] T.M. Pawlowski and C.F. Poole, Anal. Comm., 36 (1999) 71

[80] M.H. Abraham, Chem. Soc. Review, 22 (1993) 73

[81] M.H. Abraham, H.S. Chadha and A.J. Leo, J. Chromatogr. A, 682 (1994) 203

[82] J.H. Knox and J.F. Parcher, Anal. Chem., 41 (1969) 1599

[83] J.H. Knox, G.R. Laird and P.A. Raven, J. Chromatogr., 122 (1976) 129

[84] T. Farkas and G. Guiochon, Anal. Chem., 69 (1998) 4592

[85] T. Farkas, M.J. Sepaniak and G. Guiochon, J. Chromatogr. A, 740 (1996) 169

[86] U. Tallarek, E. Baumeister, K. Albert, E. Bayer and G. Guiochon, J. Chromatogr. A, 696 (1995) 1

[87] J.C. Park, K. Raghavan and S.J. Gibbs, J. Chromatogr. A, 945 (2002) 65

[88] S.G. Harding and H. Baumann, J. Chromatogr. A, 905 (2001) 19

[89] J.E. Baur, E.W. Kristensen and R.M. Wightman, Anal. Chem., 60 (1988) 2334

[90] R.A. Shalliker, B.S. Broyles and G. Guiochon, J. Chromatogr. A, 865 (1999) 83

[91] T. Yun and G. Guiochon, J. Chromatogr. A, 760 (1997) 17

[92] K. Miyabe and G. Guiochon, J. Chromatogr. A, 857 (1999) 69

[93] K. Miyabe and G. Guiochon, J. Chromatogr. A, 830 (1999) 29

[94] K. Miyabe and G. Guiochon, J. Chromatogr. A, 830 (1999) 263

[95] R.A. Shalliker, B.S. Broyles and G. Guiochon, J. Chromatogr. A, 888 (2000) 1

[96] Q.S. Yuan, A. Rosenfeld, T.W. Root, D.J. Klingenberg and E.N. Lightfoot, J. Chromatogr. A, 831 (1999) 149

[97] R.A. Shalliker, B.S. Broyles and G. Guiochon, J. Chrom. A, 994 (2003) 1

[98] W.A. Saner, J.R. Jadamec and R.W. Sager, Anal. Chem., 50 (1978) 749

[99] C. Horváth and H.-J. Lin, J. Chromatogr., 149 (1978) 43

[100] F.V. Warren and B.A. Bidlingmeyer, Anal. Chem., 60 (1988) 2821

[101] F.D. Antia and C. Horváth, J. Chromatogr., 435 (1988) 1

[102] G. Liu, N.M. Djordjevic and F. Erni, J. Chromatogr., 592 (1992) 239

[103] R. Trones, A. Iveland and T. Greibrokk, J. Microcol. Sep., 7 (1995) 505

[104] P. Molander, R. Trones, K. Haugland and T. Greibrokk, Analyst, 124 (1999) 1137

[105] J.S. Yoo, J.T. Watson and V.L. McGufin, J. Microcol. Sep., 4 (1992) 349

[106] B. Yan, J. Zhao, J.S. Brown, J. Blackwell and P.W. Carr, Anal. Chem., 72 (2000) 1253

[107] H. Poppe, J.C. Kraak, J.F. Huber and J.H. Berg, Chromatographia, 14 (1981) 515

[108] I. Halasz, R. Endele and J. Asshauer, J. Chromatogr., 112 (1975) 37

[109] H. Poppe and J.C. Kraak, J. Chrom., 282 (1983) 412

[110] O. Dapremont, G.B. Cox, M. Martin, P. Hilaireau and H. Colin, J. Chromatogr. A, 796 (1998) 81

[111] G. Mayr and T. Welsch, J. Chromatogr. A, 845 (1999) 155

[112] T. Welsch, M. Schmid, J. Kutter and A. Kálmán, J. Chromatogr. A, 728 (1996) 299

[113] R.G. Wolcott and J.W. Dolan, LC-GC, 1 (1999) 14

[114] J.W. Dolan, LC-GC, 15 (2002) 394

[115] R.G. Wolcott, J.W. Dolan, L.R. Snyder, S.R. Bakalyar, M.A. Arnold and J.A. Nichols, J. Chromatogr. A, 869 (2000) 211

[116] S. Komidas, Practical problem solving in HPLC, Wiley-VCH, Weinheim, 2000, pp. 49

[117] P.L. Zhu, L.R. Snyder, J.W. Dolan, N.M. Djordjevic, D.W. Hill, L.C. Sander and T.J. Waeghe, J. Chromatogr. A, 756 (1996) 21

[118] P.L. Zhu, J.W. Dolan and L.R. Snyder, J. Chromatogr. A, 756 (1999) 41

[119] P.L. Zhu, J.W. Dolan, L.R. Snyder, D.W. Hill, L.V. Heukelem and T.J. Waeghe, J. Chromatogr. A, 756 (1996) 51

[120] P.L. Zhu, J.W. Dolan, L.R. Snyder, N.M. Djordjevic, D.W. Hill, J.-T. Lin, L.C. Sander and L.V. Heukelem, J. Chromatogr. A, 756 (1996) 63

[121] J.W. Dolan, L.R. Snyder, T. Blanc and L.V. Heukelem, J. Chromatogr. A, 897 (2000) 37

[122] L.R. Snyder and J.W. Dolan, J. Chromatogr. A, 892 (2000) 107

[123] J.W. Dolan, L.R. Snyder, N.M. Djordjevic, D.W. Hill and T.J. Waeghe, J. Chromatogr. A, 857 (1999) 1

[124] J.W. Dolan, L.R. Snyder, N.M. Djordjevic, D.W. Hill and T.J. Waeghe, J. Chromatogr. A, 857 (1999) 21

[125] J.W. Dolan, L.R. Snyder, R.G. Wolcott, P. Haber, T. Baczek, R. Kaliszan and L.C. Sander, J. Chromatogr. A, 857 (1999) 41

[126] J.W. Dolan, L.R. Snyder and T. Blanc, J. Chromatogr. A, 897 (2000) 51

[127] J.W. Dolan, J. Chromatogr. A, 965 (2002) 195

[128] P. Molander, A. Thomassen, E. Lundanes, G. Fladseth, S. Throud, Y. Thomassen and T. Greibrokk, J. Sep. Sci., 24 (2001) 947

[129] U.D. Neue and J.R. Mazzeo, J. Sep. Sci., 24 (2001) 921

[130] N.M. Djordjevic, P.W. Fowler and F. Houdiere, J. Microcol. Sep., 11 (1999) 403

[131] T. Greibrokk and T. Andersen, J. Sep. Sci., 24 (2001) 899

[132] T. Greibrokk, Anal. Chem. (2002) 374

[133] Y. Mao and P.W. Carr, Anal. Chem., 72 (2000) 110

[134] B. Ooms, LC-GC International, 9 (1996) 574

[135] J.D. Thompson, J.S. Brown and P.W. Carr, Anal. Chem., 73 (2001) 3340

[136] K. Kimata, K. Iwaguchi, S. Onishi, K. Jinno, R. Eksteen, K. Hosoya, M. Araki and N. Tanaka, J. Chromatogr. Sci., 27 (1989) 1749

[137] Agilent, http//:www.chem.agilent.com (2002) 1

[138] ASTM, Annual book of ASTM standards, Section E 682, Vol 14.01,pp. 93

[139] The united states Pharmacopeia, XX. Revision,pp. 943

[140] B.E. Boyes and J.J. Kirkland, Peptide Research, 6 (1993) 249

[141] R.M. Smith, Retention and selectivity in liquid chromatographyJournal of Chromatography Library, Elsevier, Amsterdam, 1995, pp. 1

[142] P. Jandera, Retention and Selectivity in Liquid Chromatography, Elsevier, Amsterdam, 1995, pp. 235

[143] L.R. Snyder, J. Chromatogr., 179 (1979) 197

[144] R.M. Smith and S. Dube, Poster presentation HPLC 2001, Maastricht (2001)

[145] R.M.Smith, P. Rao, S.Dube and H.Shah, Chromatographia, 57 (2003) S-27

[146] H. D. Young, Electronic Source

[147] E. Katz, K. Ogan and P. Scott, J. Chromatogr., 260 (1983) 277

[148] A. Brand, G. Mann and W. Arlt, J. Chromatogr. A, 769 (1997) 109

[149] T. Farkas, G. Zhong and G. Guiochon, J. Chromatogr. A, 849 (1999) 35

[150] B.L. Karger, L.R. Snyder and C. Horváth, An introduction to separation science, John Wiley & Sons, Inc., New York, 1973, pp. 90

[151] G. Openhaim and E. Grushka, J. Chromatogr. A, 942 (2002) 63

[152] R.M. Smith and R.J. Burgess, J. Chromatogr. A, 785 (1997) 49

[153] T.M. Pawlowski and C.F. Poole, Anal. Comm., 36 (1999) 71

[154] P.C.Sadek, The HPLC solvent guide, John Wiley & Sons, Inc., 1996, pp. 10

[155] H. Chen and C. Horváth, J. Chromatogr. A, 705 (1995) 3

[156] C.A. Rimmer, C.R. Simmons and J.G. Dorsey, J. Chrom. A, 965 (2002) 219

[157] R. Ohmacht and B. Boros, Chromatographia, 51 (2000) 205

[158] J.E. McNair, K.C. Lewis and J.W. Jorgenson, Anal. Chem., 69 (1997) 983

[159] L.S. Ettre, LC-GC Europe, 16 (2003) 192

[160] J.P. Foley and J.G. Dorsey, Anal. Chem., 55 (1983) 730

[161] J.J. Kirkland, W.W. Yau, H.J. Stoklosa and C.H. Jr., J. Chromatogr. Sci., 15 (1977) 303

[162] B.S. Broyles, R.A. Shalliker and G. Guiochon, J. Chromatogr. A, 917 (2001) 1

[163] Y.X.Wu and .B.Ching, Chromatographia, 57 (2003) 329

[164] T. Teutenberg, O. Lerch, H.-J. Goetze and P. Zinn, Anal. Chem., 73 (2001) 3896

[165] S.M. Fields, C.Q. Ye, D.D. Zhang, B.R. Branch, X.J. Zhang and N. Okafo, J. Chromatogr. A, 913 (2001) 197

[166] S. Saha, R.M. Smith, E. Lenz and I.D. Wilson, J. Chromatogr. A, 991 (2003) 143

[167] A. Kubáová, D.j. Miller and S.B. Hawthore, J. Chromatogr. A, 923 (2001) 187

[168] R.M. Smith, J. Chromatogr. A, 975 (2002) 31

[169] S.T. Inc., Reference Technical Note 101 (2002)

[170] R.J. Burgess, ThesisLoughborough, 1999

[171] S.T. Inc., Technical Reference Note 802, (2002)

[172] W.W. Quigley, S.T. Ecker, P.G. Vahey and R.E. Synovec, Talanta, 50 (1999) 569

[173] S.T. Inc., Technical Refernce Note 803 (2002)

[174] C.F. Poole and S.A. Schuette, Contemporary practise of chromatography, Elsevier, 1984, pp. 161

[175] E.W. Hooijschuur, C.E. Kientz and U.A. Brinkman, J. Chromatogr. A, 928 (2001) 187

[176] Y. Yang, A.D. Jnes, J.A. Mathis and M.A. Francis, J. Chromatogr. A, 942 (2001) 231

[177] Y. Yang, A.D. Jones, J.A. Mathis and M.A. Francis, J. Chromatogr. A, 942 (2002) 231

[178] R.M. Smith and J. Bone, 2001 Personal Communication

[179] R.M. Smith, O. Chienthavorn, I.D. Wilson and B. Wright, Anal. Comm., 35 (1998) 261

[180] M. Godejohann, A. Preiss and C. Mügge, Anal. Chem., 70 (1998) 590

[181] K. Albert, J. Chromatogr. A, 856 (1999) 199

[182] M. Dachter, T. Glaser, K. Kohler and K. Albert, Anal. Chem., 73 (2001) 667

[183] U.D. Neue, HPLC columns -Theory, technology and practice, Wiley-VCH, New York, 1997, pp. 107

[184] K.K. Unger, Journal of Chromatography library - volume 16 - Porous Silica, its properties and use as support in column liquid chromatography, Elsevier, Amsterdam, 1979, pp. 12

[185] W. Stoeber, Kolloid-Z. (1956) 131

[186] R.K. Iler, The chemistry of silica, John Wiley & Sons, Inc., New York, 1979, pp. 62

[187] G.B. Alexander, J. Phys. Chem. (1957) 1563

[188] R.E. Majors, LC-GC North America, 18 (2000) 1214

[189] S.T. Inc., Technical Reference Note 804, 0 (2002) 0

[190] Waters, 2000, www.waters.com

[191] L. J. and C.P. W., Anal. Chem., 69 (1997) 837

[192] J. Li, Y. Hu and P.W. Carr, Anal. Chem., 69 (1997) 3884

[193] J. Li and P.W. Carr, Anal. Chem., 68 (1996) 2857

[194] J. Li and P.W. Carr, Anal. Chem., 69 (1997) 2202

[195] J. Li and P.W. Carr, Anal. Chem., 69 (1997) 2193

[196] R.G. Wolcott and J.W. Dolan, LC-GC, 17 (1999) 316

[197] R.E. Majors, LC-GC North America, 20 (2002) 516

[198] T. Enami, .Nagae and .Doshi, LC-GC Europe, 16 (2003) 418

[199] H. Kanazawa, K. Yamamoto, Y. Matsushima, N. Takai, A. Kikuchi, Y. Sakurai and T. Okano, Anal. Chem., 68 (1996) 100

[200] H. Kanazawa, Y. Kashiwase, K. Yamamoto, Y. Matsushima, A. Kikuchi, Y. Sakurai and T. Okano, Anal. Chem., 69 (1997) 823

[201] B. Ells, Y. Wang and F.F. Cantwell, J. Chromatogr. A, 835 (1999) 3

[202] A.R. Katritzky, S.M. Allin and M. Siskin, Acc. Chem. Res., 29 (1996) 399

[203] R. Burgess, PhD Thesis 1999

[204] S.T. Inc., Technical Reference Note 801 (2002)

[205] J.D. Thompson and P.W. Carr, Anal. Chem., 74 (2002) 1017

[206] J. Mann, R. Davidson, J. Hobbs, D. Banthorpe and J. Harborne, Natural Products: their chemistry and biological significance, 1996, pp. 361

[207] R. Pomponio, R. Gotti, M. Hudaib and V. Cavrini, J. Chromatogr. A, 945 (2002) 239

[208] I.D. Wilson and E. Lenz, 2002 Personal Communication

[209] Bruker, Electronic Source2003, www.bruker-biospin.de

11 APPENDIX A

Purospher RP18e

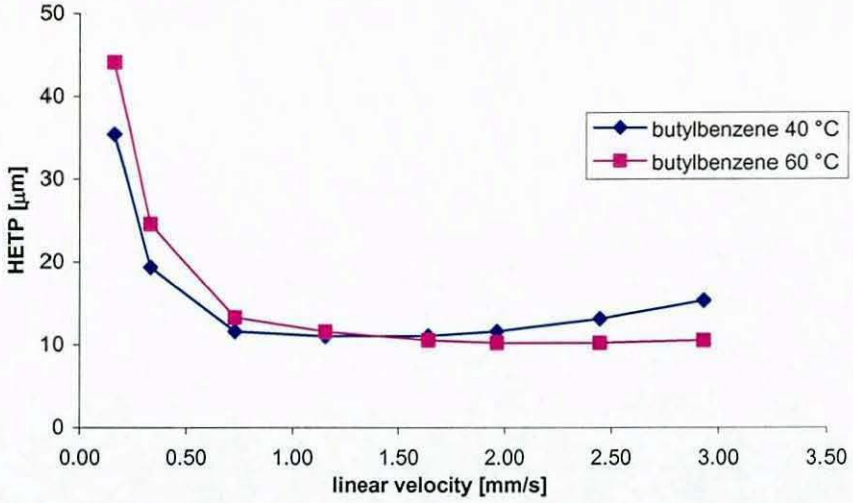

Figure 121: van Deemter curves for butylbenzene on Purospher RP18e (150 x 4.6 mm i.d.); mobile phase 75% methanol, 25% water (w/w); temperatures 40 and 60 °C controlled in water bath.

Purospher RP18

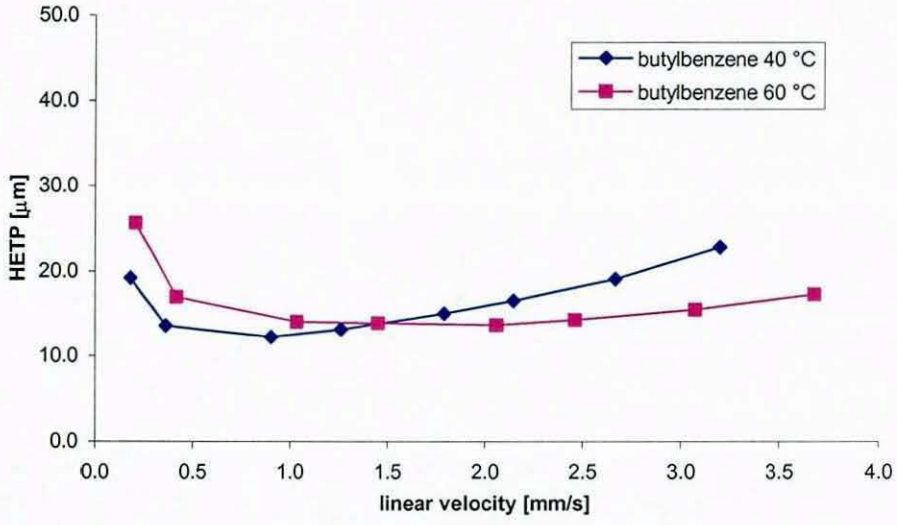

Figure 122: van Deemter curves for butylbenzene on Purospher RP18 (125 x 4.0 mm i.d.); mobile phase 75% methanol, 25% water (w/w); temperatures 40 and 60 °C controlled in water bath.

Hypersil HiPurity

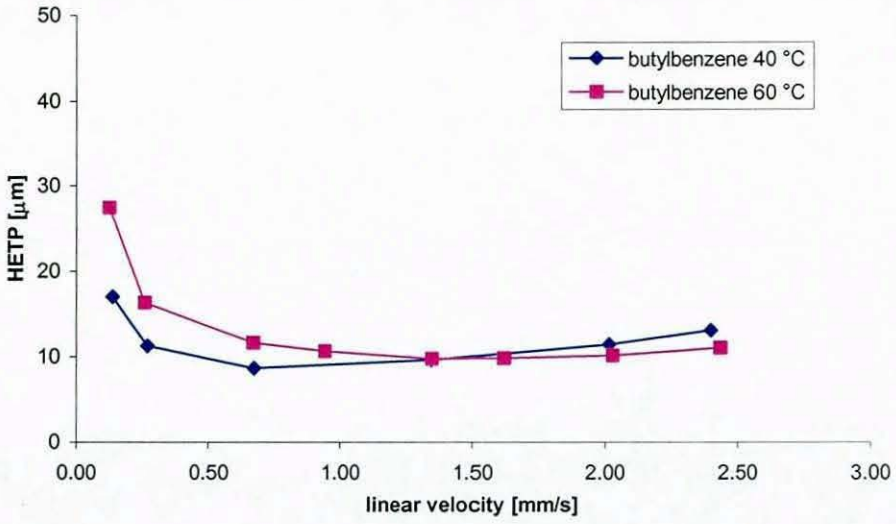

Figure 123: van Deemter curves for butylbenzene on Hypersil HiPurity (150 x 4.6 mm i.d.); mobile phase 75% methanol, 25% water (w/w); temperatures 40 and 60 °C controlled in water bath.

Prontosil

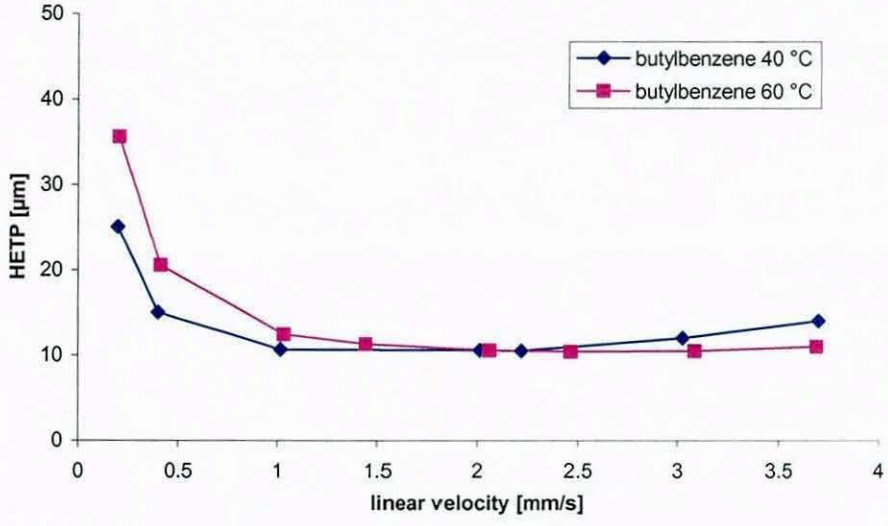

Figure 124: van Deemter curves for butylbenzene on Prontosil (150 x 4.0 mm i.d.); mobile phase 75% methanol, 25% water (w/w); temperatures 40 and 60 °C controlled in water bath.

Bischoff EU column

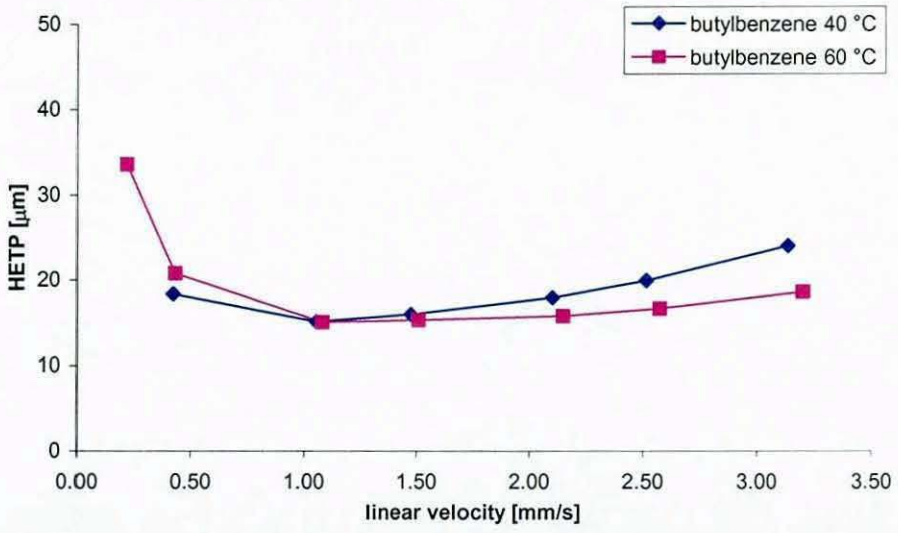

Figure 125: van Deemter curves for butylbenzene on EU column (150 x 4.0 mm i.d.); mobile phase 75% methanol, 25% water (w/w); temperatures 40 and 60 °C controlled in water bath.

12 APPENDIX B

Appendix BComparison of efficiency in water jacket and fan oven at 60 °C

Bischoff EU column

fan oven

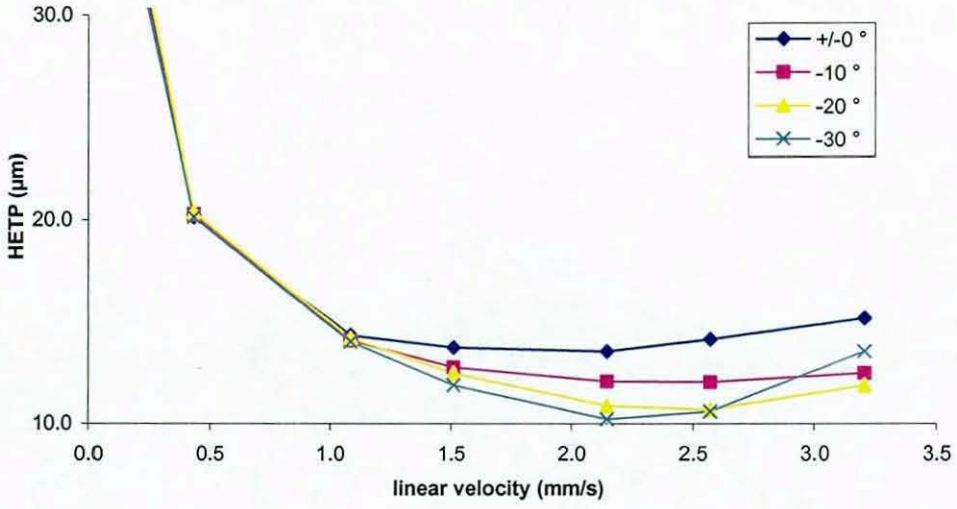

Figure 126: van Deemter curves for butylbenzene at four different mobile phase inlet temperature differentials on *EU* column (150 x 4.0 mm i.d.); 60 °C column wall temperature controlled in HP1090 fan oven; mobile phase 75 % methanol, 25 % water (w/w).

water bath

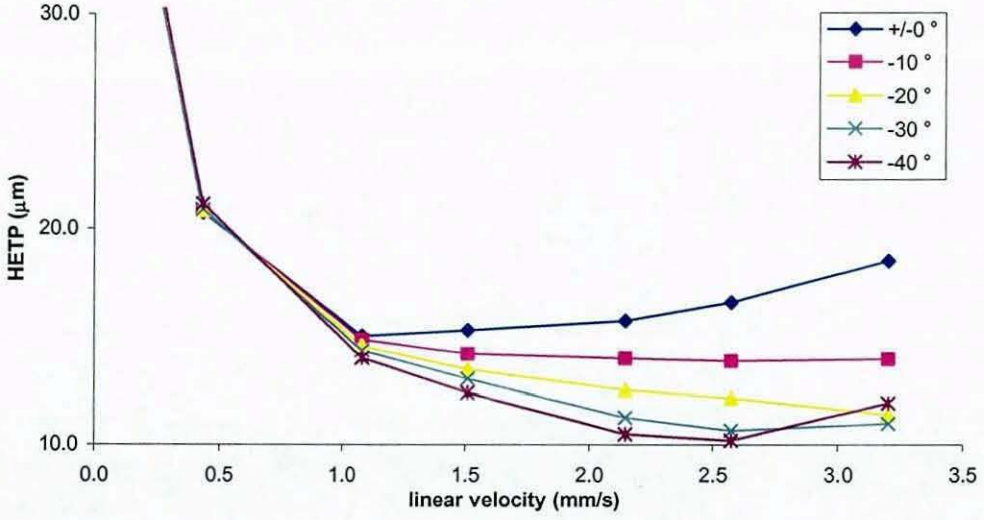

Figure 127: van Deemter curves for butylbenzene at four different mobile phase inlet temperature differences on *EU* column (150 x 4.0 mm i.d.); 60 °C column wall temperature controlled in water jacket; mobile phase 75 % methanol, 25 % water (w/w).

Appendix BComparison of efficiency in water jacket and fan oven at 60 °C

Chromolith

fan oven

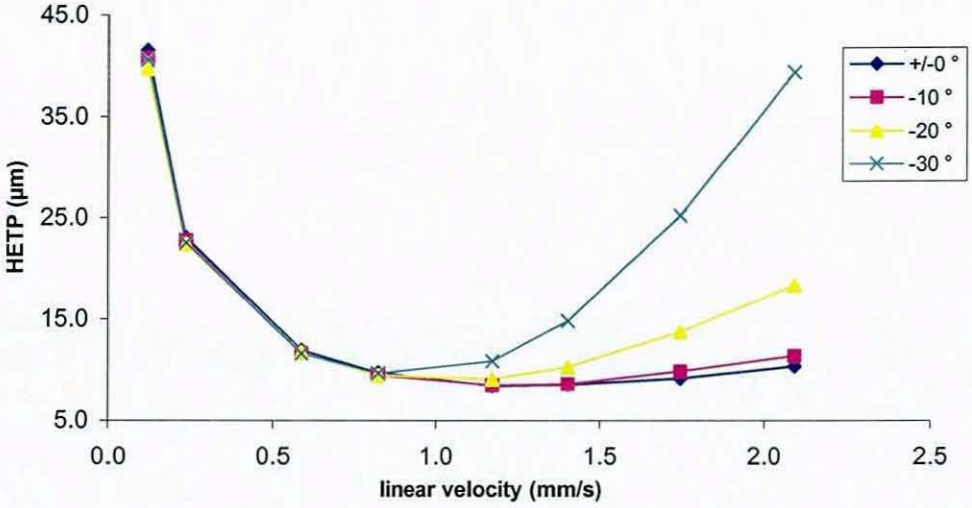

Figure 128: van Deemter curves for butylbenzene at four different mobile phase inlet temperature differences on *chromolith* column (100 x 4.0 mm i.d.); 60 °C column wall temperature controlled in HP1090 fan oven; mobile phase 75 % methanol, 25 % water (w/w).

water bath

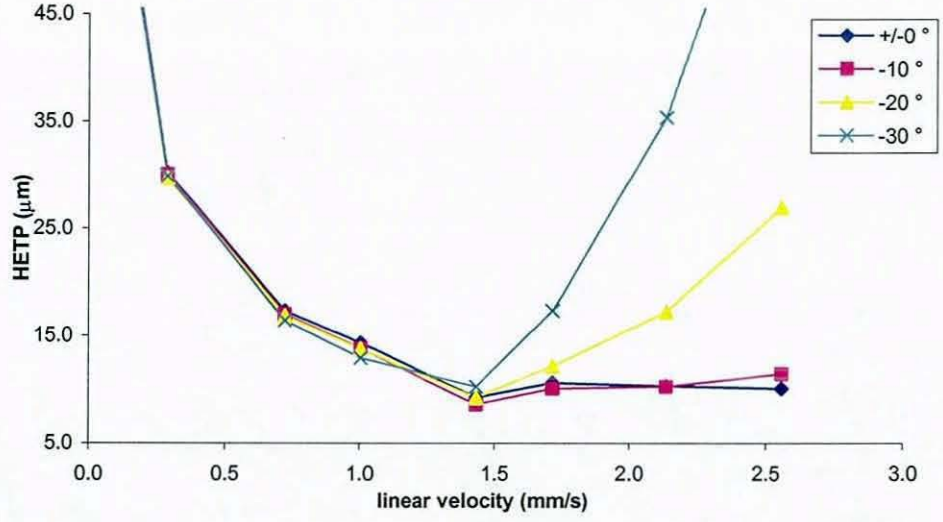

Figure 129: van Deemter curves for butylbenzene at four different mobile phase inlet temperature differences on *Chromolith* column (100 x 4.0 mm i.d.); 60 °C column wall temperature controlled in water jacket; mobile phase 75 % methanol, 25 % water (w/w).

Appendix BComparison of efficiency in water jacket and fan oven at 60 °C

Hypersil HiPurity ODS

fan oven

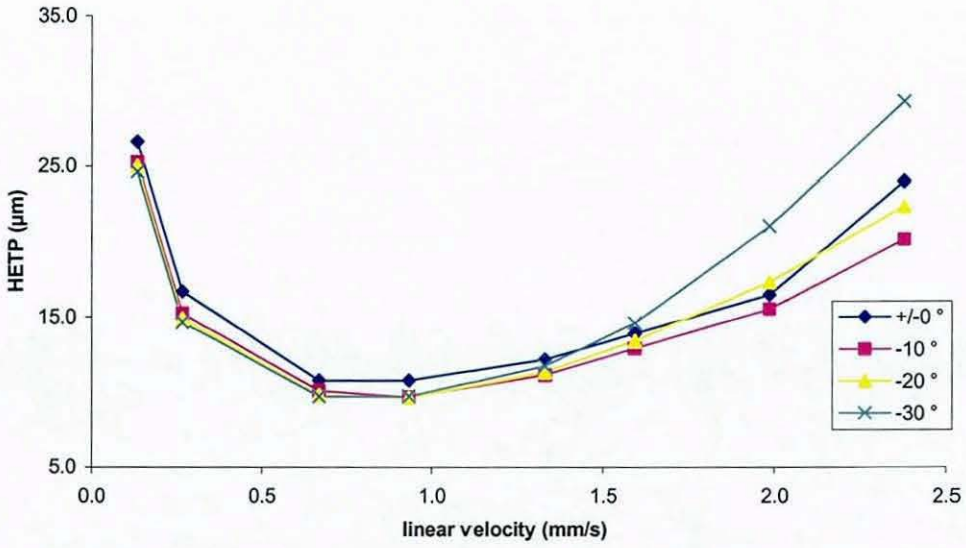

Figure 130: van Deemter curves for butylbenzene at four different mobile phase inlet temperature differences on *Hypersil ODS* column (150 x 4.6 mm i.d.); 60 °C column wall temperature controlled in HP1090 fan oven; mobile phase 75 % methanol, 25 % water (w/w).

water bath

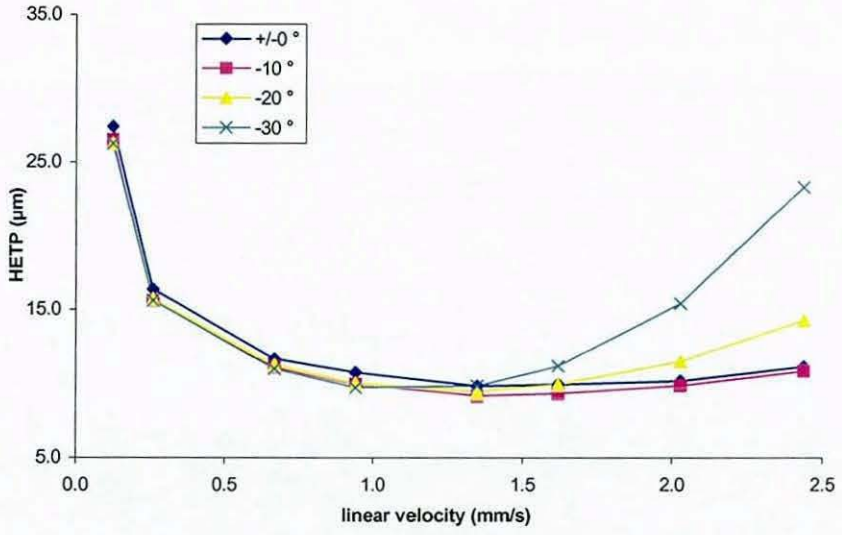

Figure 131: van Deemter curves for butylbenzene at four different mobile phase inlet temperature differences on *Hypersil ODS* column (150 x 4.6 mm i.d.); 60 °C column wall temperature controlled in water jacket; mobile phase 75 % methanol, 25 % water (w/w).

Appendix BComparison of efficiency in water jacket and fan oven at 60 °C

Kromasil

fan oven

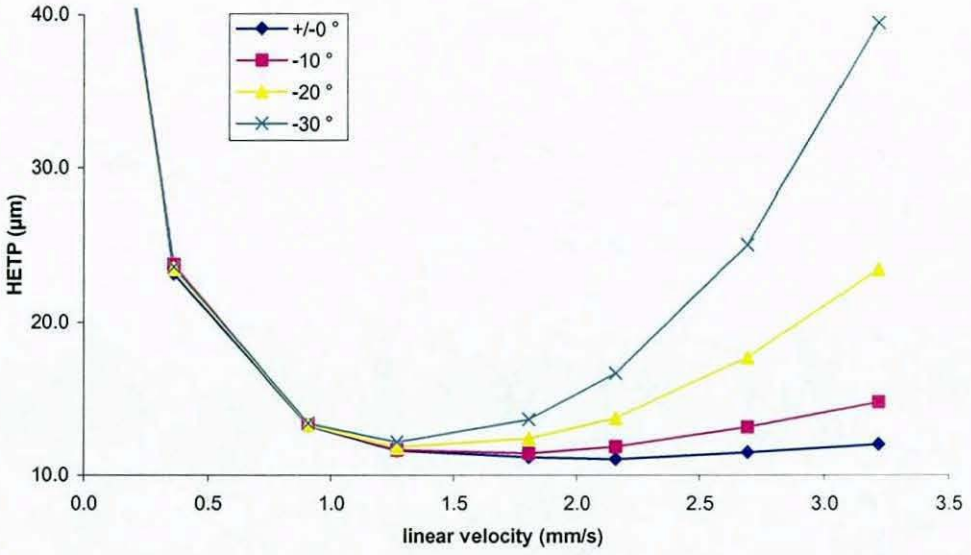

Figure 132: van Deemter curves for butylbenzene at four different mobile phase inlet temperature differences on *Kromasil* column (150 x 4.6 mm i.d.); 60 °C column wall temperature controlled in HP1090 fan oven; mobile phase 75 % methanol, 25 % water (w/w).

water bath

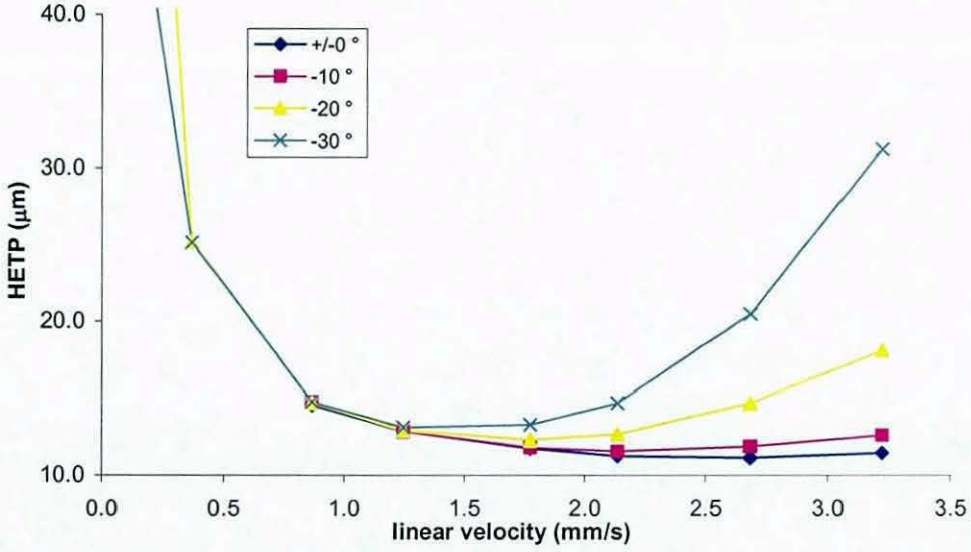

Figure 133: van Deemter curves for butylbenzene at four different mobile phase inlet temperature differences on *Kromasil* column (150 x 4.6 mm i.d.); 60 °C column wall temperature controlled in water jacket; mobile phase 75 % methanol, 25 % water (w/w).

Appendix BComparison of efficiency in water jacket and fan oven at 60 °C

Prontosil

fan oven

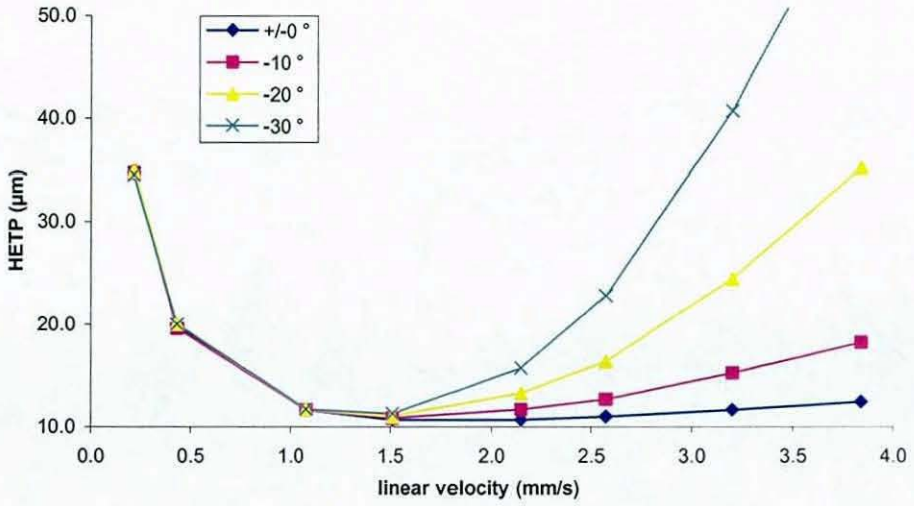

Figure 134: van Deemter curves for butylbenzene at four different mobile phase inlet temperature differences on *Prontosil* column (150 x 4.0 mm i.d.); 60 °C column wall temperature controlled in HP1090 fan oven; mobile phase 75 % methanol, 25 % water (w/w).

water bath

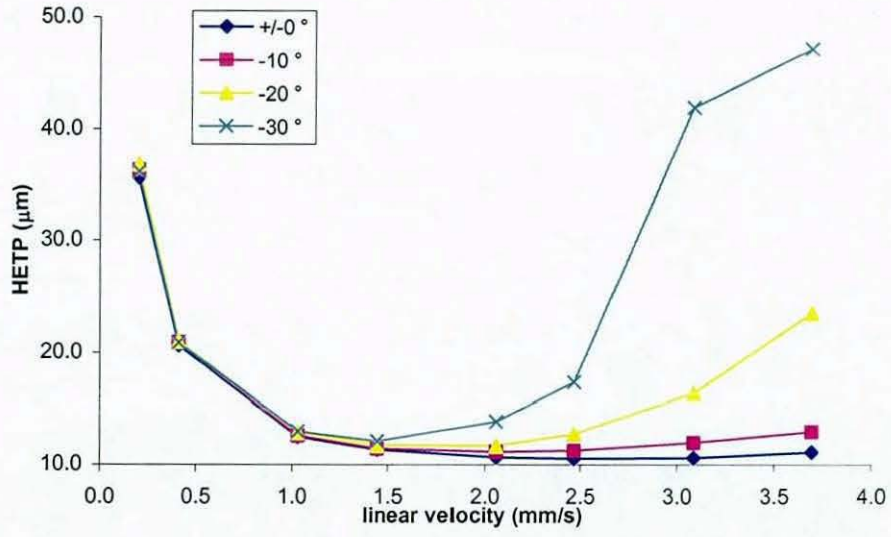

Figure 135: van Deemter curves for butylbenzene at four different mobile phase inlet temperature differences on *Prontosil* column (150 x 4.0 mm i.d.); 60 °C column wall temperature controlled in water jacket; mobile phase 75 % methanol, 25 % water (w/w).

Appendix BComparison of efficiency in water jacket and fan oven at 60 °C

Pusopher RP18

fan oven

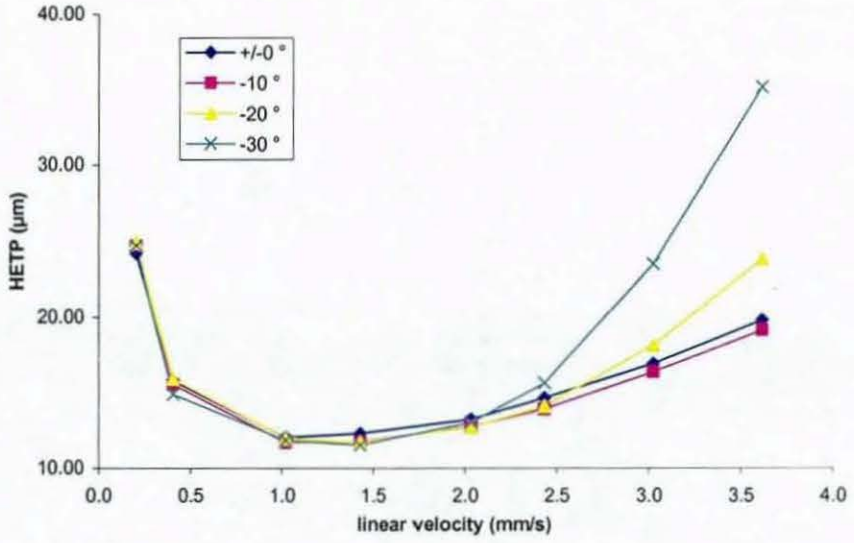

Figure 136: van Deemter curves for butylbenzene at four different mobile phase inlet temperature differences on *Purospher RP18* column (125 x 4.0 mm i.d.); 60 °C column wall temperature controlled in HP1090 fan oven; mobile phase 75 % methanol, 25 % water (w/w).

water bath

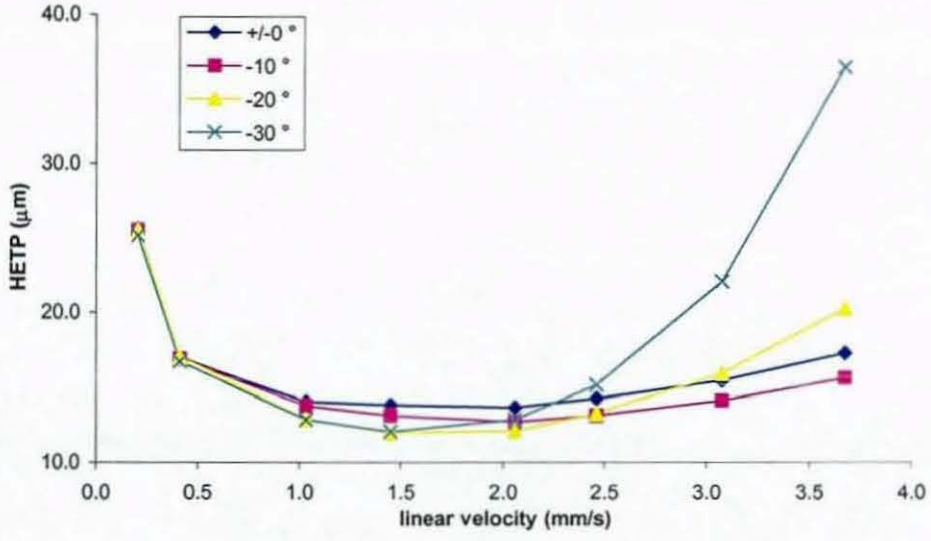

Figure 137: van Deemter curves for butylbenzene at four different mobile phase inlet temperature differences on *Purospher RP18* column (125 x 4.0 mm i.d.); 60 °C column wall temperature controlled in water jacket; mobile phase 75 % methanol, 25 % water (w/w).

Appendix BComparison of efficiency in water jacket and fan oven at 60 °C

Purospher RP18e

fan oven

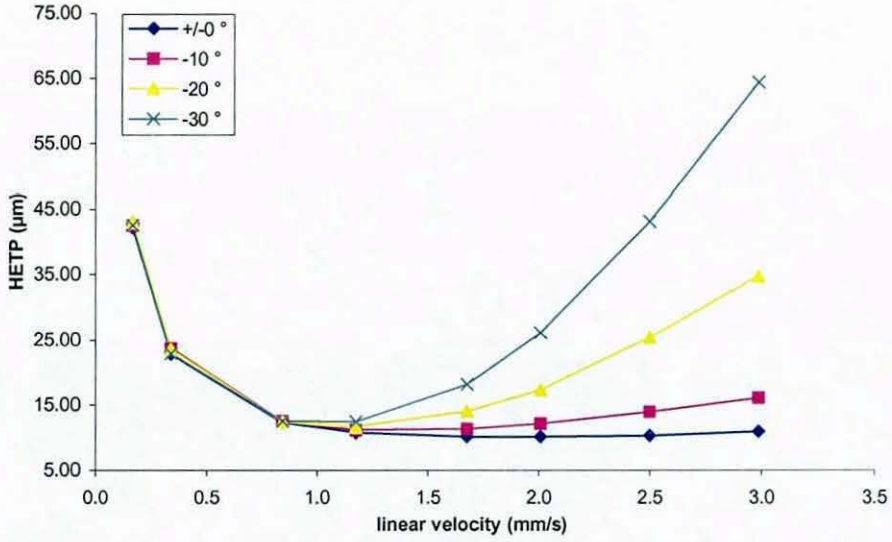

Figure 138: van Deemter curves for butylbenzene at four different mobile phase inlet temperature differences on *Purospher RP18e* column (150 x 4.6 mm i.d.); 60 °C column wall temperature controlled in HP1090 fan oven; mobile phase 75 % methanol, 25 % water (w/w).

water bath

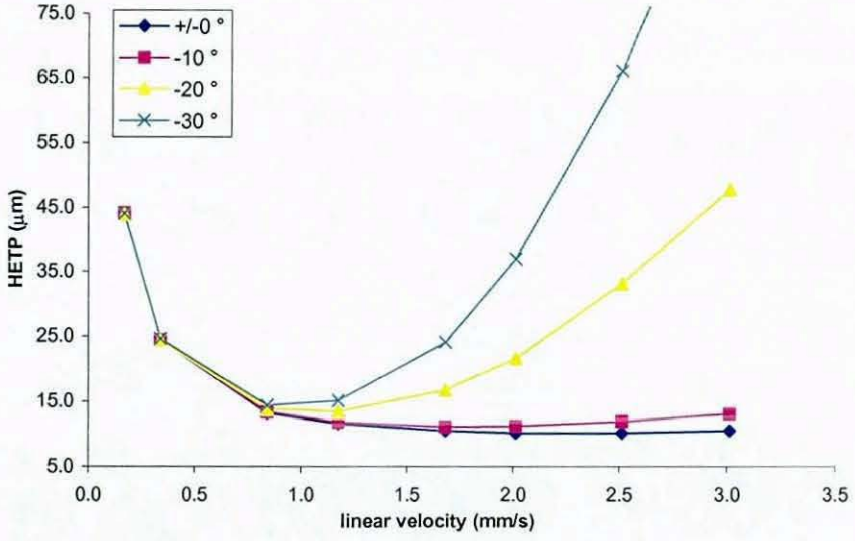

Figure 139: van Deemter curves for butylbenzene at four different mobile phase inlet temperature differences on *Purospher RP18e* column (150 x 4.6 mm i.d.); 60 °C column wall temperature controlled in water jacket; mobile phase 75 % methanol, 25 % water (w/w).

13 APPENDIX C

Bischoff EU column

fan oven

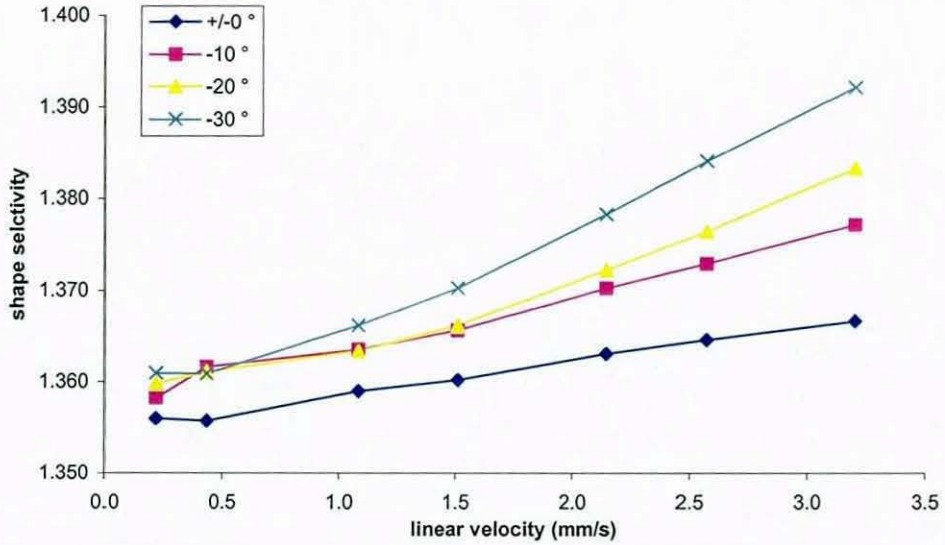

Figure 140: Change of shape selectivity with linear flow velocity and mobile phase inlet temperature on Bischoff EU column at 60 °C column temperature in HP1090 fan oven.

water bath

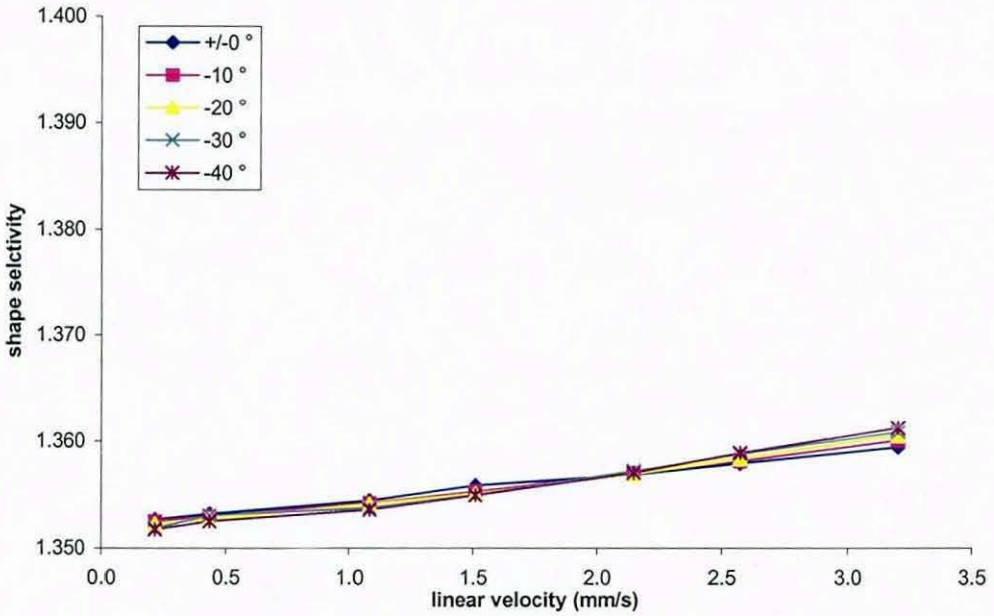

Figure 141: Change of shape selectivity with linear flow velocity and mobile phase inlet temperature on Bischoff EU column at 60 °C column temperature in water jacket.

Chromolith

fan oven

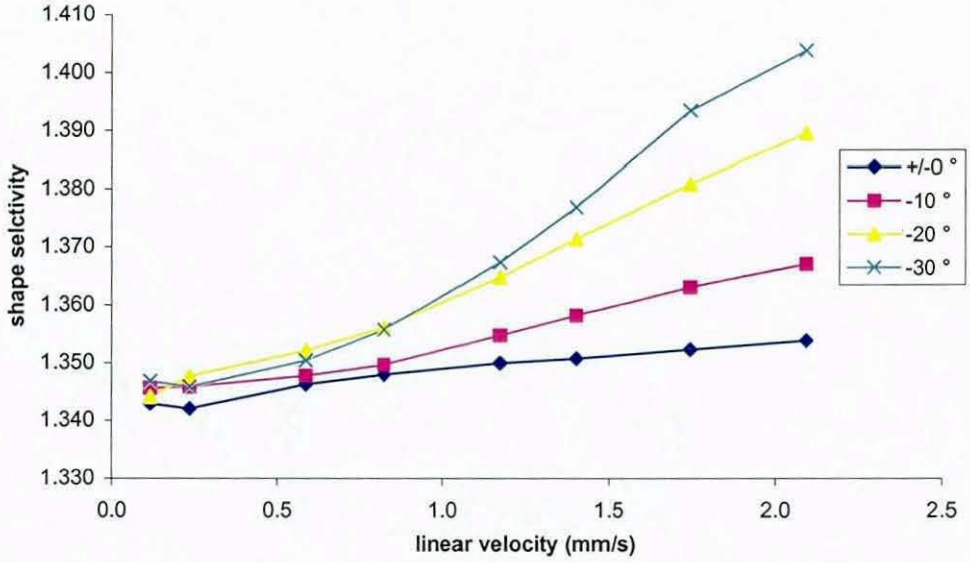

Figure 142: Change of shape selectivity with linear flow velocity and mobile phase inlet temperature on Chromolith at 60 °C column temperature in HP1090 fan oven.

water bath

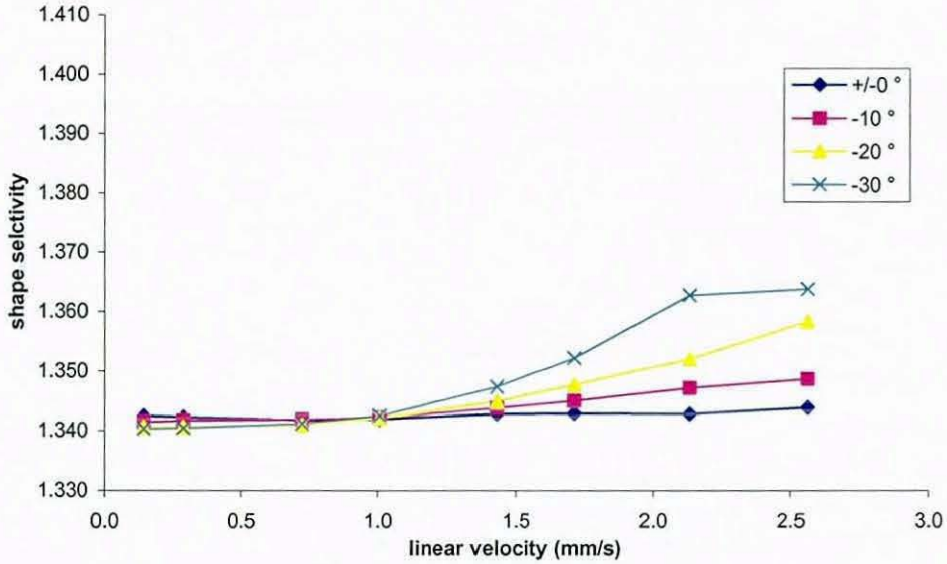

Figure 143: Change of shape selectivity with linear flow velocity and mobile phase inlet temperature on Chromolith at 60 °C column temperature in water jacket.

Appendix C Comparison of shape selectivity in water jacket and fan oven at 60 °C

Hypersil HiPurity ODS

fan oven

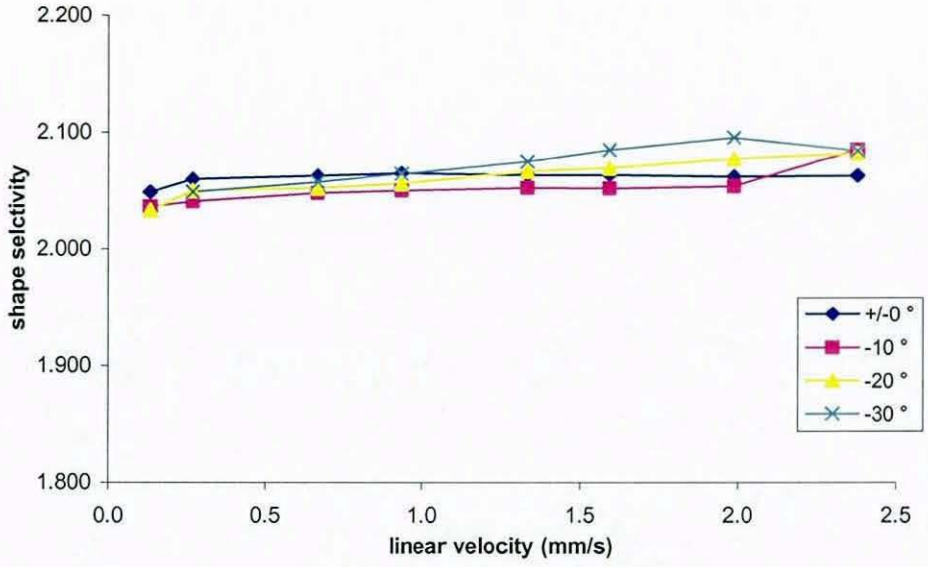

Figure 144: Change of shape selectivity with linear flow velocity and mobile phase inlet temperature on Hypersil HiPurity ODS at 60 °C column temperature in HP1090 fan oven.

water bath

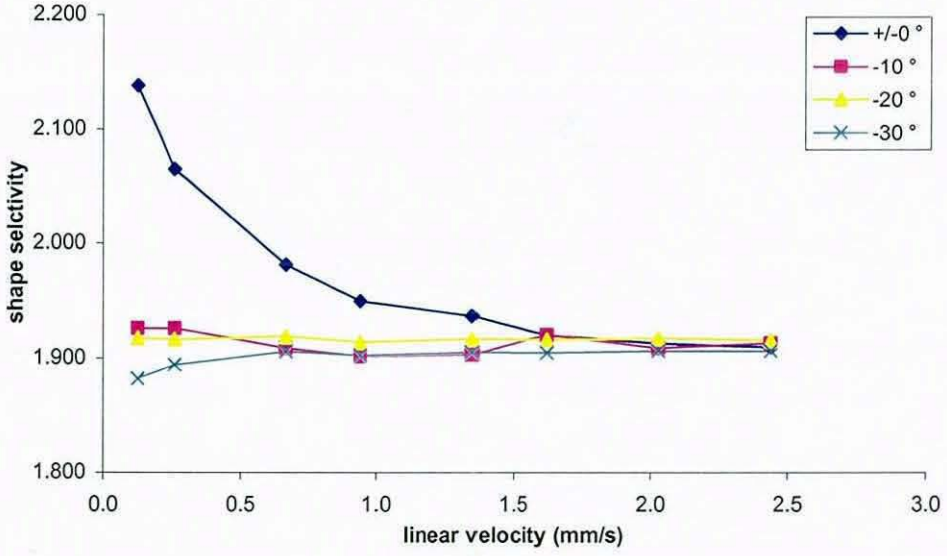

Figure 145: Change of shape selectivity with linear flow velocity and mobile phase inlet temperature on Hypersil HiPurity ODS at 60 °C column temperature in water jacket.

Kromasil

fan oven

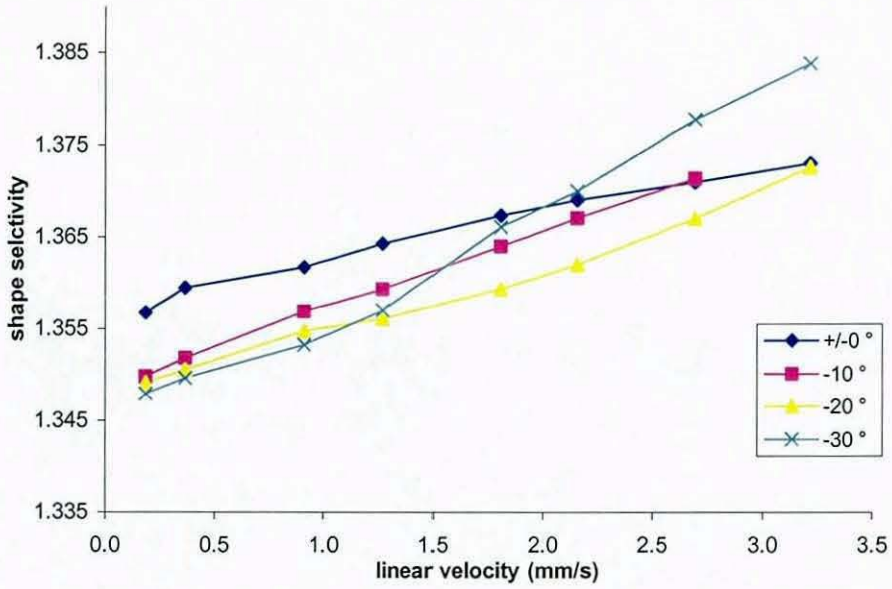

Figure 146: Change of shape selectivity with linear flow velocity and mobile phase inlet temperature on Kromasil at 60 °C column temperature in HP1090 fan oven.

water bath

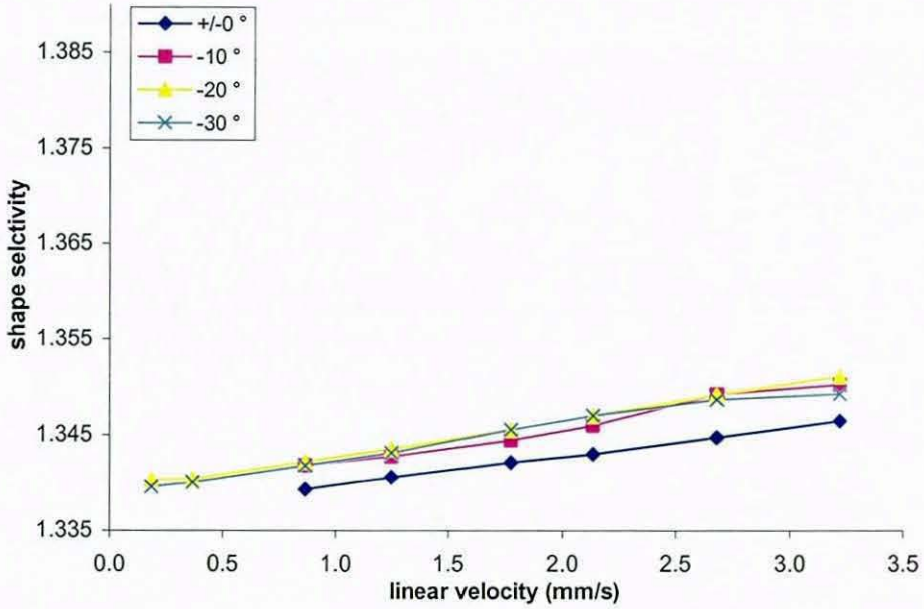

Figure 147: Change of shape selectivity with linear flow velocity and mobile phase inlet temperature on Kromasil at 60 °C column temperature in water jacket.

Prontosil

fan oven

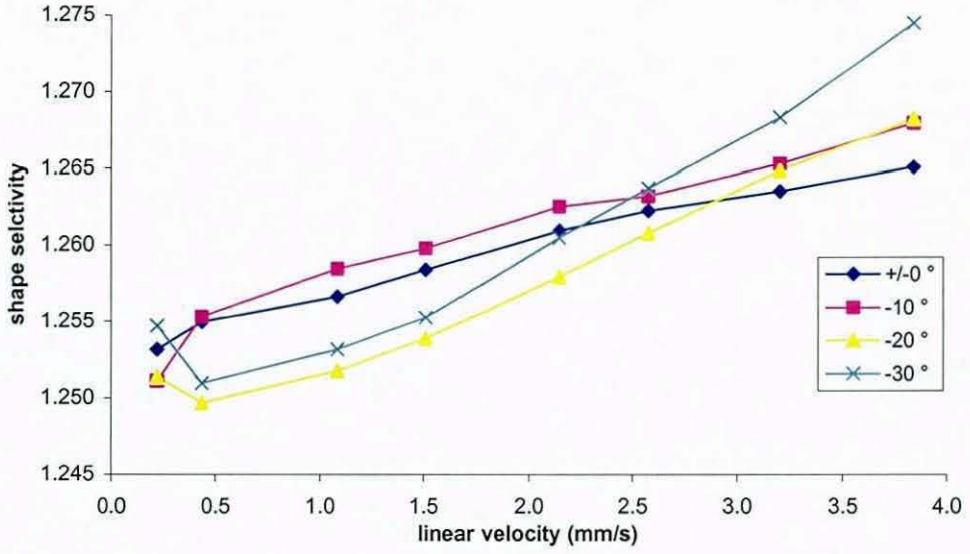

Figure 148: Change of shape selectivity with linear flow velocity and mobile phase inlet temperature on Prontosil at 60 °C column temperature in HP1090 fan oven.

water bath

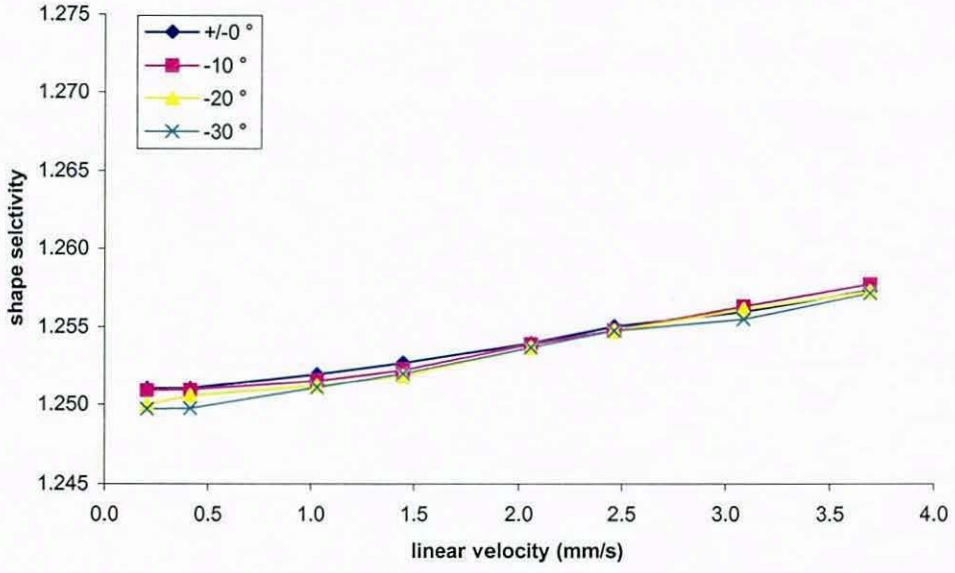

Figure 149: Change of shape selectivity with linear flow velocity and mobile phase inlet temperature on Prontosil at 60 °C column temperature in water jacket.

Purospher RP18

fan oven

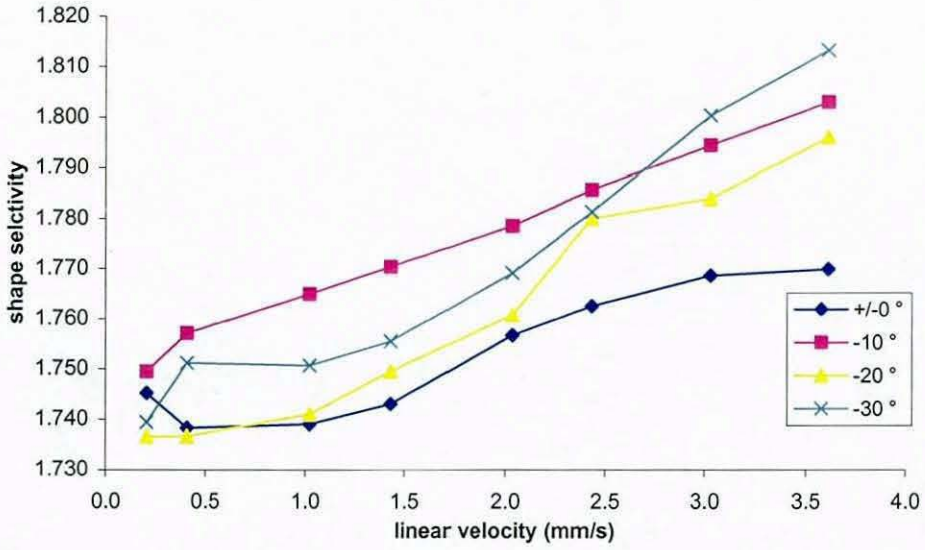

Figure 150: Change of shape selectivity with linear flow velocity and mobile phase inlet temperature on Purospher RP18 at 60 °C column temperature in HP1090 fan oven.

water bath

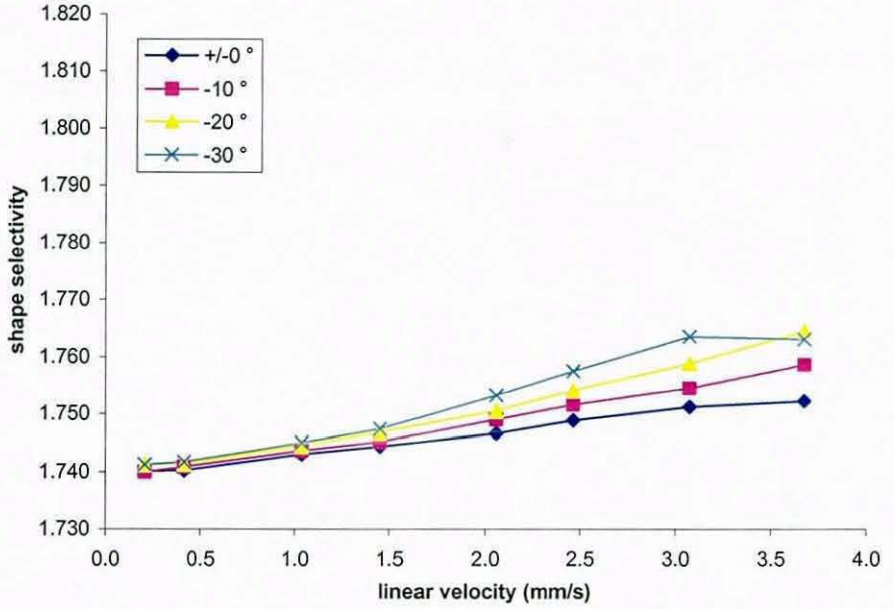

Figure 151: Change of shape selectivity with linear flow velocity and mobile phase inlet temperature on Purospher RP18 at 60 °C column temperature in water jacket.

Purospher RP18e

fan oven

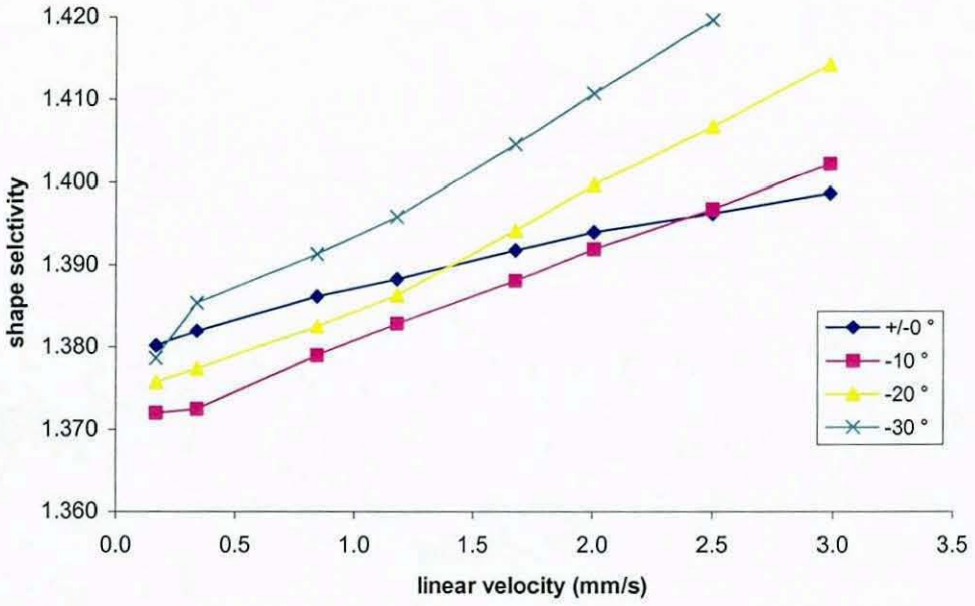

Figure 152: Change of shape selectivity with linear flow velocity and mobile phase inlet temperature on Purospher RP18e at 60 °C column temperature in HP1090 fan oven.

water bath

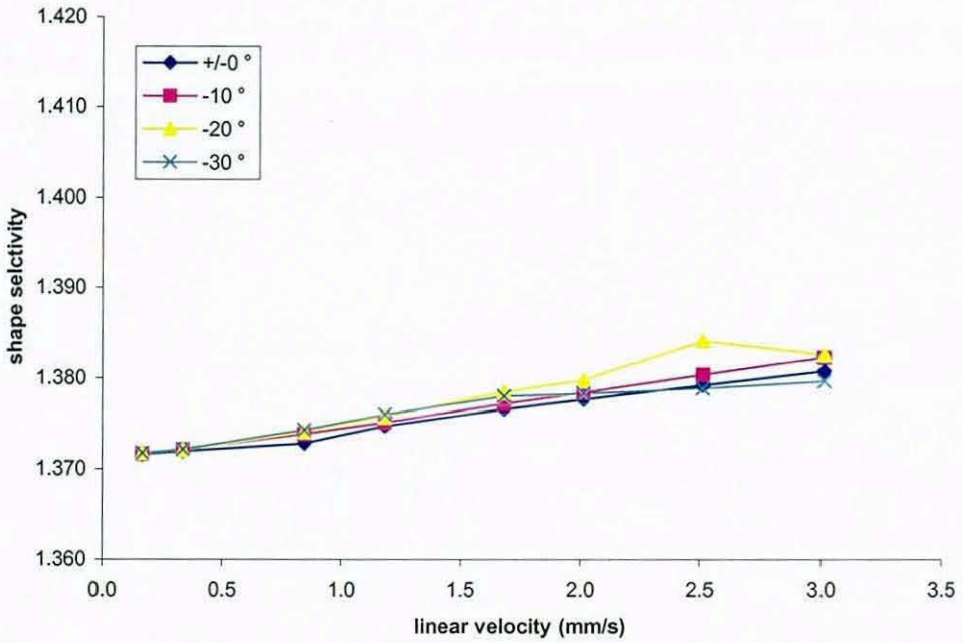

Figure 153: Change of shape selectivity with linear flow velocity and mobile phase inlet temperature on Purospher RP18e at 60 °C column temperature in water jacket.

14 APPENDIX D

Bischoff EU column

fan oven

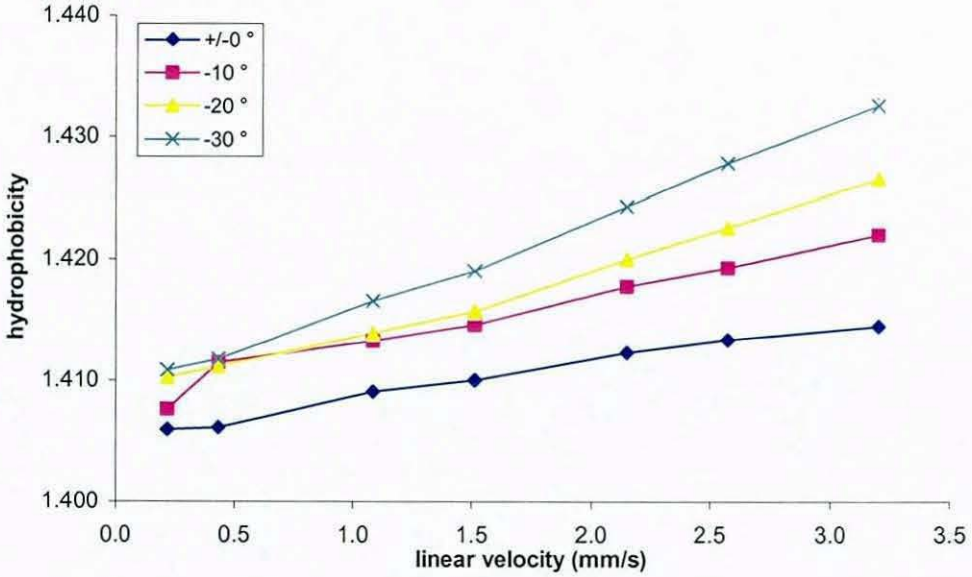

Figure 154: Change of hydrophobicity with linear flow velocity and mobile phase inlet temperature on Bischoff EU column at 60 °C column temperature in HP1090 fan oven.

water bath

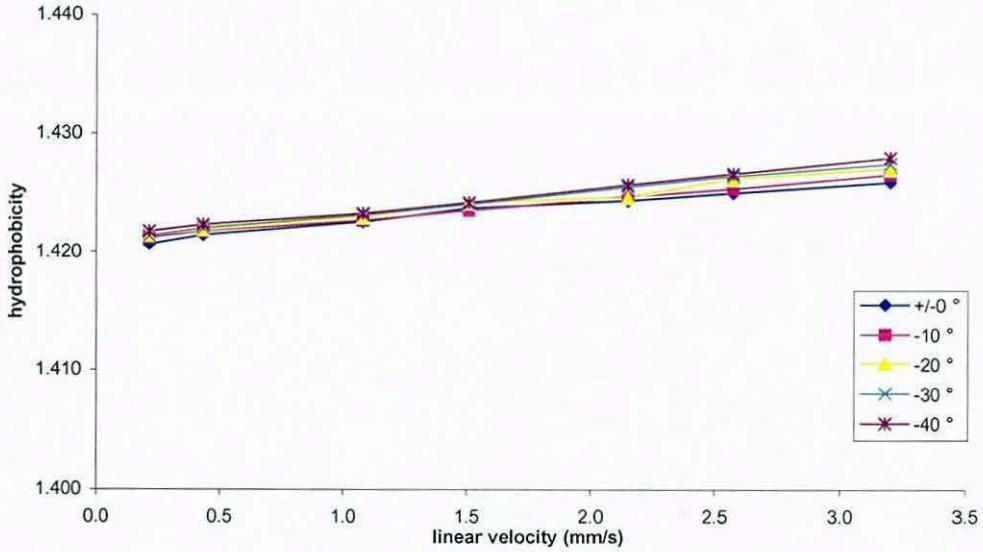

Figure 155: Change of hydrophobicity with linear flow velocity and mobile phase inlet temperature on Bischoff EU column at 60 °C column temperature in water jacket.

Chromolith

fan oven

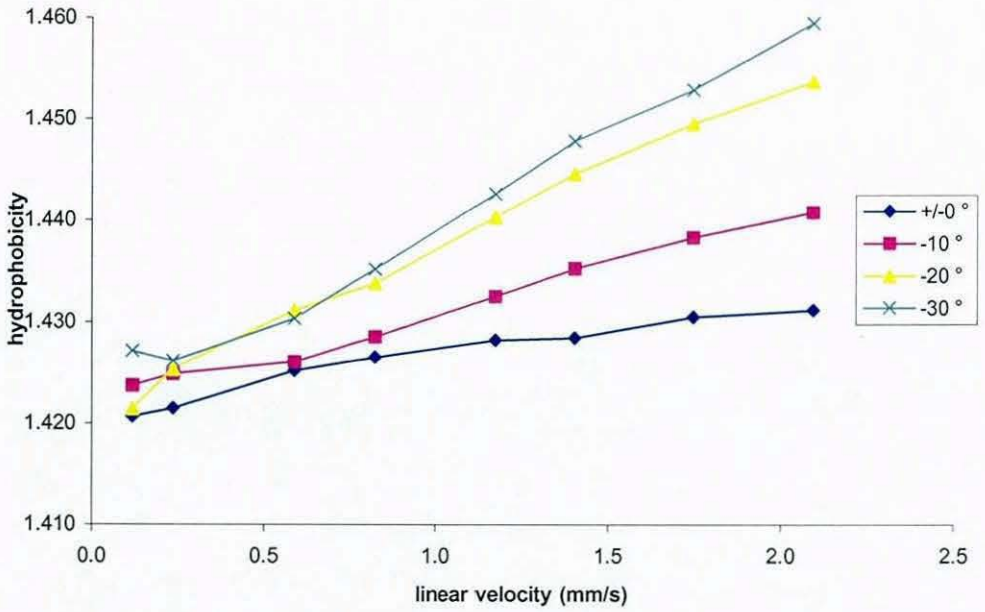

Figure 156: Change of hydrophobicity with linear flow velocity and mobile phase inlet temperature on Chromolith at 60 °C column temperature in HP1090 fan oven.

water bath

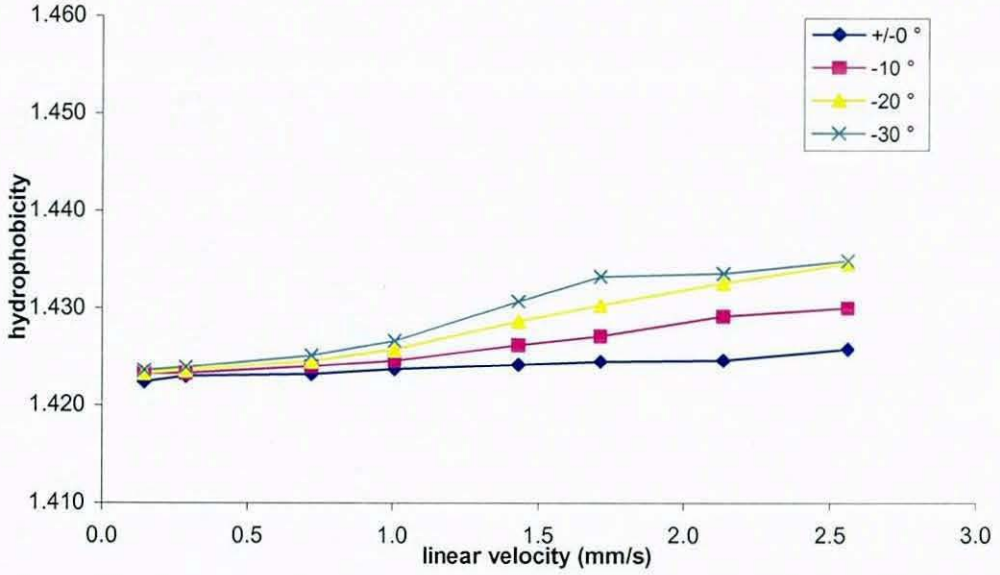

Figure 157: Change of hydrophobicity with linear flow velocity and mobile phase inlet temperature on Chromolith at 60 °C column temperature in water jacket.

Hypersil HiPutity

fan oven

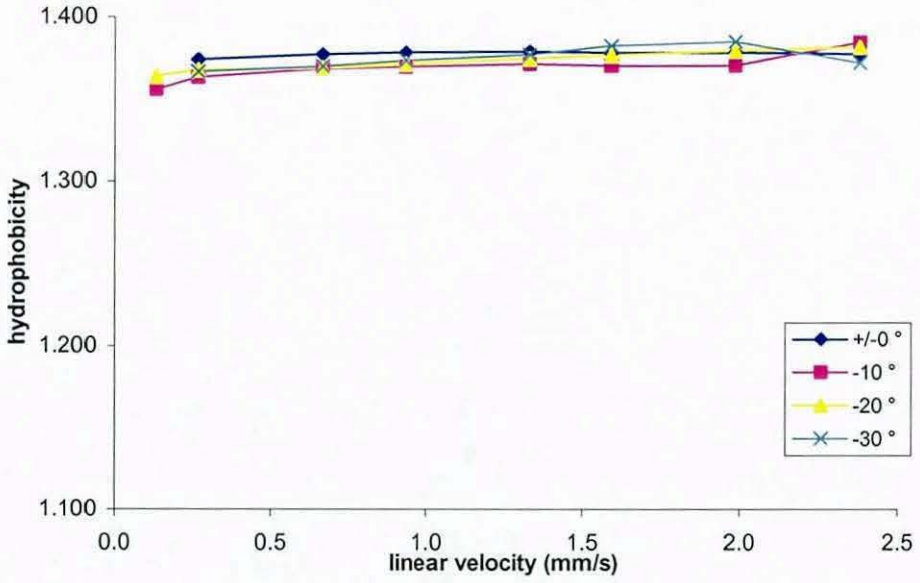

Figure 158: Change of hydrophobicity with linear flow velocity and mobile phase inlet temperature on Hypersil HiPurity ODS at 60 °C column temperature in HP1090 fan oven.

water bath

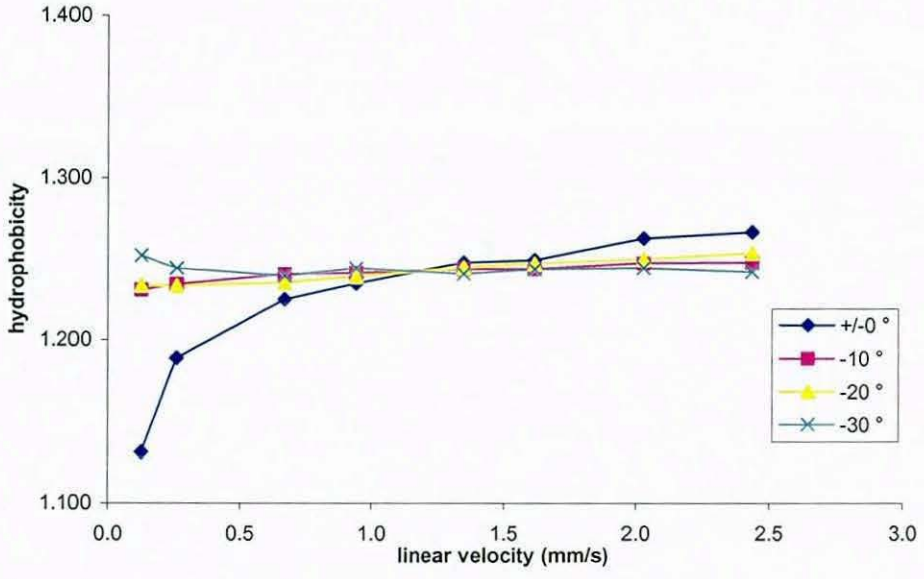

Figure 159: Change of hydrophobicity with linear flow velocity and mobile phase inlet temperature on Hypersil HiPurity ODS at 60 °C column temperature in water jacket.

Kromasil

fan oven

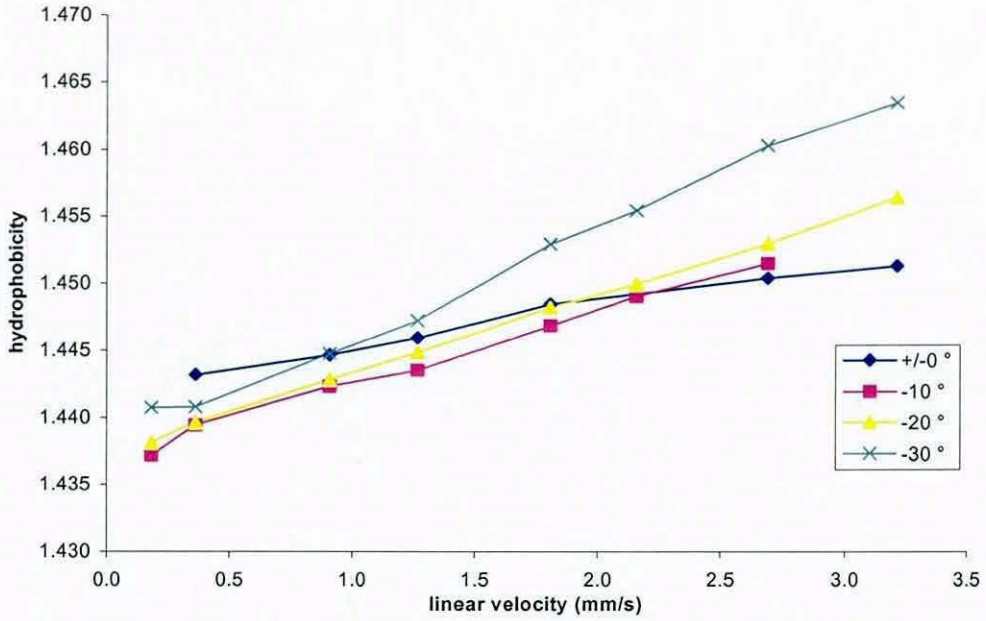

Figure 160: Change of hydrophobicity with linear flow velocity and mobile phase inlet temperature on Kromasil at 60 °C column temperature in HP1090 fan oven.

water bath

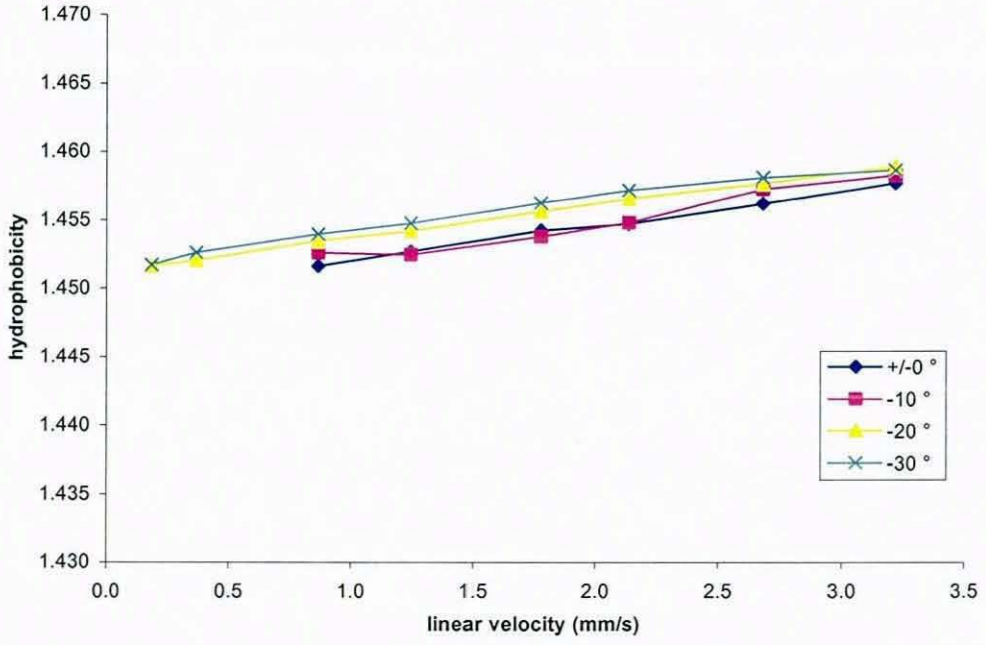

Figure 161: Change of hydrophobicity with linear flow velocity and mobile phase inlet temperature on Kromasil at 60 °C column temperature in water jacket.

Prontosil

fan oven

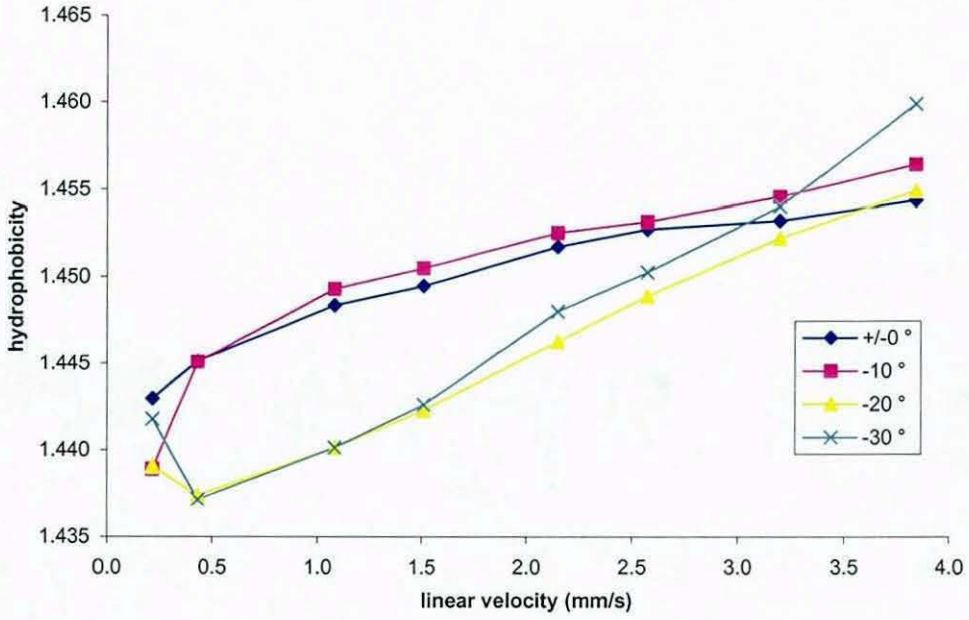

Figure 162: Change of hydrophobicity with linear flow velocity and mobile phase inlet temperature on Prontosil at 60 °C column temperature in HP1090 fan oven.

water bath

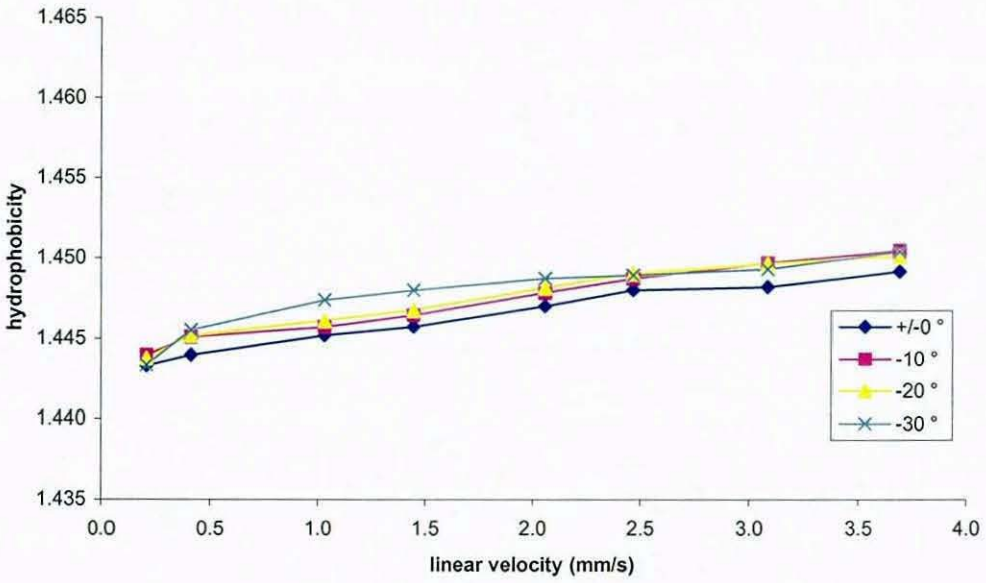

Figure 163: Change of hydrophobicity with linear flow velocity and mobile phase inlet temperature on Prontosil at 60 °C column temperature in water jacket.

Purospher RP18

fan oven

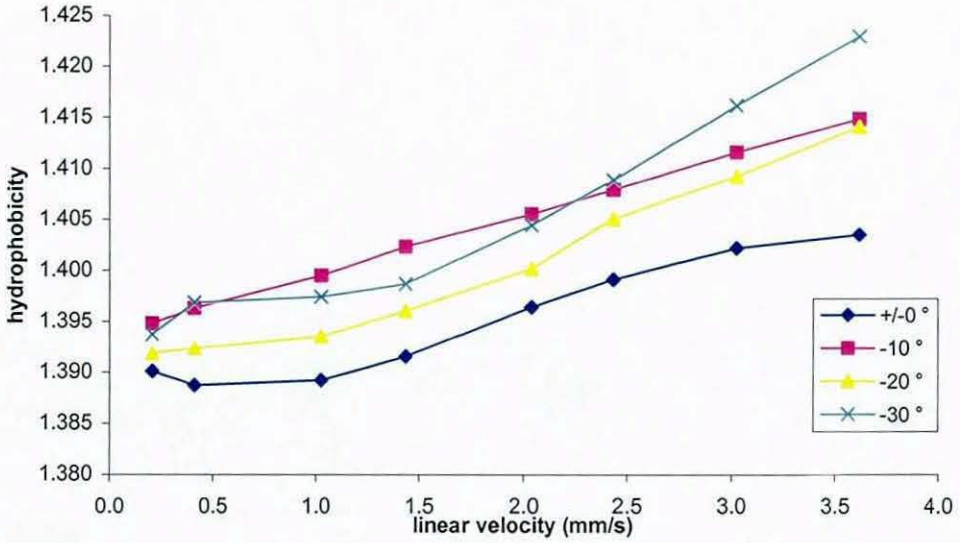

Figure 164: Change of hydrophobicity with linear flow velocity and mobile phase inlet temperature on Purospher RP18 at 60 °C column temperature in HP1090 fan oven.

water bath

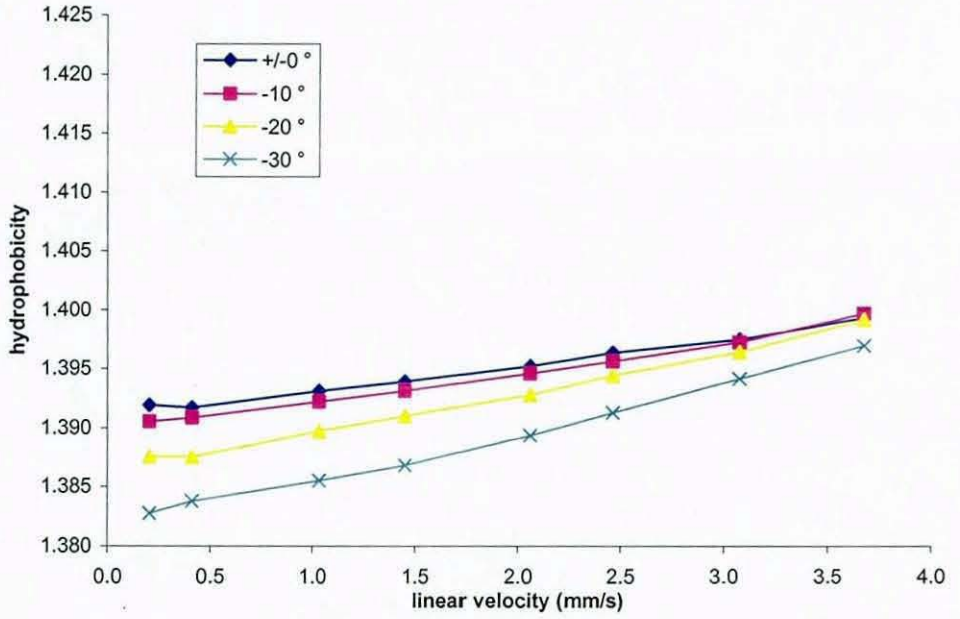

Figure 165: Change of hydrophobicity with linear flow velocity and mobile phase inlet temperature on Purospher RP18 at 60 °C column temperature in water jacket.

Purospher RP18e

fan oven

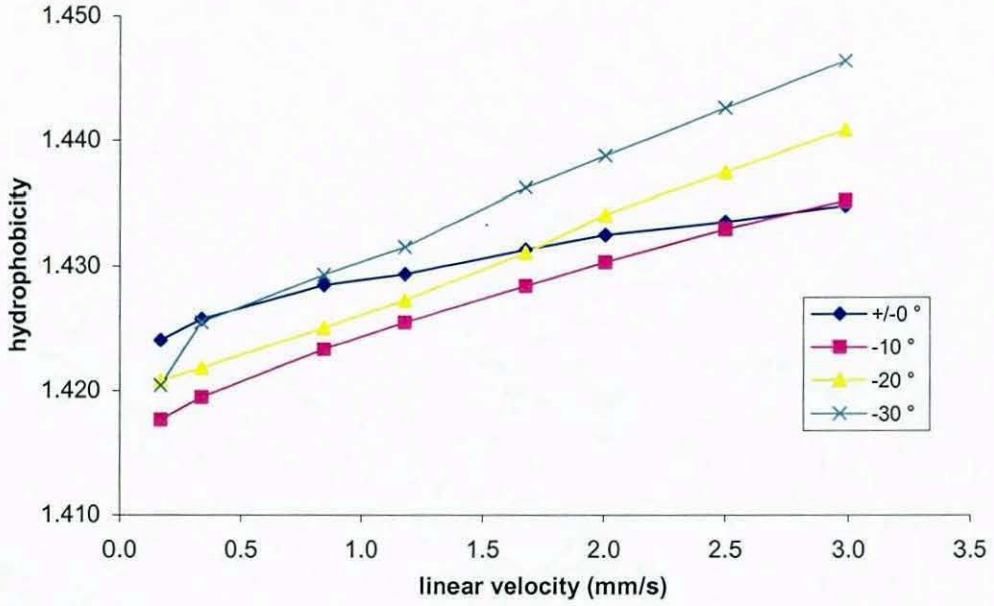

Figure 166: Change of hydrophobicity with linear flow velocity and mobile phase inlet temperature on Purospher RP18e at 60 °C column temperature in HP1090 fan oven.

water bath

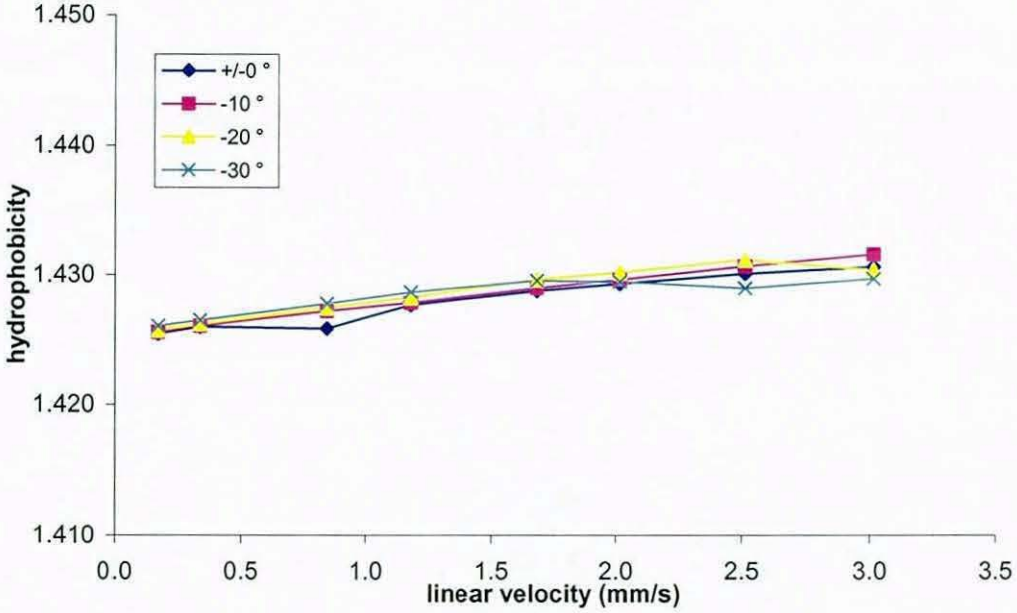

Figure 167: Change of hydrophobicity with linear flow velocity and mobile phase inlet temperature on Purospher RP18e at 60 °C column temperature in water jacket.

15 APPENDIX E

Bischoff EU column

butylbenzene

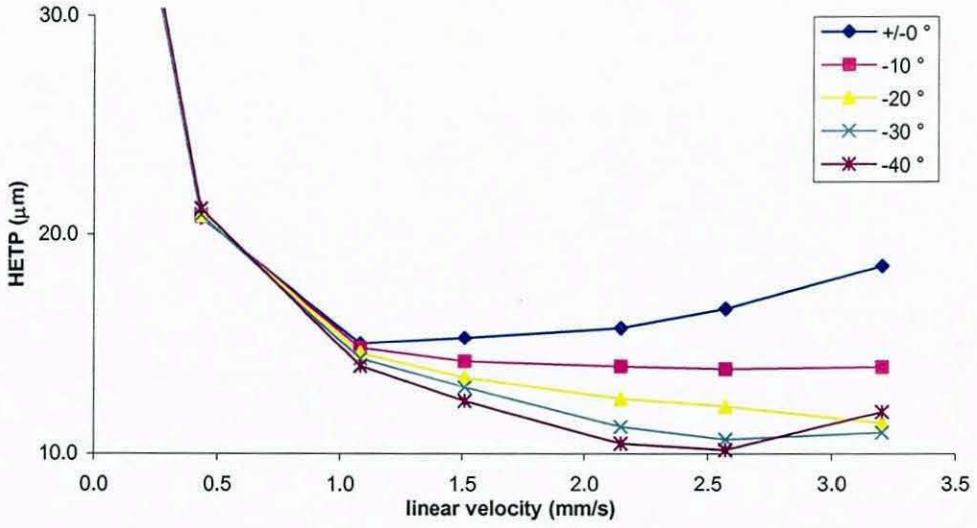

Figure 168: van Deemter curves for butylbenzene on EU column 150 x 4.0 mm i.d., mobile phase 75% methanol, 25% water (w/w), temperature 60 °C controlled in water bath, at different mobile phase inlet temperatures.

o-terphenyl

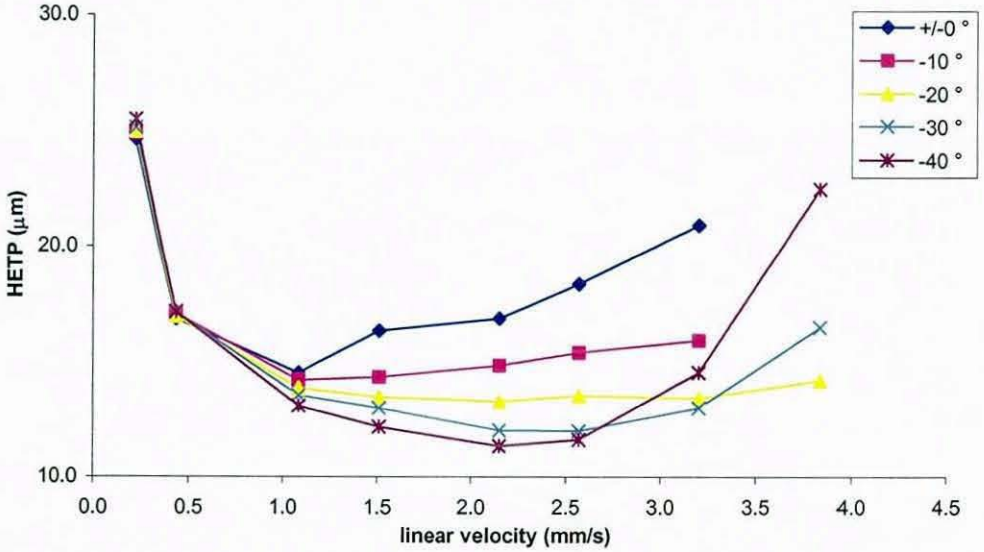

Figure 169: van Deemter curves for o-terphenyl on EU column 150 x 4.0 mm i.d., mobile phase 75% methanol, 25% water (w/w), temperature 60 °C controlled in water bath, at different mobile phase inlet temperatures.

pentylbenzene

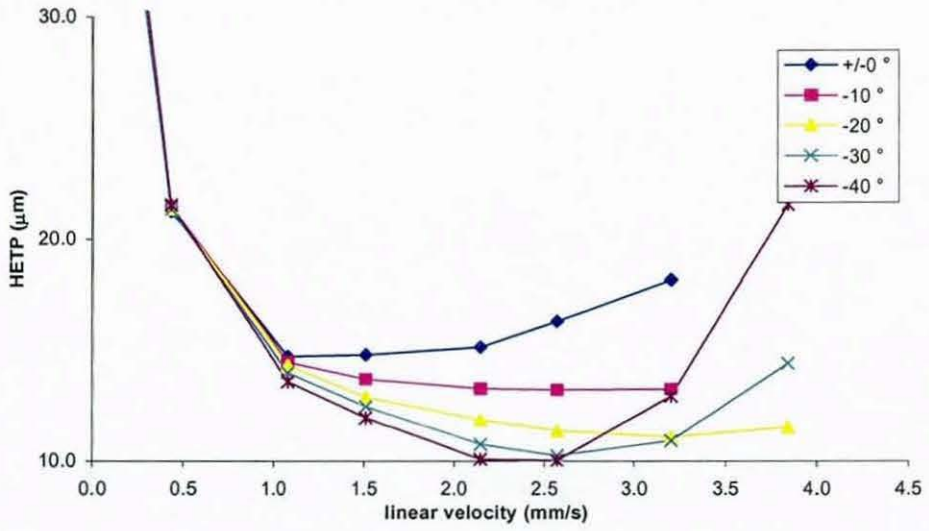

Figure 170: van Deemter curves for pentylbenzene on EU column 150 x 4.0 mm i.d., mobile phase 75% methanol, 25% water (w/w), temperature 60 °C controlled in water bath, at different mobile phase inlet temperatures.

triphenylene

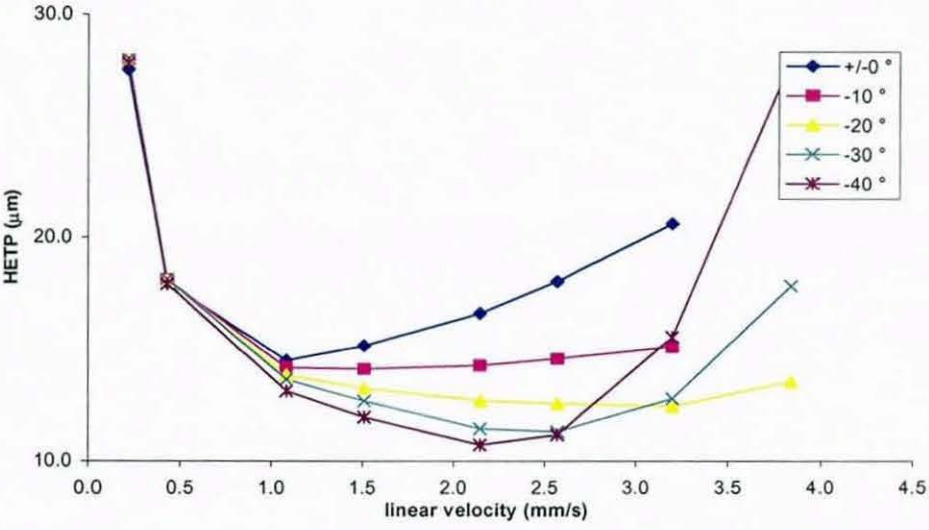

Figure 171: van Deemter curves for triphenylene on EU column 150 x 4.0 mm i.d., mobile phase 75% methanol, 25% water (w/w), temperature 60 °C controlled in water bath, at different mobile phase inlet temperatures.

Chromolith

butylbenzene

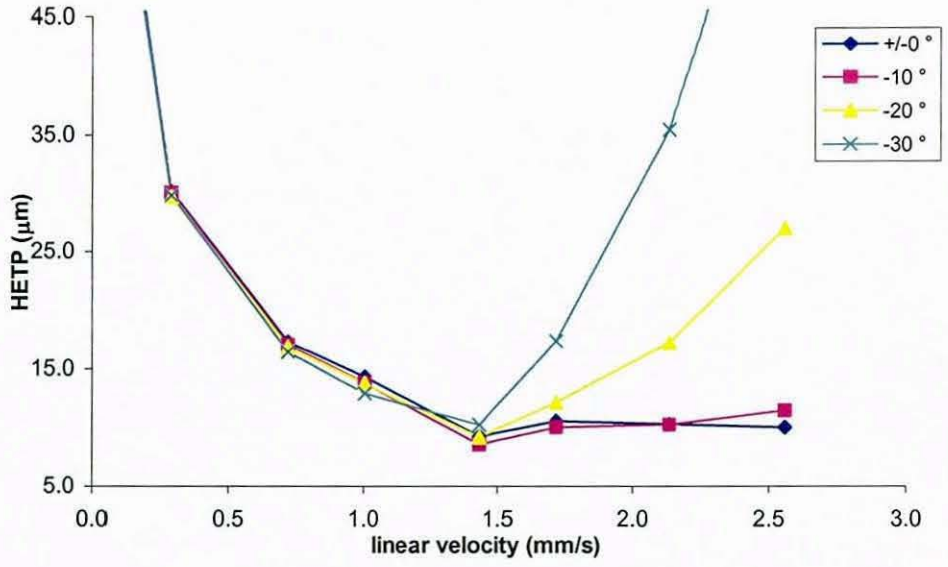

Figure 172: van Deemter curves for butylbenzene on Chromolith 100 x 4.0 mm i.d., mobile phase 75% methanol, 25% water (w/w), temperature 60 °C controlled in water bath, at different mobile phase inlet temperatures.

o-terphenyl

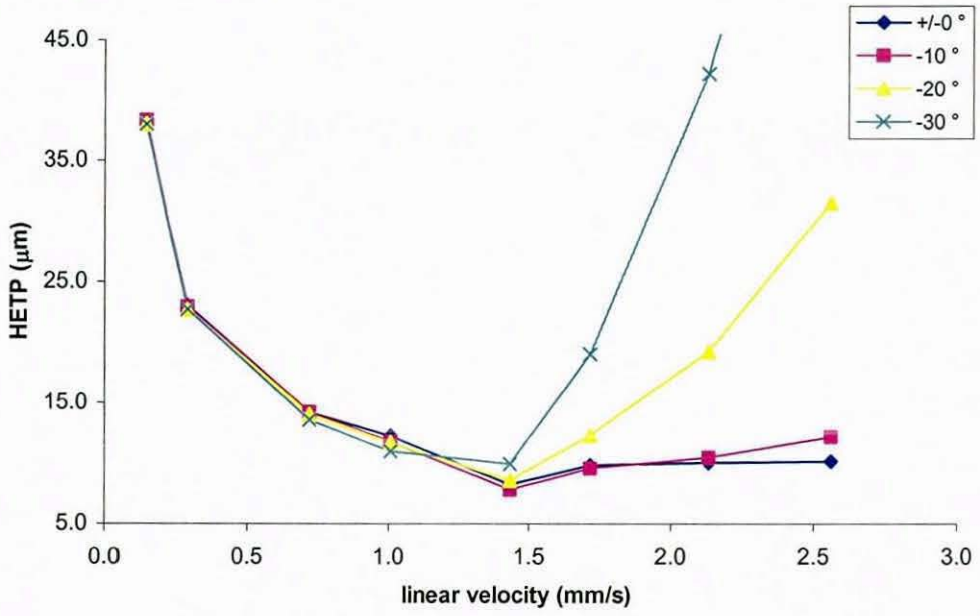

Figure 173: van Deemter curves for o-terphenyl on Chromolith 100 x 4.0 mm i.d., mobile phase 75% methanol, 25% water (w/w), temperature 60 °C controlled in water bath, at different mobile phase inlet temperatures.

pentylbenzene

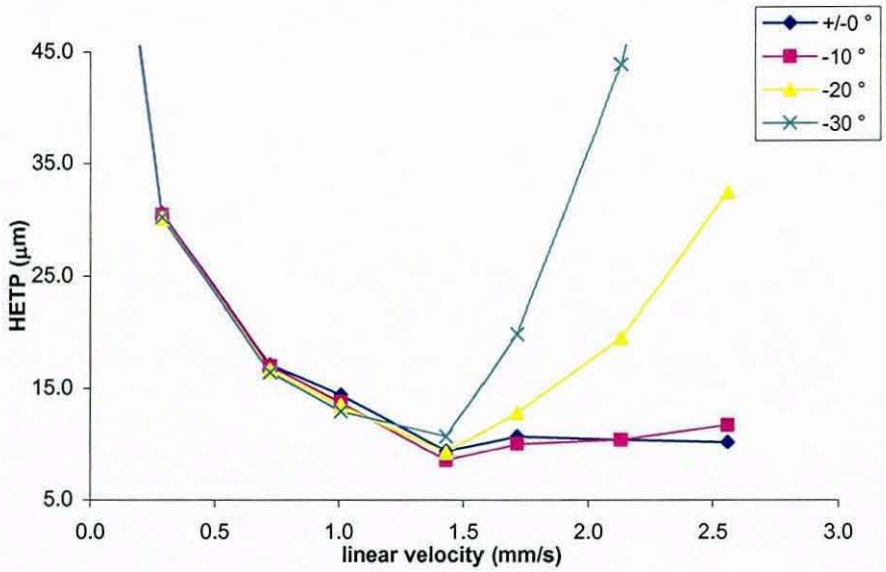

Figure 174: van Deemter curves for pentylbenzene on Chromolith 100 x 4.0 mm i.d., mobile phase 75% methanol, 25% water (w/w), temperature 60 °C controlled in water bath, at different mobile phase inlet temperatures.

triphenylene

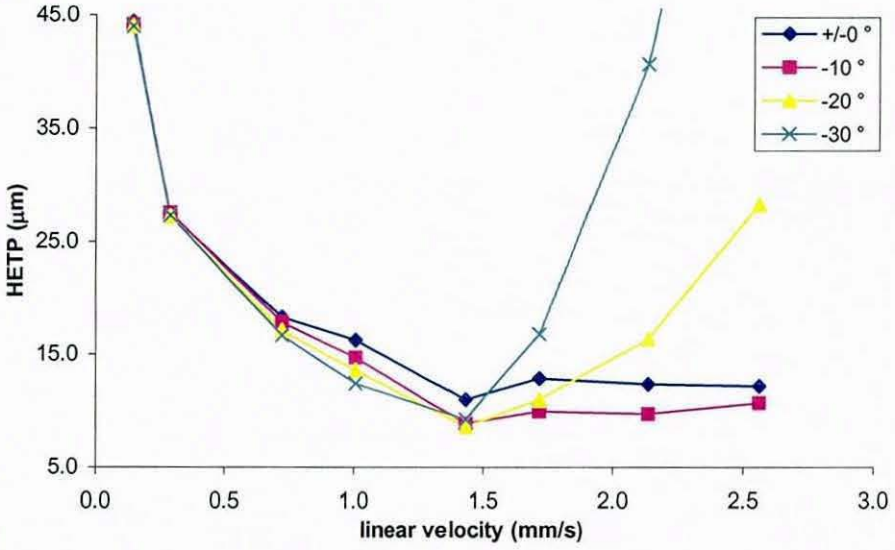

Figure 175 van Deemter curves for triphenylene on Chromolith 100 x 4.0 mm i.d., mobile phase 75% methanol, 25% water (w/w), temperature 60 °C controlled in water bath, at different mobile phase inlet temperatures.

Hypersil HiPurity ODS

butylbenzene

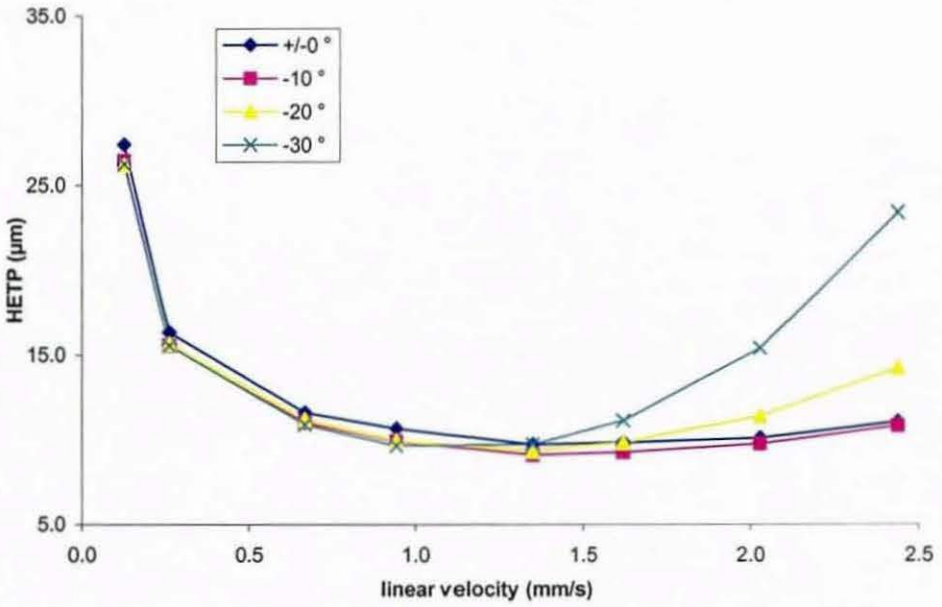

Figure 176: van Deemter curves for butylbenzene on Hypersil HiPurity ODS 150 x 4.6 mm i.d., mobile phase 75% methanol, 25% water (w/w), temperature 60 °C controlled in water bath, at different mobile phase inlet temperatures.

o-terphenyl

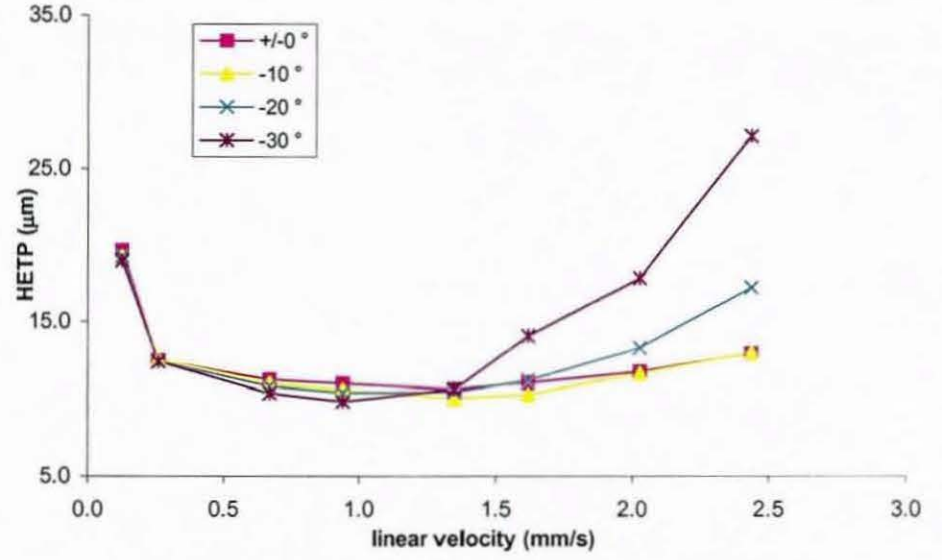

Figure 177: van Deemter curves for o-terphenyl on Hypersil HiPurity ODS 150 x 4.6 mm i.d., mobile phase 75% methanol, 25% water (w/w), temperature 60 °C controlled in water bath, at different mobile phase inlet temperatures.

pentylbenzene

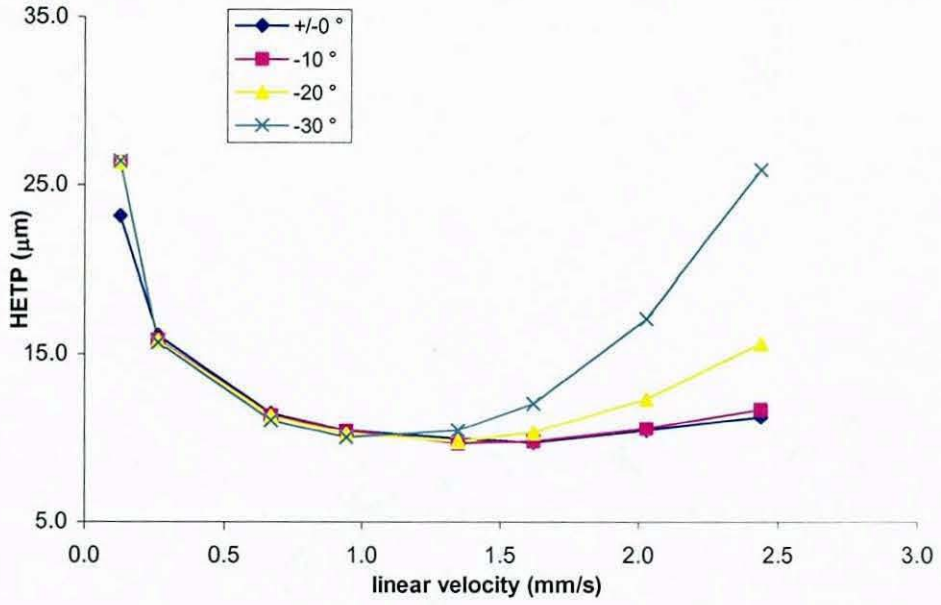

Figure 178: van Deemter curves for pentylbenzene on Hypersil HiPurity ODS 150 x 4.6 mm i.d., mobile phase 75% methanol, 25% water (w/w), temperature 60 °C controlled in water bath, at different mobile phase inlet temperatures.

triphenylene

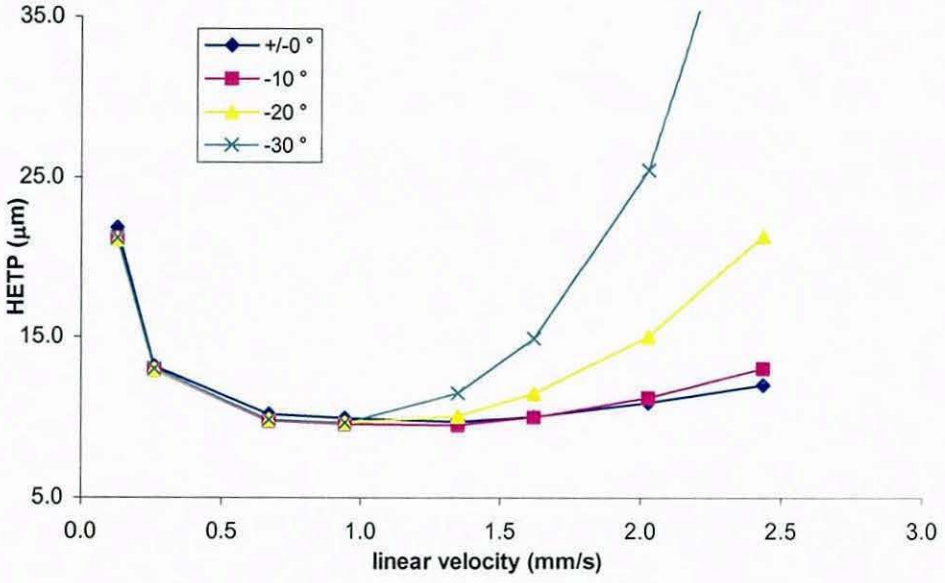

Figure 179: van Deemter curves for triphenylene on Hypersil HiPurity ODS 150 x 4.6 mm i.d., mobile phase 75% methanol, 25% water (w/w), temperature 60 °C controlled in water bath, at different mobile phase inlet temperatures.

Kromasil

butylbenzene

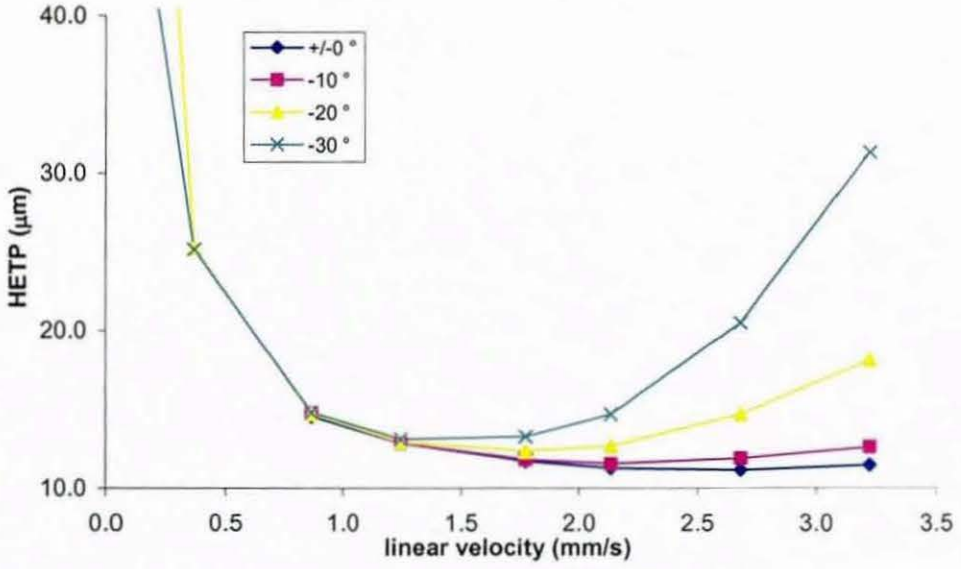

Figure 180: van Deemter curves for butylbenzene on Kromasil ODS 150 x 4.6 mm i.d., mobile phase 75% methanol, 25% water (w/w), temperature 60 °C controlled in water bath, at different mobile phase inlet temperatures.

o-terphenyl

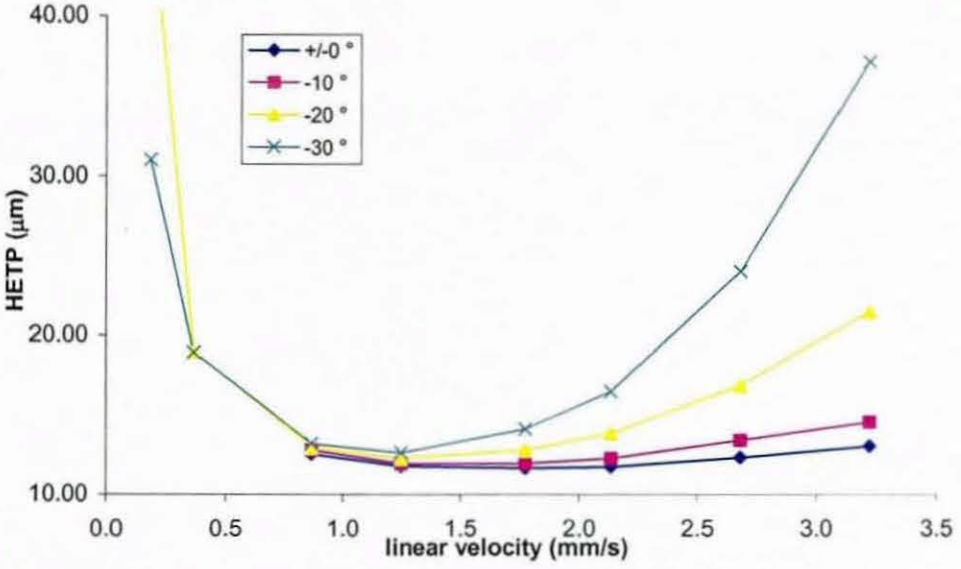

Figure 181: van Deemter curves for o-terphenyl on Kromasil ODS 150 x 4.6 mm i.d., mobile phase 75% methanol, 25% water (w/w), temperature 60 °C controlled in water bath, at different mobile phase inlet temperatures.

pentylbenzene

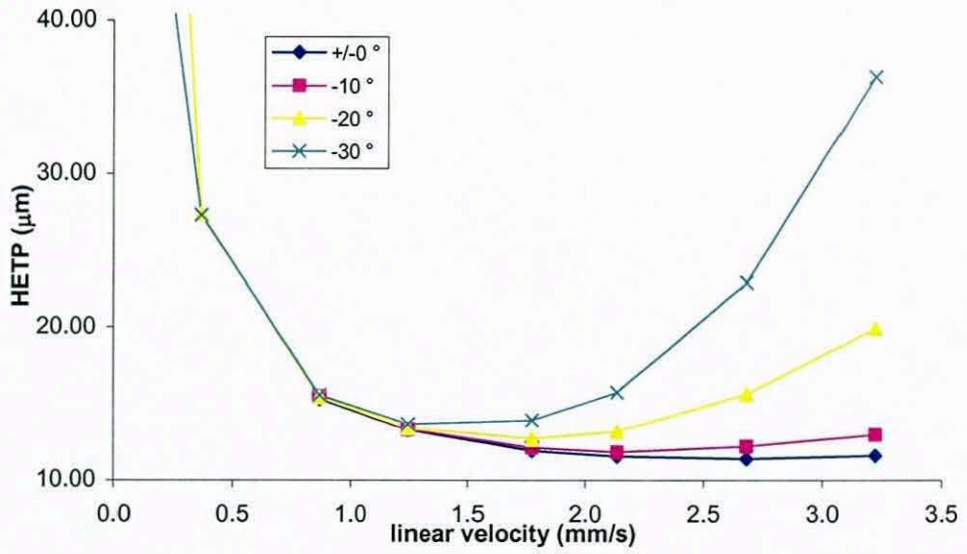

Figure 182: van Deemter curves for pentylbenzene on Kromasil ODS 150 x 4.6 mm i.d., mobile phase 75% methanol, 25% water (w/w), temperature 60 °C controlled in water bath, at different mobile phase inlet temperatures.

triphenylene

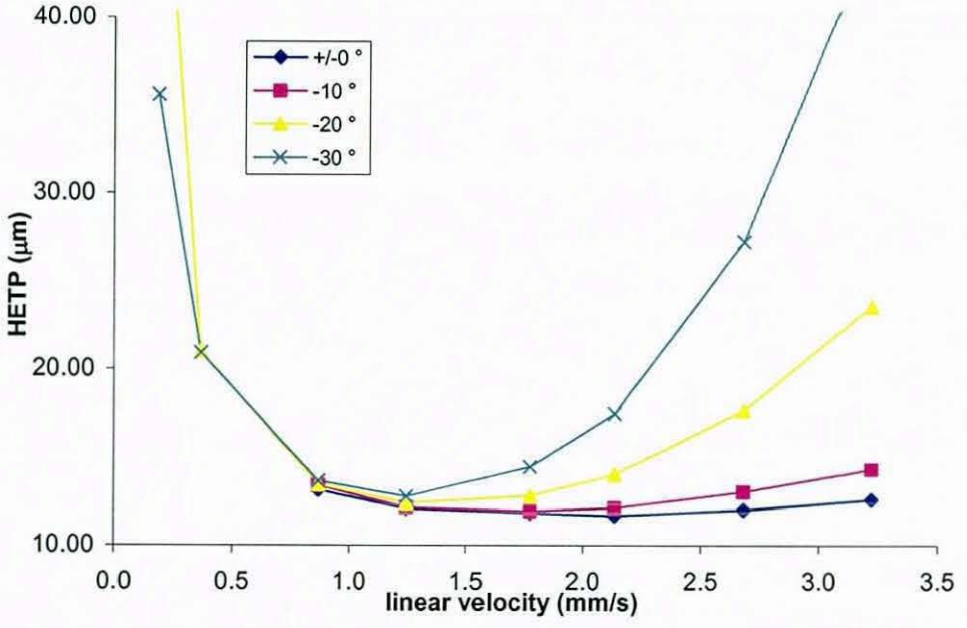

Figure 183: van Deemter curves for triphenylene on Kromasil ODS 150 x 4.6 mm i.d., mobile phase 75% methanol, 25% water (w/w), temperature 60 °C controlled in water bath, at different mobile phase inlet temperatures.

Prontosil

butylbenzene

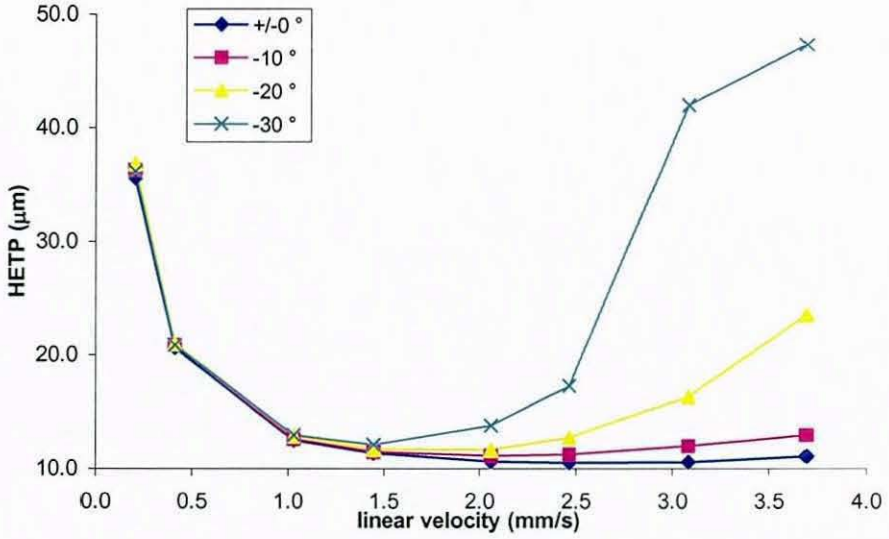

Figure 184 : van Deemter curves for butylbenzene on Prontosil ODS 150 x 4.0 mm i.d., mobile phase 75% methanol, 25% water (w/w), temperature 60 °C controlled in water bath, at different mobile phase inlet temperatures.

o-terphenyl

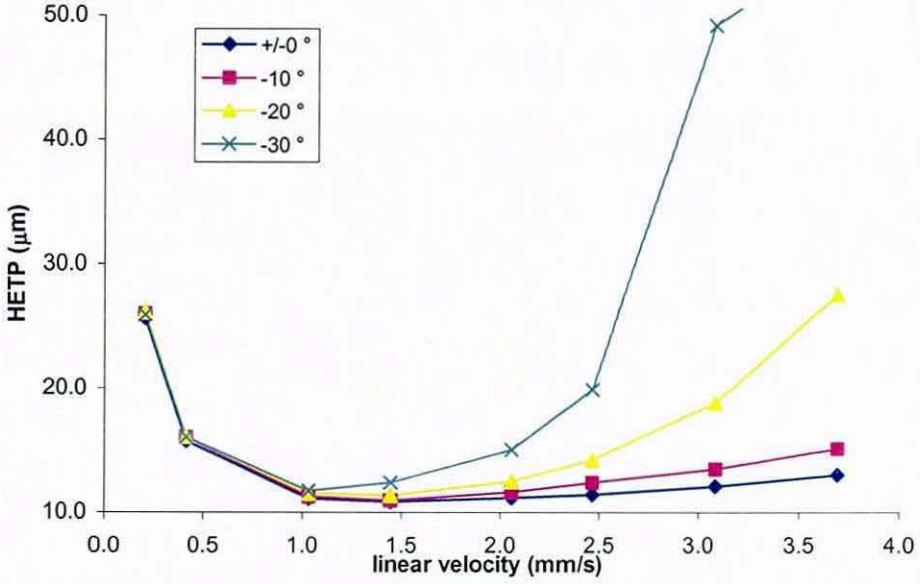

Figure 185: van Deemter curves for o-terphenyl on Prontosil ODS 150 x 4.0 mm i.d., mobile phase 75% methanol, 25% water (w/w), temperature 60 °C controlled in water bath, at different mobile phase inlet temperatures.

pentylbenzene

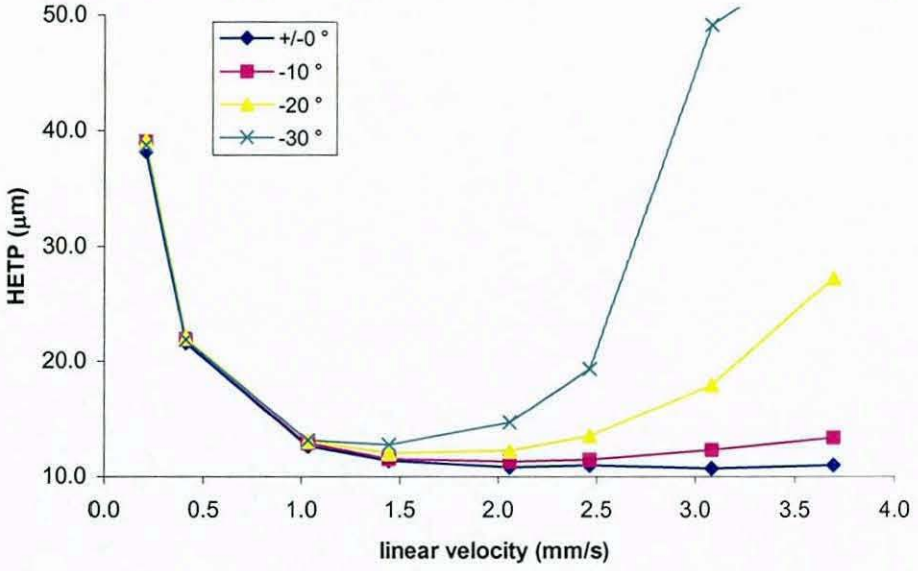

Figure 186: van Deemter curves for pentylbenzene on Prontosil ODS 150 x 4.0 mm i.d., mobile phase 75% methanol, 25% water (w/w), temperature 60 °C controlled in water bath, at different mobile phase inlet temperatures.

triphenylene

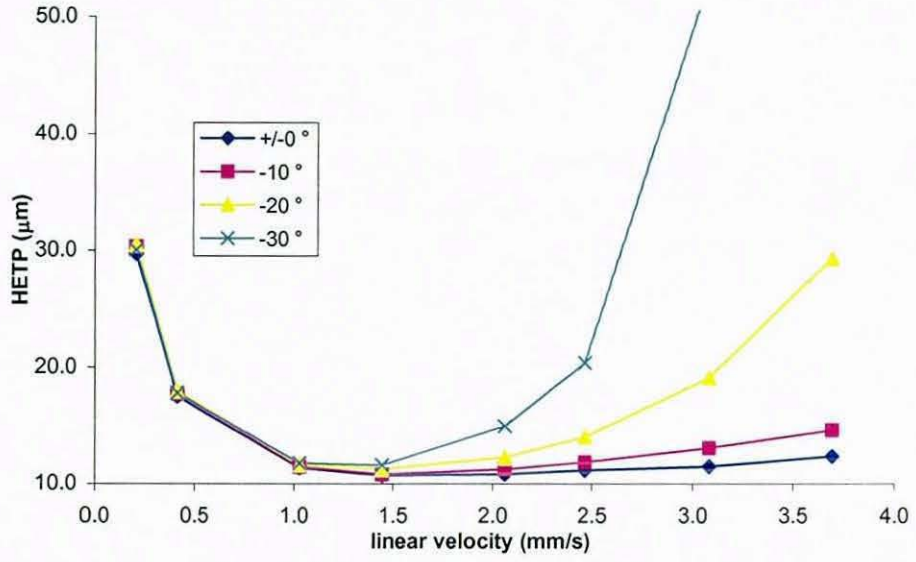

Figure 187: van Deemter curves for triphenylene on Prontosil ODS 150 x 4.0 mm i.d., mobile phase 75% methanol, 25% water (w/w), temperature 60 °C controlled in water bath, at different mobile phase inlet temperatures.

Purospher RP18

butylbenzene

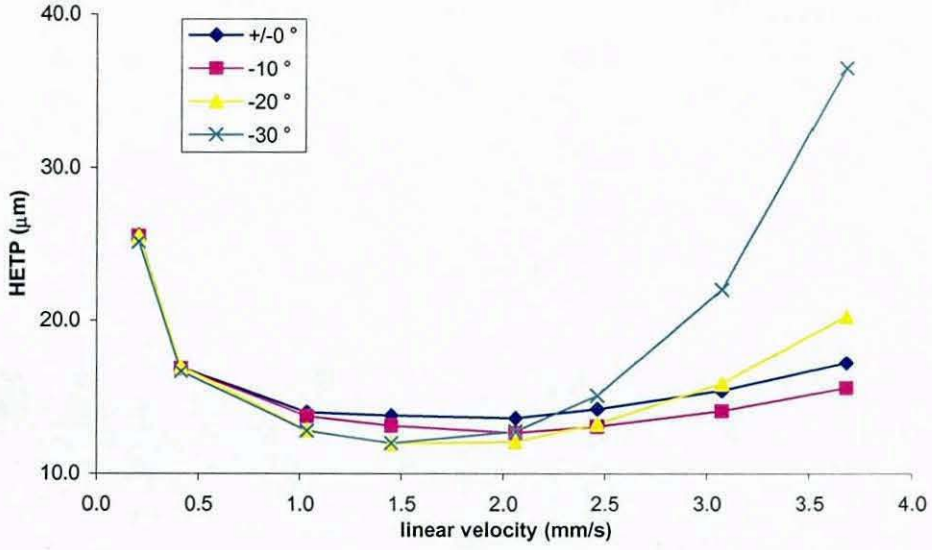

Figure 188: van Deemter curves for butylbenzene on Purospher RP18 125 x 4.0 mm i.d., mobile phase 75% methanol, 25% water (w/w), temperature 60 °C controlled in water bath, at different mobile phase inlet temperatures.

o-terphenyl

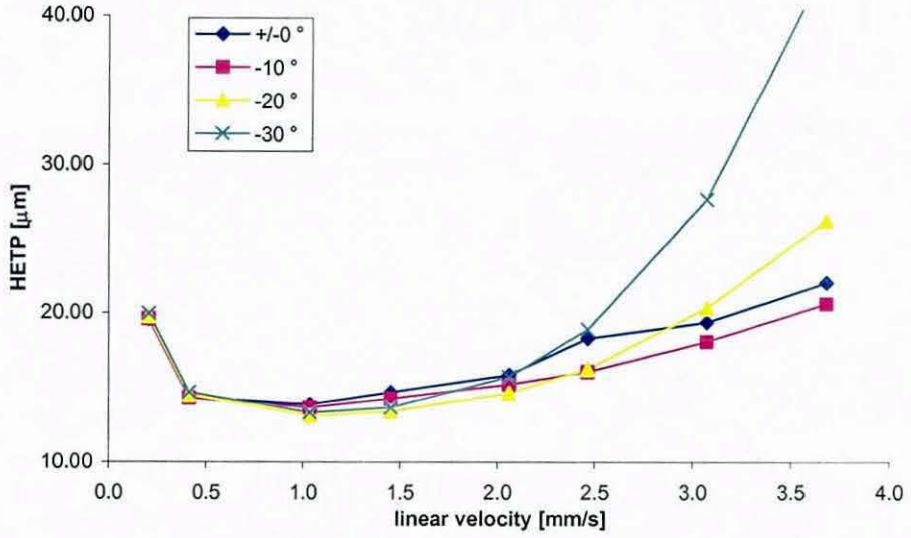

Figure 189: van Deemter curves for o-terphenyl on Purospher RP18 125 x 4.0 mm i.d., mobile phase 75% methanol, 25% water (w/w), temperature 60 °C controlled in water bath, at different mobile phase inlet temperatures.

pentylbenzene

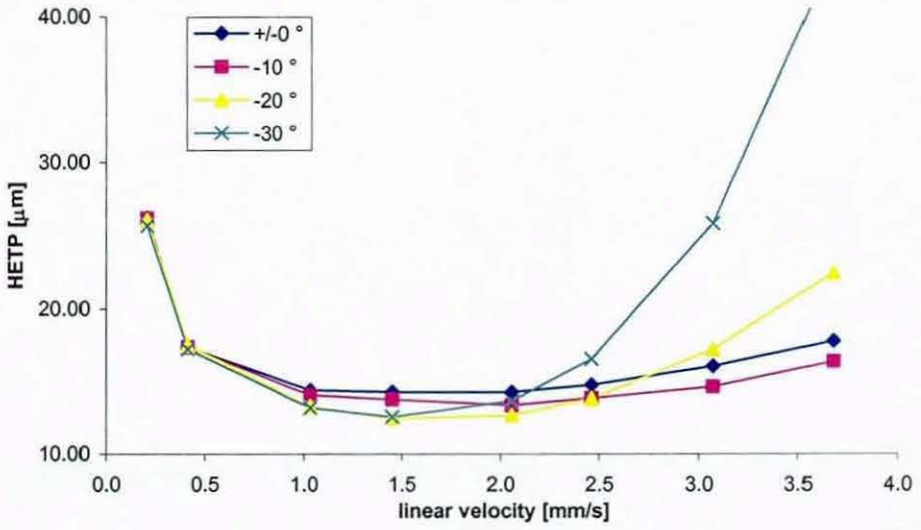

Figure 190: van Deemter curves for pentylbenzene on Purospher RP18 125 x 4.0 mm i.d., mobile phase 75% methanol, 25% water (w/w), temperature 60 °C controlled in water bath, at different mobile phase inlet temperatures.

triphenylene

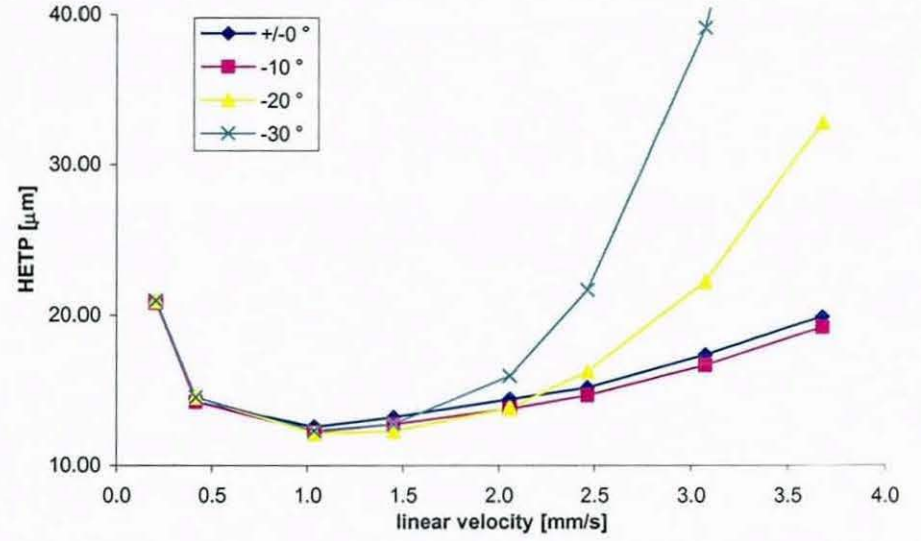

Figure 191: van Deemter curves for triphenylene on Purospher RP18 125 x 4.0 mm i.d., mobile phase 75% methanol, 25% water (w/w), temperature 60 °C controlled in water bath, at different mobile phase inlet temperatures.

Purospher RP18 125 x 3 mm

butylbenzene

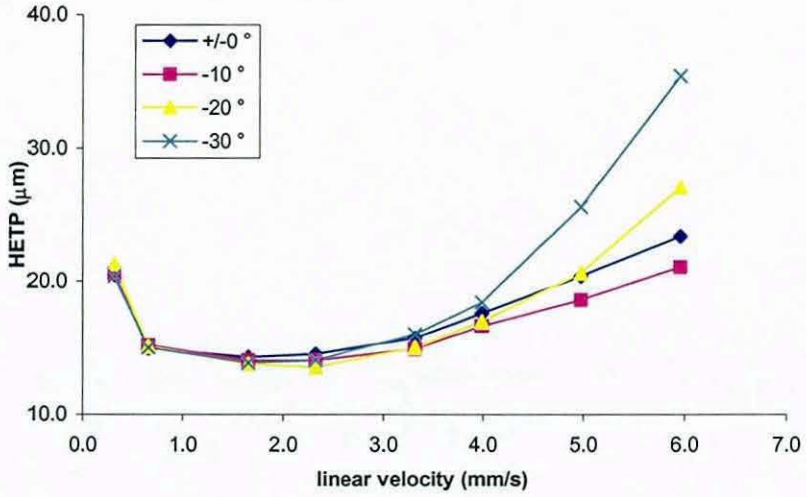

Figure 192: van Deemter curves for butylbenzene on Purospher RP18 125 x 3.0 mm i.d., mobile phase 75% methanol, 25% water (w/w), temperature 60 °C controlled in water bath, at different mobile phase inlet temperatures.

o-terphenyl

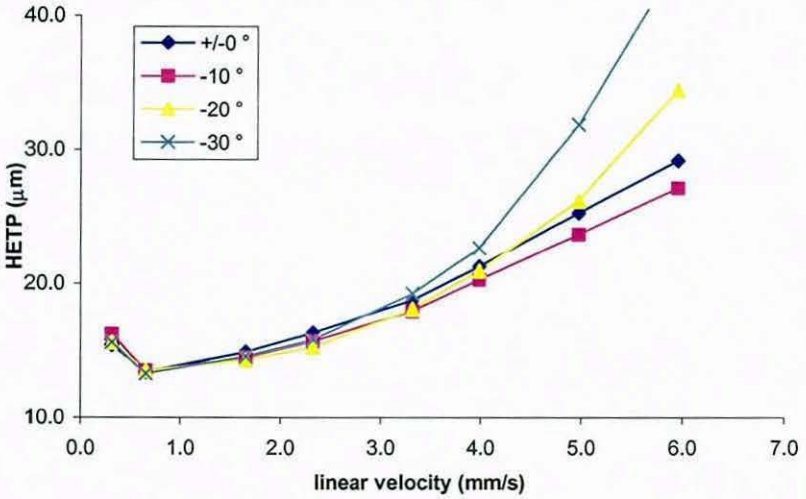

Figure 193: van Deemter curves for o-terphenyl on Purospher RP18 125 x 3.0 mm i.d., mobile phase 75% methanol, 25% water (w/w), temperature 60 °C controlled in water bath, at different mobile phase inlet temperatures.

pentylbenzene

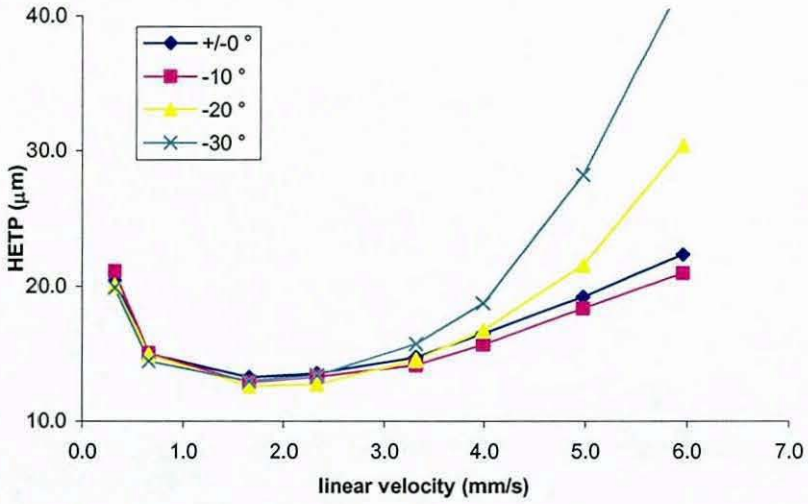

Figure 194: van Deemter curves for pentylbenzene on Purospher RP18 125 x 3.0 mm i.d., mobile phase 75% methanol, 25% water (w/w), temperature 60 °C controlled in water bath, at different mobile phase inlet temperatures.

triphenylene

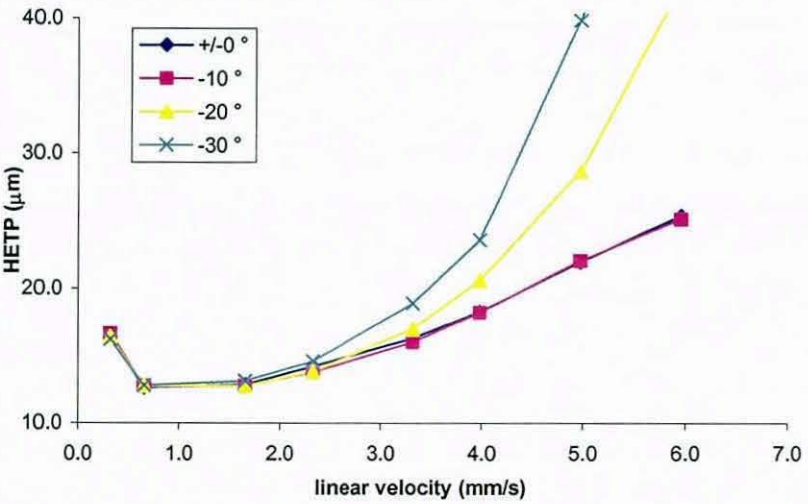

Figure 195: van Deemter curves for triphenylene on Purospher RP18 125 x 3.0 mm i.d., mobile phase 75% methanol, 25% water (w/w), temperature 60 °C controlled in water bath, at different mobile phase inlet temperatures.

Purospher RP18 125 x 2 mm i.d.

butylbenzene

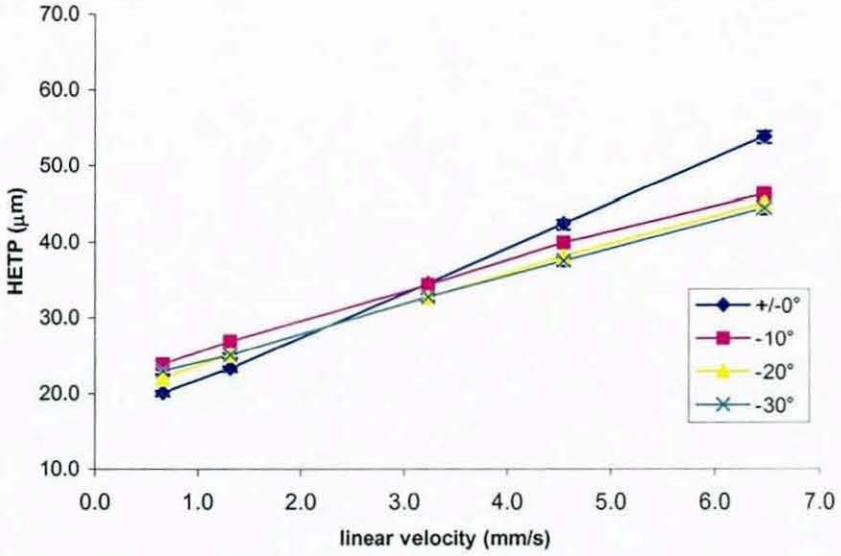

Figure 196: van Deemter curves for butylbenzene on Purospher RP18 125 x 2.0 mm i.d., mobile phase 75% methanol, 25% water (w/w), temperature 60 °C controlled in water bath, at different mobile phase inlet temperatures.

o-terphenyl

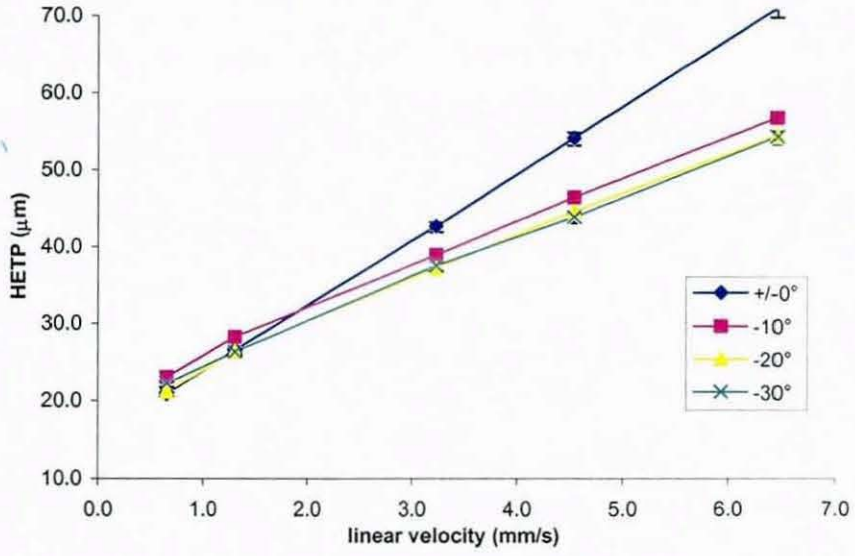

Figure 197: van Deemter curves for o-terphenyl on Purospher RP18 125 x 2.0 mm i.d., mobile phase 75% methanol, 25% water (w/w), temperature 60 °C controlled in water bath, at different mobile phase inlet temperatures.

pentylbenzene

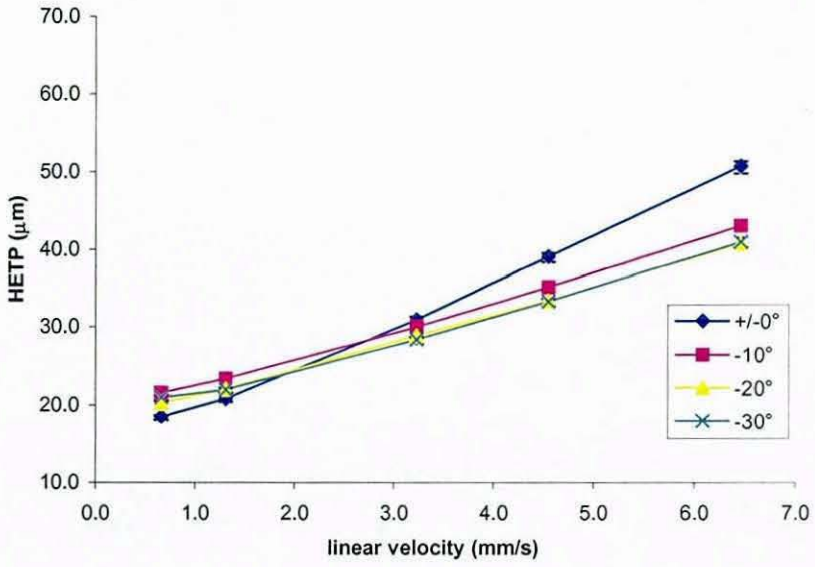

Figure 198: van Deemter curves for pentylbenzene on Purospher RP18 125 x 2.0 mm i.d., mobile phase 75% methanol, 25% water (w/w), temperature 60 °C controlled in water bath, at different mobile phase inlet temperatures.

triphenylene

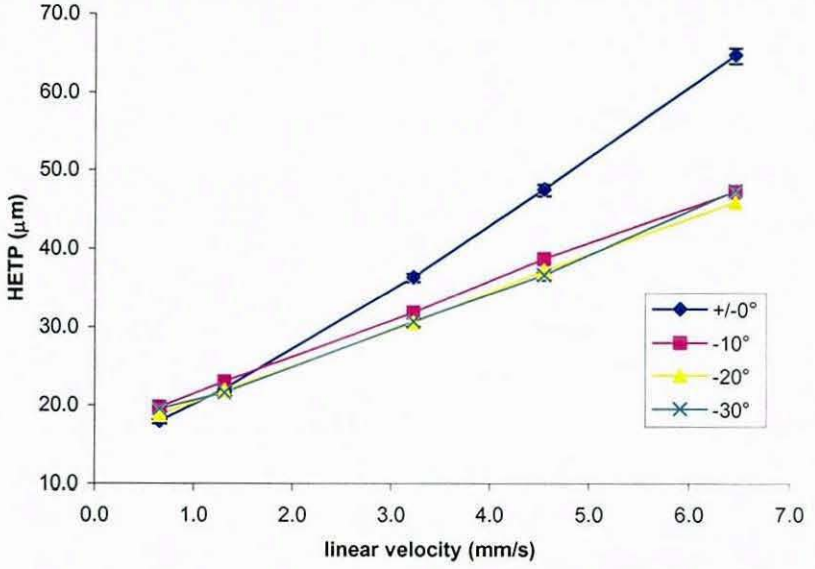

Figure 199: van Deemter curves for triphenylene on Purospher RP18 125 x 2.0 mm i.d., mobile phase 75% methanol, 25% water (w/w), temperature 60 °C controlled in water bath, at different mobile phase inlet temperatures.

Purospher RP18e 150 x 4.6 mm i.d.

butylbenzene

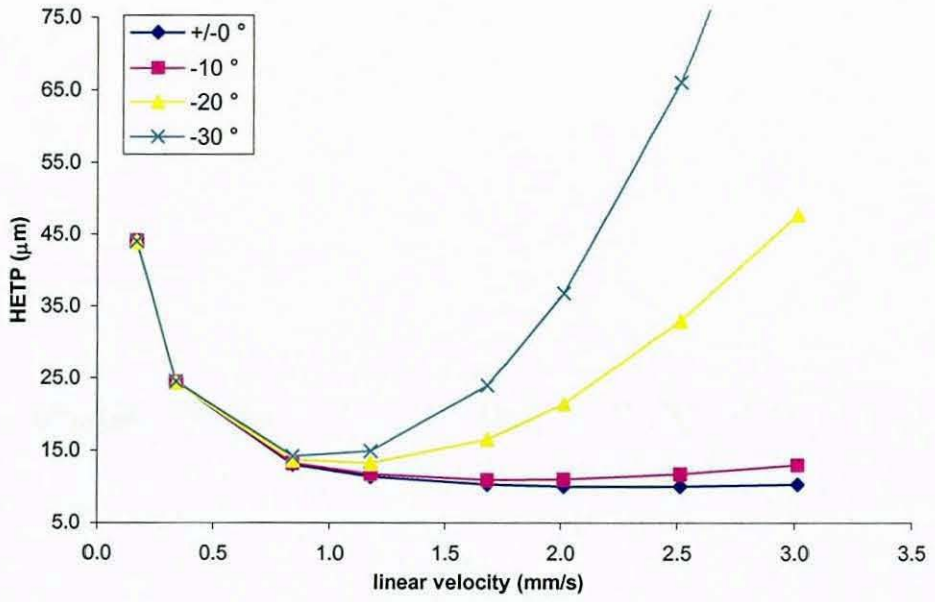

Figure 200: van Deemter curves for butylbenzene on Purospher RP18e 150 x 4.6 mm i.d., mobile phase 75% methanol, 25% water (w/w), temperature 60 °C controlled in water bath, at different mobile phase inlet temperatures.

o-terphenyl

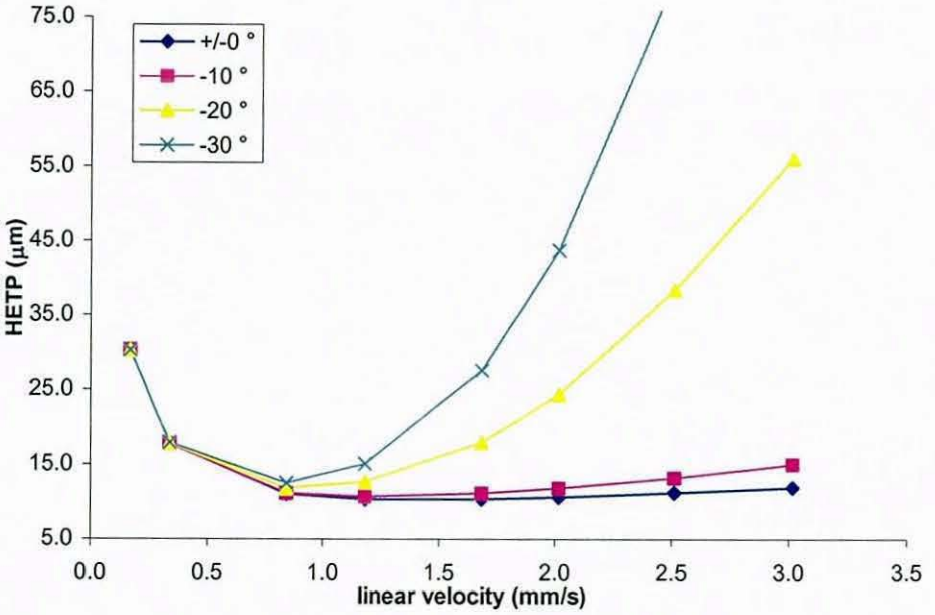

Figure 201: van Deemter curves for o-terphenyl on Purospher RP18e 150 x 4.6 mm i.d., mobile phase 75% methanol, 25% water (w/w), temperature 60 °C controlled in water bath, at different mobile phase inlet temperatures.

pentylbenzene

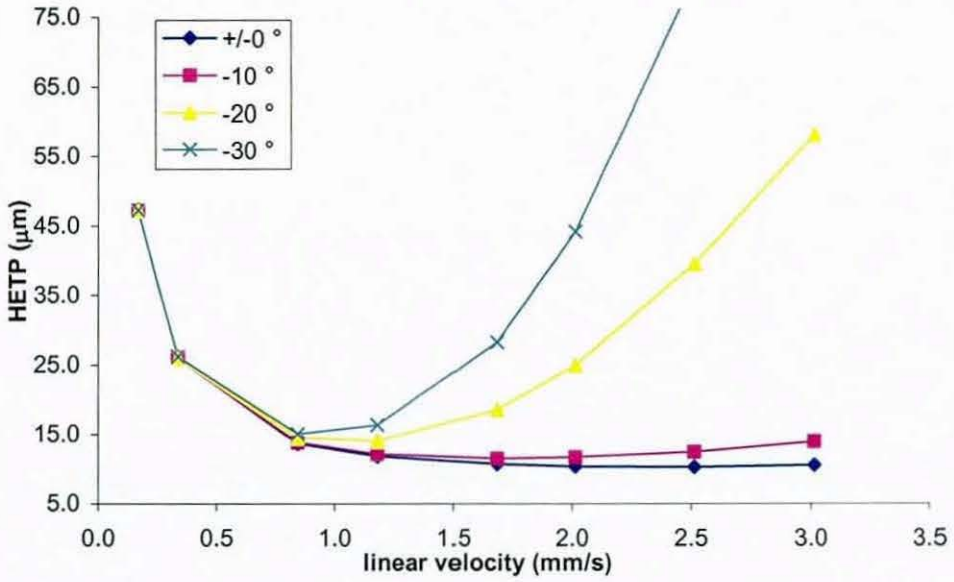

Figure 202: van Deemter curves for pentylbenzene on Purospher RP18e 150 x 4.6 mm i.d., mobile phase 75% methanol, 25% water (w/w), temperature 60 °C controlled in water bath, at different mobile phase inlet temperatures.

triphenylene

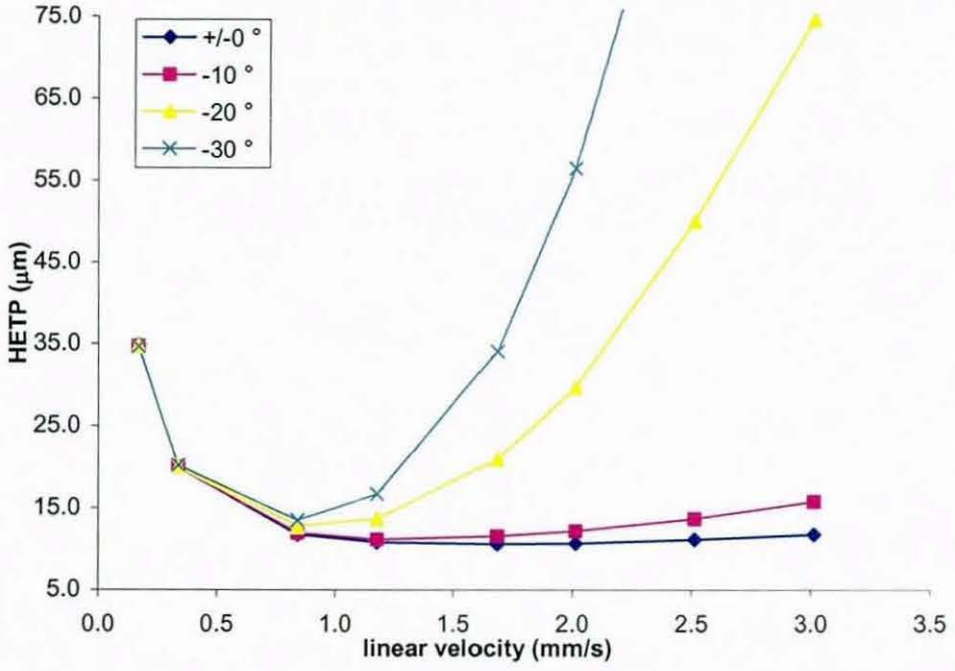

Figure 203: van Deemter curves for triphenylene on Purospher RP18e 150 x 4.6 mm i.d., mobile phase 75% methanol, 25% water (w/w), temperature 60 °C controlled in water bath, at different mobile phase inlet temperatures.

Purospher RP18e 125 x 3 mm i.d.

butylbenzene

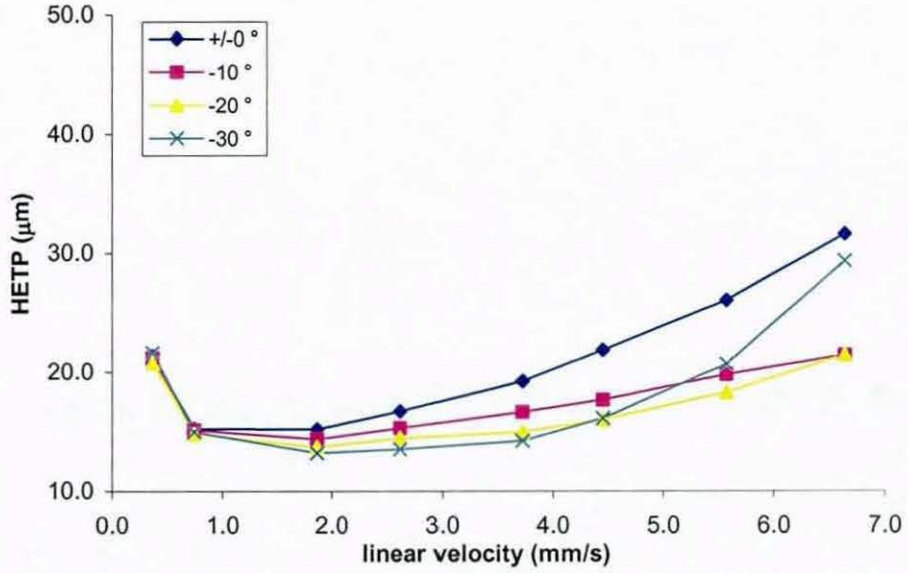

Figure 204: van Deemter curves for butylbenzene on Purospher RP18e 125 x 3.0 mm i.d., mobile phase 75% methanol, 25% water (w/w), temperature 60 °C controlled in water bath, at different mobile phase inlet temperatures.

o-terphenyl

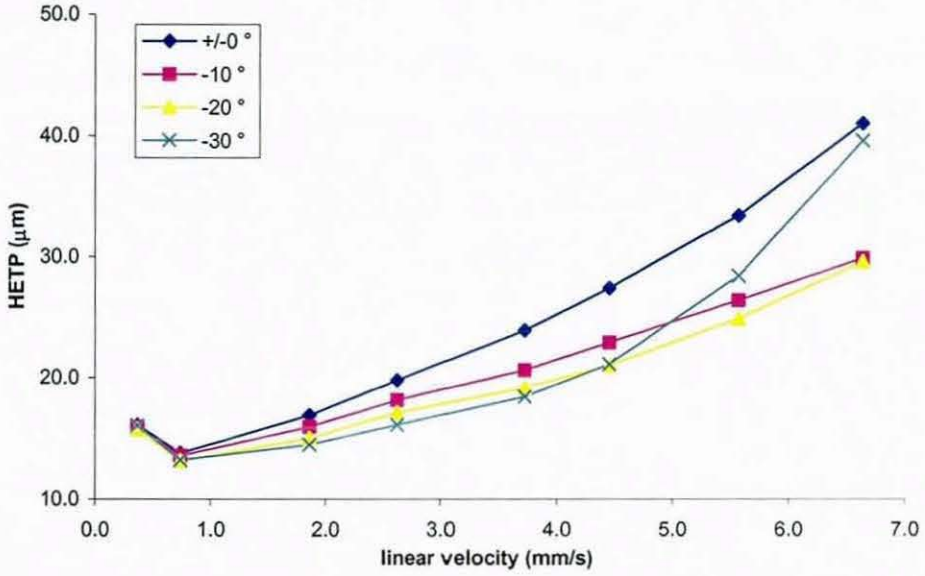

Figure 205: van Deemter curves for o-terphenyl on Purospher RP18e 125 x 3.0 mm i.d., mobile phase 75% methanol, 25% water (w/w), temperature 60 °C controlled in water bath, at different mobile phase inlet temperatures.

pentylbenzene

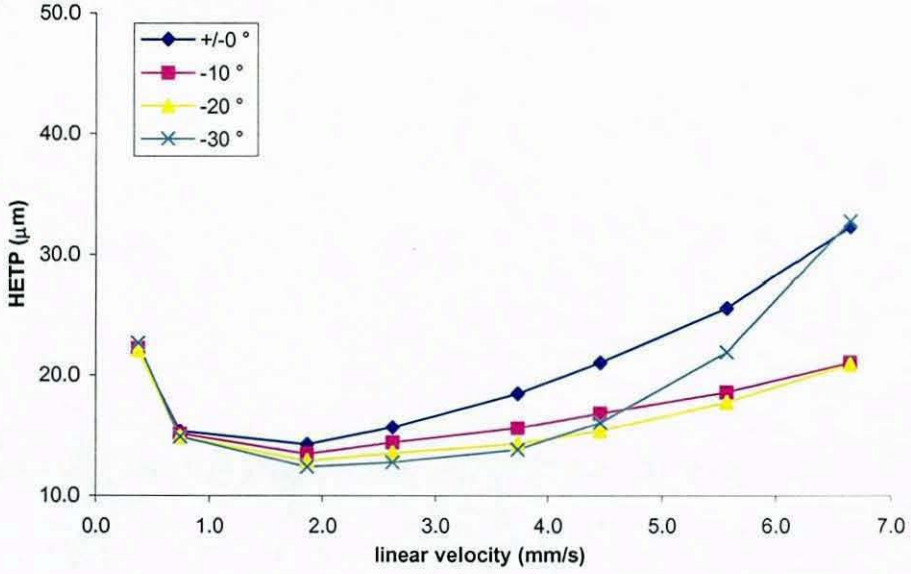

Figure 206: van Deemter curves for pentylbenzene on Purospher RP18e 125 x 3.0 mm i.d., mobile phase 75% methanol, 25% water (w/w), temperature 60 °C controlled in water bath, at different mobile phase inlet temperatures.

triphenylene

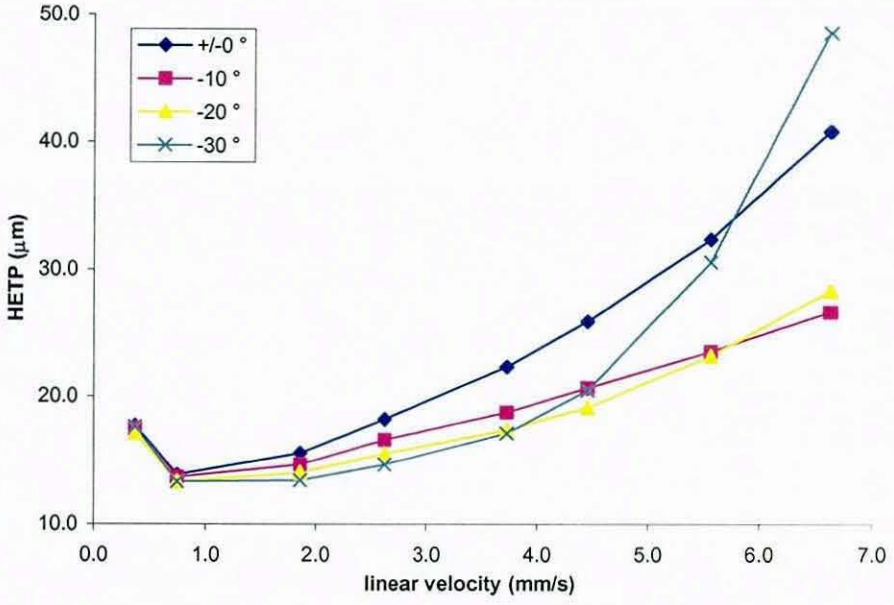

Figure 207: van Deemter curves for triphenylene on Purospher RP18e 125 x 3.0 mm i.d., mobile phase 75% methanol, 25% water (w/w), temperature 60 °C controlled in water bath, at different mobile phase inlet temperatures.

Purospher RP18e 125 x 2 mm i.d.

butylbenzene

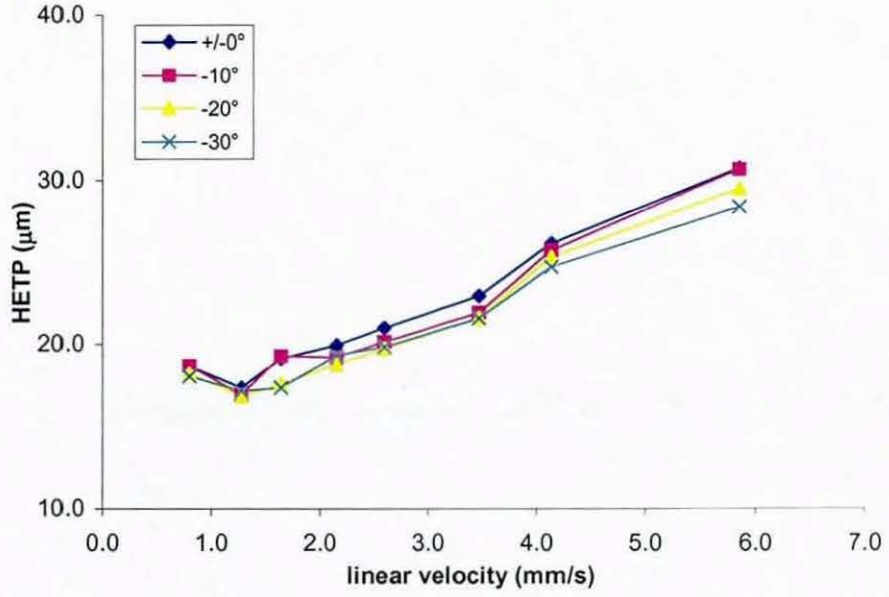

Figure 208: van Deemter curves for butylbenzene on Purospher RP18e 125 x 2.0 mm i.d., mobile phase 75% methanol, 25% water (w/w), temperature 60 °C controlled in water bath, at different mobile phase inlet temperatures.

o-terphenyl

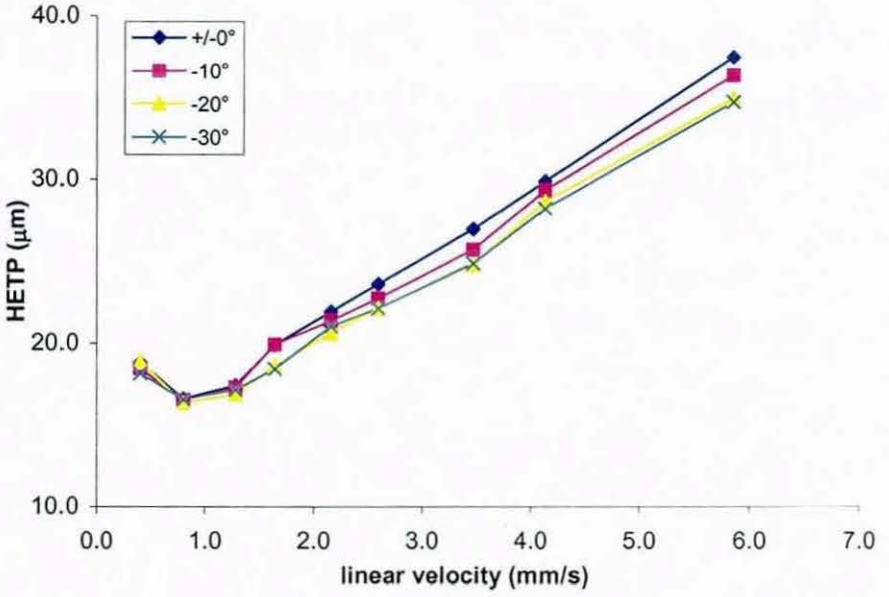

Figure 209: van Deemter curves for o-terphenyl on Purospher RP18e 125 x 2.0 mm i.d., mobile phase 75% methanol, 25% water (w/w), temperature 60 °C controlled in water bath, at different mobile phase inlet temperatures.

pentylbenzene

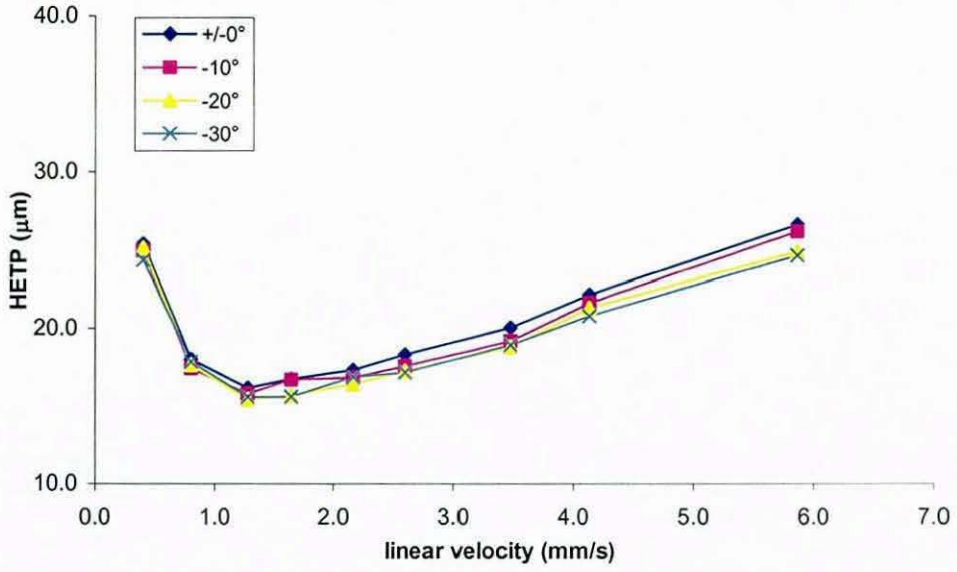

Figure 210: van Deemter curves for pentylbenzene on Purospher RP18e 125 x 2.0 mm i.d., mobile phase 75% methanol, 25% water (w/w), temperature 60 °C controlled in water bath, at different mobile phase inlet temperatures.

triphenylene

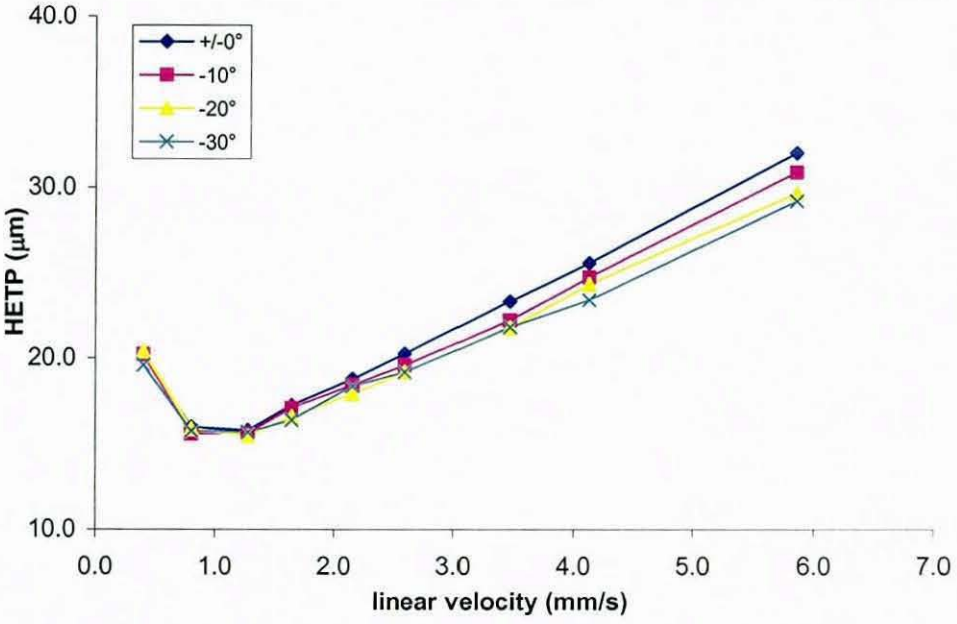

Figure 211: van Deemter curves for triphenylene on Purospher RP18e 125 x 2.0 mm i.d., mobile phase 75% methanol, 25% water (w/w), temperature 60 °C controlled in water bath, at different mobile phase inlet temperatures.

Purospher RP18e 125 x 1.0 mm i.d.

butylbenzene

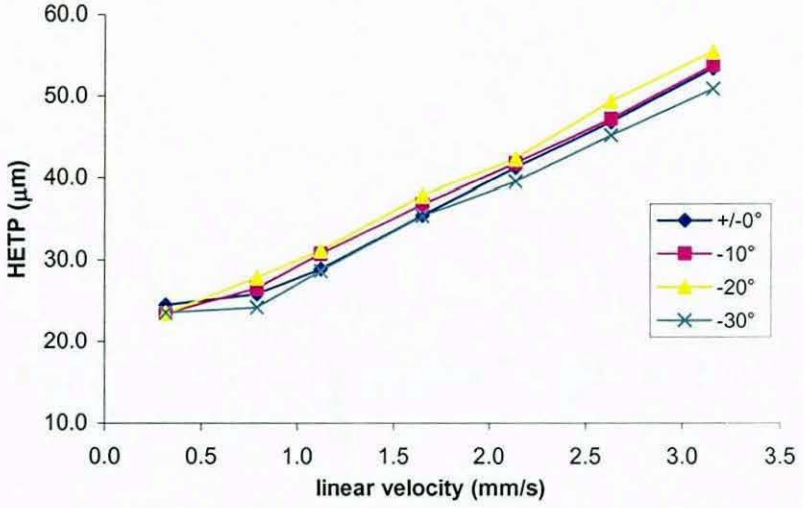

Figure 212: van Deemter curves for butylbenzene on Purospher RP18e 125 x 1.0 mm i.d., mobile phase 75% methanol, 25% water (w/w), temperature 60 °C controlled in water bath, at different mobile phase inlet temperatures.

o-terphenyl

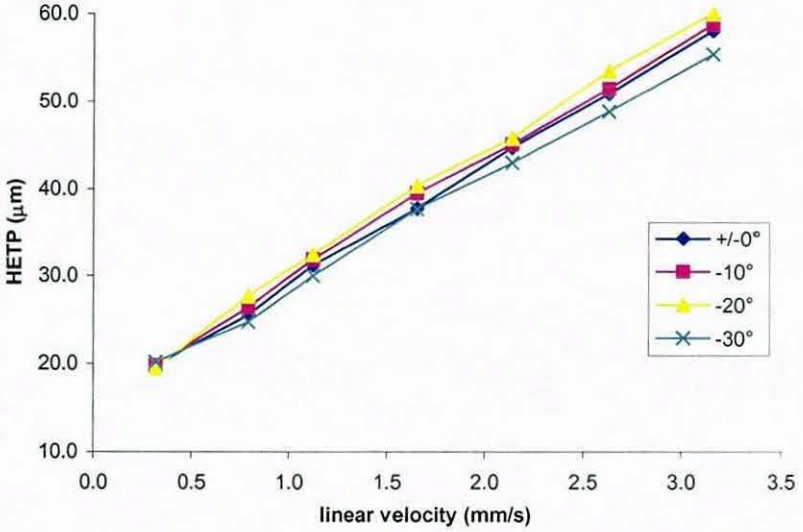

Figure 213: van Deemter curves for o-terphenyl on Purospher RP18e 125 x 1.0 mm i.d., mobile phase 75% methanol, 25% water (w/w), temperature 60 °C controlled in water bath, at different mobile phase inlet temperatures.

pentylbenzene

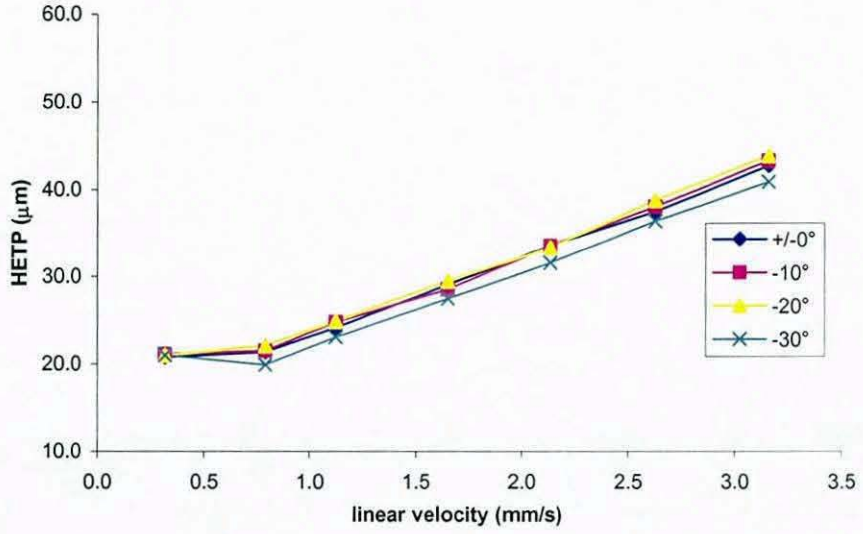

Figure 214: van Deemter curves for pentylbenzene on Purospher RP18e 125 x 1.0 mm i.d., mobile phase 75% methanol, 25% water (w/w), temperature 60 °C controlled in water bath, at different mobile phase inlet temperatures.

triphenylene

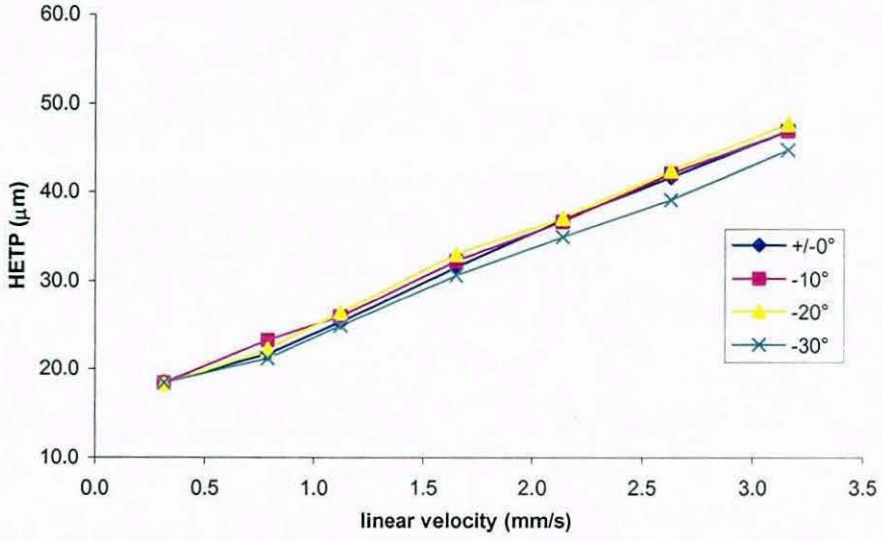

Figure 215: van Deemter curves for triphenylene on Purospher RP18e 125 x 1.0 mm i.d., mobile phase 75% methanol, 25% water (w/w), temperature 60 °C controlled in water bath, at different mobile phase inlet temperatures.

16 APPENDIX F

Bischoff EU column, 150 x 4.0 mm

butylebenzene

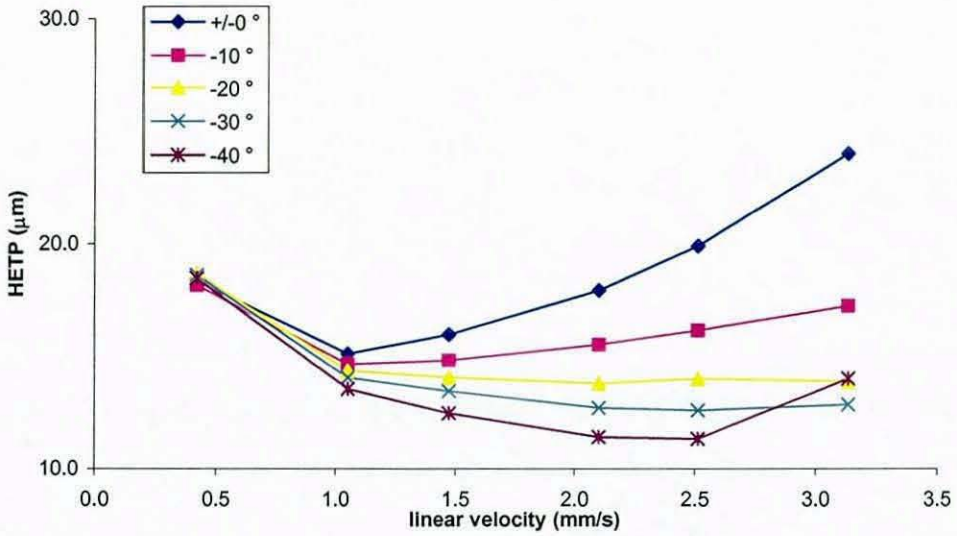

Figure 216: van Deemter curves for butylbenzene on EU column 150 x 4.0 mm i.d., mobile phase 75% methanol, 25% water (w/w), temperature 40 °C controlled in water bath, at different mobile phase inlet temperatures.

o-terphenyl

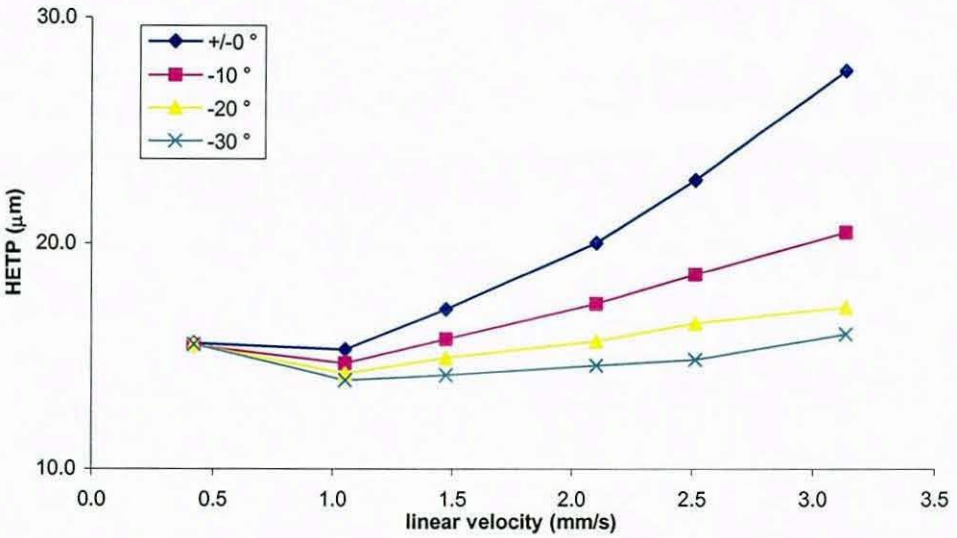

Figure 217: van Deemter curves for o-terphenyl on EU column 150 x 4.0 mm i.d., mobile phase 75% methanol, 25% water (w/w), temperature 40 °C controlled in water bath, at different mobile phase inlet temperatures.

pentylbenzene

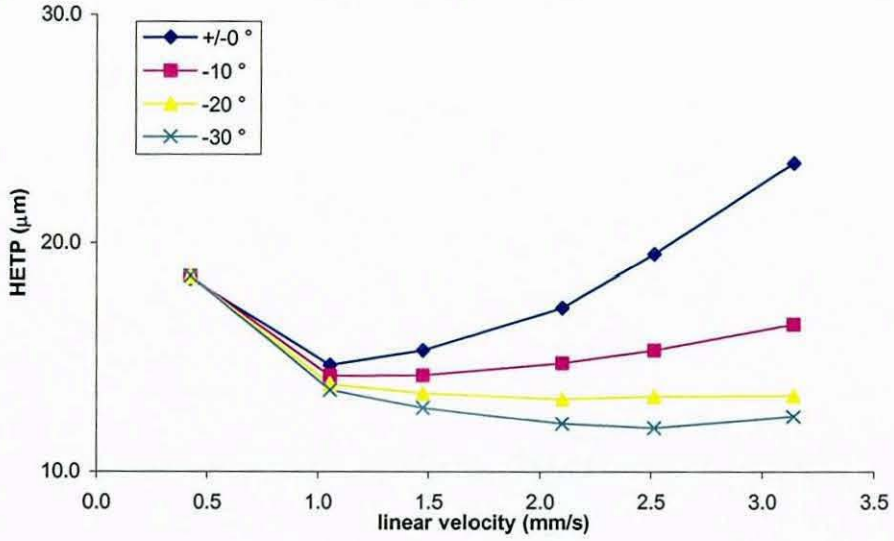

Figure 218: van Deemter curves for pentylbenzene on EU column 150 x 4.0 mm i.d., mobile phase 75% methanol, 25% water (w/w), temperature 40 °C controlled in water bath, at different mobile phase inlet temperatures.

triphenylene

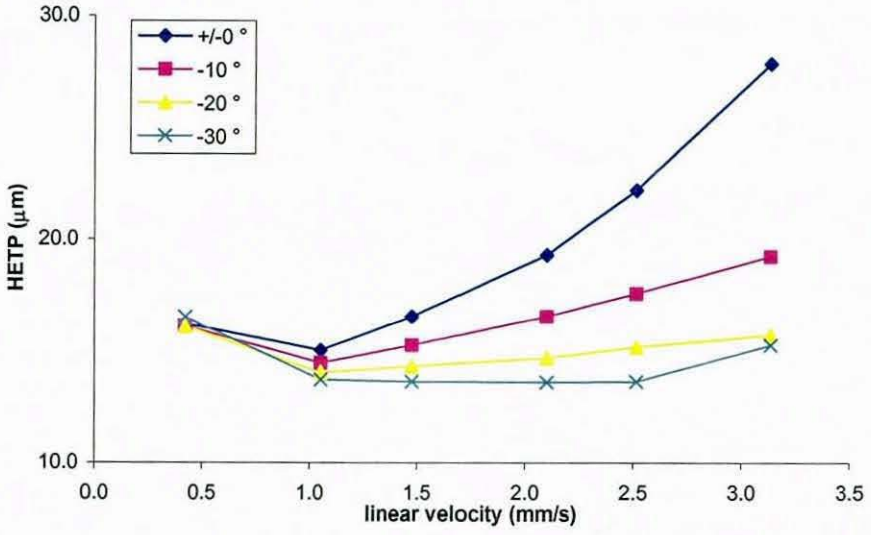

Figure 219: van Deemter curves for triphenylene on EU column 150 x 4.0 mm i.d., mobile phase 75% methanol, 25% water (w/w), temperature 40 °C controlled in water bath, at different mobile phase inlet temperatures.

Hypersil HiPurity ODS 150 x 4.6 mm

butylbenzene

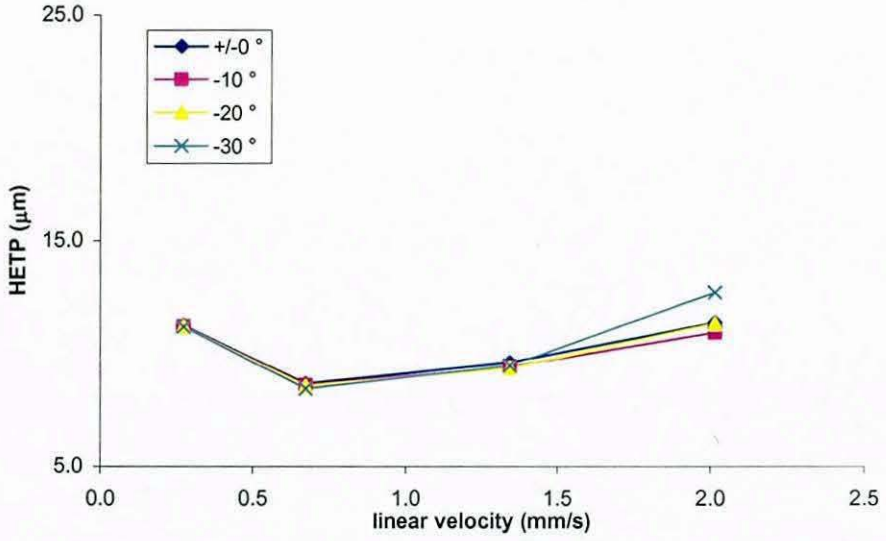

Figure 220: , van Deemter curves for butylbenzene on Hypersil HiPurity ODS column 150 x 4.6 mm i.d., mobile phase 75% methanol, 25% water (w/w), temperature 40 °C controlled in water bath at different mobile phase inlet temperatures.

o-terphenyl

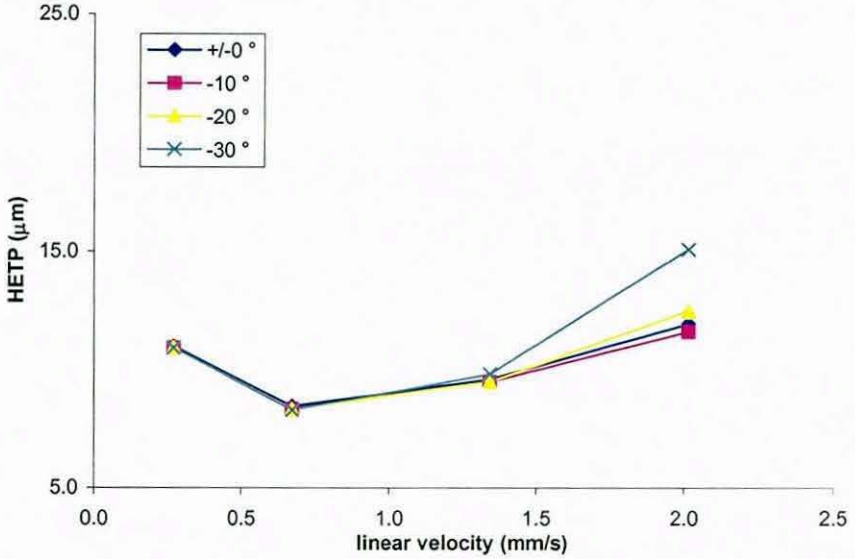

Figure 221: van Deemter curves for o-terphenyl on Hypersil HiPurity ODS column 150 x 4.6 mm i.d., mobile phase 75% methanol, 25% water (w/w), temperature 40 °C controlled in water bath, at different mobile phase inlet temperatures.

pentylbenzene

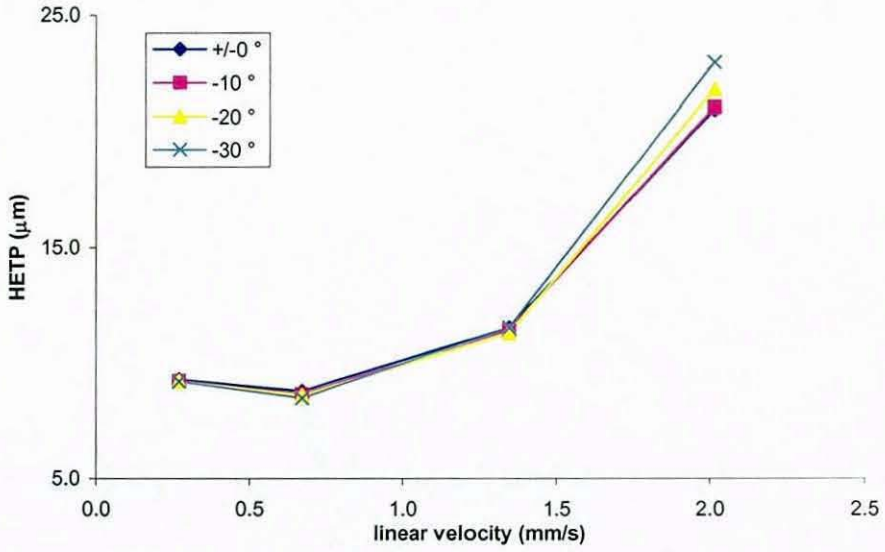

Figure 222: van Deemter curves for pentylbenzene on Hypersil HiPurity ODS column 150 x 4.6 mm i.d., mobile phase 75% methanol, 25% water (w/w), temperature 40 °C controlled in water bath, at different mobile phase inlet temperatures.

triphenylene

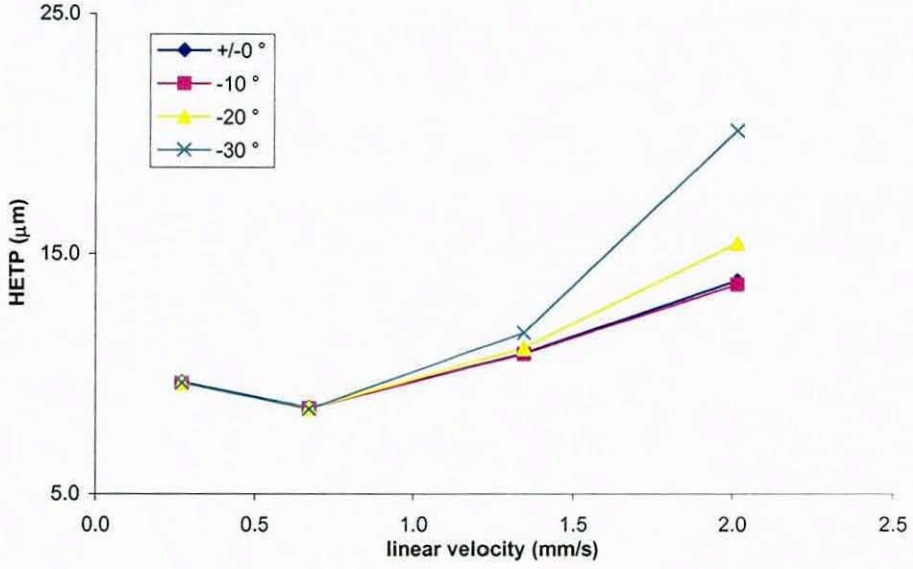

Figure 223: van Deemter curves for triphenylene on Hypersil HiPurity ODS column 150 x 4.6 mm i.d., mobile phase 75% methanol, 25% water (w/w), temperature 40 °C controlled in water bath, at different mobile phase inlet temperatures.

Prontosil ODS 150 x 4.0 mm

butylbenzene

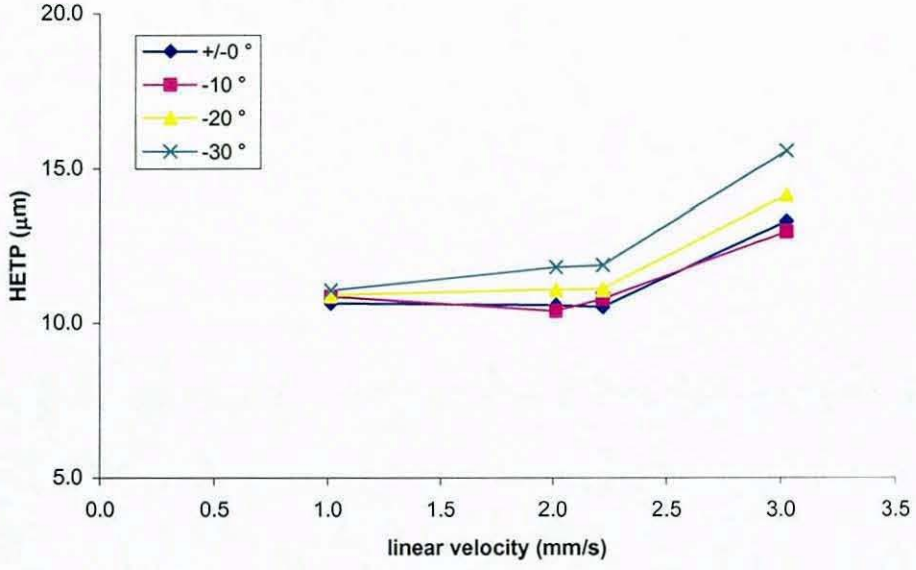

Figure 224: van Deemter curves for butylbenzene on Prontosil ODS column 150 x 4.0 mm i.d., mobile phase 75% methanol, 25% water (w/w), temperature 40 °C controlled in water bath, at different mobile phase inlet temperatures.

o-terphenyl

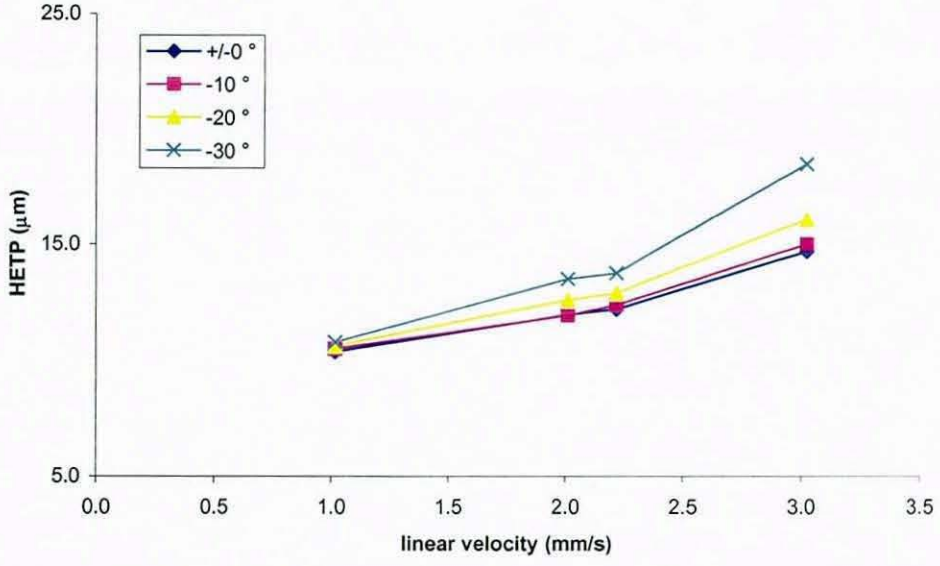

Figure 225: van Deemter curves for o-terphenyl on Prontosil ODS column 150 x 4.0 mm i.d., mobile phase 75% methanol, 25% water (w/w), temperature 40 °C controlled in water bath, at different mobile phase inlet temperatures.

pentylbenzene

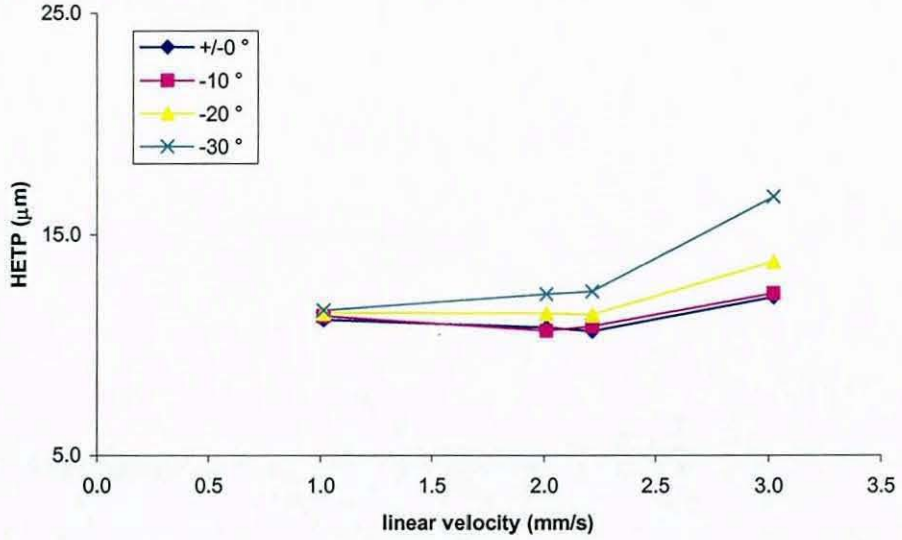

Figure 226: van Deemter curves for pentylbenzene on Prontosil ODS column 150 x 4.0 mm i.d., mobile phase 75% methanol, 25% water (w/w), temperature 40 °C controlled in water bath, at different mobile phase inlet temperatures.

triphenylene

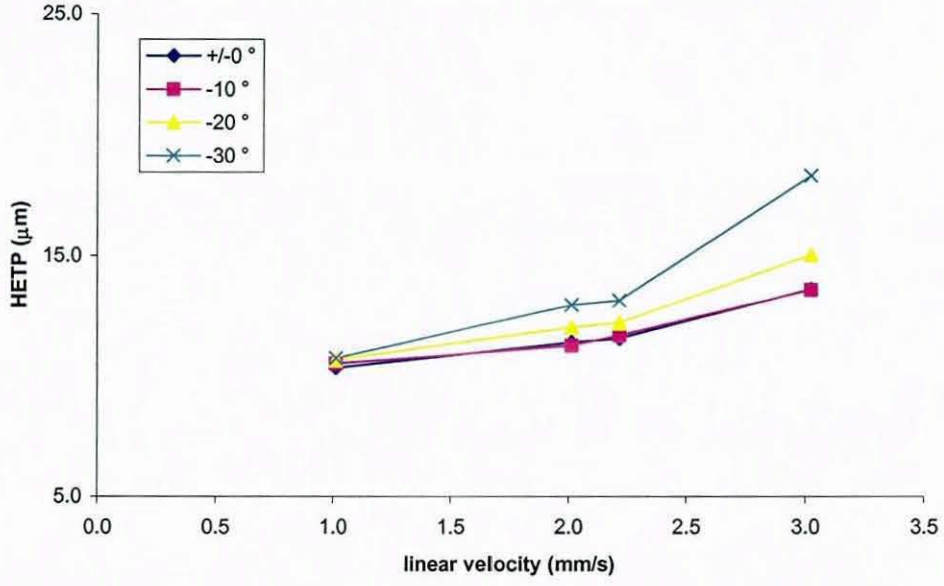

Figure 227: van Deemter curves for triphenylene on Prontosil ODS column 150 x 4.0 mm i.d., mobile phase 75% methanol, 25% water (w/w), temperature 40 °C controlled in water bath, at different mobile phase inlet temperatures.

Purospher RP18 125 x 4.0

butylbenzene

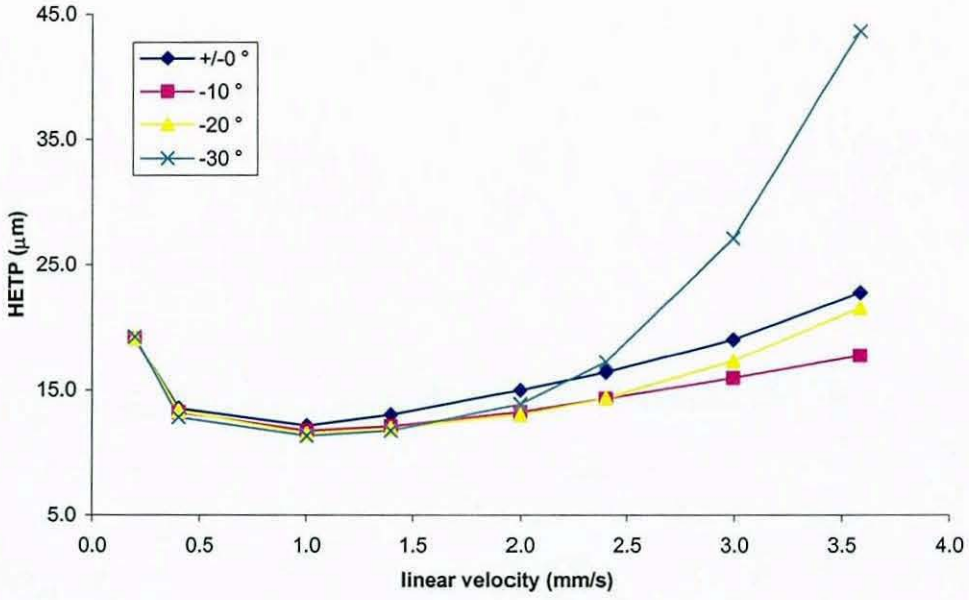

Figure 228: van Deemter curves for butylbenzene on Purospher RP18 column 125 x 4.0 mm i.d., mobile phase 75% methanol, 25% water (w/w), temperature 40 °C controlled in water bath, at different mobile phase inlet temperatures.

o-terphenyl

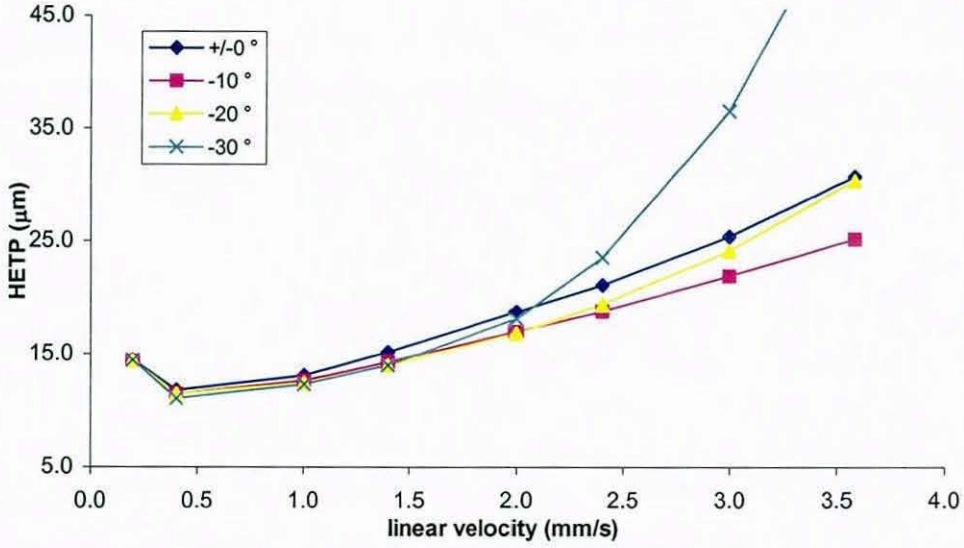

Figure 229: van Deemter curves for o-terphenyl on Purospher RP18 column 125 x 4.0 mm i.d., mobile phase 75% methanol, 25% water (w/w), temperature 40 °C controlled in water bath, at different mobile phase inlet temperatures.

pentylbenzene

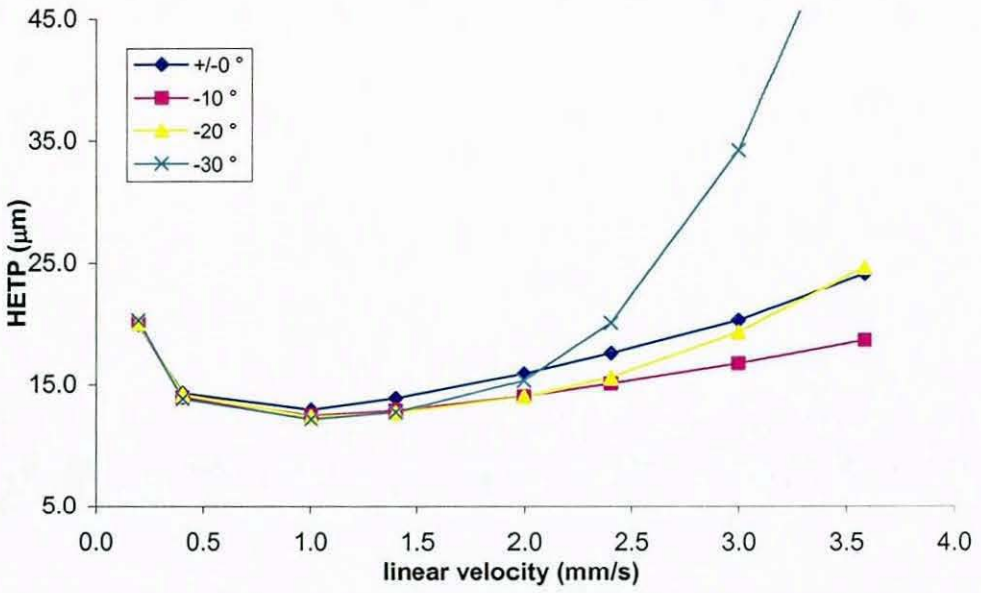

Figure 230: van Deemter curves for pentylbenzene on Purospher RP18 column 125 x 4.0 mm i.d., mobile phase 75% methanol, 25% water (w/w), temperature 40 °C controlled in water bath, at different mobile phase inlet temperatures.

triphenylene

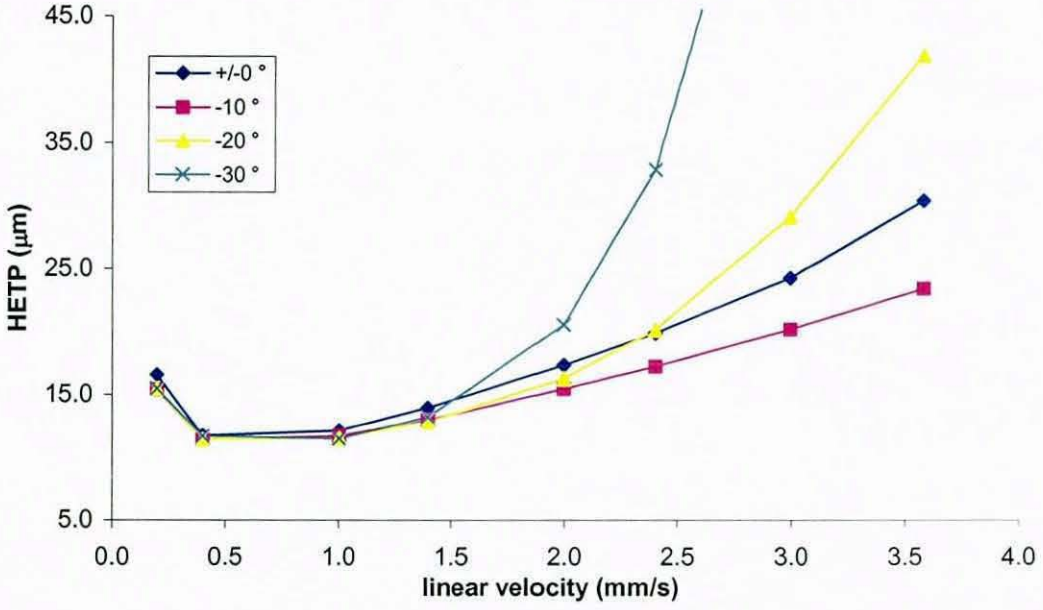

Figure 231: van Deemter curves for triphenylene on Purospher RP18 column 125 x 4.0 mm i.d., mobile phase 75% methanol, 25% water (w/w), temperature 40 °C controlled in water bath, at different mobile phase inlet temperatures.

Purospher RP18 125 x 3.0 mm

butylbenzene

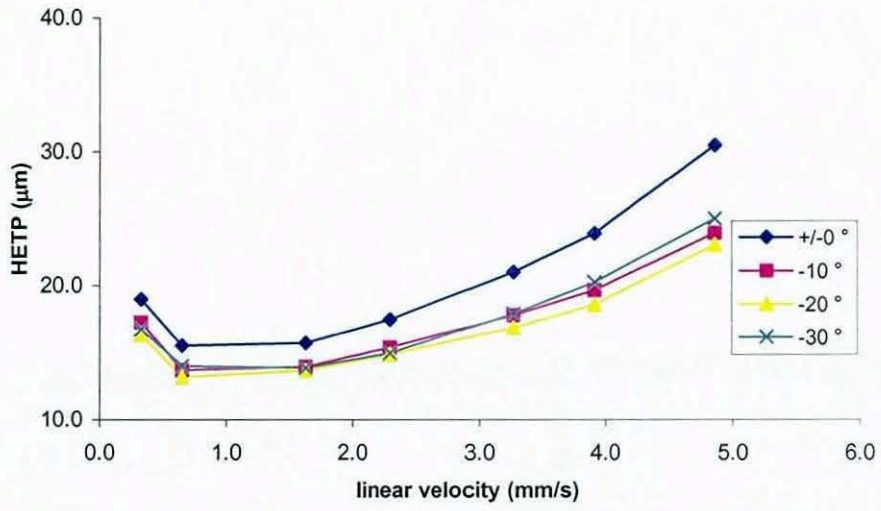

Figure 232: van Deemter curves for butylbenzene on Purospher RP18 column 125 x 3.0 mm i.d., mobile phase 75% methanol, 25% water (w/w), temperature 40 °C controlled in water bath, at different mobile phase inlet temperatures.

o-terphenyl

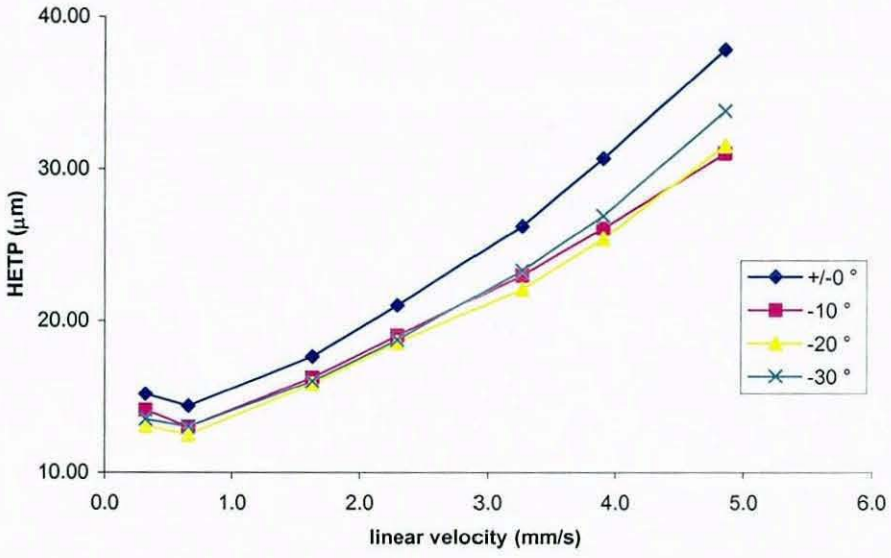

Figure 233: van Deemter curves for o-terphenyl on Purospher RP18 column 125 x 3.0 mm i.d., mobile phase 75% methanol, 25% water (w/w), temperature 40 °C controlled in water bath, at different mobile phase inlet temperatures.

pentylbenzene

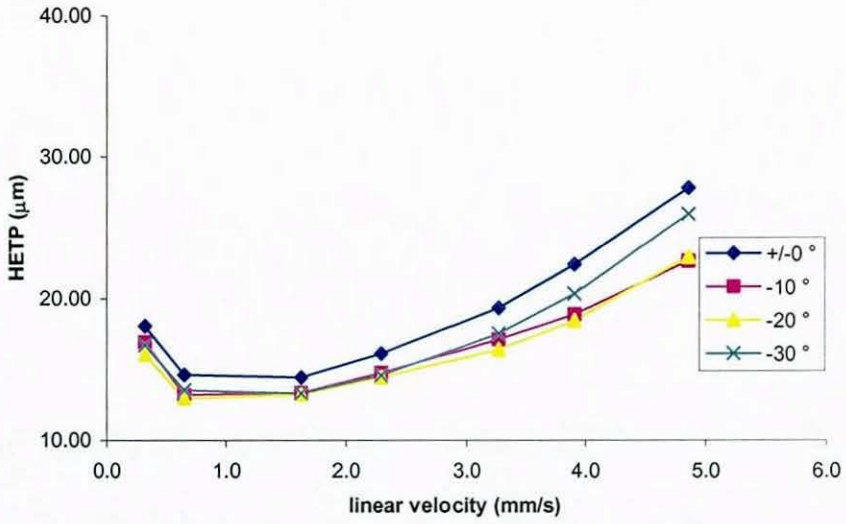

Figure 234: van Deemter curves for pentylbenzene on Purospher RP18 column 125 x 3.0 mm i.d., mobile phase 75% methanol, 25% water (w/w), temperature 40 °C controlled in water bath, at different mobile phase inlet temperatures.

triphenylene

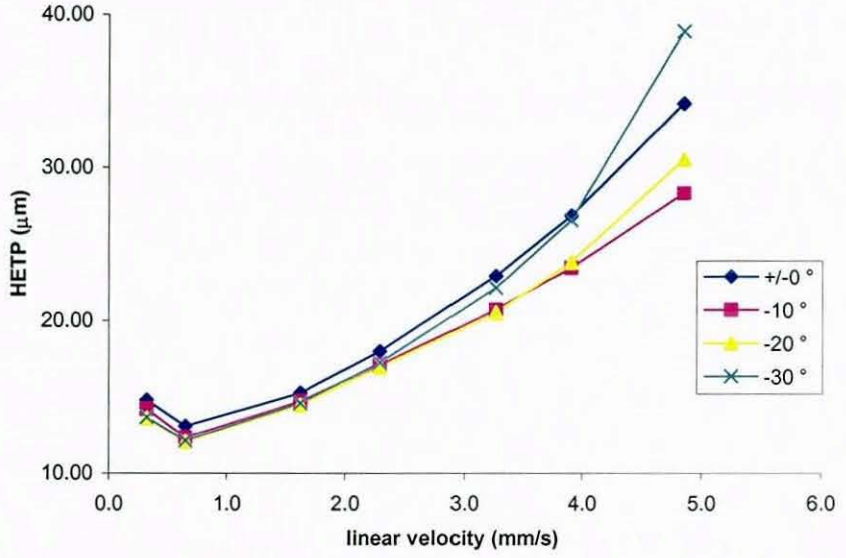

Figure 235: van Deemter curves for triphenylene on Purospher RP18 column 125 x 3.0 mm i.d., mobile phase 75% methanol, 25% water (w/w), temperature 40 °C controlled in water bath, at different mobile phase inlet temperatures.

Purospher RP18 125 x 2.0 mm

butylbenzene

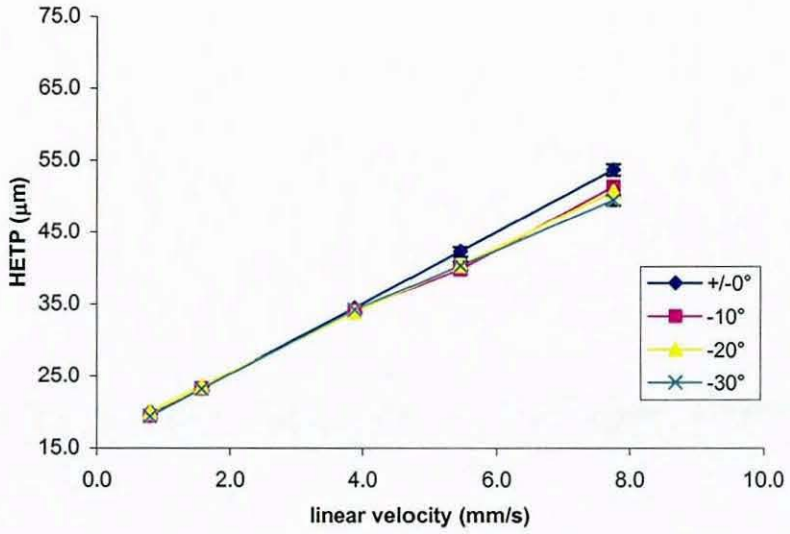

Figure 236: van Deemter curves for butylbenzene on Purospher RP18 column 125 x 2.0 mm i.d., mobile phase 75% methanol, 25% water (w/w), temperature 40 °C controlled in water bath, at different mobile phase inlet temperatures.

o-terphenyl

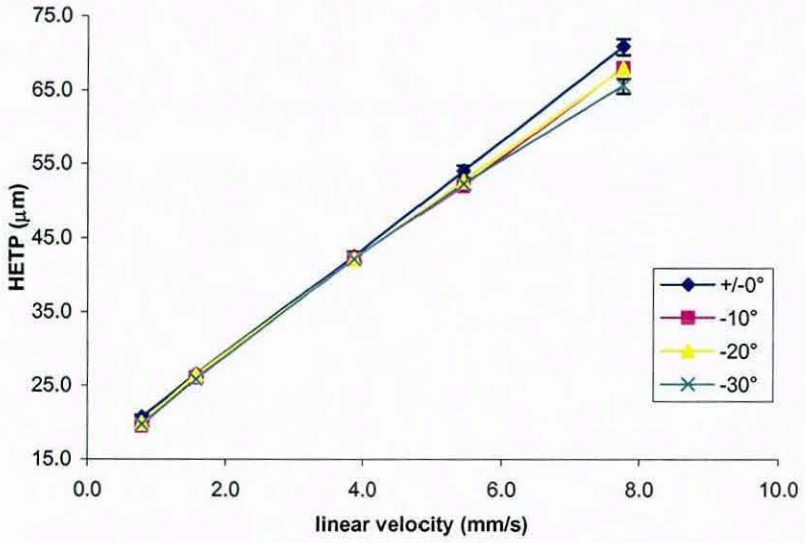

Figure 237: van Deemter curves for o-terphenyl on Purospher RP18 column 125 x 2.0 mm i.d., mobile phase 75% methanol, 25% water (w/w), temperature 40 °C controlled in water bath, at different mobile phase inlet temperatures.

penylbenzene

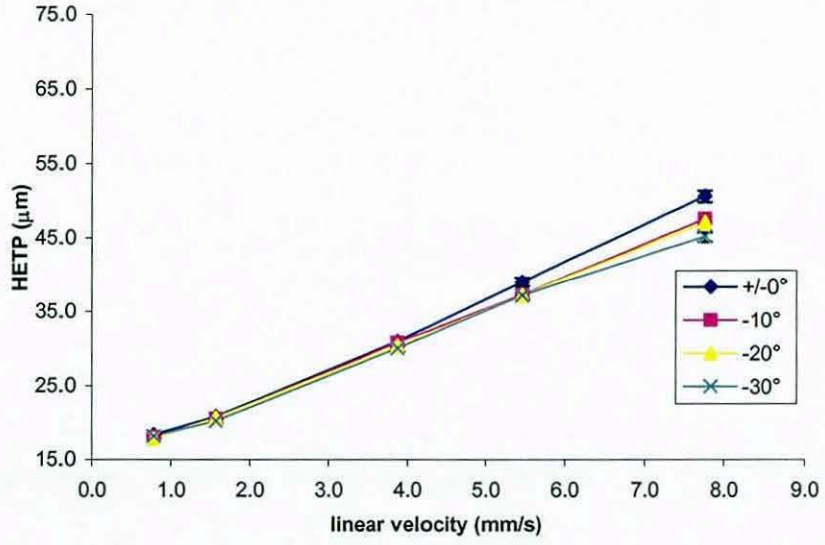

Figure 238: van Deemter curves for pentylbenzene on Purospher RP18 column 125 x 2.0 mm i.d., mobile phase 75% methanol, 25% water (w/w), temperature 40 °C controlled in water bath, at different mobile phase inlet temperatures.

triphenylene

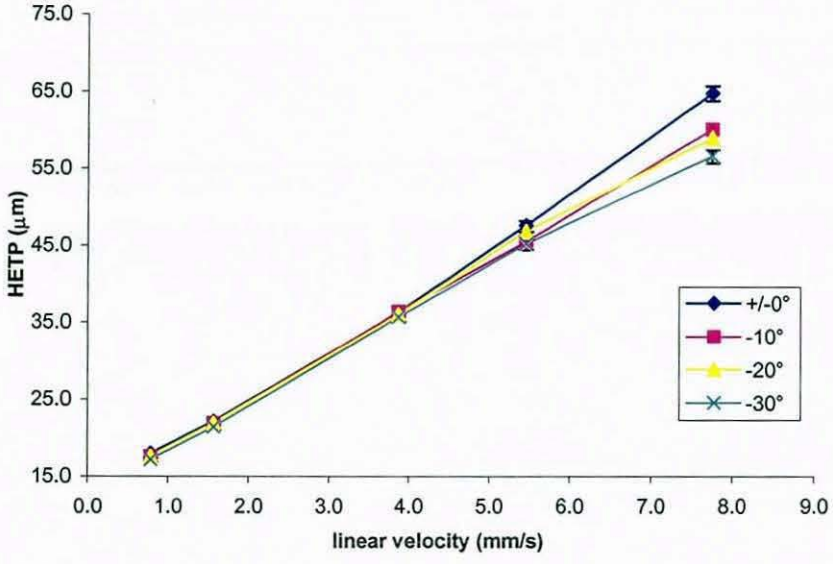

Figure 239: van Deemter curves for triphenylene on Purospher RP18 column 125 x 2.0 mm i.d., mobile phase 75% methanol, 25% water (w/w), temperature 40 °C controlled in water bath, at different mobile phase inlet temperatures.

Purospher RP18e 150 x 4.6 mm

butylbenzene

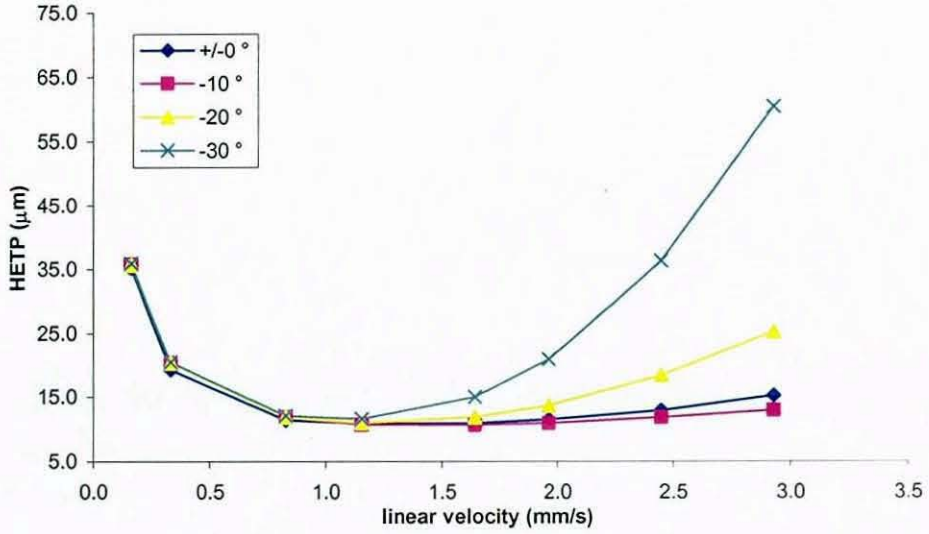

Figure 240: van Deemter curves for butylbenzene on Purospher RP18e column 150 x 4.6 mm i.d., mobile phase 75% methanol, 25% water (w/w), temperature 40 °C controlled in water bath, at different mobile phase inlet temperatures.

o-terphenyl

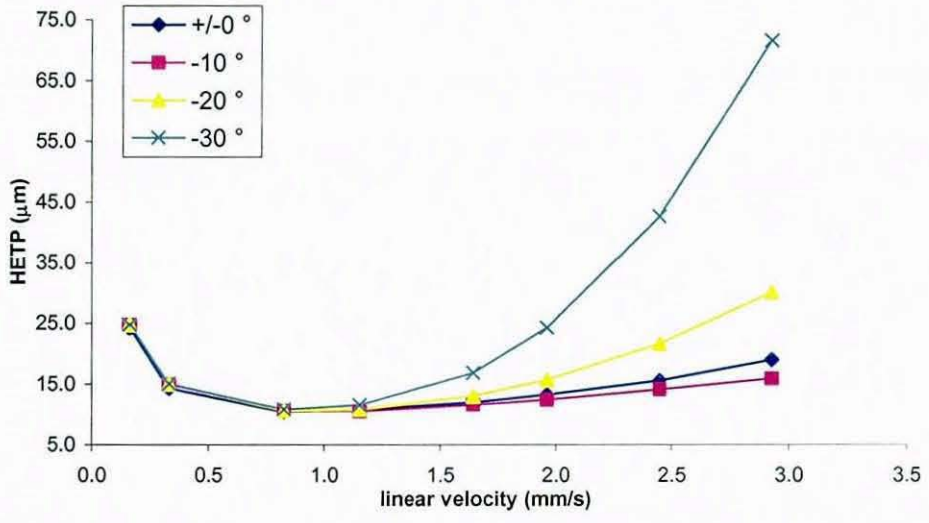

Figure 241: van Deemter curves for o-terphenyl on Purospher RP18e column 150 x 4.6 mm i.d., mobile phase 75% methanol, 25% water (w/w), temperature 40 °C controlled in water bath, at different mobile phase inlet temperatures.

pentylbenzene

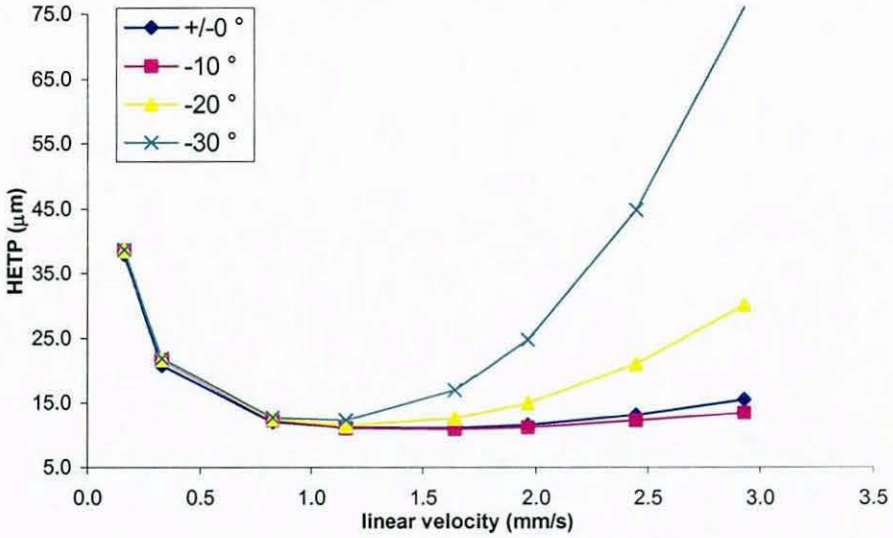

Figure 242: van Deemter curves for pentylbenzene on Purospher RP18e column 150 x 4.6 mm i.d., mobile phase 75% methanol, 25% water (w/w), temperature 40 °C controlled in water bath, at different mobile phase inlet temperatures.

triphenylene

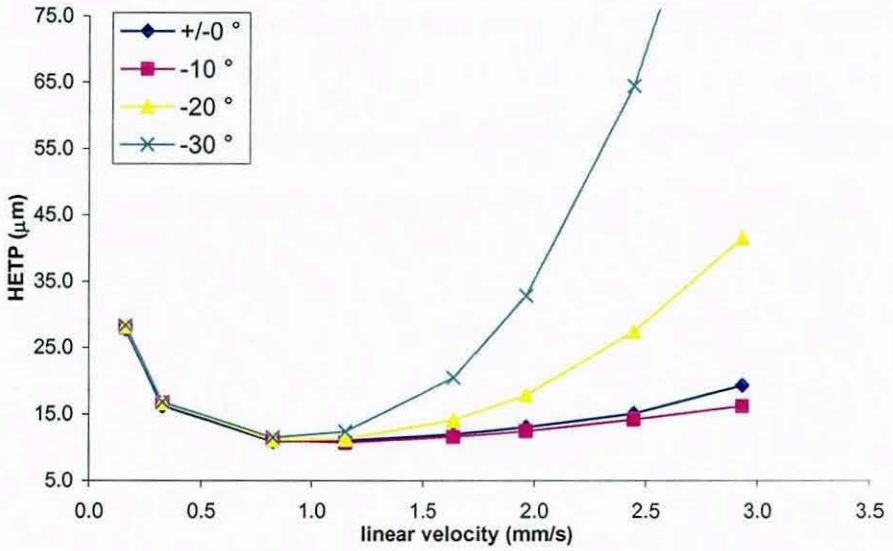

Figure 243: van Deemter curves for triphenylene on Purospher RP18e column 150 x 4.6 mm i.d., mobile phase 75% methanol, 25% water (w/w), temperature 40 °C controlled in water bath, at different mobile phase inlet temperatures.

Purospher RP18e 125 x 3.0 mm

butylbenzene

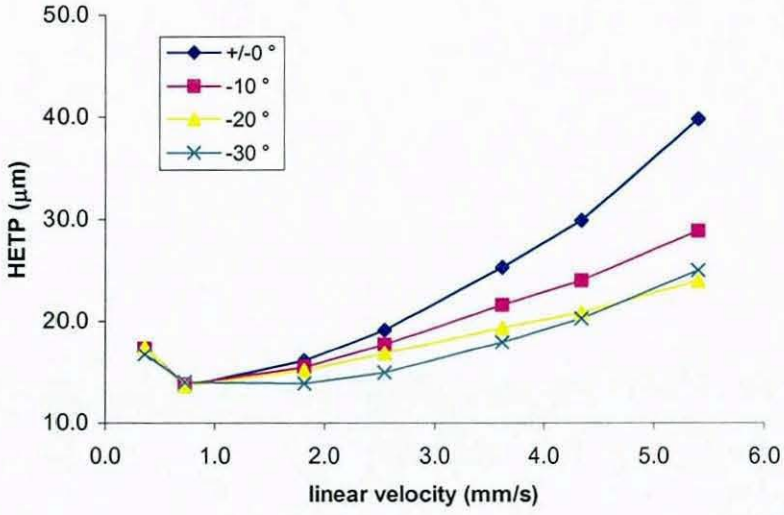

Figure 244: van Deemter curves for butylbenzene on Purospher RP18e column 125 x 3.0 mm i.d., mobile phase 75% methanol, 25% water (w/w), temperature 40 °C controlled in water bath, at different mobile phase inlet temperatures.

o-terphenyl

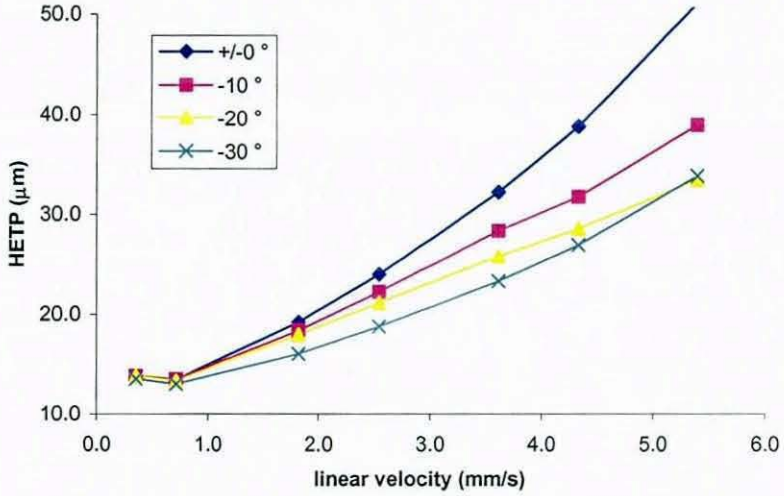

Figure 245: van Deemter curves for o-terphenyl on Purospher RP18e column 125 x 3.0 mm i.d., mobile phase 75% methanol, 25% water (w/w), temperature 40 °C controlled in water bath, at different mobile phase inlet temperatures.

pentylbenzene

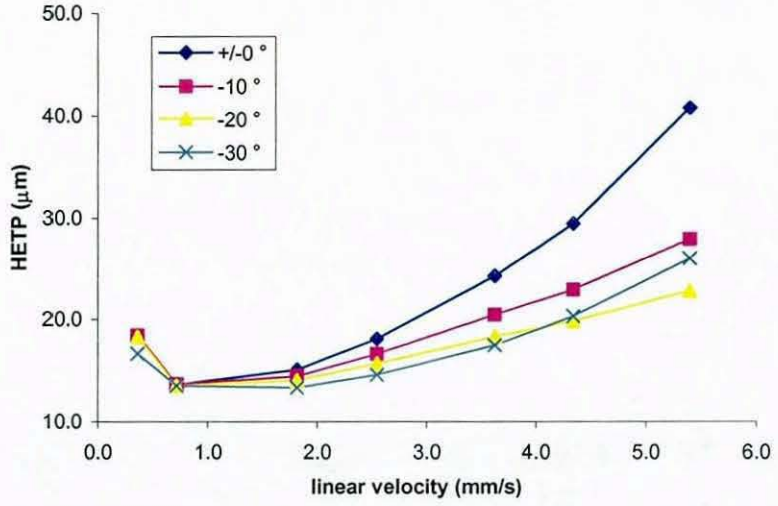

Figure 246: van Deemter curves for pentylbenzene on Purospher RP18e column 125 x 3.0 mm i.d., mobile phase 75% methanol, 25% water (w/w), temperature 40 °C controlled in water bath, at different mobile phase inlet temperatures.

triphenylene

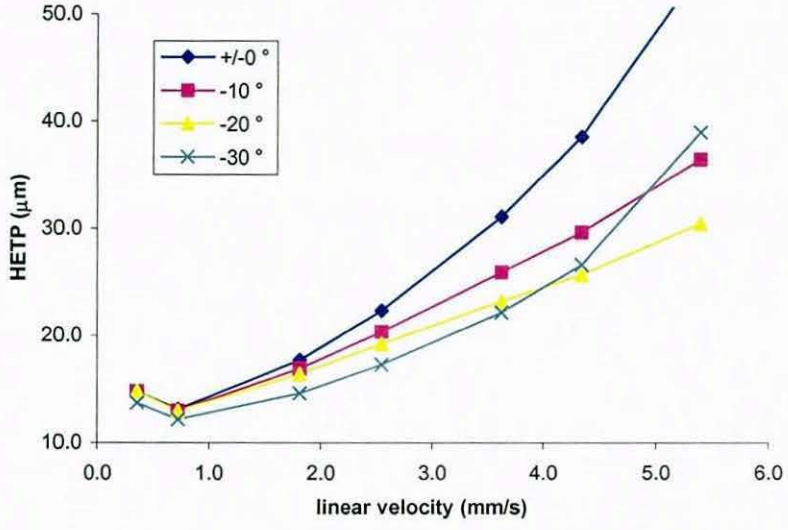

Figure 247: , van Deemter curves for triphenylene on Purospher RP18e column 125 x 3.0 mm i.d., mobile phase 75% methanol, 25% water (w/w), temperature 40 °C controlled in water bath at different mobile phase inlet temperatures.

Purospher RP18e 125 x 2.0 mm

butylbenzene

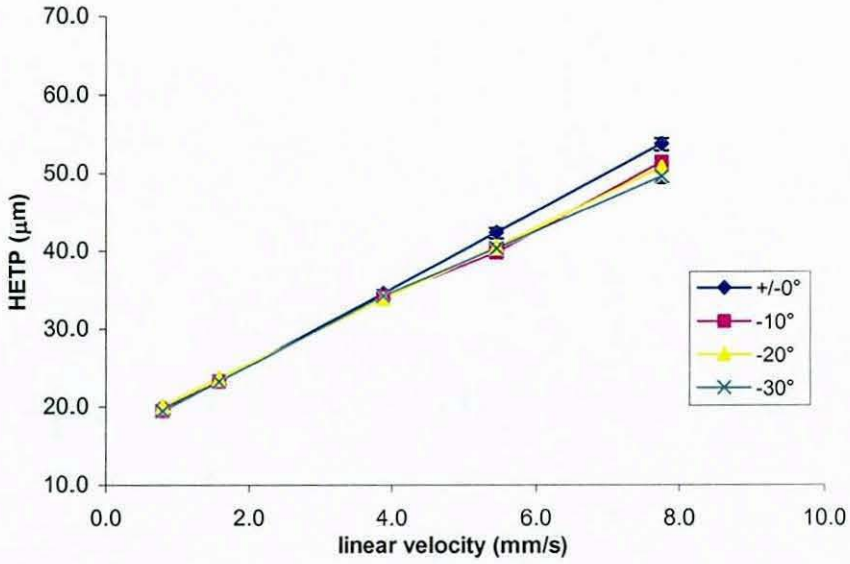

Figure 248: van Deemter curves for butylbenzene on Purospher RP18e column 125 x 2.0 mm i.d., mobile phase 75% methanol, 25% water (w/w), temperature 40 °C controlled in water bath, at different mobile phase inlet temperatures.

o-terphenyl

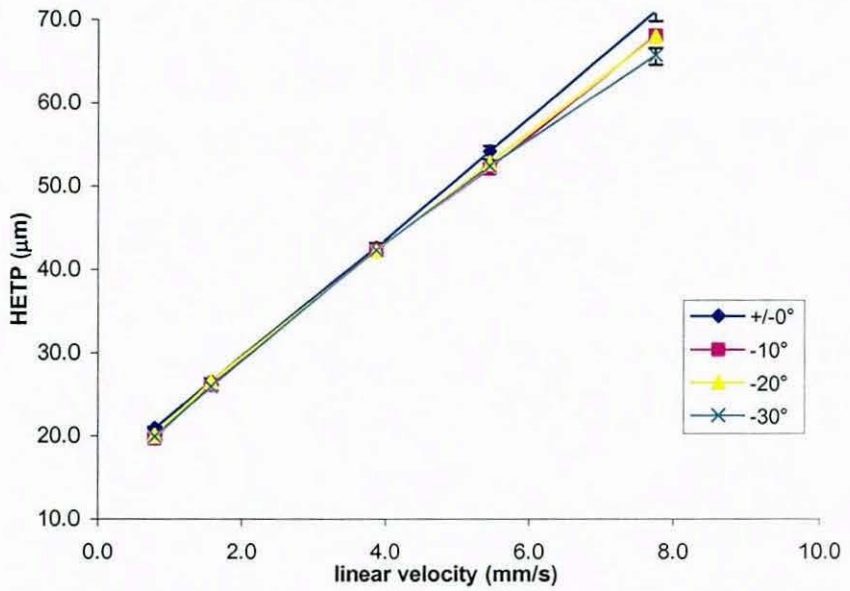

Figure 249: van Deemter curves for o-terphenyl on Purospher RP18e column 125 x 2.0 mm i.d., mobile phase 75% methanol, 25% water (w/w), temperature 40 °C controlled in water bath, at different mobile phase inlet temperatures.

pentylbenzene

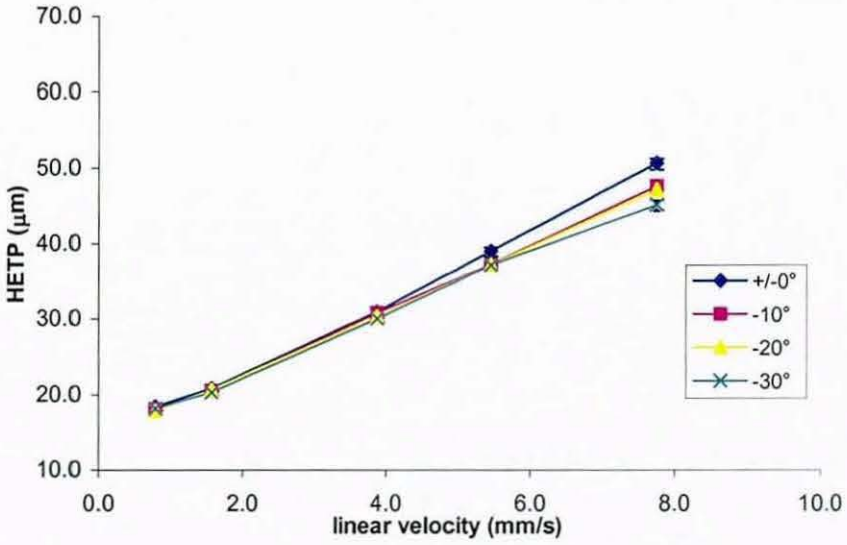

Figure 250: van Deemter curves for pentylbenzene on Purospher RP18e column 125 x 2.0 mm i.d., mobile phase 75% methanol, 25% water (w/w), temperature 40 °C controlled in water bath, at different mobile phase inlet temperatures.

triphenylene

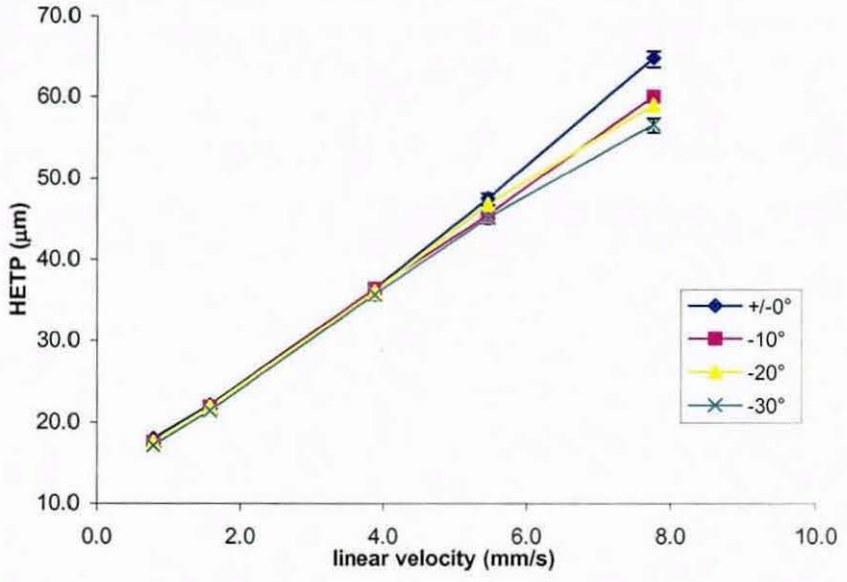

Figure 251: van Deemter curves for triphenylene on Purospher RP18e column 125 x 2.0 mm i.d., mobile phase 75% methanol, 25% water (w/w), temperature 40 °C controlled in water bath, at different mobile phase inlet temperatures.

Purospher RP18e 125 x 1.0 mm

butylbenzene

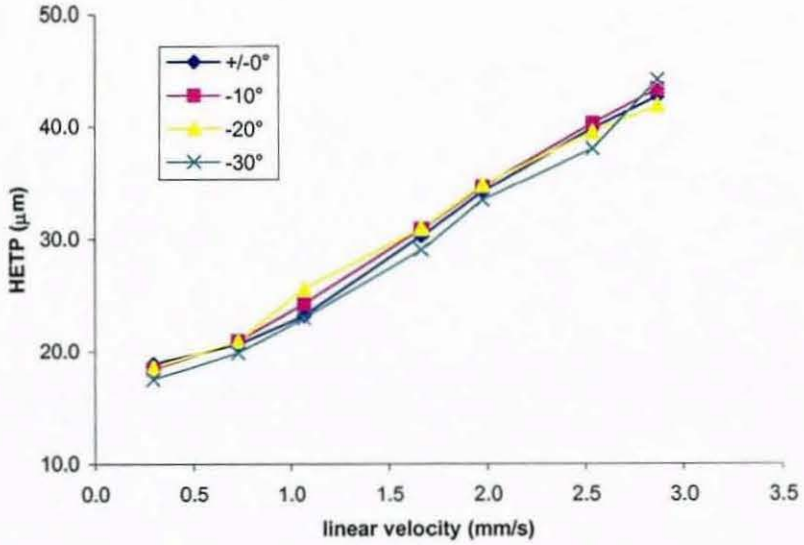

Figure 252: van Deemter curves for butylbenzene on Purospher RP18e column 125 x 1.0 mm i.d., mobile phase 75% methanol, 25% water (w/w), temperature 40 °C controlled in water bath, at different mobile phase inlet temperatures.

o-terphenyl

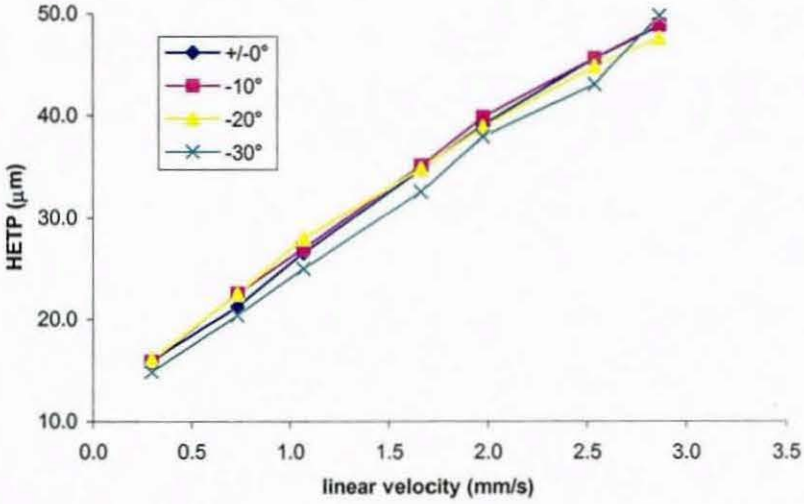

Figure 253: van Deemter curves for o-terphenyl on Purospher RP18e column 125 x 1.0 mm i.d., mobile phase 75% methanol, 25% water (w/w), temperature 40 °C controlled in water bath, at different mobile phase inlet temperatures.

pentylbenzene

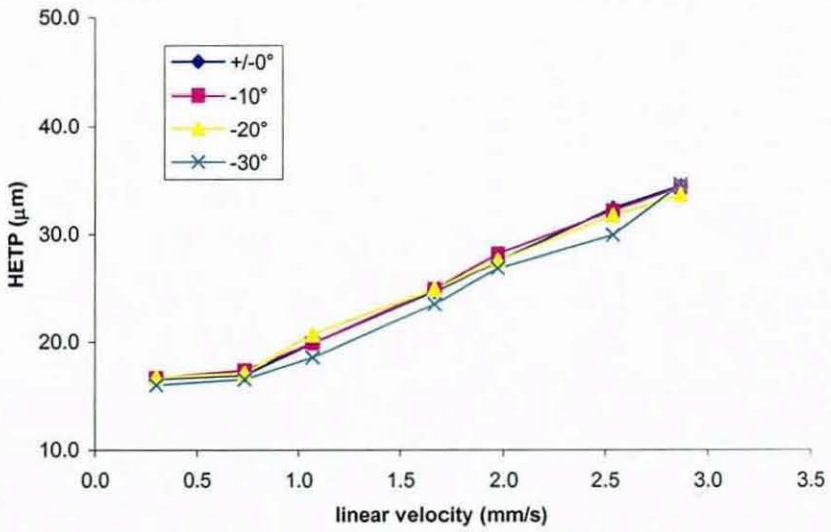

Figure 254: van Deemter curves for pentylbenzene on Purospher RP18e column 125 x 1.0 mm i.d., mobile phase 75% methanol, 25% water (w/w), temperature 40 °C controlled in water bath, at different mobile phase inlet temperatures.

triphenylene

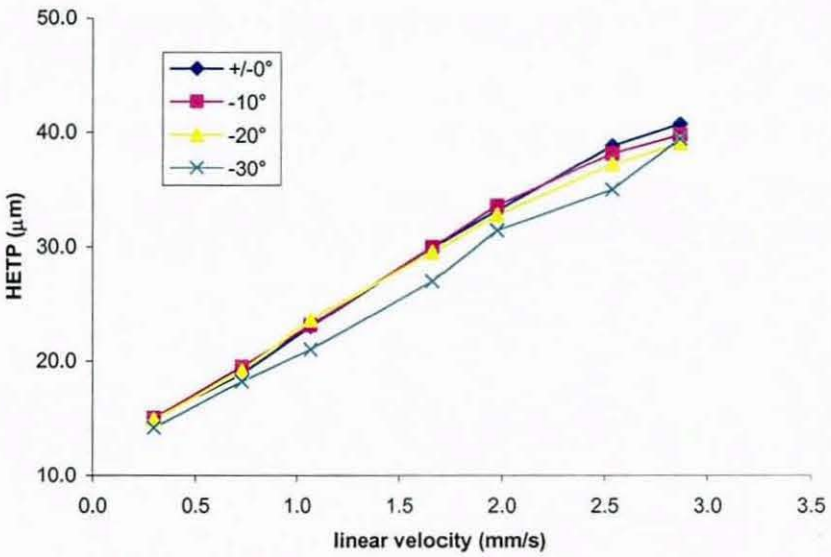

Figure 255: van Deemter curves for triphenylene on Purospher RP18e column 125 x 1.0 mm i.d., mobile phase 75% methanol, 25% water (w/w), temperature 40 °C controlled in water bath, at different mobile phase inlet temperatures.